Investigating the mechanism of renal cystogenesis in tuberous sclerosis and polycystic kidney disease

Submitted for the degree of Doctor of Philosophy at Cardiff University

Cleo Bonnet

2009

ProQuest LLC
789 East Eisenhower Parkway
P.O. Box 1346
Ann Arbor, MI 48106-1346

Summary

Tuberous sclerosis (TSC) is an autosomal dominant disorder caused by germline mutations in either *TSC1* or *TSC2* and characterised by the development of benign hamartomatous growths in multiple organs and tissues. Clinical trials are underway for the treatment of TSC-associated tumours using mammalian target of rapamycin (mTOR) inhibitors. Here, we show that many of the earliest renal lesions from $Tsc1^{+/-}$ and $Tsc2^{+/-}$ mice do not exhibit mTOR activation, suggesting that pharmacological targeting of an alternative pathway may be necessary to prevent tumour formation.

Patients with TSC often develop renal cysts and those with inherited co-deletions of the autosomal dominant polycystic kidney disease (ADPKD) 1 gene (*PKD1*) develop severe, early onset, polycystic kidneys. Using mouse models, we crossed $Tsc1^{+/-}$ and $Tsc2^{+/-}$ mice with $Pkd1^{+/-}$ mice to generate double heterozygotes. We found that $Tsc1^{+/-}Pkd1^{+/-}$ and $Tsc2^{+/-}Pkd1^{+/-}$ mice had significantly more renal lesions than their corresponding single heterozygote littermates indicating a genetic interaction between *Tsc1* and *Tsc2* with *Pkd1*. In agreement with our findings from $Tsc1^{+/-}$ and $Tsc2^{+/-}$ mice, we found that a large proportion of cysts from $Tsc1^{+/-}Pkd1^{+/-}$ and $Tsc2^{+/-}Pkd1^{+/-}$ mice failed to stain for pS6, suggesting that initiation of renal cystogenesis in these animals may occur independently of mTOR activation.

We analysed primary cilia in phenotypically normal renal tubule epithelial cells by scanning electron microscopy (SEM) and found that those from $Tsc1^{+/-}$ and $Tsc2^{+/-}$ mice were significantly shorter than those from wild-type littermates (2.122μm and 2.016μm vs. 2.233μm, respectively, $P<0.001$). Primary cilia from epithelial cells lining renal cysts of $Tsc1^{+/-}$ and $Tsc2^{+/-}$ mice were consistently longer (5.157μm and 5.091μm respectively). Interestingly, we found that *Pkd1*-deficiency coupled with either *Tsc1* or *Tsc2*-deficiency altered the length of the primary cilia from both normal renal tubule cells (restored to 'wild-type' length)

and epithelial cells lining cysts (*Tsc1*$^{+/-}$*Pkd1*$^{+/-}$ Mean 3.38μm and *Tsc2*$^{+/-}$*Pkd1*$^{+/-}$ Mean 3.09μm). These novel data demonstrate that the *Tsc* and *Pkd1* gene products help regulate primary cilia length which may prevent renal cystogenesis.

Consistent with the observation that primary cilia modulate the planar cell polarity (PCP) pathway, we found that many dividing pre-cystic renal tubule epithelial cells from *Tsc1*$^{+/-}$, *Tsc2*$^{+/-}$ and *Pkd1*$^{+/-}$ mice were highly misorientated along the tubule axis. This could potentially lead to tubule dilation and subsequent cyst formation. We therefore propose that defects in cell polarity underlie both TSC and ADPKD-associated renal cystic disease and targeting of this pathway may be of key therapeutic benefit.

Declaration

This work has not previously been accepted in substance for any degree and is not concurrently submitted in candidature for any degree.

Signed...C. Bonnet..... (candidate) Date...5/5/09....

Statement 1

This thesis is being submitted in partial fulfilment of the requirements for the degree of PhD.

Signed...C. Bonnet..... (candidate) Date...5/5/09....

Statement 2

This thesis is the result of my own independent work/investigation, except where otherwise stated. Other sources are acknowledged by explicit references.

Signed...C. Bonnet..... (candidate) Date...5/5/09...

Statement 3

I hereby give consent for my thesis, if accepted, to be available for photocopying and for inter-library loan, and for the title and summary to be made available to outside organisations.

Signed...C. Bonnet..... (candidate) Date...5/5/09....

Acknowledgements

I would like to thank the following people:

My supervisors Prof. Jerry Cheadle, who has given me helpful advice, support and constructive criticism, and Prof. Julian Sampson.

Catherine Wilson for all her training, help and support in my first year. Shelley Idziaszczyk for always being there when things don't go quite to plan and I need a good moan. Becky Harris for being an excellent lab technician and colony manager. My immunohistochemistry and SEM guru Chris von Ruhland for all his help, guidance and enthusiasm. Carol Guy, Anthony Hayes, Joanne Cable and the Biomedical Services staff at Cardiff University for technical support. Daniel St.Johnston, Eduardo Torres, Christopher Ward, Keith Davies and James Colley for helpful advice. Dorien Peters for the *Pkd1*$^{nl/nl}$ mice and Richard Sandford for the *Pkd1*$^{+/-}$ mice.

Duncan Azzopardi for being my partner in PhD crime and an excellent friend throughout the three and a half years, and many more to come! All the people in the PhD office for keeping the atmosphere fun.

All my family and friends, in particular Ryan who has been incredibly patient and understanding throughout this process, I wouldn't have been able to do it without his support. Also my mum and dad for all their support, and finally Mehri and Trefor for all their encouragement.

The Tuberous Sclerosis Association UK, the PKD Foundation and the Wales Gene Park for their funding.

Abbreviations

3D	Three dimensional
4E-BP1	eIF4E-binding protein 1
5'RACE	5' rapid amplification of cDNA ends
A/B	Apical/basal
ABC	Avidin biotin complex
ACE	Angiotensin converting enzyme
ADPKD	Autosomal dominant polycystic kidney disease
ADPLD	Autosomal dominant polycystic liver disease
AML	Angiomyolipoma
AMPK	AMP-dependent protein kinase
AP-1	Activator protein-1
APC	Adenomatosis polyposis coli
aPKC	Atypical protein kinase C
ARPKD	Autosomal recessive polycystic kidney disease
ATP	Adenosine triphosphate
AVP	Arginine vasopressin
BAX	Bcl-2-associated X protein
BBS	Bardet-Biedl syndrome
BCL2	B-cell leukemia/lymphoma 2
Bp	Base pair
BPK	BALB/C polycystic kidneys
BSA	Bovine serum albumin
BUN	Blood urea nitrogen
Ca^{2+}	Calcium
CaM	Calmodulin
cAMP	Cyclic adenosine monophosphate
CDK1	Cyclin-dependent kinase 1
cDNA	Complementary DNA
CICR	Ca^{2+}-induced Ca^{2+} release

CPK	Congenital polycystic kidneys
CRISP	Consortium for Radiologic Imaging Studies of PKD
CRR	Cystein-rich regions
CT	Computed tomography
DAB	3,3'-diaminobenzidine
DAPI	4',6-diamidino-2-phenylindole
DBA	*Dolichos biflorus* agglutinin
DCT	Distal convoluted tubule
DHPLC	Denaturing high-performance liquid chromatography
Dkk	Dickkopf
DNA	Deoxyribonucleic acid
dNTP	Deoxynucleotidetriphosphates
DPX	Dibutyl phthalate and xylene
Dsh	Dishevelled
Dub	Duboraya
E	Embryonic day
EDTA	Ethylenediaminetetraacetic acid
EF	E and F helixes of parvalbumin
EGFR	Epidermal growth factor receptor
eIF4E	Eukaryotic translation initiation factor 4E
ENU	N-ethyl-nitrosourea
ER	Endoplasmic reticulum
ERα	Estrogen receptor α
ERK	Extracellular signal regulated kinase
ERM	Ezrin-radixin-moezin
ES	Embryonic stem
ESRD	End-stage renal disease
ET	Endothelin
FAK	Focal adhesion kinase
FAP	Familial adenomatous polyposis
FBS	Foetal bovine serum

F.F	Filtration fraction
FGFR	Fibroblast growth factor receptor
FIP200	Focal adhesion kinase family interacting protein of 200KD
FITC	Fluorescein isothiocyanate
FKBP	FK506-binding protein
FoxO1	Forkhead box O1
FTase	Farnesyltransferase
Fz	Frizzled
GAP	GTPase-activating protein
GDP	Guanosine diphosphate
GFR	Glomerular filtration rate
GPS	G-protein coupled receptor proteolytic site
GSK	Glycogen synthase kinase
GTP	Guanosine triphosphate
H&E	Haematoxylin and eosin
HIF	Hypoxia-inducible factor
HMDS	Hexamethyldisilazane
ICA	Intracranial aneurysm
Id	Inhibitor of DNA binding
IFT	Intraflagellar transport
IHC	Immunohistochemistry
IKK	Inhibitory κB kinase
IMCD	Inner medullary collecting duct
Inv	Inversion of embryonic turning
IRES	Internal ribosome entry site
IRI	Ischaemic/reperfusion injury
IRS	Insulin receptor substrate
JCK	Juvenile cystic kidney
JCPK	Juvenile congenital polycystic kidney
JPS	Juvenile polyposis syndrome
KAP3	Kinesin superfamily-associated protein 3

KAT	Kidney, anaemia, testis
Kb	Kilobase
kDa	Kilodalton
KIF3a	Kinesin family member 3a
KIP	Kinase interacting protein
LAM	Lymphangioleiomyomatosis
LCM	Laser capture microdissection
LDL	Low-density lipoprotein A
LEF	Lymphoid enhancer factor
LH2	Lipoxygenase homology
LOH	Loss of heterozygosity
LRP	Lipoprotein receptor-related protein
LRR	Leucine-rich repeats
LST8	Lethal with SEC13 protein 8
LTL	*Lotus tetragonolobus* lectin
LVH	Left ventricular hypertrophy
MAP	Mean arterial pressure
MAPK	Mitogen activated protein kinase
Mb	Megabase
MDCK	Madin-Darby canine kidney
MEF	Mouse embryonic fibroblast
MEK	Mitogen extracellular kinase
MK2	MAPK activated protein kinase 2
MRI	Magnetic resonance imaging
mRNA	Messenger ribonucleic acid
mTOR	Mammalian target of rapamycin
mTORC	Mammalian target of rapamycin complex
NaCl	Sodium chloride
NEK	NIMA-related kinase
NF-1	Neurofibromatosis type-1
NF-L	Neurofilament-L

NIMA	Never in mitosis A
NLS	Nuclear localisation sequence
NPHP	Nephronophthisis
OCT	Optimum cutting temperature
OFD1	Oral-facial-digital syndrome type 1
ORF	Open reading frame
ORPK	Oak Ridge polycystic kidney
PALS	Protein associated with Lin-seven
PAM	Protein associated with Myc
PATJ	PALS1-associated TJ protein
PBFG	Phosphate buffered formaldehyde glutaraldehyde
PBP	Polycystic breakpoint protein
PBS	Phosphate buffered saline
PC1	Polycystin-1
PC2	Polycystin-2
PCK	Polycystic kidneys
PCP	Planar cell polarity
PCR	Polymerase chain reaction
PCY	Polycystic kidney disease
PI3K	Phosphoinositide 3-kinase
PFGE	Pulsed field gel electrophoresis
PIKK	Phosphoinositide 3-kinase-related kinase
PJS	Peutz-Jeghers syndrome
PKB	Protein kinase B
PKD	Polycystic kidney disease
PKHD	Polycystic kidney and hepatic disease
PLC	Phospholipase C
PTEN	Phosphatase and tensin homologue
PTHS	PTEN-hamartoma tumour syndrome
Raptor	Regulatory associated protein of mTOR
RAAS	Renin-angiotensin-aldosterone system

RCC	Renal cell carcinoma
REJ	Sperm receptor for egg jelly
Rheb	Ras homologue enriched in brain
Rictor	Rapamycin insensitive companion of mTOR
RPF	Renal plasma flow
RSK1	Ribosomal protein S6 kinase 1
RT-PCR	Reverse transcription-polymerase chain reaction
RxRα	Retinoid x receptor α
S6K	S6 kinase
SAD	Synapses of amphids defective
SAP	Shrimp alkaline phosphatase
SDS	Sodium dodecyl sulphate
SEGA	Subependymal giant cell astrocytoma
SEM	Scanning electron microscope
SEN	Subependymal nodule
sFRP	Secreted frizzled-related protein
SIN1	Stress activated protein kinase interacting protein 1
STAT6	Signal transducer and activator of transcription protein 6
TAD	Transcription activating domain
TBS	Tris buffered saline
TCF	T-cell factor
TGF	Transforming growth factor
THP	Tamm-Horsfall glycoprotein
TNF	Tumour necrosis factor
TNFR	Tumour-necrosis-factor receptor
TOR	Target of rapamycin
TOS	TOR signalling
TrCP	Transducin repeat-containing protein
TRITC	Tetramethyl rhodamine isothiocyanate
TRP	Transient receptor potential
TSC	Tuberous sclerosis

TUNEL	Terminal dUTP nick-end labelling
UV	Ultraviolet
V_2	Vasopressin
Vang	Vang Gogh
VDR	Vitamin D receptor
VEGF	Vascular endothelial growth factor
VHL	von Hippel-Lindau
WIF-1	Wnt inhibitory factor 1
WPK	Wistar polycystic kidneys
WSC	Cell wall integrity and stress response component
WT	Wild-type

Contents

List of figures

List of tables

CHAPTER ONE: General introduction

1.1 Tuberous sclerosis complex

Tuberous sclerosis complex (TSC) is a tumour suppressor gene syndrome characterised by benign hamartomatous growths in multiple organs.

1.1.1 A brief history of TSC

Désiré-Magloire Bourneville first discovered and described TSC in 1879, giving it the name "tuberous sclerosis of the cerebral convolutions" (Bourneville 1880). In 1908 Vogt proposed a clinical triad of seizures, mental handicap and adenoma sebaceum as indicative of cerebral tuberous sclerosis and also noted that cardiac and renal tumours occurred (Vogt 1908). Prior to the 1970's, estimates of the prevalence of TSC ranged from 1:20,000 to 1:150,000 (Gunther and Penrose 1935, Ross and Dickerson 1943, Dawson 1954, Paulson and Lyle 1966, Zaremba 1968, Stevenson and Fischer 1956, Nevin and Pearce 1968, Singer 1971). During the 1970's and 1980's, new technologies such as computed tomography (CT), echocardiography, renal ultrasound and magnetic resonance imaging (MRI) provided reliable non-invasive methods of diagnosis allowing identification of patients who did not present with the complete Vogt's triad or those that presented with no signs of impaired intelligence (Lagos and Gomez 1967). Due to these new technologies and publication of primary and secondary diagnostic criteria by Gomez in 1979, population studies became far more accurate and many more patients were included (Gomez 1979). Since this, many more population studies have been undertaken and by 2006 the prevalence of TSC was estimated between 1:14,492 to 1:26,500 (Shepherd *et al.* 1991a, Webb *et al.* 1996, Devlin *et al.* 2006). The two genes responsible for TSC have now been characterised (The European Chromosome 16 Tuberous Sclerosis Consortium 1993, van Slegtenhorst *et al.* 1997) and genetic testing is available for the diagnosis of TSC in adults, children and infants, both pre- and post-natally (Jones *et* al. 2000, Bénit *et al.* 2001). Table 1.1 lists further important discoveries in the history of TSC.

Table 1.1 History of the tuberous sclerosis complex.

Date	Name	Discoveries, developments and genetics
1835	Pierre François Olive Rayer	A picture in skin disease atlas closely resembled facial angiofibromas seen in TSC patients.
1862	Friedrich Daniel von Recklinghausen	Presented a newborn infant with heart tumours and brain scleroses, now commonly known as cardiac rhabdomyomas and cortical tubers.
1879	Désiré-Magloire Bourneville	Coined term "tuberous sclerosis of the cerebral convolutions" after examining brain of epileptic and mentally handicapped girl (Bourneville 1880).
1885	Balzer, Ménétrier and Pringle	Recognised and named "adenoma sebaceum", a facial lesion found in TSC patients.
1905	Campbell	Described ocular pathology.
1905	Perusini	Observed association of cerebral, renal and cardiac lesions with facial angiofibromas.
1908	Vogt	Clinical triad of seizures, mental handicap and adenoma sebaceum (Vogt 1908).
1910	Kirpicznik & Berg	Hereditary nature of tuberous sclerosis.
1920 and 1935	Van der Hoeve	Noted retinal phakomas and a similarity between TSC, neurofibromatosis and von Hippel-Lindau disease, introduced concept of phakomatosis.
1932	Critchley & Earl	Published very complete description of TSC and emphasized the diagnostic value of white spots (hypomelanotic skin macules).
1942	Moolten	Recognised the complexity and hamartial nature of tuberous sclerosis, renamed it "the tuberous sclerosis complex" (Moolten 1942).
1967	Lagos & Gomez	38% of their patients were found to have average intelligence.
1979	Gomez	New criteria for diagnosis; decline of Vogt's triad.
1987	Fryer *et al.*	Assigned *TSC1* to chromosome 9q34 (Fryer *et* al. 1987).
1992	Kandt *et al.*	Assigned *TSC2* to chromosome 16p13 near the region of *PKD1* (Kandt *et* al. 1992).
1993	The European Chromosome 16 TSC Consortium	*TSC2* cloned and its protein product tuberin identified. Found region of homology to the GTPase-activating protein GAP3.
1994	Green *et al.* & Carbonara *et al.*	Loss of heterozygosity found in renal, cardiac and brain lesions from TSC patients (Green *et al.* 1994, Carbonara *et* al. 1994).
1997	Van Slegtenhorst *et al.*	*TSC1* cloned and its protein product hamartin identified (van Slegtenhorst *et* al. 1997).
1998	Van Slegtenhorst *et al.*	Hamartin and tuberin associate physically *in vivo* (van Slegtenhorst *et al.* 1998).
2002	Tee *et al.*	Hamartin and tuberin function together to inhibit the mammalian target of rapamycin (mTOR) pathway (Tee *et al.* 2002).

Unless otherwise stated, references are from Gomez *et al.* 1999.

1.1.2 TSC manifestations

TSC can cause hamartomatous lesions in most organs of the body, notably the central nervous system, skin, kidneys, retina and heart. Skin lesions are the most common findings in TSC patients (apparent in approximately 96% of patients), closely followed by cerebral pathology in 90% of patients. Approximately 84% have had seizures, 60% have renal pathology and nearly 50% have retinal hamartomas (Gomez *et al.* 1999). Other tissues that may be affected include the lungs, spleen, lymph nodes, adrenal and thyroid glands, gonads, nasal mucosa, pituitary gland, the aorta and large calibre arteries, bones, dental enamel, gums, liver, pancreas, and gastrointestinal tract (Gomez 1988). The spinal cord is rarely involved and the skeletal muscles and peripheral nerves are not known to be affected. Table 1.2 lists the characteristic lesions of TSC in more detail. Age is a factor in the type of lesions present in a patient. Angiomyolipomas (AMLs) tend to not appear until later in life, usually becoming apparent towards the end of the second decade, whereas cardiac rhabdomyomas appear in foetal life and often disappear in infancy (Roach and Sparagana 2004).

Hamartomas are the most common type of lesion in TSC, however there are actually three different types of lesion (Moolten 1942):

- Hamartias are misaligned groups of dysplastic cells that are intrinsic to the tissue they are located in. The undifferentiated cells do not multiply or grow more rapidly than the surrounding normal cells (e.g. cortical tubers).
- Hamartomas are groups of dysplastic cells that tend to multiply excessively and grow into benign tumours (e.g. renal angiomyolipomas).
- Hamartoblastomas are rare malignant tumours derived from hamartomas (e.g. renal cell carcinomas).

	Subependymal giant cell astrocytoma (SEGA)	Histologically identical to SEN but diff their propensity to grow. Lie adjacent foramina of Monro.
Skin	Hypomelanotic macule	Often present at birth and appear as c white patches commonly over the trur buttocks.
	Facial angiofibroma (adenoma sebaceum)	Red to pink papules or nodules with a smooth, glistening surface. Bilaterally symmetrical, distributed over the cent areas.
	Shagreen patch	Found on the dorsal body surfaces, particularly the lumbosacral region. Ap slightly elevated, yellowish, brown or colour and texture of orange peel.
	Ungual fibroma	Dull, red- or flesh-coloured papules or nodules arising from the finger or toe bed.
	Café-au-Lait macule	Oval or round, flat, hyperpigmented m of 1 to 5cm in length. Can create diag confusion with neurofibromatosis.
Kidney	Cyst Angiomyolipoma Renal cell carcinoma	Described in text below.
Heart	Cardiac rhabdomyoma	Grey-white to yellow-tan lesions that v from several millimetres to several centimetres. Occur more commonly in ventricles than atria.

		tumours, mixed tumours and retinal depigmented spots.
Lungs	Lymphangioleiomyomatosis (LAM)	Found in up to 50% of women with TS CT scan. Affected lungs may be twice heavy as normal. Lung tissue replace many cysts varying from a few millim several centimetres diameter.
Liver	Angiomyolipoma	Less commonly found in the liver than kidneys. Consists of abnormal blood smooth muscle cells and adipose tiss
The endocrine system	Angiomyolipoma Adenoma	Organs involved include adrenal glan thyroid gland, pancreas, gonads, hypothalamus, pituitary and parathyro glands.
Digestive tract	Mouth - Nodular tumours, fibromas, papillomas Rectum - Hamartomatous colorectal polyps	Appear between 4 and 10 years of ag puberty. Uncommon, mainly occur in adults. T non-neoplastic and have no malignan potential.
Teeth	Enamel pits	Occur in primary or deciduous teeth.
Spleen	Nodular tumours	Very rare. Can reach up to 11cm in di
Arteries	Wall defects	Result in aneurysm of the aorta or subclavian, cranial, or renal arteries.
Skeleton	Phalangeal cysts Sclerotic lesions	Present early in childhood. Non-speci fibrous tissue replaces bone. Un-accompanied by symptoms. Calva sclerosis appears within the first deca life in about half of TSC patients.

Information obtained from Gomez *et al.* 1999, Rosser *et al.* 2006 and Lendva and Marshall 2003.

1.1.2.1 Renal manifestations

After neurologic complications, renal manifestations are the second most common cause of morbidity and mortality in TSC (Shepherd *et al.* 1991b). Renal lesions can be divided into three types: cysts and AMLs (strongly associated with TSC) and renal cell carcinomas (RCCs) (rarely seen).

AMLs are the most common renal lesions in TSC, seen in as many as 80% of patients (Bernstein and Robbins 1991, Casper *et al.* 2002). Females appear to be more often affected with larger and more numerous AMLs compared to males (Ewalt *et al.* 1998). AMLs are classified as benign tumours of abnormal blood vessels, immature smooth muscle cells and adipose tissue (Henske 2005). The lesions are often multiple and bilateral and increase in size and number with age (Roach and Sparagana 2004). Smaller AMLs are asymptomatic, but lesions larger than 4cm in diameter are at greater risk of spontaneous haemorrhage and are often treated with prophylactic embolization (Casper *et al.* 2002).

The second most common renal lesions in TSC patients are cysts, occurring in 17% of children and up to 47% of adults (Rosser *et al.* 2006). Cysts are more commonly the cause of renal insufficiency and hypertension than AMLs (Lendvay and Marshall 2003). Like AMLs, the incidence of cysts between the sexes appears to vary with 20% of males and 9% of females affected (Torres *et al.* 1995). Cysts may be focal or diffuse, can be several centimetres in diameter and are usually present throughout the cortex and medulla. They are characteristically lined with a hyperplastic epithelium consisting of large cells often containing large, hyperchromatic nuclei with occasional mitotic figures (Gomez 1988). Occasionally TSC patients present with severe cystic kidneys, often at a young age, similar to those seen in advanced autosomal dominant polycystic kidney disease (ADPKD). Almost all of these patients have an inherited deletion spanning both the *TSC2* and *PKD1* genes which lie adjacent to each other on chromosome 16 (Brook-Carter *et al.* 1994, Sampson *et al.* 1997 and Laas *et al.* 2004).

TSC patients can also develop RCC and oncocytomas although these are quite rare phenotypes. The incidence of TSC associated RCC has been reported to be 2.5% to 4%, which is higher than that of the general population (Lendvay and Marshall 2003, Al-Saleem *et al.* 1998). There are also many reports in children with TSC (Al-Saleem *et al.* 1998, Robertson *et al.* 1996), and one report in an infant (Breysem *et al.* 2002). RCCs in TSC patients occur at an average age of 28 years, compared to sporadic RCCs which occur at a mean age of 55 in the general population (Washecka and Hanna 1991, Bjornsson *et al.* 1996). Clear cell carcinomas are the predominant cancer cell type, with papillary, sarcomatoid and chromophobe carcinomas also seen (Bjornsson *et al.* 1996, Al-Saleem *et al.* 1998). It is believed that RCCs evolve from hyperplastic cystic epithelia rather than AML lesions (Al-Saleem *et al.* 1998, Robertson *et al.* 1996).

1.1.3 Clinical diagnosis of TSC

For decades, Vogt's triad of seizures, mental retardation and facial angiofibromas was thought to be the complete clinical manifestation of TSC. However Gomez found that the three features of the triad are only found in 29% of patients with TSC, and perhaps more importantly 6% of TSC patients displayed none of the triad (Gomez 1988). In 1979 Gomez devised a new criterion for the diagnosis of TSC (Gomez 1979). This was later reassessed in 1998 at the Consensus Conference on TSC, and an even more detailed diagnostic criterion was devised (Roach *et al.* 1998). The new criteria were divided into major and minor features with the outcome consisting of a definitive, probable or possible diagnosis of TSC. Table 1.3 shows the full diagnostic criteria. Since 2001 genetic testing, using techniques such as denaturing high-performance liquid chromatography (DHPLC), has also been employed to diagnose TSC by screening patients DNA for mutations in *TSC1* or *TSC2* (Bénit 2001).

Table 1.3 Clinical diagnostic criteria for TSC.

Major features
Facial angiofibromas or forehead plaque
Nontraumatic ungula or periungual fibroma
Hypomelanotic macules (more than 3)
Shagreen patch (connective tissue nevus)
Multiple retinal nodular hamartomas
Cortical tuber *
Subependymal nodule
Subependymal giant cell astrocytoma
Cardiac rhabdomyomas, single or multiple
Lymphangioleiomyomatosis †
Renal angiomyolipomas †
Minor features
Multiple randomly distributed pits in dental enamel
Hamartomatous rectal polyps ‡
Bone cysts §
Cerebral white matter migration lines * §
Gingival fibromas
Nonrenal hamartomas ‡
Retinal achromic patch
"Confetti" skin lesions
Multiple renal cysts ‡
Definite TSC: either 2 major features or 1 major feature with 2 minor features.
Probable TSC: 1 major feature and 1 minor feature.
Possible TSC: either 1 major feature or 2 or more minor features.

Table adapted from Roach *et al.* 1998.
* When cerebral cortical dysplasia and cerebral white matter migration tracts occur together, they should be counted as 1 rather than 2 features of TSC.
† When both lymphangioleiomyomatosis and renal angiomyolipomas are present, other features of TSC should be present before definitive diagnosis is assigned.
‡ Histologic confirmation is suggested.
§ Radiographic confirmation is sufficient.

1.1.4 Identification of the TSC genes

TSC was first recognised as a genetic condition in 1910 by Kirpicznik, and later in 1913, Berg reported that the disease was hereditary (Kirpicznik 1910, Berg 1913). Gunther and Penrose in 1935 demonstrated the dominant inheritance and also suggested a high mutation rate was present in TSC (Gunther and Penrose 1935). It was not until the 1980s that progress was made in identifying the genes responsible for TSC. Fryer *et al.* undertook a genetic linkage study of 19 TSC families and found linkage to the ABO blood group gene on chromosome 9q34 (Fryer *et al.* 1987). The locus was named *TSC1* for tuberous sclerosis complex type 1, however evidence for genetic heterogeneity suggested that there must be at least one additional TSC-causing locus elsewhere in the genome (Sampson *et al.* 1989, Haines *et al.* 1991, Northrup *et al.* 1992). In 1991 a genome-wide search testing five families affected by TSC revealed linkage to a polymorphic marker near the autosomal dominant polycystic kidney disease type 1 (ADPKD1) locus on chromosome 16p13 (Kandt *et al.* 1992). This locus was named *TSC2* and subsequent studies indicated that >90% of TSC families showed strong evidence of linkage to *TSC1* or *TSC2* with no conclusive evidence of a third locus.

1.1.4.1 The TSC1 gene

In the early 1990s, analysis of key meiotic recombination events in TSC1 families suggested that the disease gene was located in a 4-cM interval between loci D9S149 and D9S114 (Povey *et al.* 1994). Conflicting recombination data (Gilbert *et al.* 1993, Kwiatkowski *et al.* 1993, Pitiot *et al.* 1994, Nellist *et al.* 1993) and the lack of any clues from chromosome rearrangements or large deletions led to the construction of a 1.7 Megabase (Mb) cosmid contig which covered the *TSC1* candidate region (Hornigold, *et al.* 1997). The candidate region was soon narrowed to 900 kilobases (kb) between the markers D9S2127 and DBH (van Slegtenhorst 1997). This *TSC1* region proved to be gene-rich with over 30 genes identified and several of these were highlighted as good candidates based on probable roles in signal transduction pathways. However, no mutations in these genes were identified in patients with TSC (van Slegtenhorst 1997) and so complete genome

sequencing of the region was initiated to predict further putative exons and genes. Systematic amplification and mutation screening of exons by heteroduplex analysis of a set of 60 DNA samples from 20 unrelated familial TSC cases with linkage to 9q34 and 40 sporadic cases, revealed mobility shifts corresponding to small truncating mutations in the 62nd exon screened (van Slegtenhorst 1997). This exon corresponded to previously identified complementary DNA (cDNA) clones and a combination of 5' rapid amplification of cDNA ends (5'RACE), reverse transcription-polymerase chain reaction (RT-PCR) and isolation of other cDNA clones defined the remainder of the open reading frame (ORF) of *TSC1* (van Slegtenhorst 1997). The complete genomic structure of *TSC1* was finally determined by comparison of the genomic and cDNA sequences (van Slegtenhorst 1997).

The *TSC1* gene spans approximately 43kb of genomic DNA and consists of 23 exons, of which the last 21 contain coding sequence (van Slegtenhorst 1997). The initiator ATG codon occurs at nucleotide 222 (in exon 3) and the first stop codon is at nucleotide 3738 in exon 23, leaving a 4.5 kb 3' untranslated region (van Slegtenhorst 1997). The 8.6 kb full length transcript encodes a 1164 amino acid, 130 kDa protein called hamartin (Figure 1.3) (van Slegtenhorst 1997).

1.1.4.2 The TSC2 gene

Linkage studies in 1992 identified a 1.5 Mb region of chromosome 16p as the probable location of the *TSC2* gene (Kandt *et al.* 1992). Around the same time a family with TSC and ADPKD was found to segregate a translocation between chromosomes 16p and 22q (Cheadle *et al.* 2000). The mother and daughter had typical ADPKD; however the son had symptoms of both TSC and ADPKD. The translocation breakpoint on chromosome 16 in this family was shown to disrupt the *PKD1* gene. It was concluded that the son had TSC as well as ADPKD due to a deletion of one copy of *TSC2*, the implied location of which was telomeric to the translocation breakpoint on chromosome 16p13.3, and a 1.4 Mb *TSC2* candidate region was identified. A further 1.1 Mb of this region was excluded following identification of another breakpoint in a patient with no signs of TSC who had a *de novo* truncation of

16p (Wilkie *et al.* 1990). Progress in identifying *TSC2* was rapid due to advanced mapping of 16p13.3 already available and in depth information on chromosomal rearrangements in the region, which narrowed down the search substantially (Gomez *et al.* 1999). A cosmid contig was developed for the remaining 300 kb *TSC2* candidate region and pulsed field gel electrophoresis (PFGE) and southern blotting were used to examine a panel of 255 unrelated TSC patients for rearrangements (The European Chromosome 16 Tuberous Sclerosis Consortium 1993). Five TSC associated deletions at 16p13.3 were identified and mapped to a 120 kb region from which 4 genes were isolated by screening cDNA libraries. One gene was interrupted by all 5 PFGE deletions making it a strong candidate for *TSC2*. Further analysis of this gene revealed 4 smaller intragenic deletions thus confirming the identity of the *TSC2* gene. (The European Chromosome 16 Tuberous Sclerosis Consortium 1993).

TSC2 is approximately 44 kb in length and comprises 41 exons and a non-coding leader exon (Kobayashi *et al.* 1997). The initiator ATG codon occurs at nucleotide 19 in exon 1 and the stop codon is at nucleotide 5440 in exon 41 .The *TSC2* transcript is roughly 5.5 kb and encodes a 1807 amino acid, 198 kDa protein called tuberin (Figure 1.3) (The European Chromosome 16 Tuberous Sclerosis Consortium 1993).

1.1.5 Mutation analysis and genotype/phenotype correlations

To date more than 680 disease-causing mutations have been identified in either *TSC1* or *TSC2* (Au *et al.* 2007). Most identified mutations are small changes such as small deletions or insertions and missense, nonsense or splice site mutations (Dabora *et al.* 2001, Sancak *et al.* 2005) (Figure 1.1). Large rearrangements, missense mutations and in-frame deletions are very rare in the *TSC1* gene; however TSC patients with large deletions and rearrangements in *TSC2* have often been found (Au *et al.* 1997, Sancak *et al.* 2005) (Figure 1.1). In a recent study, few or no mutations were found in exons 22 and 23 of *TSC1* and exons 6, 25, 31, and 41 of *TSC2* (Au *et al.* 2007). Approximately 70% of *TSC1* mutations were located in or near exons 8, 9, 10, 15, 17, and 18, and approximately 70% of *TSC2* mutations were located in or near exons 9, 13, 14, 16, 23, 24, 29, 30, 33, and 35 to 40 (Au *et al.* 2007).

Missense mutations in the *TSC2* Rheb-GAP-domain (exons 35-40) accounted for approximately 6% of all mutations suggesting that the GAP domain exons are a major target for missense mutation probably linked to a key role in the regulation of cellular growth (Au *et al.* 2007). Another frequently mutated codon, R611 of *TSC2* (accounting for 6% of all mutations) has been demonstrated to be important in regulating mammalian target of rapamycin (mTOR)/pS6K function (Nellist *et al.* 2001, Au *et al.* 2007). Both somatic and germline mosaicism for *TSC1* and *TSC2* mutations have also been found in TSC patients (Cheadle *et al.* 2000).

Approximately two-thirds of TSC patients present as sporadic cases caused by a *de novo* mutation in either *TSC1* or *TSC2*, with neither parent displaying signs of TSC (The European Chromosome 16 Tuberous Sclerosis Consortium 1993, van Slegtenhorst 1997). In *de novo* cases, mutations in *TSC2* are found at a much higher frequency (*TSC1*:*TSC2* = 1:4) compared to familial cases where approximately half show linkage to *TSC1* and half to *TSC2* (Au *et al.* 2007, Sancak *et al.* 2005, Jones *et al.* 1999). This difference has been attributed to the smaller size and less complex structure of *TSC1*, and the rarity of large DNA rearrangements and missense mutations at this locus (Sancak *et al.* 2005). In general, milder TSC phenotypes are observed in familial cases compared to spontaneous cases (Au *et al.* 2007). Many studies have been conducted on large cohorts of patients to examine genotype/phenotype correlations (Jones *et al.* 1999, Dabora *et al.* 2001, Sancak *et al.* 2005, Au *et al.* 2007). Au *et al.* (2007) recently reported a higher rate of neurologic, renal and skin lesions in patients with a *TSC2* mutation. Sancak *et al.* (2005) found patients with a *TSC1* mutation were less often mentally retarded and had fewer renal AMLs, renal cysts, retinal phakomas and retinal depigmentations. Not only are there differences in phenotype when comparing genotype, but also there are differences between the sexes. Males have more neurologic features as well as more retinal phakomas, ungula fibromas and renal cysts (Au *et al.* 2007). Two possible reasons for these differences between the sexes are modifier genes coded for on the X chromosome or differential effects of hormonal influences between genders (Smalley 1992, Kwiatkowski 2002, Au *et al.* 2007).

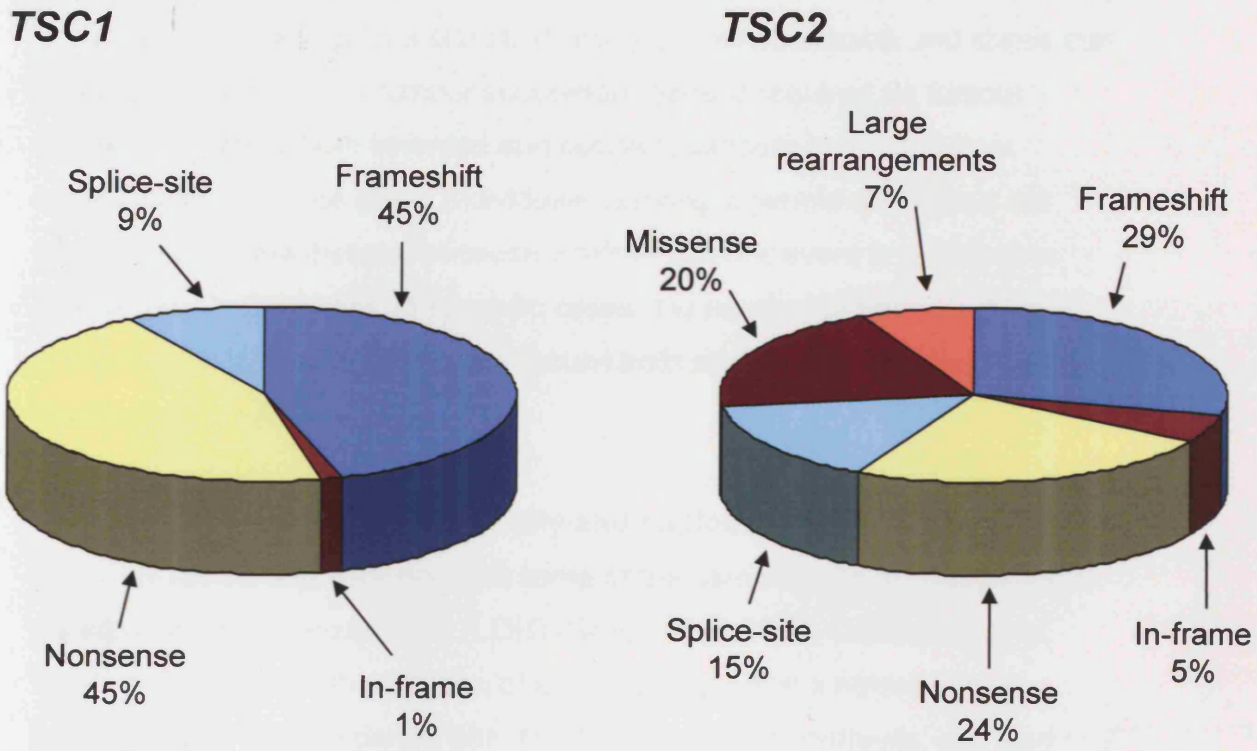

Figure 1.1 Types and frequencies of the mutations found in *TSC1* and *TSC2*. Data taken from Sancak *et al.* 2005.

1.1.6 Knudson's two-hit hypothesis

Tumourigenesis generally requires mutations in both the maternal and paternal alleles of tumour suppressor genes as described by Knudson's two-hit hypothesis (Figure 1.2) (Knudson 1971). Knudson's two-hit hypothesis was formulated from results of a statistical study on retinoblastoma and states that biallelic inactivation of a tumour suppressor gene is required for tumour formation and that both inherited and sporadic cancers can result from mutations of the same gene. Individuals carrying a germline mutation are predisposed to the disease because a single somatic event is sufficient to initiate tumour formation. In sporadic cases, the number of tumours is lower and cancer occurs at a later age because both alleles must be somatically inactivated (Knudson 1971).

1.1.7 Loss of heterozygosity and haploinsufficiency

In 1994 it was reported that some of the hamartomas in TSC patients showed loss of heterozygosity (LOH) (Green *et al.* 1994, Carbonara *et al.* 1994). LOH involves the deletion of a wild-type allele in a heterozygous individual and, in accordance with Knudson's two-hit hypothesis, can lead to tumour formation (Knudson 1971). The finding that some TSC hamartomas appeared to fit with Knudson's two-hit hypothesis suggested a role for *TSC1* and *TSC2* as tumour suppressor genes, which restrict cell proliferation under normal conditions (Vogelstein and Kinzler 2004). LOH at *TSC1* and *TSC2* has been found in SEGAs, AMLs, RCCs, rhabdomyomas and other lesions (Green *et al.* 1994, Carbonara *et al.* 1994, Parry *et al.* 2001), however it appears to be more apparent in certain lesions. Henske *et al.* (1996) found LOH of the TSC genes in over 50% of renal AMLs and cardiac rhabdomyomas, but only 4% of brain lesions, suggesting a different pathogenic mechanism for tumour formation in different organs.

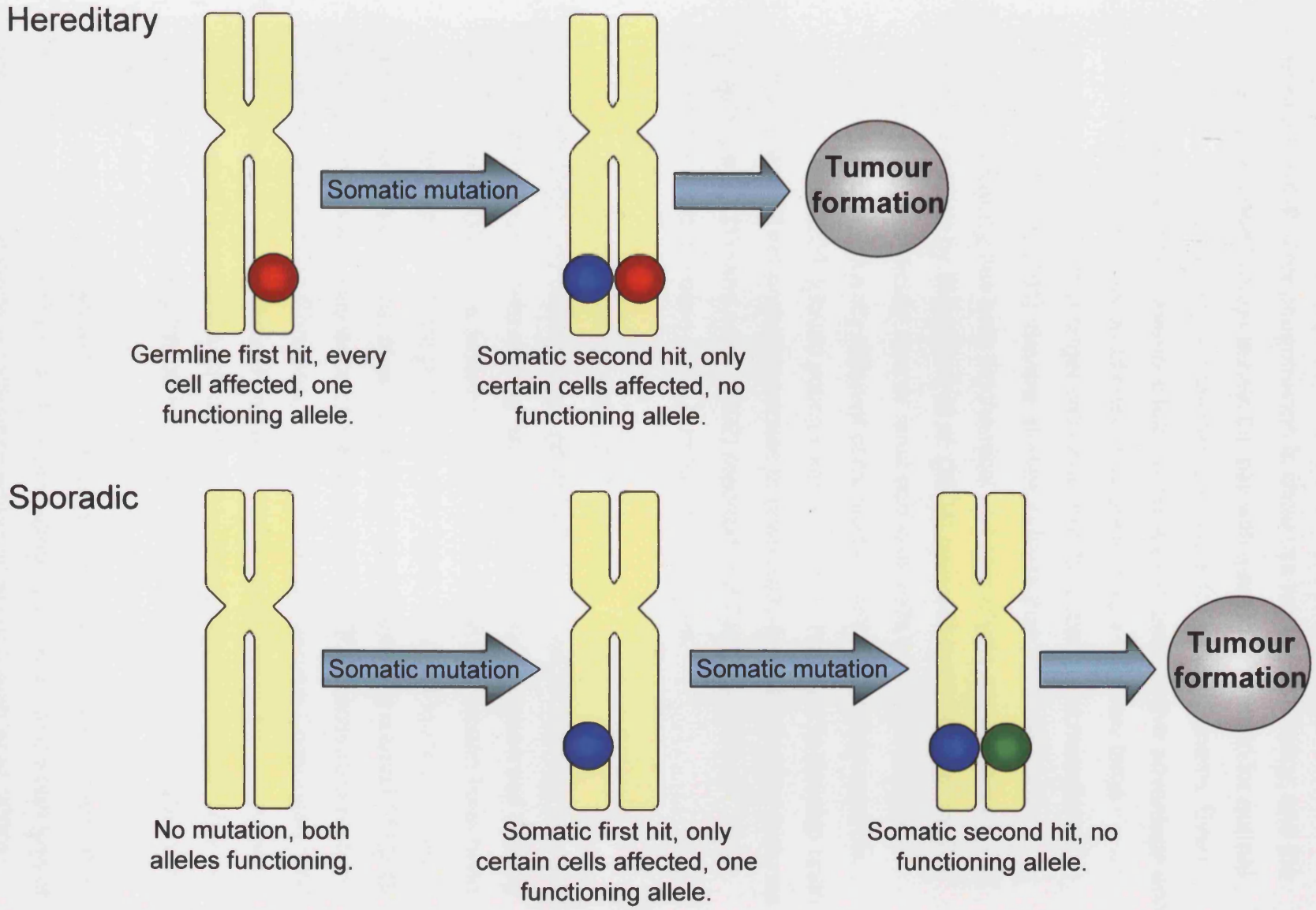

Figure 1.2 Knudson's two-hit model for hereditary and sporadic tumourigenesis. LOH, loss of heterozygosity.

There is increasing evidence that the loss of only one allele of a tumour suppressor gene might also contribute to tumourigenesis (Santarosa and Ashworth 2004). This phenomenon is known as haploinsufficiency, and the reduction in gene dosage leaves the cell with insufficient protein for normal functions, thus conferring a selective advantage for tumourigenesis. Even weak haploinsufficient events could confer a small proliferative advantage and allow the clonal expansion of cells, thus presenting a relatively large sensitised population of target cells available for subsequent mutagenesis (Quon and Berns 2001). Several studies indicate that *TSC1* or *TSC2* haploinsufficiency has both biochemical and phenotypic consequences. For example a study by Stoyanova *et al.* (2004) revealed that gene expression profiles of phenotypically normal renal epithelial cells from *TSC* mutation carriers were significantly different compared to similar cells from controls. Waltereit *et al.* (2006) found young Eker rats, which have yet to develop brain tumours, exhibit enhanced responses to chemically-induced kindling (induces seizures) and Uhlmann *et al.* (2002) reported that $Tsc1^{+/-}$ and $Tsc2^{+/-}$ mice exhibit a 1.5 fold increase in the number of astrocytes.

1.1.8 Biochemistry of the TSC proteins

Hamartin and tuberin share no homology with each other and very little with other proteins, however they are highly evolutionarily conserved (Huang and Manning 2008). The protein domains of hamartin and tuberin have been extensively studied and are summarised in Table 1.4 and Figure 1.3. They contain multiple domains, of which the best characterised is a small *TSC2* C-terminus region with sequence similarity to Rap1-GTPase-activating protein (GAP) (The European Chromosome 16 Tuberous Sclerosis Consortium 1993, Wienecke *et al.* 1995, Maheshwar *et al.* 1997). GAPs inhibit the Ras-related family of small G proteins such as Rap1 and Rheb (Ras homologue enriched in brain) by accelerating the conversion of the active GTP-bound state to the inactive GDP-bound state (Piedimonte *et al.* 2006). Less is known about the function of hamartin. Hamartin possesses a domain which interacts with the ezrin-radixin-moezin (ERM) family of actin-binding proteins, and when loss of hamartin occurs, defects in cell-matrix adhesion occur (Lamb *et al.* 2000). Hamartin also associates with neurofilament-L (NF-L) suggesting that it may

function as an integrator of the neuronal intermediate filament and the actin cytoskeletal network (Haddad *et al.* 2002). These proposed functions of hamartin indicate that it may act as a scaffolding protein for tuberin localisation (Astrinidis and Henske 2005).

1.1.8.1 Interaction of hamartin and tuberin

Hamartin and tuberin physically interact to form a heterodimer complex through strong association of specific binding motifs within their N-termini (van Slegtenhorst *et al.* 1998, Hodges *et al.* 2001) (Figure 1.3). Yeast two-hybrid screening revealed that this association occurs between amino acids 302-430 of hamartin and amino acids 1-418 of tuberin (Hodges *et al.* 2001) (Figure 1.3). The hamartin-tuberin interaction appears to be important for the stability of each protein. Benvenuto *et al.* (2000) found that binding of hamartin to tuberin protects it from ubiquitination, and conversely, hamartin, which is also ubiquitinated, was found to be stabilised by co-expression of tuberin. Tuberin can also act as a cytosolic chaperone, preventing hamartin self-aggregation (Nellist *et al.* 1999). Phosphorylation of tuberin may also affect the stability of the hamartin-tuberin complex. Aicher *et al.* (2001) found that tuberin undergoes phosphorylation at serine and tyrosine residues (Figure 1.3), and when not phosphorylated, tuberin was unable to interact with hamartin and the tumour suppressor activity of the complex was lost. Similar results were also found by Nellist *et al.* (2001). These studies indicate that the stability and optimum function of the hamartin-tuberin complex is dependent on the activity of the two proteins.

Although hamartin has no GAP activity, evidence suggests that it may be important for the function of tuberin as a GAP. Hamartin and tuberin together enhanced Rheb GTPase activity by more than 100-fold over the activity of either protein on its own, indicating that hamartin and tuberin form a GTPase-activating protein complex that greatly enhances the intrinsic GTPase activity of Rheb (Tee *et al.* 2003). Astrinidis *et al.* (2003) reported that phosphorylation of hamartin by the cyclin-dependent kinase 1 (CDK1) leads to decreased tuberin GAP activity during G_2/M phase of the cell-cycle.

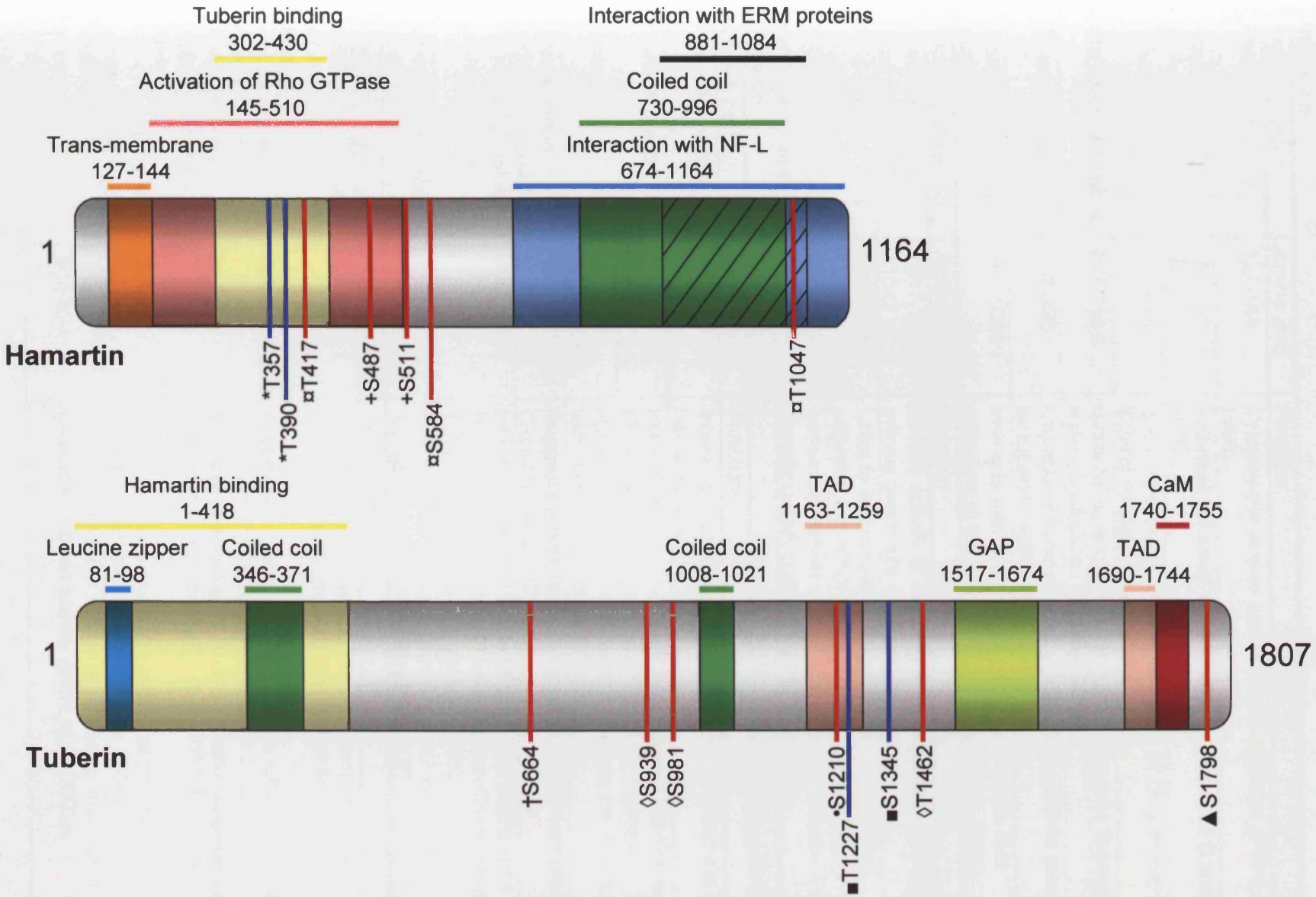

Figure 1.3 Schematic diagram of the functional/structural domains and phosphorylation sites of hamartin and tuberin. Sites of inhibitory phosphorylation events are in red, sites of activating phosphorylation events are in blue. Phosphorylating kinases are indicated by the following symbols: *GSK3β, +IKKβ, ¤CDK1, †ERK2, •MK2, ◊AKT, ■AMPK, ▲RSK1. Abbreviations: ERM; ezrin-radixin-moezin, NF-L; neurofilament-L, TAD; transcription activating domain, CaM; calmodulin, GAP; GTPase activating protein.

Table 1.4 Domains and phosphorylation sites of hamartin and tuberin.

Hamartin		
Protein domain	*Amino acid*	*Function*
Trans-membrane	127-144	Cytoplasmic vesicle membrane localisation (Plank *et al.* 1998).
Activation of Rho GTPase	145-510	Activates the small GTP-binding protein Rho (Lamb *et al.* 2000).
Tuberin binding	302-430	Interacts strongly with the hamartin binding domain of tuberin (Hodges *et al.* 2001).
Interaction with NF-L	674-1164	Binds NF-L, anchors neuronal intermediate filaments to actin cytoskeleton (Haddad 2002).
Coiled coil	730-996	Capable of hamartin self aggregation which is prevented by tuberin (Nellist *et al.* 1999).
Interaction with ERM proteins	881-1084	Interacts with ERM family of proteins which aids adhesion to the cell substrate (Lamb *et al.* 2000).
Phosphorylated by	*Amino acid*	*Function*
CDK1 (cyclin dependent kinase)	T417, S584, T1047	Inhibits activity of hamartin-tuberin complex during mitosis (Astrinidis *et al.* 2003).
IKKβ (inhibitory κB kinase)	S487, S511	Links to inflammation. Suppresses hamartin and activates the mTOR pathway. (Lee *et al.* 2007).
GSK3β (glycogen synthase kinase)	T357, T390	Increases stability of hamartin-tuberin complex: β-catenin signalling attenuation (Mak *et al.* 2005).
Tuberin		
Protein domain	*Amino acid*	*Function*
Hamartin binding	1-418	Interacts strongly with the tuberin binding domain of hamartin (Hodges *et al.* 2001).
Leucine zipper	81-98	Involved in protein-protein interactions (The European Chromosome 16 Tuberous Sclerosis Consortium 1993).
Coiled coil	346-371, 1008-1021	Necessary but not sufficient to mediate the interaction with hamartin (Hodges *et al.* 2001).
Transcription activating domain	1163-1256, 1690-1744	Suggests a potential role for tuberin in transcription (Tsuchiya *et al.* 1996).
GTPase activating protein (GAP)	1517-1674	Inhibit Ras-related family of small G proteins such as Rap1, Rab5 and Rheb (The European Chromosome 16 Tuberous Sclerosis Consortium 1993).
Calmodulin (CaM) binding	1740-1755	Potential role in transcription by modulation of steroid receptor function (Noonan *et al.* 2002).
Phosphorylated by	*Amino acid*	*Function*
ERK (extracellular signal regulated kinase)	S664	Growth factor activated. Disrupts hamartin-tuberin complex, activation of mTOR (Ma *et al.* 2005).
Akt (or protein kinase B (PKB))	S939, S981, T1462	Growth factor activated. Inactivates tuberin and causes activation of mTOR (Manning *et al.* 2002).
MK2 (MAPK activated protein kinase 2)	S1210	Promotes binding with 14-3-3 proteins, sequesters tuberin from substrates (Li *et al.* 2003b).
RSK1 (ribosomal protein S6 kinase)	S1798	Growth factor activated. Inhibits heterodimer complex, increased mTOR signalling (Roux 2004).
AMPK (AMP-dependent protein kinase)	T1227, S1345	Phosphorylated in response to energy deprivation which increases tuberin activity (Inoki *et al.* 2003).

1.1.8.2 Localisation of hamartin and tuberin

Consistent with the fact that hamartin and tuberin form a heterodimer complex, the proteins are co-expressed in most tissues, particularly those affected by TSC. Immunohistochemical analyses have localised hamartin and tuberin to the brain, kidney, heart, adrenal gland, gut, liver, lung, pancreas and prostate (Plank *et al.* 1991, Johnson *et al.* 2001). Minimal expression has also been found in the lymph node, spleen, testes and thymus (Johnson *et al.* 2001). Within the cell, hamartin and tuberin show transient membrane localisation indicating that they are not integral membrane proteins but appear to be mainly cytoplasmic (Yamamoto *et al.* 2002, Nellist *et al.* 1999). Hamartin has been localised to cytoplasmic vesicles and the centrosome (Plank *et al.* 1998, Astrinidis *et al.* 2006), whilst tuberin has been localised to the Golgi apparatus and the nucleus (Wienecke *et al.* 1996, Lou *et al.* 2001).

1.1.8.3 The mTOR pathway

Target of rapamycin (TOR), a protein kinase expressed by all eukaryotic cells, regulates cell size through control of mRNA translation in response to nutrient and growth signals (Tee *et al.* 2005). TOR proteins function as serine/threonine kinases of the phosphoinositide 3-kinase-related kinase (PIKK) family and have also been found to regulate cell proliferation, survival and metabolism in certain settings (Huang and Manning 2008, Fingar and Blenis 2004). mTOR (mammalian target of rapamycin) exists in two functionally distinct protein complexes: mTORC1 (mTOR complex 1) and mTORC2 (mTOR complex 2). mTORC1 forms a complex with Raptor (regulatory associated protein of mTOR) and LST8 (lethal with SEC13 protein 8) and is sensitive to inhibition by the naturally occurring compound rapamycin, whereas mTORC2, which complexes with Rictor (rapamycin insensitive companion of mTOR), SIN1 (stress activated protein kinase interacting protein 1) and LST8, is insensitive to rapamycin (Huang and Manning 2008). Little is known about the biochemical role of mTORC2. It has been found to function upstream of Rho GTPases to regulate the actin cytoskeleton (Jacinto *et al.* 2004). mTORC2 also acts as a motif kinase for Akt (also known as protein kinase B (PKB)) and phosphorylates it at S473, thus activating Akt downstream of growth factors (Sarbassov *et al.* 2005).

mTORC1 (referred to as mTOR from now on) has two major downstream phosphorylation targets: ribosomal protein S6 kinase (S6K) and 4E-BP1 (eIF4E (eukaryotic translation initiation factor 4E)-binding protein 1) which both have TOR signalling (TOS) motifs (Astrinidis and Henske 2005). When p70S6K is activated by mTOR, S6K becomes phosphorylated resulting in increased ribosome biogenesis (Astrinidis and Henske 2005). Inhibitory phosphorylation of 4E-BP1 by mTOR prevents binding of the protein to eIF4E which is then free to facilitate mRNA translation (Gingras *et al.* 2001).

A link was established between the hamartin-tuberin complex and mTOR after studies in *Drosophila* revealed an increase in cell size in *dTsc1* and *dTsc2* mutant cells (Gao and Pan 2001, Potter *et al.* 2001). This work suggested that the *TSC* genes function together in the insulin signalling pathway downstream from Akt. Akt was later found to directly phosphorylate tuberin and inhibit the hamartin-tuberin complex confirming the downstream location of *TSC1* and *TSC2* (Manning *et al.* 2002, Potter *et al.* 2002). In 2002 the *TSC1/TSC2* complex was shown to inhibit mTOR mediated signalling to S6K and 4E-BP1 (Tee *et al.* 2002). It was unclear how exactly this inhibition of mTOR occurred until Tee *et al.* (2003) presented evidence that the hamartin-tuberin complex inhibited Rheb by reverting Rheb-GTP back into Rheb-GDP, through the function of tuberin's GAP domain which stimulated the intrinsic GTPase activity of Rheb. Rheb had previously been shown to potently activate mTOR, although the mechanism by which it does this is still unclear (Saucedo *et al.* 2003). Figure 1.4 shows the role of the hamartin-tuberin complex in the mTOR pathway.

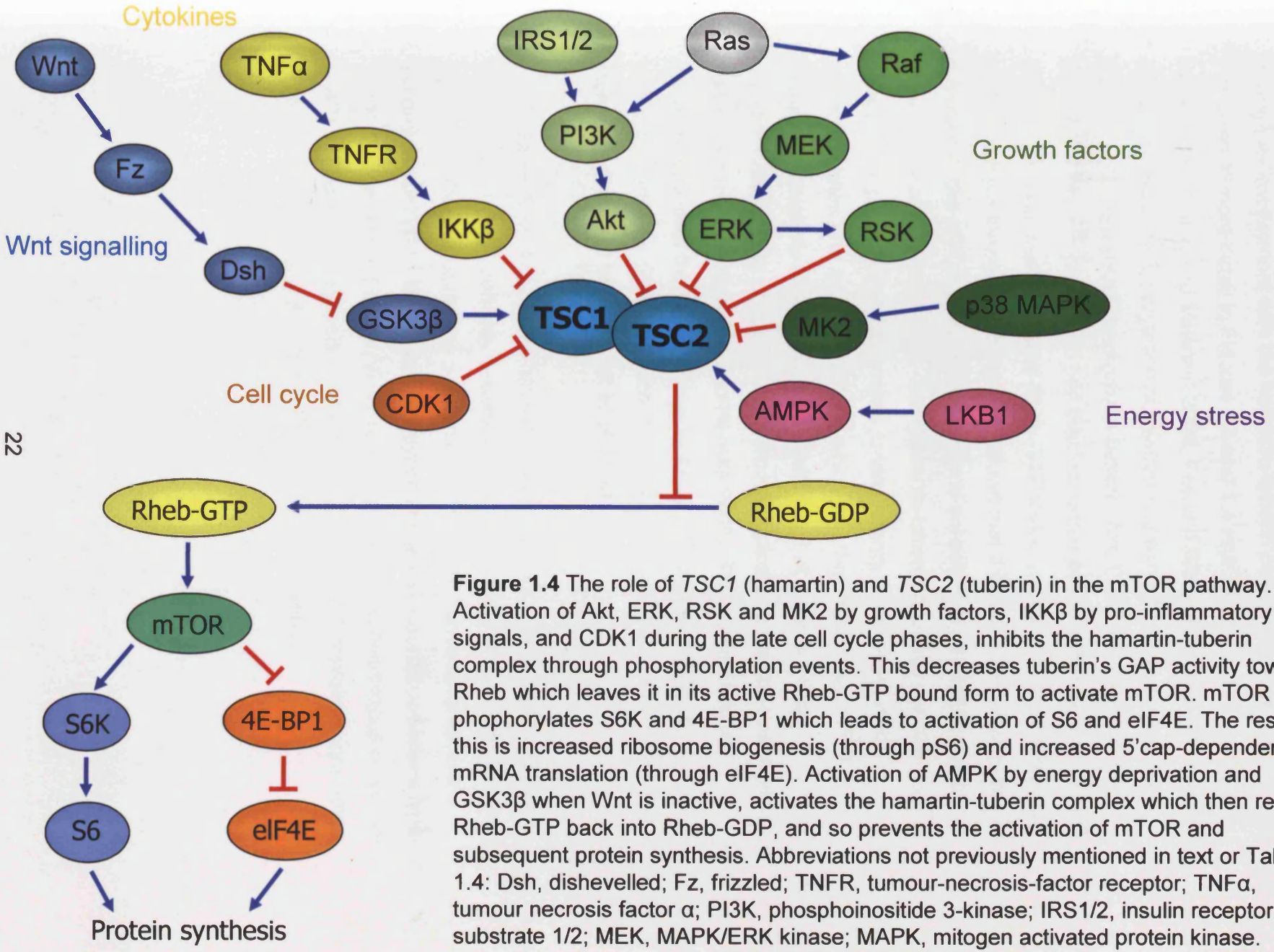

Figure 1.4 The role of *TSC1* (hamartin) and *TSC2* (tuberin) in the mTOR pathway. Activation of Akt, ERK, RSK and MK2 by growth factors, IKKβ by pro-inflammatory signals, and CDK1 during the late cell cycle phases, inhibits the hamartin-tuberin complex through phosphorylation events. This decreases tuberin's GAP activity towards Rheb which leaves it in its active Rheb-GTP bound form to activate mTOR. mTOR then phophorylates S6K and 4E-BP1 which leads to activation of S6 and eIF4E. The result of this is increased ribosome biogenesis (through pS6) and increased 5'cap-dependent mRNA translation (through eIF4E). Activation of AMPK by energy deprivation and GSK3β when Wnt is inactive, activates the hamartin-tuberin complex which then reverts Rheb-GTP back into Rheb-GDP, and so prevents the activation of mTOR and subsequent protein synthesis. Abbreviations not previously mentioned in text or Table 1.4: Dsh, dishevelled; Fz, frizzled; TNFR, tumour-necrosis-factor receptor; TNFα, tumour necrosis factor α; PI3K, phosphoinositide 3-kinase; IRS1/2, insulin receptor substrate 1/2; MEK, MAPK/ERK kinase; MAPK, mitogen activated protein kinase.

The mTOR pathway can be inhibited and activated in a variety of ways through its involvement with the hamartin-tuberin complex. These are displayed in more detail in Figures 1.3 and 1.4 and Table 1.4. For extensive reviews see Huang and Manning 2008, Tee and Blenis 2005 and Krymskaya 2003. Inhibitory phosphorylation of hamartin/tuberin by cell-cycle kinases (CDK1), cytokines (IKKβ) and growth factors (Akt, ERK, RSK and MK2) inactivates the complex which can then no longer prevent the accumulation of Rheb-GTP. With the build up of Rheb-GTP levels, mTOR becomes activated and protein synthesis is increased. It follows that if TSC1/2 are inactive due to a mutation, the mTOR pathway will become constitutively activated due to increased levels of Rheb-GTP. The hamartin-tuberin complex can also be activated by phosphorylation events. Under energy deprivation, AMPK phosphorylates and activates tuberin which can then inhibit the mTOR pathway through its association with Rheb (Inoki *et al* 2003). This phosphorylation may protect the cells from apoptosis caused by prolonged energy deprivation (Astrinidis and Henske 2005). The hamartin-tuberin complex also links the Wnt pathway to the mTOR pathway through its phosphorylation by GSK3β, which increases the stability of the complex and thus its inhibition of mTOR (Mak *et al.* 2005).

Aside from TSC, other hamartoma and tumour syndromes have been linked to the mTOR pathway (extensively reviewed in Inoki *et al.* 2005). These include PTEN- (phosphatase and tensin homologue) hamartoma tumour syndromes (PTHSs), Peutz-Jeghers syndrome (PJS), neurofibromatosis type-1 (NF-1), von Hippel-Lindau (VHL) syndrome, familial adenomatous polyposis (FAP) and juvenile polyposis syndrome (JPS). Table 1.5 contains more detail on these diseases and their link with the mTOR pathway.

Table 1.5 Hamartoma syndromes and their link to mTOR.

Disease	Gene mutated	Link to mTOR	Clinical characteristics
TSC	*TSC1, TSC2*	Form a complex which inhibits formation of Rheb-GTP.	Hamartomas in multiple organs, hypomelanocytic macules.
Cowden disease	*PTEN*	Reduces intracellular levels of PI3K, inhibits Akt activation.	Hamartomas in multiple organs, lentigenes.
Bannayan-Riley-Ruvalcaba syndrome	*PTEN*	Reduces intracellular levels of PI3K, inhibits Akt activation.	Hamartomas in multiple organs, lentigenes.
Proteus syndrome	*PTEN*	Reduces intracellular levels of PI3K, inhibits Akt activation.	Hamartomas in multiple organs.
Lhermitte-Duclos disease	*PTEN*	Reduces intracellular levels of PI3K, inhibits Akt activation.	Hamartomas in brain.
PJS	*LKB1/STK11*	Phosphorylates and activates AMPK.	Hamartomas in the gastrointestinal tract, lentigenes.
NF-1	*NF1*	GTPase activating protein for the Ras small G protein.	Neurofibromas.
VHL syndrome	*VHL*	Degradation of hypoxia-inducible factor (HIF) of which mTOR is a regulator.	Angiomas of the retina, haemangioblastomas of the central nervous system, renal carcinoma.
FAP	*APC*	Loss of *APC* causes β-catenin activation. mTOR has been linked to Wnt pathway.	Polyps or carcinomas in the gastrointestinal tract.
JPS	*SMAD4, BMPR1A*	SMAD3, binding partner of SMAD4, physically interacts with Akt and tuberin.	Hamartomas in the gastrointestinal tract.

Information obtained from Inoki *et al.* 2005.

1.1.8.4 Other functions of hamartin and tuberin

Hamartin and tuberin have other functions in the cell including roles in transcriptional activation and cell cycle control (Table 1.6) (Refer to Krymskaya 2003 and Rosner *et al.* 2008 for extensive reviews). These observations are perhaps not surprising given the central role of the mTOR pathway in so many biological processes. Importantly, *TSC1* and *TSC2* do not always function through the mTOR pathway, suggesting that hamartin and

tuberin play unique roles in cellular signalling, independent of mTOR activation.

Table 1.6 Cell signalling functions of hamartin and tuberin.

(Continued on the next page).

Cellular function	Evidence
Transcriptional activation	▪ Loss of functional tuberin triggers accumulation of HIF and upregulation of the expression of HIF-responsive genes including VEGF. ▪ Tuberin interacts with Pam, a binding partner for the transcription factor c-myc, although the functional relevance of this interaction is yet to be determined. ▪ Tuberin was found to interact with SMAD2 and SMAD3 to regulate TGFβ responsive gene transcription. ▪ Tuberin is a modulator of transcription events mediated by steroid/nuclear receptor family members i.e. ERα, RxRα and VDR. ▪ Tuberin physically associates with the forkhead transcription factor FoxO1, which interacts with several kinds of protein and regulates their function and vice versa. ▪ In renal carcinomas of the Eker rat (which has an insertion in the *TSC2* locus, discussed later), the transcription factor AP-1 is overexpressed, suggesting that loss of tuberin promotes AP-1 gene translation.
Cell adhesion and the cytoskeleton	▪ Hamartin interacts with the ERM-family proteins ezrin, radixin and moesin which are involved in cleavage furrows during cell division and cell adhesion. This interaction is required for activation of the small GTP-binding protein Rho by serum and is involved in the regulation of cell adhesion. ▪ Interaction of hamartin with ERM and NF-L (a major cytoskeletal element in nerve axons and dendrites) proteins suggests that hamartin could function as an integrator of the neuronal intermediate filament and the actin cytoskeletal skeleton. ▪ Hamartin binds to FIP200 which is a protein inhibitor for FAK which is an integral part of focal adhesions at the cell membrane.

Table 1.6 Cell signalling functions of hamartin and tuberin.

(Continued from previous page).

Cellular function	Evidence
Cell cycle regulation	▪ Loss of function of either hamartin or tuberin shortens the G1 phase of the cell cycle, subsequently leading to cell proliferation. ▪ Tuberin has been found to bind to cyclins D1, D2 and D3 which are expressed during early G1 phase. ▪ Hamartin and tuberin stabilise protein levels of p27KIP1, a CDK inhibitor, and thus inhibit the activity of CDKs and cell cycle progression. ▪ Cyclin B1 and Cdk1, which regulate the transition from G2 to M phase (mitosis), interact with the hamartin/tuberin complex and cyclin A (also involved in G2 to M phase transition) interacts with tuberin.
GAP for Rap1A and Rab5	▪ Tuberin shows modest GAP activity towards Rap1A which has mitogenic and oncogenic properties and also a possible role in mitogen-activated protein-kinase-mediated neuronal differentiation. ▪ Tuberin has modest GAP activity for the GTPase Rab5, which serves a role in regulating endosome fusion.
Interaction with 14-3-3 proteins	▪ Akt phosphorylated tuberin interacts with 14-3-3 proteins which function as adaptor molecules modulating interactions/functions of components involved in signal transduction and cell cycle control.

HIF = hypoxia-inducible transcription factor, VEGF = vascular endothelial growth factor, Pam = protein associated with c-myc, TGFβ = transforming growth factor beta, FoxO1 = forkhead box O1, ERα = oestrogen receptor alpha, RxRα = retinoid X receptor alpha, VDR = vitamin D receptor, AP-1 = activator protein-1, KIP1 = kinase interacting protein 1, CDK = cyclin-dependent kinase, ERM = ezrin-radixin-moesin, NF-L = light-chain neurofilament, FIP200 = focal adhesion kinase family interacting protein of 200KD, FAK = focal adhesion kinase. Information and references obtained from Cheadle *et al.* 2000, Krymskaya 2003 and Rosner *et al.* 2008.

1.1.9 Treatment of TSC

Since loss of *TSC1* or *TSC2* leads to activation of the mTOR pathway, it followed that the natural inhibitor of mTOR, rapamycin, could be used for treatment of the disease. Rapamycin (also known as sirolimus) is an antifungal agent derived from a bacterium (*Streptomyces hygroscopicus*) found in the soil of Easter Island in the 1970s (Vézina *et* al. 1975, Sehgal *et al.* 1975). It has been used as an immunosuppressant in organ transplantation for many years, but recently, due to its high specificity towards the immunophilin FKBP12 and subsequent binding to mTOR, it has been trialled for use in the treatment of TSC (Inoki *et al.* 2005). Research into the effect of rapamycin treatment in the Eker rat model of TSC revealed a significant decrease in the size of renal tumours, accompanied by down regulation of ribosomal S6 kinase activity, reduction in cell size, and induction of apoptosis (Kenerson *et al.* 2005). Interestingly no effect on the number of microscopic precursor lesions was found indicating that other mechanisms, besides activation of the mTOR pathway, may be involved in tumour initiation. Rapamycin treatment has also been found to prevent seizures and prolong survival in mice with conditional inactivation of the *Tsc1* gene in glia (Zeng *et al.* 2008), and a reduction in subcutaneous tumours has been seen following the topical application of rapamycin in a nude TSC mouse model (Rauktys *et al.* 2008). Results are now beginning to emerge from rapamycin studies and clinical trials in patients. Two small studies revealed that rapamycin caused the regression of astrocytomas and renal AMLs in TSC patients (Franz *et al.* 2006, Herry *et al.* 2007). Recently the results from a two year clinical trial of sirolimus use in TSC patients were published by Bissler *et al.* (2008). Sirolimus was administered for the first year only, after which the patient's progress was followed up for a year. The results were encouraging, with AMLs regressing during the year of sirolimus therapy, however, after treatment had stopped AMLs tended to increase in volume. Interim results from a two year study by Davies *et al.* (2008) also reveal shrinkage of AMLs in all TSC patients treated with sirolimus. These clinical trials present encouraging data for the effective treatment of TSC with rapamycin, however concerns have been expressed over the long-term usage of the drug, which may increase the risk of malignant tumours. This is due to the identification of

an Akt feedback loop, which upon rapamycin usage restores insulin signalling toward Akt (Manning 2004). Further work however is needed to fully understand this phenomenon.

1.1.10 TSC models

Studies in animal models have enhanced our knowledge of the genetic and biochemical mechanisms that underlie many diseases, including TSC. *TSC1* and *TSC2* homologues have been identified in non-mammalian organisms such as *Schizosaccharomyces pombe* and *Drosophila*. As with hamartin and tuberin, the protein products of *S. pombe Tsc1* and *Tsc2* were found to physically interact. Deletion of *Tsc1* or *Tsc2* resulted in defective uptake of nutrients from the environment and also a defect in conjugation (Matsumoto *et al.* 2002). Recently, a gene, *cpp1*, encoding the β-subunit of a farnesyltransferase (FTase) was found to suppress most of the phenotypes associated with loss of function of *Tsc1/Tsc2* in *S. pombe*, prompting the authors to speculate that an inhibitor of FTase should be considered as an anti-TSC drug (Nakase *et al.* 2006). Studies in *Drosophila* were among the first to identify the *Tsc1/Tsc2* genes as downstream targets of Akt in the mTOR pathway (as explained above) (Gao and Pan 2001, Potter *et al.* 2001, Potter *et al.* 2002). The *Drosophila TSC1/TSC2* homologues were identified in 1999, during which it was found that mutation of *dTsc2* (*gigas)* resulted in enlarged cells which repeated S phase without entering M phase (Ito and Rubin 1999). This suggested that a defect in cell-cycle control may be an underlying cause of TSC, a theory supported by work from Astrinidis *et al.* (2003) on CDK1.

1.1.10.1 TSC rodent models

A large number of mammalian genes do not have orthologues in invertebrates. Murine models are therefore invaluable, specifically mouse models as they share considerable physiological, anatomical and genomic similarities with humans (Yu and Bradley 2001). They can also be interbred, allowing assessment of the effects of multiple genetic changes, and controlled breeding is relatively simple. Rats are also a valuable model organism, however genetic manipulation of the rat genome has proved difficult due to a

lack of suitable methods for generating targeted mutations (Piedimonte *et al.* 2006, Jacob and Kwitek 2002). Targeted mutation of the genome is desirable as spontaneous mutations of biomedical interest occur infrequently, and radiation or chemical mutagenesis of the genome is limited by the fact that the final results of the induced rearrangements cannot be predetermined (Yu and Bradley 2001). Therefore, the production of mouse models is typically carried out in two ways: random insertion of cloned DNA into the pronuclei of fertilised mouse eggs using microinjection, and site specific genetic manipulation of embryonic stem (ES) cells which are injected into blastocysts which are then injected into pseudopregnant foster mothers (Kobayashi *et al.* 2005, Yu and Bradley 2001). ES cell technology is an extremely powerful technique, and has been used to develop TSC mouse models.

1.1.10.1.1 Tsc1 knockout mice

Three conventional *Tsc1* knockout mouse models have been developed (Kobayashi *et al.* 2001, Kwiatkowski *et al.* 2002, Wilson *et al.* 2005), the most recent of which exhibited a more severe phenotype than existing models (Wilson *et al.* 2005). To knockout a germ line copy of *Tsc1*, Wilson *et al.* (2005) constructed a targeting vector designed to inactivate *Tsc1* by deleting an internal region of the gene comprising the 3' half of exon 6 and all of exons 7 and 8 and replacing this region with a β-galactosidase reporter/neomycin selection cassette. The linearised vector was electroporated into embryonic day (E) 14 Tg2aIV ES cells and $Tsc1^{+/-}$ clones were injected into C57BL/6 blastocysts and transferred into pseudopregnant females. $Tsc1^{+/-}$ F1 mice (50% 129ola/50% C57BL/6) were backcrossed with inbred C57BL/6, Balb/c and C3H mice to assess the effects of background on the $Tsc1^{+/-}$ phenotype. The deletion event produced an unpredicted spliced transcript that lacked exons 6-8, and joined exons 5 and 9, causing a shift in the reading frame and the introduction of a premature termination codon in exon 9.

$Tsc1^{-/-}$ mice were found to die *in utero* between E10.5 and E12.5, similar to what was found in two previous mouse models (Kobayashi *et al.* 2001, Kwiatkowski *et al.* 2002). These null embryos were generally smaller

and developmentally retarded, with some displaying exencephaly and abnormal morphology of myocardial cells (Kobayashi *et al.* 2001, Kwiatkowski *et al.* 2002, Wilson *et al.* 2005). Kobayashi *et al.* (2001) observed that about one third of *Tsc1* null embryos displayed failed neural tube closure at the head region.

The frequency and severity of renal lesions from *Tsc1*$^{+/-}$ mice is dependent on background. This was examined thoroughly by Wilson *et al.* (2005) who found that more *Tsc1*$^{+/-}$ mice (44%) on a C3H background developed macroscopically and microscopically visible renal lesions at the early age of 3-6 months, compared to those on a C57BL/6 (8%) or Balb/c (13%) background. They also found that 80% of 15-18 month mice on a Balb/c background showed progression to RCC, far more than on C3H or C57BL/6 backgrounds. Regardless of background, by 15-18 months all mice showed microscopic renal lesions. These renal lesions varied from cysts, atypical cysts with papillary projections, branching cysts with branching papillary projections to solid carcinomas. The authors also noted that these lesions displayed a clear progression from small cysts to carcinomas (Wilson *et al.* 2005). Extra-renal lesions were also reported in *Tsc1*$^{+/-}$ mice, including liver haemangiomas and hepatomas, uterine leiomyoma/leiomyosarcomas, tail or paw haemangiomas (Kobayashi *et al.* 2001, Kwiatkowski *et al.* 2002, Wilson *et al.* 2005) and RCC metastases in the lungs (Wilson *et al.* 2005).

Molecular analysis of renal and extra-renal lesions revealed that LOH at the *Tsc1* locus was present in five out of 12 renal lesions, two out of five hepatic haemangiomas, one out of two uterine lesions and one out of one lung lesion (Wilson *et al.* 2005). Kobayashi *et al.* (2001) found two out of six renal lesions with loss of the wild-type *Tsc1* allele. These LOH analyses suggest that a second hit in *Tsc1* may be necessary for the development of renal tumours in *Tsc1*$^{+/-}$ mice.

1.1.10.1.2 Tsc2 knockout mice

Two groups have developed conventional *Tsc2* knockout mouse models using similar homologous recombination and targeting vector techniques. Onda *et al.* (1999) disrupted exon 2 with a neomycin gene targeting construct, whereas Kobayashi *et al.* (1999) deleted part of exon 2 through to exon 5 with a LacZ/neomycin reporter selection cassette. Both of these gene targeting events resulted in early truncation of the protein product, which was confirmed by a lack of tuberin staining in immunoblot assays.

Similar to *Tsc1*$^{-/-}$ mice, homozygous *Tsc2* mutant embryos died *in utero* between E9.5 and E12.5 (Onda *et al.* 1999, Kobayashi *et al.* 1999). *Tsc2*$^{-/-}$ embryos appeared less developed by approximately 1-2 embryonic days and showed signs of exencephaly and a hypoplastic liver (Onda *et al.* 1999). The nonclosure of the neural tube in the head region was also a prominent feature, and was found in approximately 50% of *Tsc2*$^{-/-}$ embryos at E9.0-11.5 (Kobayashi *et al.* 1999).

Most *Tsc2*$^{+/-}$ mice displayed renal cysts and adenomas by 6 months of age, and rose to complete penetrance by 15 months (Onda *et al.* 1999, Kobayashi *et al.* 1999). Histological examination revealed that all *Tsc2*$^{+/-}$ renal lesions were located in the cortical region of the kidney, and, similar to findings from *Tsc1*$^{+/-}$ mice, renal lesions appeared as pure cysts, cysts with papillary projections and solid adenomas (Onda *et al.* 1999, Kobayashi *et al.* 1999). Extra-renal lesions included liver haemangiomas, angiosarcomas in the foot, tail and lip, alveolar adenomas and RCC metastases in the lungs (Onda *et al.* 1999, Kobayashi *et al.* 1999).

LOH analysis revealed loss of the wild-type *Tsc2* allele in nine out of 37 renal cystadenomas and carcinomas, and seven out of 14 liver haemangiomas (Onda *et al.* 1999). Kobayashi *et al.* (1999) found LOH of *Tsc2* in four out of 11 renal lesions. As with the LOH data from *Tsc1*$^{+/-}$ mice, these results indicate that loss of the wild-type *Tsc2* allele may contribute to tumour development.

1.1.10.1.3 The Eker rat

The Eker rat was the first hereditary cancer animal model to be described (Eker 1954, Okimoto *et al.* 2000). It presented as an autosomal dominant, hereditary model of predisposition to renal carcinoma with near complete penetrance, and displayed kidney lesions ranging from atypical tubules, pure cysts, cysts with papillary projections to solid adenomas (Eker *et al.* 1981, Hino *et al.* 1994). Homozygous mutant mice were found to die *in utero* at approximately 10 days of embryonic life (Hino *et al.* 1993a). Eker rats also developed tumours in the spleen, uterus and pituitary and, to a lesser extent, brain hamartomas resembling human TSC subependymal hamartomas and cortical tubers have also been observed (Hino *et al.* 1994, Yeung *et al.* 1997, Mizuguchi *et al.* 2000). The gene responsible for the Eker rat phenotype was localised to chromosome 10q12 using linkage analysis (Hino *et al.* 1993b, Yeung *et al.* 1993). Hino *et al.* (1994) demonstrated that the Eker rat gene was tightly linked to *TSC2*, with further analyses confirming that the mutation involved insertion of an approximately 5kb DNA fragment in the 3' portion of the gene proximal to the putative rap1GAP domain, resulting in aberrant RNA expression from the mutant allele (Yeung *et al.* 1994, Kobayashi *et al.* 1995).

LOH studies in Eker rats have revealed 40-60% of renal tumours show LOH, compared to 0% of splenic haemangiomas, 36% of uterine leiomyomas, 35% of pituitary adenomas and 0% of subependymal and subcortical hamartomas (Yeung *et al.* 1995, Yeung *et al.* 1997, Kubo *et al.* 1995). Screening for intragenic mutations has shown that some LOH-negative RCCs from Eker rats carry point mutations (7 out of 21 spontaneous RCCs) however, many lesions do not contain these mutations (Kobayashi *et al.* 1997). This data, as with the *Tsc1*$^{+/-}$ and *Tsc2*$^{+/-}$ mouse data, indicates that second hits are an important feature of tumour development, however, they are not apparent in all lesions, suggesting perhaps other mechanisms are also responsible for tumourigenesis.

1.2 Autosomal dominant polycystic kidney disease

Polycystic kidney diseases (PKDs) are a large family of disorders characterised by the occurrence of multiple renal cysts often leading to end-stage renal disease (ESRD). They frequently arise through genetic mutations with autosomal dominant or autosomal recessive PKD being the most prevalent inherited PKDs (Ibraghimov-Beskrovnaya and Bukanov 2008). Autosomal recessive PKD (ARPKD) occurs at an incidence of 1:20,000, and is observed primarily in infancy and childhood (Torres and Harris 2006). ARPKD is characterised by bilateral cystic kidneys and congenital hepatic fibrosis and is responsible for significant paediatric morbidity and mortality (Ibraghimov-Beskrovnaya and Bukanov 2008). The gene responsible for ARPKD lies on chromosome 6p21.1-p12 and is called *PKHD1* (polycystic kidney and hepatic disease 1) (Zerres *et al.* 1994, Guay-Woodford *et al.* 1995). The protein product of *PKHD1* is known as fibrocystin (Ward *et al.* 2002) (or polyductin (Onuchic *et al.* 2002)) which functions as a membrane associated receptor or ligand, however its exact role is unknown (Menezes and Onuchic 2006). Autosomal dominant PKD (ADPKD) is one of the most common life-threatening genetic diseases, occurring at a higher incidence than ARPKD, and will be the focus of this chapter.

1.2.1 A brief history of ADPKD

ADPKD was previously known as adult polycystic kidney disease, however this name did not encompass the true pathology of the disease (Zhou and Pei 2008). ADPKD is in fact an inherited systemic disease that can occur at any time in life and can affect multiple organs such as the kidneys, liver and heart (Zhou and Pei 2008). It later became known as autosomal dominant PKD after a study by Dalgaard in 1957 confirmed an autosomal dominant pattern of inheritance (Dalgaard 1957). During this study the prevalence of ADPKD was estimated at 1:1,000 from a Danish population, however a more recent North American study provided a prevalence estimate of 1:400 (Iglesias *et al.* 1983). These figures make ADPKD the most common genetic disorder of the kidney, with over 50,000 people affected in the United Kingdom alone, and up to 12.5 million worldwide (Yoder *et al.* 2006). In 1985 and 1993 the two genes responsible for ADPKD, *PKD1* and *PKD2*, were

localised, and later their protein products identified (Reeders *et al.* 1985, Peters *et al.* 1993, Kimberling *et al.* 1993, Hughes *et al.* 1995, The International Polycystic Kidney Disease Consortium 1995, Mochizuki *et al.* 1996). Genetic testing is now available to test those with equivocal renal imaging results and those with a negative family history (Rossetti *et al.* 2001).

1.2.2 ADPKD manifestations

ADPKD is characterised by progressive formation and enlargement of bilateral, multiple, renal cysts, leading to chronic renal failure by the sixth to eighth decade of life. Typical symptoms of ADPKD include abdominal discomfort, back pain, macroscopic haematuria and urine infections (Yoder *et al.* 2006). It is a multisystemic disorder with cysts also occurring in the liver (70% of patients) and pancreas (5-10%), and rarely in other organs such as the spleen (Yoder *et al.* 2006). Numerous hepatic cysts can give rise to polycystic liver disease in patients with advanced renal disease. Hepatic cysts arise from the biliary epithelia and are rarely associated with impairment of hepatic function (Sandford *et al.* 1999). Although men and women with ADPKD are equally as susceptible to hepatic cysts, massive polycystic liver disease occurs almost exclusively in women (Gabow *et al.* 1990). Polycystic liver disease is not to be confused with autosomal dominant polycystic liver disease (ADPLD), another monogenic disorder due to mutations of different genes, with few or no renal cysts present in patients (Qian *et al.* 2003a).

Of the non-cystic manifestations, cardiovascular system abnormalities are the most common and often most lethal (Fick *et al.* 1995). Hypertension is a major feature of ADPKD, occurring in 50-70% of patients often before any significant reduction in renal function (Ecder and Schrier 2001). Cardiac valvular heart disease is also widespread, with mitral valve prolapse occurring in 25% of ADPKD patients (Sandford *et al.* 1999). Ruptured intracranial aneurysms (ICAs) are rare but life threatening complications, occurring in 8% of ADPKD patients compared with ~1% of the general population (Chapman *et al.* 1992, Ruggieri *et al.* 1994, Rinkel *et al.* 1998). Renal and extra-renal manifestations of ADPKD have also been reported in children and even rarely *in utero* or in the early postnatal period (Boucher and Sandford 2004).

1.2.2.1 Renal manifestations

The formation of renal cysts is age dependent and occurs in all ADPKD patients. In most cases only a few renal cysts are detected in patients before 30 years of age, however, by the fifth decade of life, hundreds to thousands of renal cysts may be present, leading to enlargement of the kidneys by up to 40cm in length (compared with 10-12cm in normal individuals) and 8kg in weight (compared with 400-500g in normal individuals) (Gabow 1993). Renal cysts occur bilaterally and arise from epithelial cells lining the renal tubule, but unlike ARPKD cysts, which derive from collecting ducts, ADPKD cysts arise from all segments of the nephron and collecting ducts (Torres and Harris 2006). The main complications associated with renal cysts include renal failure, back or flank pain, cyst infection and haemorrhage, and renal stones (Table 1.7). RCC occurs very rarely in ADPKD and does not appear to arise at a greater frequency than the general population (Keith *et al.* 1994). Progression to ESRD in ADPKD patients typically occurs in late middle age with less than 5% of patients under 40 years of age, and up to 80% of those 70 years of age suffering from it (Zhou and Pei 2008).

Table 1.7 Renal manifestations of ADPKD.

Symptom	**Caused by**
Renal function abnormalities	Urine concentrating defect Reduced urine ammonium relative to pH Reduced renal blood flow
Renal pain	Cyst haemorrhage Renal calculi Renal infection
Haematuria	Cyst haemorrhage Renal calculi Renal cell carcinoma
Proteinuria	Low grade excretion of urinary protein (<1g/day).
Hypertension	Activation of renin-angiotensin system Impaired endothelial-dependent vascular relaxation Increased sympathetic nerve activity
Renal disease progression	Compression atrophy Tubular obstruction Renal ischemia Interstitial inflammation Apoptosis of tubular epithelial cells

Table adapted from Zhou and Pei 2008.

1.2.3 Clinical diagnosis of ADPKD

The most frequently used methods of diagnosis for ADPKD are trans-abdominal ultrasound scanning, CT, and MRI (Boucher and Sandford 2004, Nascimento *et al.* 2001). Ultrasound is the preferred diagnostic imagining method for both adults and children as it is simple, highly sensitive, widely available and non-invasive (Boucher and Sandford 2004). CT and MRI are often used when ultrasound results are equivocal, and additional information on renal structure and function is required (Nascimento *et al.* 2001).

ADPKD is typically diagnosed in adults when they present with bilaterally enlarged kidneys with multiple cysts and a positive family history consistent with autosomal dominant inheritance (Pei 2006). Other symptoms that contribute towards a positive ADPKD diagnosis are the presence of liver and other extra-renal cysts, cardiovascular system abnormalities indicative of the disease, and also the absence of symptoms of other cystic kidney disorders (Table 1.8) (Pei 2006). However occasionally ADPKD will appear in children and may be easily confused with ARPKD. In these instances, the presence of a positive family history of ADPKD and renal cyst size differences will help to differentiate the two (ADPKD renal cysts are generally larger than ARPKD cysts (Avni *et al.* 2002)). In some patients where ADPKD is suspected, a family history may not be present, indicating a possible *de novo* mutation or an undiscovered *PKD2* family history with very mild symptoms (Pei 2006).

For individuals born with a 50% risk of inheriting ADPKD from a *PKD1*-linked family, diagnostic criteria revised by Ravine *et al.* (1994) are commonly used (listed below). This diagnostic criteria is also believed to be sufficient for the diagnosis of ADPKD from *PKD2*-linked families, however some refinement is needed to reduce the false-negative rate (Pei 2006).

- Younger than 30 years of age – at least two renal cysts (unilateral or bilateral).
- Between 30 and 59 years of age – at least two cysts in each kidney.
- Older than 60 years of age – at least four cysts in each kidney.

Genetic testing is also available for the diagnosis of ADPKD when renal ultrasonography is inconclusive and there is a negative family history (Rossetti *et al.* 2002b). This involves the use of techniques such as DHPLC mutation screening of the entire *PKD1* and *PKD2* coding sequence and splice junctions. Expense is however a problem and a definitive mutation is maybe found in no more than approximately two thirds of the test subjects (Pei 2006).

Table 1.8 Potential ADPKD diagnostic confusion with other renal cystic disorders.

Disorder	Prevalence	Inheritance	Differences to ADPKD
Syndromic			
TSC	~1:10,000	Autosomal dominant	Skin lesions, retinal hamartomas, seizures, mental retardation, brain lesions, cardiac rhabdomyoma, LAM, renal angiomyolipoma.
VHL syndrome	~1:50,000	Autosomal dominant	Central nervous system and retinal haemangioblastoma, pancreatic cysts, pheochromocytoma, RCC, papillary cystadenoma of epididymis.
Medullary sponge kidney	~1:5,000	Familial clustering uncommon	Medullary nephrocalcinosis, "paintbrush" appearance of renal papillae on intravenous pyelogram.
Oro-facio-digital syndrome	Very rare	X-linked dominant inheritance	Lethal in affected males. Oral anomalies, facial anomalies, digital anomalies.
Nonsyndromic			
Simple renal cysts	Common	None	Rare under 30 years, but increase with age.
Acquired renal cystic disease	Common	None	Chronic renal insufficiency or ESRD with multiple renal cysts associated with normal sized or small kidneys.

Table adapted from Pei 2006.

1.2.4 Identification of the ADPKD genes

The first ADPKD gene locus, now designated the *PKD1* locus, was localised in 1985 to the α-globin cluster on the short arm of chromosome 16 (Reeders *et al.* 1985). Families in which there was no linkage to markers on chromosome 16p were soon identified (Kimberling *et al.* 1988, Romeo *et al.* 1988), leading to the discovery of a second ADPKD locus (*PKD2*) on chromosome 4q13-q23 (Peters *et al.* 1993, Kimberling *et al.* 1993). It is estimated that approximately 85% of ADPKD is due to mutations in *PKD1*, with *PKD2* accounting for the remaining 15% (Peters and Sandkuijl 1992, Peral *et al.* 1993). However, since patients with *PKD2* mutations have a milder disease phenotype and sometimes go un-diagnosed, there may be a bias towards identifying families with *PKD1* mutations, thus the proportion of families with ADPKD2 may be higher than 15% (Hateboer *et al.* 1999).

1.2.4.1 The PKD1 gene

Localisation of the *PKD1* region was further refined in the early 1990s to chromosome band 16p13.3 using extensive linkage analysis and panels of somatic cell hybrids (The European Polycystic Kidney Disease Consortium 1994). Within this region the *PKD1* locus was located in an interval of approximately 600kb between the markers *GGG1* and *SM7*, which was rich in gene sequences (Harris *et al.* 1990, Germino *et al.* 1992, Harris *et al.* 1991, Somlo *et al.* 1992). Investigators then went on to examine families with TSC for information on the possible location of ADPKD causing genes as it was known that some TSC patients developed renal cystic lesions that resembled those of ADPKD. One ADPKD family was found to have inherited a balanced translocation near the *TSC2* locus with a breakpoint in a novel gene named the polycystic breakpoint protein (*PBP*) gene (The European Polycystic Kidney Disease Consortium 1994). Further mutations of the *PBP* gene, which encodes a 14kb transcript, were found in ADPKD1 patients, confirming that *PBP* was in fact the *PKD1* gene (The European Polycystic Kidney Disease Consortium 1994). A year later the *PKD1* sequence was extended by 2689 amino acids (The International Polycystic Kidney Disease Consortium 1995). The delay in revealing the entire *PKD1* sequence was due to the presence of several transcriptionally active copies of *PKD1*-like sequences located in the

more proximal region 16p13.1 (The European Polycystic Kidney Disease Consortium 1994). This made it very difficult to distinguish the *PKD1* locus transcript from those of the *PKD1*-like loci.

PKD1 is approximately 53kb in length and is organised into 46 exons encoding a 14.5kb mRNA (The International Polycystic Kidney Disease Consortium 1995). Exon 1 is located 16kb away from exon 2 with an in-frame start codon located at 212bp and an ORF of 12,906bp (Hughes *et al.* 1995). The *PKD1* genomic region has a high GC content and multiple simple repeats (Hughes *et al.* 1995). Interestingly, intron 21 contains a 2.5kb polypyrimidine tract which may interfere with replication and transcription (Van Raay *et al.* 1996). The 14.5kb transcript encodes a 4,302 amino acid, 460 kDa protein called polycystin-1 (PC1) (Hughes *et al.* 1995).

1.2.4.2 The PKD2 gene

Unlike the *PKD1* gene, *PKD2* is a single copy gene and so its identification was much simpler. Peters *et al.* (1993) localised the *PKD2* locus to the long arm of chromosome 4, flanked by the DNA markers D4S231 and D4S423. Around the same time, Kimberling *et al.* (1993) further localised *PKD2* to chromosome 4q13-q23, and in 1996, the *PKD2* gene sequence was mapped using cDNA clones (specifically clone cTM-4) (Mochizuki *et al.* 1996).

PKD2 is approximately 68kb in length and contains 15 exons which encode a 5.4kb transcript. An initiator ATG codon is located 67bp from the 5' end, and is followed by a 2904bp ORF. The *PKD2* transcript encodes a 968 amino acid, 110 kDa protein called polycystin-2 (PC2) (Mochizuki *et al.* 1996).

1.2.4.3 A possible PKD3 gene?

The existence of a third gene, *PKD3*, is suspected but has not yet been confirmed. This theory arose due to the identification of a small proportion of families linked neither to *PKD1* nor to *PKD2* (Daoust *et al.* 1995, de Almeida *et al.* 1995, Turco *et al.* 1996, Ariza *et al.* 1997, McConnel *et al.* 2001). However, before these unlinked families can be confidently assigned to the putative *PKD3* gene, potential confounders must first be eliminated. The

common confounders that may lead to false exclusion of linkage to *PKD1* and *PKD2* include: genotyping errors, DNA sample mix up, non-paternity and misdiagnosis (Paterson and Pei 1998, Paterson and Pei 1999). Detailed haplotype analysis using multiple markers must be performed in all putative *PKD3* families before the existence of this gene can be confirmed and potentially located.

1.2.5 Mutation analysis of *PKD1* and *PKD2*

A mutation detection rate in *PKD1* and *PKD2* of approximately 76% has been achieved using conventional and long-range PCR (Boucher and Sandford 2004). Most of these mutations are unique to a single family, as seen in other autosomal dominant and X-linked diseases (Peters and Breuning 2001). Mutations have been identified in all parts of *PKD1* and are predicted to produce a truncated PC1 protein (Rossetti *et al.* 2001). Most mutations are nonsense (33%) or frameshifting (28%), however small deletions (6%), splicing defects (14%) and missense mutations (19%) are also common, (Rossetti *et al.* 2001) and in total approximately 270 different *PKD1* mutations have been described (Rossetti *et al.* 2007). Large deletions of *PKD1* are rare but can include the adjacent *TSC2* gene, causing a contiguous gene deletion syndrome (discussed in more detail in section 1.2.6) (Brook-Carter *et al.* 1994, Sampson *et al.* 1997 and Laas *et al.* 2004).

Nearly 70 different mutations have been found in *PKD2*, most of which are predicted to be inactivating (Rossetti *et al.* 2007). These mutations are dispersed over the entire coding sequence with no significant clustering or hotspots, however none have been found in exons 3 and 15 (Magistroni *et al.* 2003). Of the mutations reported, most are nonsense (37%) or frameshifting (39%), but splicing (17%) and missense mutations (6%) also occur (Magistroni *et al.* 2003). One family has been found to have a complete deletion of *PKD2* (Magistroni *et al.* 2003).

Evidence suggests that *PKD1* is more susceptible to mutagenic events than *PKD2*, with a *de novo* germline mutation rate four to five times higher (Rossetti *et al.* 2001). A number of reasons have been proposed to explain

formation and recombination; however a recent report by Kozlowski *et al.* (2007) found no evidence for an enhanced rate of genomic deletions near this tract.

1.2.6 Genotype/phenotype correlations

ADPKD1 is a more severe disease than ADPKD2, with earlier diagnosis, a higher incidence of hypertension and haematuria, a greater history of urinary tract infection, and ESRD occurring approximately 15 years earlier (Hateboer *et al.* 1999, Ravine *et al.* 1992). Allelic effects within each gene may also influence renal disease severity in ADPKD. The location of mutations in *PKD1*, but not the type, appears to be associated with disease severity differences in the ADPKD1 population. Patients with mutations in the 5' portion of the gene (0-7812bp) were found to have a lower mean age of ESRD than the 3' group (beyond 7812bp) (Rossetti *et al.* 2002a). In addition, Rossetti *et al.* (2003) revealed that 5' mutations were more commonly associated with vascular disease, becoming especially clear in patients with aneurismal rupture, early rupture or families with more than one vascular case. By contrast, a large study of ADPKD2 patients, found that the location of mutations did not influence the age of onset of ESRD (Magistroni *et al.* 2003). This study did however reveal that patients with splice site mutations appear to have milder renal disease compared with other mutation types. Interestingly Magistroni *et al.* (2003) found a significant correlation between gender and disease severity, reporting that female ADPKD2 patients had a later mean age of ESRD onset compared to males. However, in studies of *PKD1*, gender was not found to correlate significantly with disease severity (Hateboer *et al.* 1999, Rossetti *et al.* 2002a).

Renal disease severity in ADPKD can also be greatly affected by two rare Mendelian syndromes. The first, known as the TSC2/ADPKD1 contiguous gene syndrome, involves a large genomic deletion of both *PKD1* and *TSC2* (Brook-Carter *et al.* 1994). These genes lie immediately adjacent to each other (approximately 60bp apart) on chromosome 16p13.3 in a tail-to-tail orientation (Sampson *et al.* 1997). Large *TSC2/PKD1* contiguous deletions were first discovered during the search for the *TSC2* gene (Brook-Carter *et al.* 1994, The European Chromosome 16 Tuberous Sclerosis Consortium 1993, The European Polycystic Kidney Disease Consortium 1994). The first TSC patient with this deletion was only three months old and was found to have grossly enlarged and polycystic kidneys (Brook-Carter *et al.* 1994). Five further TSC patients with similar polycystic kidneys in infancy were studied, and deletions involving *TSC2* and *PKD1* were found in each case (Brook-Carter *et al.* 1994). In contrast, severe early onset cystic kidney disease was not found in TSC patients with no mutations in *PKD1*, suggesting that constitutional deletion of *PKD1* is necessary for the development of this phenotype in some TSC patients (Brook-Carter *et al.* 1994). The severity of the TSC2/ADPKD1 contiguous gene syndrome indicates that an interaction between *TSC2* and *PKD1* exists and perhaps the signalling pathways downstream from PC1 and tuberin converge at some crucial point (Rossetti and Harris 2007). To date approximately 20 cases (75% paediatric and 25% adult cases) of the disease have been observed, often arising in patients with no family history of the disease or those with somatic mosaic parents with subtle disease (Bisceglia *et al.* 2008 for case references).

The second syndrome involves bilineal inheritance of two independently segregating *PKD1* and *PKD2* mutations. During the search for the putative *PKD3* gene a large ADPKD family was studied which had previously been excluded from linkage to both the *PKD1* locus and the *PKD2* locus (Pei *et al.* 2001). Out of 48 members of the family, 28 were affected with ADPKD, two of which were shown to have *trans*-heterozygous germline *PKD1* and *PKD2* mutations. These two individuals had more severe renal disease than the other family members who had either mutation alone, and also developed ESRD approximately 20 years earlier. The authors proposed two

signalling complex below a "threshold", which would predispose more cells to a cystic phenotype (Pei *et al.* 2001). These rare syndromes provide unique evidence for the role of interaction between cystogenes (*PKD1* with *TSC2*, and *PKD1* with *PKD2*) in modifying renal cystic disease severity (Zhou and Pei 2008).

1.2.7 Loss of heterozygosity and haploinsufficiency

Similar to Knudson's classic "two-hit" model of tumourigenesis, a two-hit model of cystogenesis has been proposed for ADPKD (Reeders 1992). As with most cystic kidney diseases, the majority of nephrons remain normal in ADPKD whilst a minority (around 10%) contain cysts, and yet every cell within the nephron carries a germline mutation (Reeders 1992). This suggests that the germline mutation is not in itself sufficient to produce a cyst and a "second hit" is also required. Recent studies have provided evidence that this event is a major mechanism of cystogenesis in ADPKD. By isolating epithelial cells from single renal cysts, thus minimising contamination by other cells, two laboratories independently reported that ADPKD1 renal cysts are monoclonal (Qian *et al.* 1996, Brasier *et al.* 1997). LOH of *PKD1* was found in 17-24% of cysts, however small somatic mutations were not examined (Qian *et al.* 1996, Brasier *et al.* 1997). Second hits have also been found in extra renal tissue such as the liver; in which one group found small intragenic mutations in up to 30% of *PKD1* liver cysts (Watnick *et al.* 1998). Studies of *PKD2* have revealed similar findings, with LOH and small intragenic mutations reported in up to 10% and 40% of human *PKD2* renal and liver cysts, respectively (Pei *et al.* 1999, Torra *et al.* 1999, Koptides *et al.* 1999). Of note, inactivating somatic *PKD1* mutations have been reported in approximately 8% of *PKD2* cysts, and conversely, somatic *PKD2* mutations in approximately 13% of *PKD1* cysts, suggesting a *trans*-heterozygous two-hit model may be a mechanism for

two-hit model of cystogenesis (Ong and Harris 1997). First, it was argued that a higher rate of somatic PKD mutations should be reported if second hits are indeed required for cystogenesis. However, none of the earlier studies examined the entire length of *PKD1* and *PKD2* for somatic mutations, and also mutation screening of *PKD1* is challenging due to its large size and complexity. To address this issue, a recent study screened the entire *PKD2* gene for somatic mutations using a highly sensitive single-stranded conformational analysis (Watnick *et al.* 2000). The analysis, which included all 15 exons and flanking splice junctions, revealed somatic mutations in 71% of cysts. This study reveals that when using sensitive mutation detection techniques, a high rate of somatic mutation can be detected, however, a large proportion of cysts still show no second hit. The second concern involves evidence from studies showing strong immunoreactivity for PC1 and PC2 in the majority of cystic epithelia (Ong *et al.* 1999a, Ong *et al.* 1999b). These results appear incompatible with a two-hit model of cystogenesis, and so several explanations have been proposed. Ong *et al.* (1999b) suggested that the problem could be reconciled if the majority of somatic mutations are missense, which could then functionally inactivate the "normal" polycystin protein while allowing its expression and detection. However, the majority of PKD mutations identified so far are stop or frame-shifting changes (Rossetti *et al.* 2001, Magistroni *et al.* 2003). Another explanation stems from *trans*-heterozygous inactivation of *PKD1* and *PKD2* (Watnick *et al.* 2000, Koptides *et al.* 2000). Expression of PC1 and PC2 is expected in these cysts, however *trans*-heterozygous inactivation only occurs in approximately 10% of ADPKD cysts and so cannot account for the majority of polycystin immunoreactivity (Pei 2001). Finally, unreliable antibodies and cross-reactivity could lead to polycystin positive cysts (Pei 2001).

only 13-20% normally spliced PC1, Lantinga-van Leeuwen *et al.* (2004) found that a reduced dosage of *Pkd1*, but not complete loss, was sufficient to initiate cystogenesis. Similar results were obtained by Jiang *et al.* (2006) using a conditional *Pkd1* knockout mouse model, resulting in partially inhibited *Pkd1* expression. Mice homozygous for the targeted allele appeared normal at birth but developed polycystic kidneys whilst low levels of full-length PC1 continued to be produced. Haploinsufficiency in *Pkd2* mouse mutants has also been reported to result in a cystic phenotype. Chang *et al.* (2006) found an increased proliferative index in non-cystic tubules 5-10 times that of normal control tissue. The effects of haploinsufficiency in *trans*-heterozygous *Pkd1* and *Pkd2* mutations have also been studied using mouse models (Wu *et al.* 2002). The severity of cystic disease was found to be increased in $Pkd1^{+/-}$ $Pkd2^{+/-}$ mice in excess of that predicted by a simple additive affect based on cyst formation in $Pkd1^{+/-}$ or $Pkd2^{+/-}$ mice alone. Together, the data from these haploinsufficient models suggest that severe reduction, but not complete loss of PC1, possibly coupled with other genetic and environmental factors, may induce cystogenesis. Two other studies have suggested that increased levels of PC1 expression may also cause renal cystic disease. Transgenic mice over expressing *Pkd1* were found to have multiple tubular and glomerular cysts, as well as hepatic cysts and bile duct proliferation, characteristic of ADPKD (Pritchard *et al.* 2000, Thivierge *et al.* 2006). Interestingly, analysis of tissues from ADPKD patients has revealed enhanced PC1 immunoreactivity in the majority of cysts (Ward *et al.* 1996, Geng *et al.* 1996). These studies suggest that overexpression of PC1 alone may also be sufficient to trigger cystogenesis.

Table 1.9 The polycystin protein family.

Protein	Gene and locus	Localisation	Biological role
PC1-like			
Polycystin-1	*PKD1*, 16p13.3	Widespread	Mechanotransducti regulator of cell growth, proliferatior and differentiation
Polycystin-REJ	*PKDREJ*, 22q13	Testis, coincident with the timing of sperm maturation	Regulator of ion channels during fertilisation?
Polycystin-1L1	*PKD1L1*, 16p12-13	Relatively widespread with higher levels in heart and testis	Unknown
Polycystin-1L2	*PKD1L2*, 16q23	Relatively widespread with higher levels in heart and testis	Unknown
Polycystin-1L3	*PKD1L3*, 16q22	Relatively widespread, but not in skeletal muscle	Unknown
PC2-like			
Polycystin-2	*PKD2*, 4q21-23	Widespread	Mechanotransducti regulator of cell growth, proliferatior and differentiation
Polycystin-L	*PKDL*, 10q24-25	Relatively widespread	Unknown
Polycystin-2L2	*PKD2L2*, 5q31	Heart and testis	Fertilisation?

Table adapted from Zhou and Pei 2008, Delmas *et al.* 2004.

PC1 is a receptor-like molecule with a large extracellular N-terminal domain, 11 transmembrane domains and a C-terminal cytoplasmic domain o approximately 200 amino acids (Figure 1.5) (Sandford *et al.* 1999). The N-terminus contains a number of adhesive regions, suggesting a diverse role a

for the normal function of the protein. Qian *et al.* (2002) found that cleavage deficient Madin-Darby canine kidney (MDCK) cells could only form cyst-like structures compared to cells transfected with wild-type PC1, which consistently developed tubule like structures in 3-dimesional collagen gels. Cleavage of the cytoplasmic C-terminal tail is believed to be involved in nuclear signalling and will be discussed in more detail later. The C-terminal domain of PC1 is known to be phosphorylated at a number of sites. Cyclic adenosine monophosphate (cAMP)-dependent protein kinase A, but not protein kinase C, phosphorylates PC1 at S4159 and S4252, whilst it is suggested that T4237 might be phosphorylated by c-src (Parnell *et al.* 1999, Li *et al.* 1999).

PC2 is a non-selective cation channel with a high permeability to calcium (Ca^{2+}) modulated by intracellular Ca^{2+} concentration (Anyatonwu and Ehrlich 2005). It contains six transmembrane domains and a pore region thought to be located between the fifth and sixth transmembrane domains (Anyatonwu and Ehrlich 2005) (Figure 1.5) (Table 1.10). Both N- and C-terminal domains of PC2 are located intracellularly. PC2 shares significant homology with transient receptor potential (TRP) channels and is considered a member of the TRP channel superfamily TRPP2 (Delmas *et al.* 2004). An EF-hand domain (EF stands for E and F helixes of parvalbumin) is present in the C-terminal of PC2 and is thought to play a significant role in Ca^{2+} binding and regulation of ion channel functions (Cai *et al.* 1999). PC2 associates with the coiled coil domain of PC1 through its C-terminal tail (Qian *et al.* 1997).

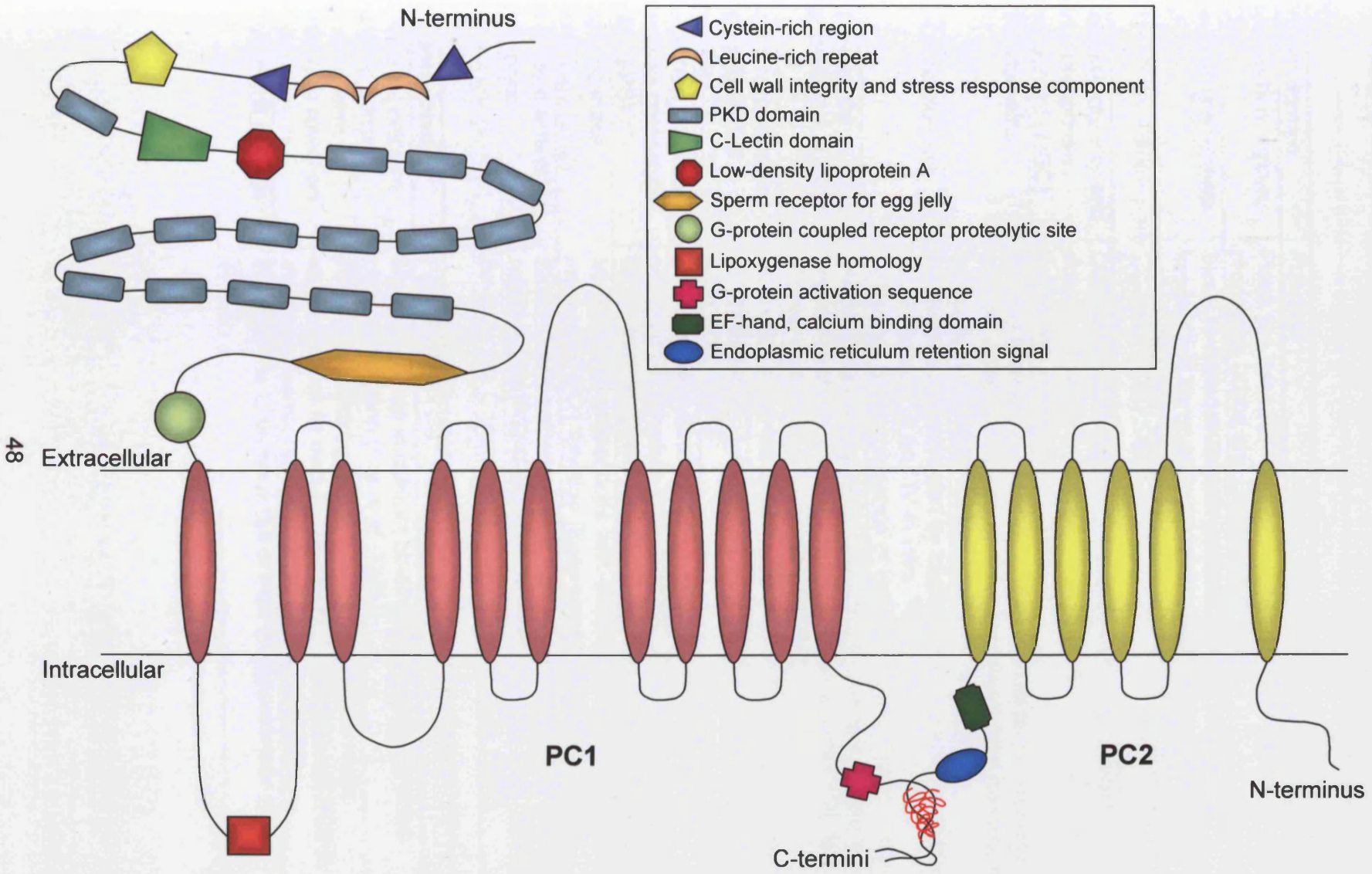

Figure 1.5 The predicted structure of human PC1 and PC2. A coiled-coil domain (red spiral) in the C-terminus of PC1 interacts with a predicted coiled-coil domain (red spiral) in the C-terminus of PC2. PC1 has 11 transmembrane domains (pink ovals) and PC2 has 6 transmembrane domains (yellow ovals). All other domains are indicated in the key above. Domains not drawn to scale.

	cell proliferation has been observed *in vitro* (Malnas *et a* 2002).
Cell wall integrity and stress response component (WSC)	Definite function unknown. Putative carbohydrate-bindir domain, possibly acting as a regulator of stress-activate pathways (Weston *et al.* 2003).
PKD domains	Display homology to immunoglobin-like domains. Involv cell-cell adhesion by strong calcium-independent homo interactions (Ibraghimov-Beskrovnaya *et al.* 2000).
C-Lectin domain	Involved in cell adhesion by binding carbohydrate matri and collagen I, II and IV *in vitro*. This binding is greatly enhanced by the presence of calcium (Weston *et al.* 20
Low-density lipoprotein A (LDL)	Involved in protein-protein interactions. Binding partner unclear as there is some confusion as to whether LDL i definite motif in PC1 (Weston *et al.* 2003).
Sperm receptor for egg jelly (REJ) domain	Regulator of ion transport in the acrosome reaction. Un of function in PC1, but could be involved in ionic regulat (Moy *et al.* 1996).
G-protein coupled receptor proteolytic site (GPS)	Site of proteolytic cleavage, a process that requires the adjacent REJ module to be present. Cleavage could be for PC1 to exhibit full biological activity (Qian *et al.* 2002
Lipoxygenase homology (LH2)	May mediate interactions with other membrane proteins involved in PC1 function (Bateman and Sandford 1999)
G-protein activation sequence	Binds to and activates G proteins. This activity is physic regulated by PC2 (Parnell *et al.* 1998, Delmas *et al.* 20
Coiled coil domain	Binds to the C-terminal tail of PC2 (Qian *et al.* 1997).
PC2	
Protein domain	*Function*
EF-hand, calcium binding domain	May play a role in calcium binding and regulation of ion channel function (Cai *et al.* 1999).
Endoplasmic reticulum retention signal	Prevents trafficking to the surface membrane when expressed on its own. Responsible for retention of PC2 the endoplasmic reticulum (ER) (Cai *et al.* 1999).
Coiled coil domain	Binds to the C-terminal tail of PC1 (Foggensteiner *et al.* 2000).

the cell membrane, they form a mechanosensory complex which helps regulate normal renal tissue morphogenesis (discussed in more detail in section 1.3) (Nauli *et al.* 2003). PC2 can also regulate the subcellular distribution of PC1. Grimm *et al.* (2003) observed that when PC1 is expressed alone, it localises to the cell membrane, whereas co-transfection with PC2 results in ER localisation of PC1 along with PC2. Interestingly it has also been shown that PC2 remains in the nodal cilia of PC1 knockout mice, suggesting that PC2 targeting can also be independent of PC1 (Geng *et al.* 2006). It is clear that further studies are required to elucidate the full interdependent and independent functions of PC1 and PC2.

1.2.8.2 Localisation of PC1 and PC2

PC1 and PC2 have a wide tissue distribution, being highly expressed in kidney, brain, liver, pancreas and vasculature (Wilson 2001). Expression of PC1 is developmentally regulated, with high levels in developing tissue, but only low levels in adult tissue (Geng *et al.* 1997, Van Adelsberg *et al.* 1997). In the mouse kidney, PC1 levels peak at embryonic day 15 and fall to a low level 2 weeks after birth (Geng *et al.* 1997). This low level is then maintained throughout adult life. Within the kidney, PC1 is found predominantly in the collecting duct, although lower levels are also found in nearly all tubule segments of the nephron (Foggensteiner *et al.* 2000). The subcellular localisation of PC1 has been greatly debated, although it is now generally accepted as a cell membrane protein specifically located at the apical membrane and the adherent and desmosomal junctions (Geng *et al.* 1996, Huan and van Adelsberg 1999, Scheffers *et al.* 2000). More recently PC1 has been localised to the primary cilium of renal tubules *in vivo* and in cell culture (Nauli *et al.* 2003, Yoder *et al.*, 2002, Luo *et al.* 2003).

Unlike PC1, PC2 maintains high levels of tubular expression in adult kidney (Foggensteiner *et al.* 2000). PC2 expression is highest in the thick ascending limb of the loop of Henle and the distal convoluted tubule (DCT) in normal adult kidney (Foggensteiner *et al.* 2000). The subcellular location of PC2 has been controversial, with cytoplasmic, apical and basolateral membrane localisation reported *in vivo* (Cai *et al.* 1999, Foggensteiner *et al.* 2000). PC2 is also found in the ER, and some groups believe this to be its primary location (Cai *et al.* 1999, Koulen *et al.* 2002). Finally PC2 has been localised to the primary cilium along with PC1, where they are believed to act as a mechanosensory complex (Yoder *et al.* 2002).

1.2.8.3 PC1 and PC2 signalling pathways

The mechanosensation and calcium influx properties of PC1 and PC2 are one of the most interesting and possibly most important functions of these proteins and will be discussed in detail in section 1.3. PC1 and PC2 are also believed to be involved in other significant signalling pathways, such as the Wnt pathway and the mTOR pathway.

1.2.8.3.1 The JAK-STAT pathway

Recent studies in the kidney have shown that the C-terminal cytoplasmic tail of PC1 can be cleaved in response to fluid flow stress (discussed in more detail in section 1.3) (Chauvet *et al.* 2004, Low *et al.* 2006). This cleaved C-tail then translocates to the nucleus where it initiates nuclear signalling by binding to the transcription factor STAT6 (signal transducer and activator of transcription protein 6) and its co-activator P100 (Low *et al.* 2006) (Figure 1.6). The researchers suggest that this nuclear localisation of STAT6 has a pathologic role in ADPKD. They found that cyst lining cells in ADPKD showed elevated levels of nuclear STAT6, P100 and the PC1 tail. It was proposed that in normal renal tubular lumens with fluid flow and normal PC1, STAT6 is sequestered in the cilia by PC1. Under the absence of urine flow or PC1, STAT6 translocates from the cilia to the nucleus to initiate STAT6-dependent transcription (Figure 1.6).

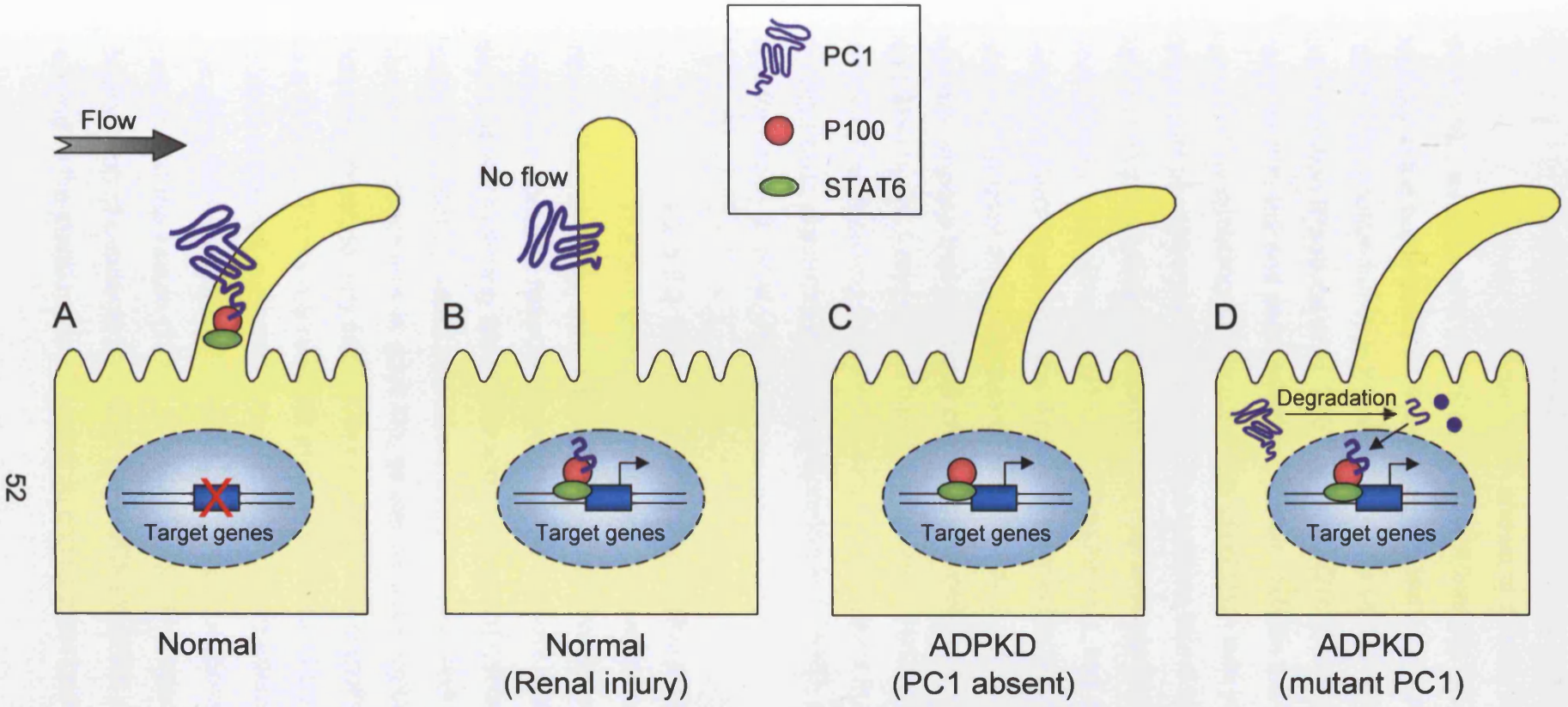

Figure 1.6 A working model of the role of PC1, primary cilia and flow sensing in the JAK/STAT pathway. Under normal flow conditions (**A**), PC1 localises to primary cilia, where it is in a complex with P100 and STAT6. The normal function of PC1 would be to sequester STAT6 and prevent the expression of STAT6/P100-dependent genes. This state remains stable as long as the cilia remain bent by luminal fluid flow. Renal injury resulting in cessation of fluid flow (**B**) will trigger cleavage of the cytoplasmic tail of PC1 by a yet unknown mechanism and protease. This is accompanied by STAT6 tyrosine phosphorylation, nuclear translocation of the PC1 tail/STAT6/P100 complex, and activation of gene expression. If PC1 is lost, STAT6 cannot be sequestered at the cilia and may be constitutively activated (**C**). It is more commonly observed in ADPKD that PC1 is actually highly expressed in cyst-lining epithelial cells. However, overexpressed mutant PC1 may be mis-folded and degraded, which may release a biologically active fragment corresponding to the C-terminal half of the tail. In this scenario (**D**), not only would STAT6 fail to be sequestered at the cilia, but the PC1 tail would further increase STAT6-dependent transcription. Adapted from Low *et al.* 2006.

1.2.8.3.2 The inhibitor of DNA binding pathway

Recently, PC2 has been shown to directly associate with the protein Id2, a member of the inhibitor of DNA binding (Id) protein family that belongs to the superfamily of helix-loop-helix transcription factors (Li *et al.* 2005). This protein family is known to promote cellular growth and inhibit differentiation (Pagliuca *et al.* 2000). Li *et al.* (2005) showed that PC2 interacts with Id2 and sequesters the protein outside the nucleus in the cytosol, thus inhibiting its function. This interaction was regulated by PC1-dependent phosphorylation of PC2. The authors found increased Id2 expression and nuclear translocation in cyst lining epithelia in the kidneys from patients with either *PKD1* or *PKD2* mutations, and also renal epithelial cells from *Pkd1* targeted mice. This is in contrast to the normal kidney, in which a low level of Id2 expression was detected, primarily in the cytosol. The authors propose that Id2 has a crucial role in cell-cycle regulation that is mediated by PC1 and PC2. Their data indicates that aberrant Id2 nuclear translocation resulting from loss of function mutations in either *PKD1* or *PKD2* contributes to abnormal cellular proliferation in ADPKD, which is a trigger for cyst formation (Li *et al.* 2005).

1.2.8.3.3 The canonical Wnt signalling pathway

The Wnt signalling pathway is an evolutionarily conserved signal transduction pathway used extensively during development. This highly conserved complex network of proteins can regulate multiple aspects of development including the proliferation, fate specification, polarity and migration of cells (Habas and Dawid 2005). It also plays a role in normal physiologic processes in adult life, as well as pathological roles in many diseases, most notably cancer. In canonical Wnt signalling, Wnt proteins bind to a Frizzled (Fz) family receptor and a coreceptor of the LRP family, both located at the cell surface (Clevers 2006). Fz then interacts with the cytoplasmic phosphoprotein Dishevelled which functions upstream of β-catenin and the kinase GSK-3 (Clevers 2006). This interaction inhibits the degradation of β-catenin by the APC/Axin/CK1/GSK3β destruction complex, leading to the stabilization of β-catenin and its translocation to the nucleus

Conflicting evidence exists over whether PC1 modulates Wnt signalling. The controversy mainly revolves around the potential interaction between the membrane-anchored C-terminal tail of PC1 and β-catenin. Kim *et al.* (1999) reported that the PC1 C-terminal tail stabilizes β-catenin and stimulates TCF-dependent gene transcription in human embryonic kidney cells. They state that their findings indicate that PC1 has the capacity to modulate Wnt signalling during renal development. However, two recent studies have shown that neither the membrane anchored nor the cleaved soluble PC1 C-terminal tails were able to modulate Wnt signalling using a variety of assays (Le *et al.* 2004, Low *et al.* 2006). This conflicting data requires further investigation before the potential link between polycystins and Wnt signalling can be confidently resolved.

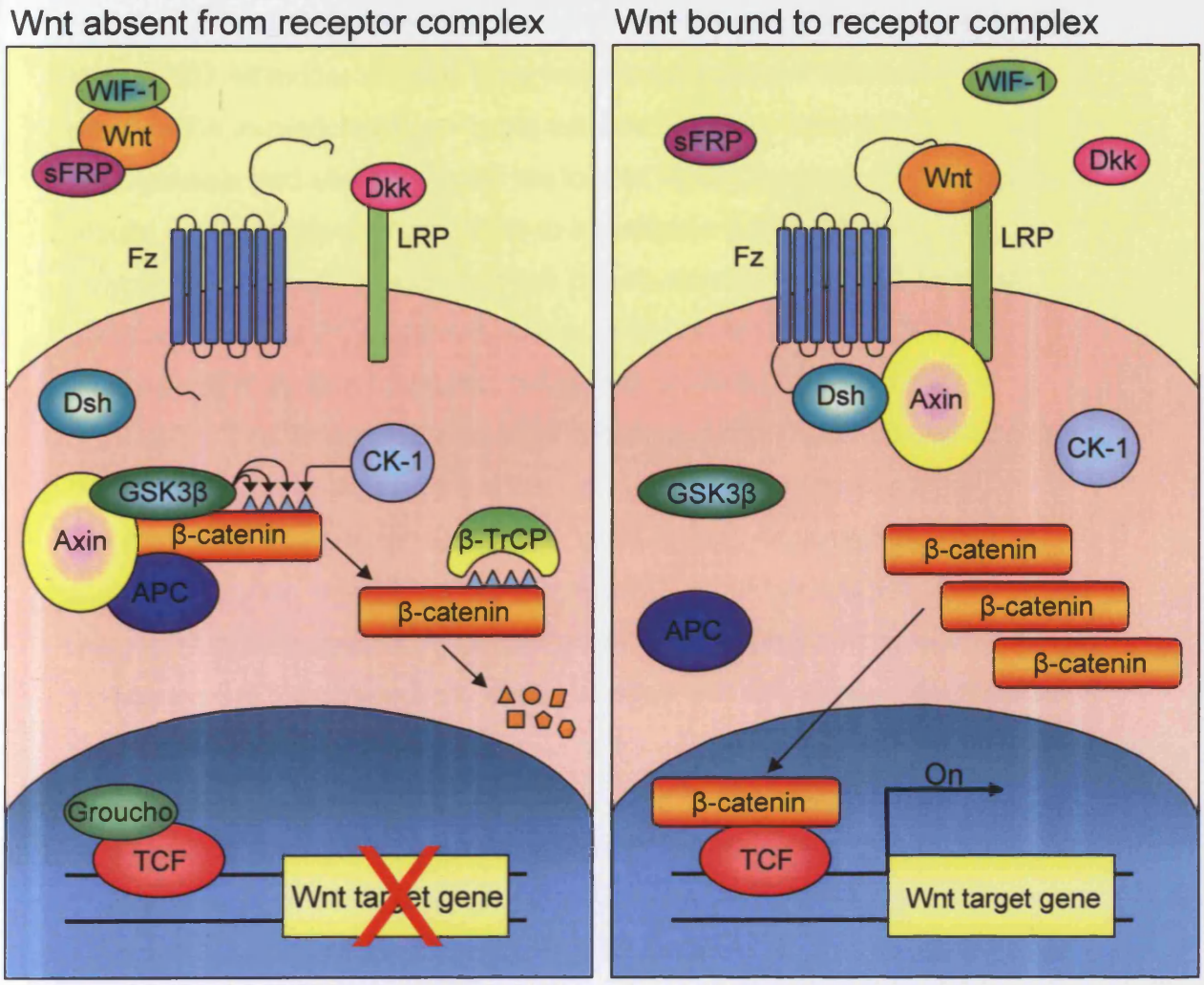

Figure 1.7 Overview of the canonical Wnt signalling pathway. (Left panel) When the Wnt receptor complex is not bound by Wnt ligand, cytoplasmic β-catenin is bound to its destruction complex, consisting of APC, axin/conductin and GSK3β. After CK-1 phosphorylates β-catenin on Ser 45 residue, β-catenin is further phosphorylated on Thr 41, Ser 37 and Ser 33 residues by GSK3β. Phosphorylated β-catenin is recognised by ubiquitin ligase β-TrCP and undergoes ubiquitination and degradation. Therefore, the cytoplasmic level of β-catenin is kept low in the absence of Wnt/Fz signalling. In the nucleus, the binding of Groucho to TCF (T cell factor) inhibits the transcription of Wnt target genes. WIF-1, sFRP and/or Dkk can inhibit the Wnt/Fz signalling by binding to Wnt ligands or LRP. (Right panel) Once bound by Wnt, the Fz/LRP coreceptor complex activates the canonical signalling pathway. Dsh is recruited and phosphorylated by Fz. Phosphorylated Dsh in turn recruits axin, which dissociates from the β-catenin destruction complex. Beta-catenin therefore escapes from phosphorylation and subsequent ubiquitination and accumulates in the cytoplasm. This accumulated cytoplasmic β-catenin then enters the nucleus where it displaces Groucho, binds to TCF/LEFs and activates the transcription of Wnt target genes. Information obtained from Eisenmann 2005.

polycystins in mTOR signalling. Their results showed that the C-terminal cytoplasmic tail of PC1 interacts with tuberin and the kinase mTOR. Interestingly they also found that the mTOR pathway is inappropriately activated in cyst-lining epithelial cells in human ADPKD and mouse models (*Pkd1*, *MAL* and *orpk* mouse models), and when given rapamycin, a significant reduction in renal size was found in both end-stage ADPKD patients and PKD mouse models (*Orpk* and *bpk* mouse models). The authors suggest that dysregulation of mTOR underlies changes in renal epithelial cells that cause the formation of polycystic kidneys. It is proposed that a function of the PC1 tail may be to assemble a complex with tuberin and mTOR and when PC1 is mutated, for example in ADPKD patients, the tuberin-mTOR complex is not formed and mTOR is rendered constitutively active (Figure 1.8) (Shillingford *et al.* 2006, Mostov 2006). These results also led the authors to speculate that rapamycin and other mTOR inhibiting drugs may be excellent candidates to help prevent or delay the onset of PKD (Shillingford *et al.* 2006).

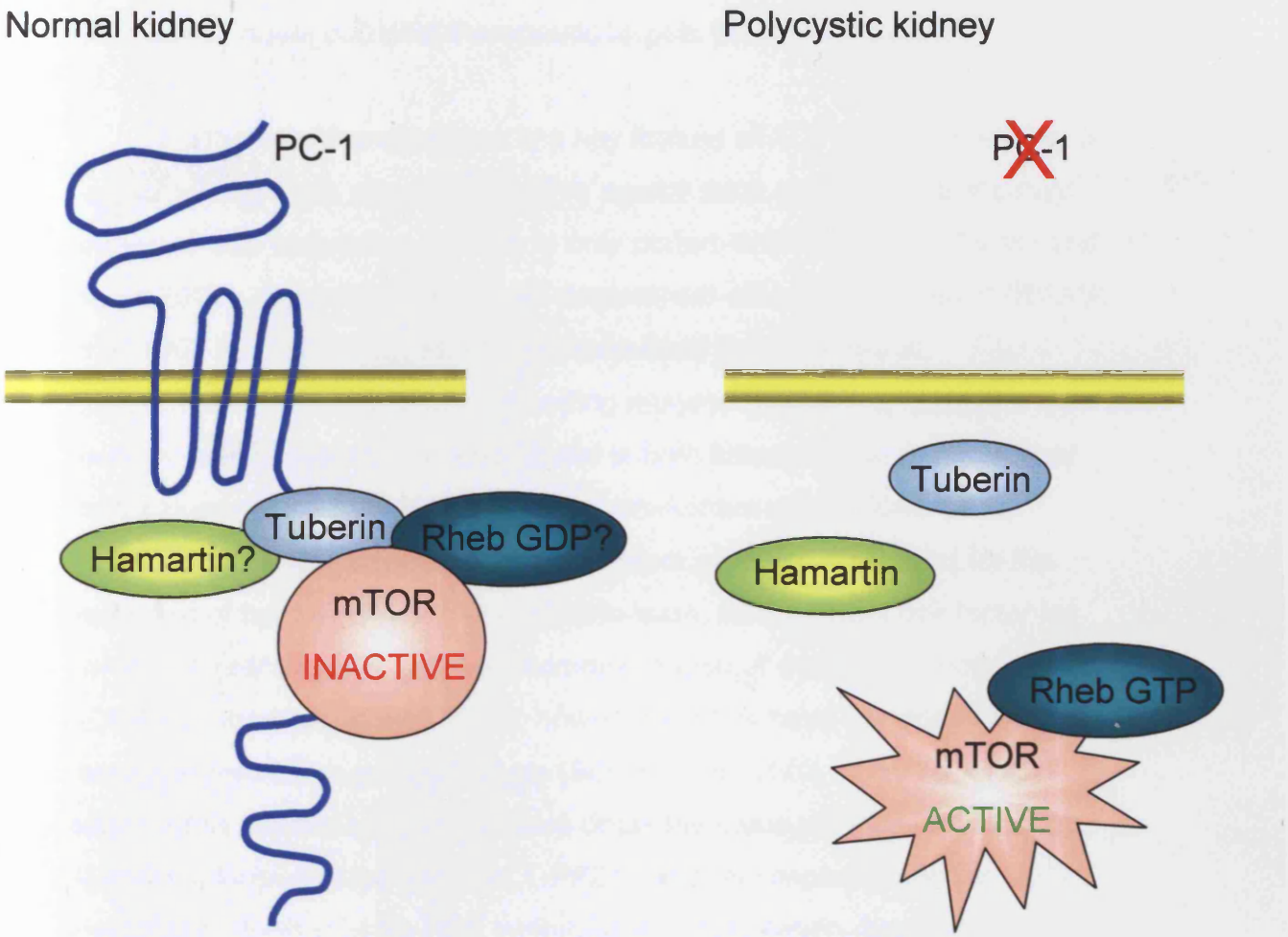

Figure 1.8 Model of the possible regulation of mTOR by PC1. Interaction data suggests that a function of the PC1 tail may be to assemble a complex with tuberin and mTOR. However, tuberin does not directly interact with mTOR and instead inhibits Rheb, reverting it from active RhebGTP to inactive RhebGDP. This perhaps suggests that Rheb should be part of the PC1/tuberin/mTOR complex, however this has not yet been proven. Another unanswered question is whether hamartin is part of the complex. The hamartin-tuberin interaction appears to be important for the stability of each protein and so the presence of hamartin must be established. When PC1 is mutated, for example in ADPKD patients, the tuberin/Rheb/mTOR complex does not form (or not as efficiently). Under these conditions, tuberin may be subject to phosphorylation by kinases such as Akt or Erk, which destabilise the hamartin/tuberin complex. Without the stable hamartin/tuberin complex, RhebGTP binds to mTOR and the mTOR pathway is rendered constitutively active. Adapted from Mostov 2006.

has stimulated trials of antiproliferative agents such as taxanes and c-myc antisense with satisfactory results in only certain animal models (Torres and Harris 2007). Activation of the renin-angiotensin-aldosterone system (RAAS) in ADPKD has been suggested, with increased levels of rennin, angiotensinogen, angiotensin converting enzyme (ACE), angiotensin II type 1 receptor and angiotensin II being found in both kidney tissue and cyst fluid from patients (Torres *et al.* 1992, Loghman-Adham *et al.* 2004). ACE inhibitors and angiotensin II receptor blockers are frequently used for the treatment of hyperlipidaemia and hypertension, an important risk factor for cardiovascular disease, the most common cause of death in patients with ADPKD (Torres and Harris 2007), however studies have not demonstrated a renoprotective effect of these drugs (Schrier *et al.* 2002, Chapman 2007). To address this issue and asses in more detail the value of RAAS inhibition in ADPKD, a large clinical trial (HALT-PKD) has been implemented to investigate whether using ACE inhibitors and angiotensin receptor blockers in combination is beneficial in comparison with ACE inhibitors alone (Chapman 2007). Rapamycin studies in three rodent models of PKD have shown encouraging results, with a significant reduction in the rate of cyst expansion and improved renal function (Shillingford *et al.* 2006, Tao *et al.* 2005, Wahl *et al.* 2006). Clinical trials of sirolimus and everolimus are now underway (Torres and Harris 2007). EGFR tyrosine kinase inhibitors, mTOR inhibitors, vasopressin V2 receptor antagonists and octreotide are currently the therapies best supported by preclinical studies and are being tested in ongoing ADPKD clinical trials (Table 1.11) (Torres and Harris, 2007, Ibraghimov-Beskrovnaya and Bukanov 2008).

Table 1.11 Summary of existing drugs and potential experimental agents for the treatment of PKD.

System	Drug	Mechanism	Physiological effects	Trial results/status
RAAS	Enalapril	ACE-inhibitor	⇑ RFP ⇑ GFR ⇓ F.F ⇓ Alb/Cr (M>F)	LVH reversal ⇓ Albuminuria
Vasopressin	Mozavaptan (rat) Tolvaptan (human)	V_2-receptor antagonist	⇓ cAMP ⇓ Ras ⇓ ERK	⇓ Disease progression ⇓ Kidney weight ⇓ BUN NA in fibrocystic liver disease
	Water	AVP suppression	⇓ cAMP	⇓ Cyst growth ⇓ Kidney weight ⇑ Renal function
Endothelin	Bosentan	$ET_{A/B}$ receptor antagonist	⇓ MAP ⇑ GFR ⇑ RPF	Acute treatment
	Darusentan LU 224332	$ET_{A/B}$ receptor antagonists (especially ET_A)	⇑ Cyst volume ⇑ Cell proliferation	⇑ Kidney weight (not recommended)
Calcium channel	Verapamil BAPTA-AM	Calcium channel antagonist	⇑ cAMP	
mTOR	Sirolimus Temsirolimus Everolimus	mTOR inhibitor	⇓ Cell proliferation ⇓ Cyst volume ⇓ Renal volume	Phase I and II clinical trials
MEK	PD-098059	MEK inhibitor	⇓ Cell proliferation	
Caspase	IDN-8050	Pan-caspase inhibitor	⇓ Cyst volume ⇓ Kidney size	Reduction in BUN (rat)
Somatostatin	Octreotide	Somatostatin receptor type 2 agonist	⇓ cAMP ⇑ PLC ⇑ Phospholipase ⇓ Cyst growth	6 month clinical trial

AVP = arginine vasopressin, BUN = blood urea nitrogen, cAMP = cyclic adenosine monophosphate, ERK = extracellular signal-regulated kinase, ET = endothelin, F.F = filtration fraction, GFR = glomerular filtration rate, LVH = left ventricular hypertrophy, MAP = mean arterial pressure, MEK = mitogen extracellular kinase, NA = data not available, PLC = phospholipase C, RAAS = rennin-angiotensin-aldosterone system, RPF = renal plasma flow, V_2 = vasopressin, ⇑ indicates increase, ⇓ indicates decrease. Table adapted from Masoumi *et al.* 2007.

The main challenge in ADPKD clinical trials is the utilisation of renal function as the primary outcome measure. Renal function remains normal for decades, and only begins to decline late in the course of the disease when the kidneys are markedly enlarged, obliterated by cysts and unlikely to benefit from potential treatment. Reliable, more sensitive measures of kidney function are required for more beneficial early intervention trials. Results from the CRISP (Consortium for Radiologic Imaging Studies of PKD) study indicate that the rate of renal growth is a good indicator of kidney function decline, and justifies the measurement of kidney volume by MRI as a reliable indicator of clinical outcome.

1.2.10 PKD models

Animal models of PKD have been critical in supporting studies of disease pathogenesis and in testing potential therapies. For extensive reviews please refer to Guay-Woodford 2003 and Torres and Harris 2007. Murine PKD models have arisen from spontaneous mutations, random mutagenesis, transgenic technologies and gene-specific targeting and generally resemble human ARPKD or ADPKD with respect to renal cyst pathology and disease progression (Guay-Woodford 2003). For example, those models that display cysts distributed along the entire nephron, extra-renal manifestations and slower disease progression most closely resemble the human ADPKD phenotype (Guay-Woodford 2003).

Although there are a number of spontaneous animal models of PKD, none are due to mutations in *Pkd1* or *Pkd2* (Torres and Harris 2007). Table 1.12 lists many of these models, including the *jcpk* (Flaherty *et al.* 1995) and *orpk* (Moyer *et al.* 1994) mouse models which arose from chemical and insertional mutagenesis programmes respectively. Several of them, particularly the *cpk*, *bpk*, *orpk* and *pcy* mice and the *Han:SPRD* and *pck* rats, have been used to test potential therapies (Torres and Harris 2007). In general, the ideal model for this purpose should carry a mutation in an orthologous gene to the human disease-carrying gene and reproduce the typical phenotype of human ADPKD or ARPKD, however few, if any, meet these requirements (Torres and Harris 2007). For example, the *cpk* (Fry *et al.*

1985, Preminger *et al.* 1982) and *bpk* (Nauta *et al.* 1993) mice present with a phenotype resembling ARPKD, however they are caused by mutations in *Cys1* and *Bicc1* respectively, genes which are not known to be associated to human ARPKD pathology (Hou *et al.* 2002).

Table 1.12 Murine models of PKD.

Model	Inheritance	Gene	Protein	Renal pathology	Extra-renal pathology	Progression	Human homologue
Mouse							
cpk	AR	*Cys1*	Cystin	PT⇒CD	BD, P	Rapid	?
bpk	AR	*Bicc1*	Bicaudal C	PT⇒CD	BD	Rapid	?
jcpk	AD/AR	*Bicc1*	Bicaudal C	GI/all tubules	BD	Slow/rapid	?
orpk	AR	*TgN737*	Polaris	PT⇒CD	BD, PD	Rapid	?
inv	AR	*Invs*	Inversin	PT⇒CD	BA, P, SI	Rapid	*NPH2*
jck	AR	*Nek8*	Nek8	C, OM	-	Slow	?
kat	AR	*Nek1*	Nek1	GI, PT	FD, MS, HC, An	Slow	
pcy	AR	*Nphp3*	Nephro-cystin-3	CD, nephron	ICA	Slow	*NPH3*
Rat							
Han: SPRD-cy	AD/AR	*Pkdr1*	SamCystin	PT	L	Slow	?
wpk	AR	*Mks3*	Meckelin	PT⇒CD	HC	Rapid	*MKS3*
pck	AR	*Pkhd1*	Fibrocystin	CD, DN	BD	Slow	*PKHD1*

Cpk = congenital polycystic kidneys, *bpk* = BALB/C polycystic kidneys, *jcpk* = juvenile congenital polycystic kidney, *orpk* = Oak Ridge polycystic kidney, *inv* = inversion of embryonic turning, *jck* = juvenile cystic kidney, *kat* = kidney, anaemia, testis, *pcy* = polycystic kidney disease, *wpk* = Wistar polycystic kidneys, *pck* = polycystic kidneys, AR = autosomal recessive, AD = autosomal dominant, PT = proximal tubule, CD = collecting duct, GI = glomeruli, C = cortex, OM = outer medulla, DN = distal nephron, BD = biliary dysgenesis, P = pancreatic cysts or fibrosis, PD = polydactyl, BA = biliary atresia, SI = *situs inversus*, ICA = intracranial aneurysm, FD = facial dysmorphism, MS = male sterility, HC = hydrocephalus, An = anaemia. Information and references from Guay-Woodford 2003, Torres and Harris 2007.

Mice with targeted mutations of *Pkd1* or *Pkd2* have been created (Table 1.13); however, the renal phenotype in heterozygous animals is often normal or only very mild, with cystic change late in life (Ibraghimov-Beskrovnaya and Bukanov 2008). Homozygous animals develop renal and pancreatic cysts at E15.5, however death occurs perinatally (Guay-Woodford 2003). Exceptions to the mild cystic phenotype include those models with a hypomorphic *Pkd1* allele such as $Pkd1^{nl}$ (Lantinga-van Leeuwen *et al.* 2004) and $Pkd1^{L3}$ (Jiang *et al.* 2006) which results in a low expression of PC1, thus preventing homozygous lethality. These mice develop polycystic kidney disease within the first month after birth, however the variability of the phenotype limits their usefulness for therapeutic trials. The $Pkd2^{-/WS25}$ mouse (Lakshmanan and Eysselein 1993) with one null allele and one unstable allele (WS25) develops renal and liver cysts within 3 months, however, due to a very high degree of phenotypic heterogeneity in combination with difficulties in measuring disease progression, this model is more suitable as a secondary confirmatory model in therapeutic testing (Torres and Harris 2007).

As previously mentioned, murine models with a simple targeted mutation in *Pkd1* or *Pkd2* develop very mild renal cystic disease, therefore making them unsuitable for therapeutic testing (Ibraghimov-Beskrovnaya and Bukanov 2008), however, they may provide an insight into early cystogenesis events. The $Pkd1^{del17\text{-}21\beta geo}$ mouse (Boulter *et al.* 2001) carries a truncating mutation in the *Pkd1* gene, replacing exons 17-21 with a *lacZ-neomycin* fusion gene (*βgeo*) downstream of a splice acceptor site and an internal ribosome entry site (IRES). The resulting transcript is predicted to encode a truncated form of PC1, which includes only the extracellular domains up to and including the PKD repeats, and thus represents a common class of mutation found in ADPKD patients.

Table 1.13 Mouse models with *Pkd1* and *Pkd2* targeted mutations.

Strain	Mutation	*Pkd1*$^{-/-}$	K/P cysts	Cardiovascular defects	Oedema	Skeletal defects	*Pkd1*$^{+/-}$
Pkd1^{del34}	Exon 34 deletion	Lethal/ perinatal	K, P	None	Yes	Yes	K, L, P cysts
Pkd1^{null}	Exon 4 insertion	Lethal	K, P	Subcutaneous bleeding seen in <1% of animals	Yes	Yes	K, L, P cysts
Pkd1^{L}	Exon 43-45 deletion	Lethal	K, P	Vascular leak	Yes	n.d.	n.d.
Pkd1$^{del17-21\beta geo}$	Exon 17-20 deletion	Lethal	K	Conotruncal defects	Yes	Yes	K, L cysts
Pkd1^{-}	Exon 2-4 deletion with in-frame *lacZ*	Lethal	K, P	Double outlet right ventricle	Yes	n.d.	n.d.
Pkd1^{-}	Exon 2-6 deletion	Lethal	K	Conotruncal defects	Yes	n.d.	n.d.
Pkd1^{-}	Exon 1 disruption	Lethal	K, P	n.d	Yes	n.d.	K, L cysts
Pkd1^{-}	Point change due to ENU mutagenesis	Lethal	K	n.d.	Yes	n.d.	K, L, P cysts
Pkd1^{nl}	Insertion of neo cassette in intron 1, aberrant splicing	Viable. 40% at 1 month, 10% >1 year	K, P	Aorta aneurysms	No	n.d.	No cysts
Pkd1^{L3}	Aberrant transcription and/or splicing	Viable. 50% at 1-2 months, 10% >1 year	K, P	n.d.	No	n.d.	No cysts
Pkd1^{cond}	Exon 2-4 *MMTV.Cre*	Viable	K (few)	None	No	No	No cysts
Pkd2^{-}	Exon 1 disruption	Lethal	K, P	Yes	Yes	n.d.	K, L cysts
Pkd2^{WS25}	Exon 1 duplication. Unstable allele	Viable	K, P	n.d.	n.d.	n.d.	K cysts
Pkd2^{LacZ}	Exon 1 deletion with LacZ promoter trap	Lethal	K, P	Yes	Yes	Yes	n.d.

Pkd1$^{-/-}$ = homozygous for the targeted mutation, *Pkd1*$^{+/-}$ = heterozygous for the targeted mutation, ENU = N-ethyl-nitrosourea, K = kidney, L = liver, P = pancreas, n.d. = not described. Information and references obtained from Guay-Woodford 2003, Torres and Harris 2007, Zhou and Pei 2008.

As with other *Pkd1* and *Pkd2* targeted mouse models, homozygous *Pkd1*$^{del17\text{-}21\beta geo}$ embryos died before birth at E13.5-E14.5. The cause of death is believed to be from a primary cardiovascular defect that includes double outflow right ventricle, disorganised myocardium and abnormal atrio-ventricular septation. Although skeletal abnormalities have not been recognised in ADPKD patients, skeletal development in homozygous embryos was found to be severely compromised, with abnormal axial skeleton and long bones found.

Approximately 50% of *Pkd1*$^{del17\text{-}21\beta geo}$ heterozygous (*Pkd1*$^{del17\text{-}21\beta geo/+}$) mice developed renal cysts by 9 months of age and cysts were detected as early as 3 months. Indicative of ADPKD, cysts arose throughout the nephron and were often lined with hyperplastic cells or apoptotic cells. Liver cysts, another feature of human ADPKD, were found occasionally in heterozygous mice from 19 months of age. *Pkd1* expression was found to correlate well with the onset of renal cyst formation in other *Pkd1* mouse models, with a low expression prior to E15.5, and a dramatic increase in the differentiating tubules of the nephron and collecting duct system from E15.5 to E18.5. *Pkd1* was also expressed highly throughout the cardiovascular system, with highest levels in the aortic outflow tract and atrial appendages and in the endothelial and vascular smooth muscle cells of the major vessels including the aorta and intracranial arteries. Cardiovascular defects are a major feature of ADPKD and are often the most lethal. Combined with the lethal cardiovascular phenotype of *Pkd1*$^{del17\text{-}21\beta geo}$ null mice, this expression pattern suggested a role for PC1 in cardiovascular development.

1.3 Primary cilia

The first documented mention of ciliary structures occurred as far back as 1676 by Antony van Leeuwenhoek in a letter sent to the Royal Society of London describing his discovery of protozoa with cilia and flagella (Haimo and Rosenbaum 1981). For the next 200 years cilia and flagella were found on a variety of cells and theories began to be developed to explain flagellar beating. It was not until 1954 when, thanks to the development of the electron microscope, the internal structure of the cilium was described (Fawcett and Porter 1954).

1.3.1 Ciliary localisation and structure

Cilia (and flagella, which are distinguished by distinctive patterns of movement) are microtubule based hair-like organelles that protrude from the apical surface of most types of eukaryotic cell, with the exception of higher plants and fungi (Bisgrove and Yost 2006). Exceptions within the body include mucosal epithelium of the gut, hepatocytes and small lymphocytes (Wheatley *et al.* 1996). Although cilia are extensively found in vertebrate cells, they are restricted to sensory neurons in invertebrates (Wheatley *et al.* 1996). For a complete list of ciliated cells please visit http://www.bowserlab.org/primarycilia/cilialist.html.

Structurally, the cilium consists of nine peripheral microtubule doublets, the axoneme, covered by a specialised plasma membrane that extends from the cell surface into the extra-cellular space (Figure 1.9) (Davenport and Yoder 2005). The microtubule doublets emerge from the nine triplet microtubules of the basal body (the elder centriole in a centrosome), which anchors the cilium to the cell and acts as a microtubule-organising centre (Simons and Walz 2006). There is a transition zone at the junction of the basal body and the ciliary axoneme consisting of Y-shaped fibres which, in combination with the internal structure of the basal body, functions as a filter for the cilium (Bisgrove and Yost 2006). The distal tips of cilia link the ends of the axonemal microtubules to the ciliary membrane, thus forming a microtubule-capping structure (Sloboda 2005).

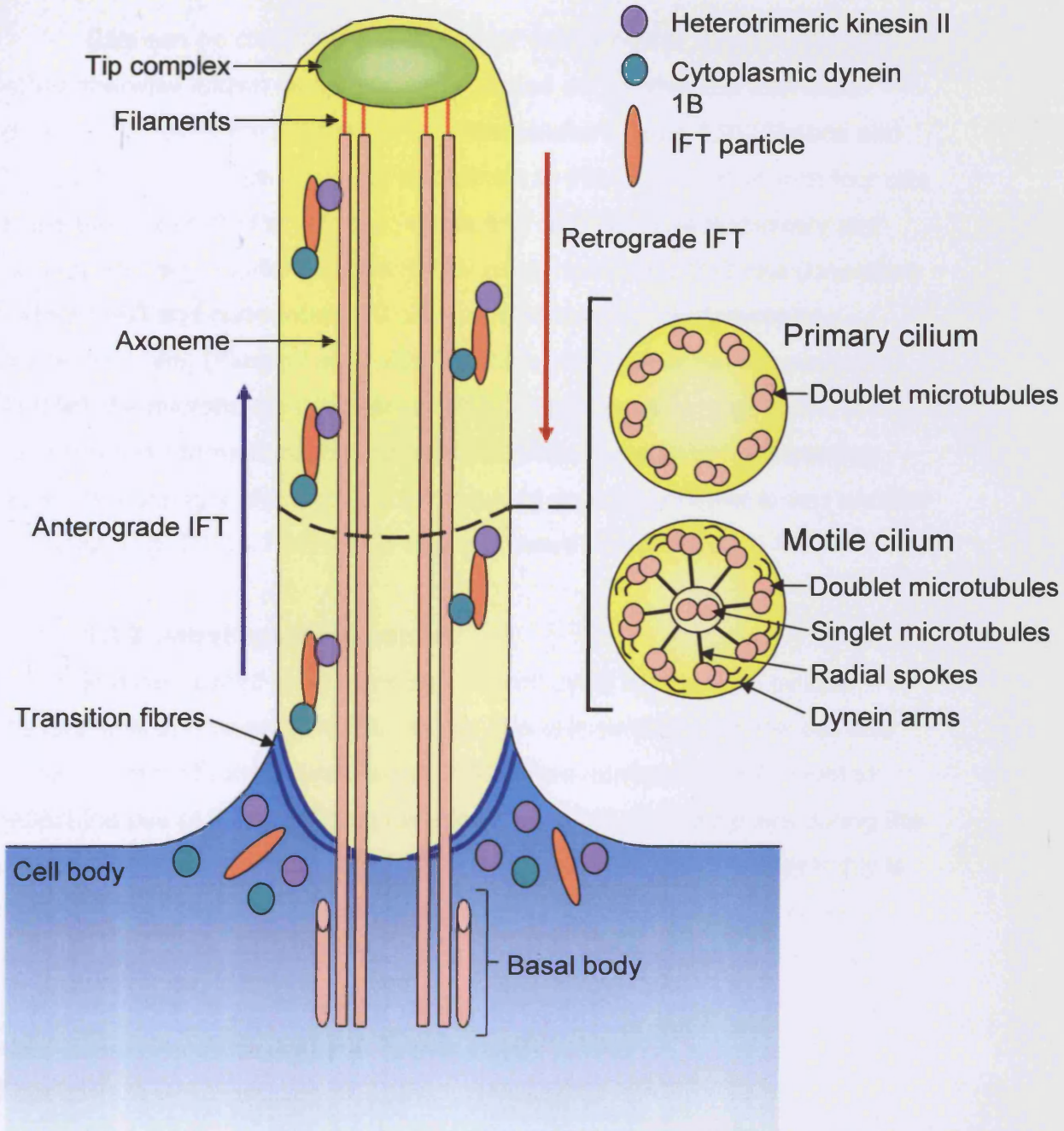

Figure 1.9 Cilia structure and intraflagellar transport (IFT). A typical cilium consists of an axoneme of nine microtubule doublets which arise from the nine triplet microtubules of the basal body (the elder centriole in a centrosome). The transition zone at the junction of the basal body and the ciliary axoneme consists of Y-shaped fibres and functions as a filter for the cilium. The distal tips of cilia link the ends of the axonemal microtubules to the ciliary membrane, thus forming a microtubule tip complex. Motile cilia generally have a central pair of microtubule singlets as well as outer dynein arms which are important for ciliary motility. These features are generally absent from primary cilia. Ciliary assembly and maintenance is accomplished by IFT, which relies on the microtubule motor proteins kinesin II and cytoplasmic dynein to transport IFT particles and their associated cargo up and down the length of the cilium. At the ciliary tip, anterograde cargo is unloaded, turnover cargo is picked up, the kinesin II motor is inactivated for transport back to the cytoplasm, and cytoplasmic dynein is activated to power the retrograde trip back to the cytoplasm.

Cilia can be classified as either '9+2' motile cilia or '9+0' non-motile cilia (otherwise known as primary cilia), based on whether the axoneme includes an additional central pair of microtubules (Figure 1.9) (Simons and Walz 2006). There are of course exceptions to this classification with four cilia types being identified in humans: motile 9+2 cilia (such as respiratory and ependymal cilia), motile 9+0 cilia (nodal cilia), non-motile 9+2 cilia (kinocilium of hair cells) and non-motile 9+0 cilia (renal monocilia, photoreceptor-connecting cilia) (Fliegauf *et al.* 2007). Motile cilia usually have dynein arms that link the microtubule doublets, exerting ciliary movement by ATP-dependent conformational changes and transient binding to neighbouring doublets, leading to the sliding of microtubule doublets relative to one another (Fliegauf *et al.* 2007). Non-motile cilia lack these dynein arms.

1.3.2 Intraflagellar transport

In most ciliated cells, entry into the cell-cycle is preceded by cilia disassembly and resorption, followed by cilia reassembly once the cell has exited mitosis (Quarmby and Parker 2005). This relationship is thought to reflect the use of the basal body/centrioles as mitotic spindle poles during the cell-cycle (Quarmby and Parker 2005). Cilia disassembly and reassembly is carried out by a specialised microtubule based conveying system called intraflagellar transport (IFT) (Figure 1.9, reviewed extensively in Scholey 2003), an essential process considering cilia are devoid of ribosomes and so cannot make their own proteins (Yoder 2007).

IFT was first identified in *Chlamydomonas* as the rapid bidirectional movement of particles along the length of the flagellar axoneme on raft-like transport structures located between the outer doublet microtubules and the axoneme membrane (Kozminski *et al.* 1993). Ciliary proteins and transport 'rafts' are assembled at the base of the cilia near the transition fibres and basal body into complexes called IFT particles (Davenport and Yoder 2005). These particles are then transported in an anterograde manner toward the tip of the axoneme by the action of the heterotrimeric kinesin II motor complex (Kif3a, Kif3b and Kap3 in mammalian systems) (Kozminski *et al.* 1993, Davenport and Yoder 2005). Once the particle reaches the tip of the cilia

axoneme, it undergoes a poorly understood transition resulting in inactivation of the kinesin and the retrograde return of the raft to the base of the cilium via a cytoplasmic dynein motor protein (Davenport and Yoder 2005). Because cilia lack the ability to carry out protein synthesis, IFT is thought to be essential for transporting proteins required for cilia assembly, maintenance and sensory and signalling functions to their location in the axoneme, as well as delivering signals from the cilium in response to external environmental stimuli (Wang *et al.* 2006, Yoder 2007).

1.3.3 Physiological functions of cilia

In mammals, motile cilia are normally found in large numbers and beating in a coordinated wave on the apical surface of epithelial cells (Yoder 2007). Examples include motile cilia lining the trachea, where they sweep mucus and dirt out of the lungs, ependymal cells of the brain ventricles involved in cerebrospinal fluid movement, and the Fallopian tubes, where they move the ovum from the ovary to the uterus (Eley *et al.* 2005). An exception to the usual 9+2 motile cilia structure is the solitary nodal cilium. Although motile, nodal cilia have a 9+0 microtubule arrangement, and are present in the embryonic node where they act as a specialised signalling structure in the early mammalian embryo (Yost 2003). The circular twirling of these cilia generates a leftward flow of extraembryonic fluid which is essential for the correct development of left-right asymmetry (i.e. ensuring the heart is on the left of the body whilst the liver is on the right) (Nonaka *et al.* 2005).

In contrast, primary cilia are solitary, non-motile organelles, present on most cells in the mammalian body, including specialised cells such as olfactory cells and rod and cone cells in the retina. During olfaction, odorants bind to olfactory receptors on the ciliary membrane of olfactory sensory neuron cilia, causing an increase in Ca^{2+} inside the cilia, an effect that is converted into an electrical signal (Menini 1999). Photoreception involves rod and cone photoreceptors which possess a primary cilium that transports photoreceptor discs and visual pigments to an expanded tip called the outer segment where the reception and transduction of light can occur (Singla and Reiter 2006). These functions clearly demonstrate the chemo- and

photosensation properties of primary cilia, thus allowing a cell or an organism to interact with and respond appropriately to its environment. Primary cilia lining renal tubules may also have a chemosensory function, extending from the apical cell surface into the tubule lumen where they can sense specific ligands and transmit this information to surrounding cells (Zhang *et al.* 2004). However, perhaps the most interesting function of these renal primary cilia is their role as a mechanosensor, detecting fluid flow (urine) through the lumen of the tubule. This detection involves deflection of the cilium in response to fluid flow, quickly followed by an influx of extracellular Ca^{2+}, probably mediated by PC1 and PC2 (Praetorius and Spring 2001 & 2003, Nauli *et al.* 2003). Nauli *et al.* (2003) proposed that PC1 and PC2 function in this Ca^{2+} response by the large extracellular domain of PC1 sensing fluid shear stress as the cilia bends, thus acting as a mechano-fluid sensory molecule, then transmitting this mechanical stress signal to tightly associated PC2, which in turn produces sufficient extracellular Ca^{2+} influx to trigger intra-organellar Ca^{2+} release inside the cytoplasm through Ca^{2+} induced Ca^{2+} release (Figure 1.10). The resulting local increase in the cytosolic Ca^{2+} concentration may then alter various cell functions such as growth, differentiation, gene expression and polarity.

In addition to functioning as a calcium influx inducing mechanosensor, deflection of the cilia axoneme and the polycystins has effects on gene expression. In the presence of normal flow conditions, PC1 localises to the primary cilium in association with STAT6 and P100, thus preventing the expression of STAT6/P100-dependent genes (Figure 1.6a) (Low *et al.* 2006). However, when fluid flow is impeded for example from renal injury, the C-terminal tail of PC1 is proteolytically cleaved and translocates to the nucleus with STAT6 and P100 to activate target genes (Figure 1.6b) (Low *et al.* 2006). As previously mentioned (section 1.2.8.3.1), if PC1 is absent, for example during ADPKD, STAT6 and P100 are no longer sequestered in the cilium, and may be constitutively activated in the cell nucleus (Figure 1.6c) (Low *et al.* 2006). Similarly, when primary cilia, PC1 or PC2 are absent or inhibited, Ca^{2+} influx is impeded, demonstrating the importance of this organelle in Ca^{2+} mediated signalling (Nauli *et al.* 2003).

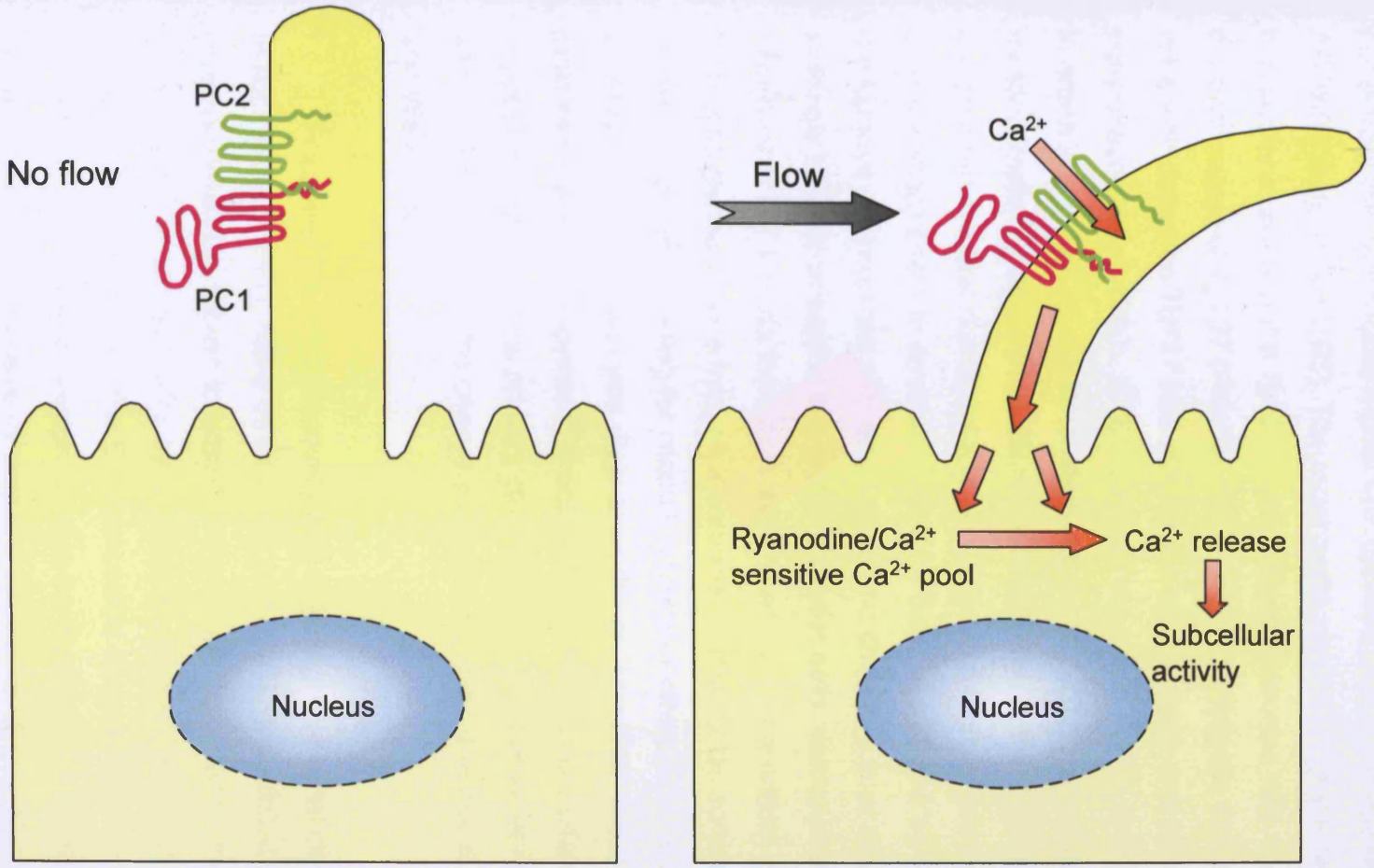

Figure 1.10 Schematic diagram of mechanisms of fluid shear stress and Ca^{2+} signalling in primary cilia. PC1 and PC2 physically interact to form a mechanosensory complex at the plasma membrane of primary cilia which act as antennae to sense fluid movement. The large extracellular domain of PC1 acts as a sensory molecule which senses fluid shear stress, transmitting this signal from the extracellular fluid environment to PC2, which, in turn, produces sufficient Ca^{2+} influx to activate intracellular ryanodine receptors through Ca^{2+}-induced Ca^{2+} release (CICR). The resulting local increase in the cytosolic Ca^{2+} concentration then regulates numerous molecular activities inside the cell that contribute to tissue development. When fluid flow is absent, the cilium does not bend, therefore no Ca^{2+} influx is triggered due to the lack of fluid shear stress acting on PC1. Information obtained from Nauli *et al.* 2003.

1.3.4 The ciliary hypothesis of cyst formation

The first clue that cilia might be involved in the pathogenesis of PKD came from the *orpk* mouse model with disease phenotypically resembling ARPKD (Yoder *et al.* 1995). The renal cystic phenotype is the result of a hypomorphic allele of the *Tg737* gene. *Chlamydomonas* with mutated IFT88, the homologue of *Tg737* (Polaris), fail to assemble flagella and similarly, *orpk* mice with defective *Tg737* lack cilia on the ventral node and tubular epithelial cells (Pazour *et al.* 2000). IFT88 is one of the components of the IFT complex in green algae (Qin *et al.* 2001). Mice with a *kif3a* (subunit of the IFT kinesin II motor complex) knockout specifically in the kidney (conventional knockouts are embryonic lethal due to defects in cardiac looping and left-right axis determination) begin to develop cysts by 5 days of age and by 5 weeks of age the kidneys are replaced with large cysts and fibrosis (Lin *et al.* 2003). Most strikingly cilia are absent in the cystic epithelial cells, demonstrating the necessity of IFT for cilia formation. More evidence for a critical role of cilia in PKD cystogenesis came from an insertional mutagenesis screen in zebrafish, in which 7 genes encoding for ciliary functions or ciliogenesis were among 11 isolates with pronephric cysts (Sun *et al.* 2004). Together, these findings indicated that IFT is important for both flagella and primary cilia formation, and suggested that functional primary cilia are linked to normal renal function, which ultimately led to the ciliary hypothesis of cystic disease in PKD (Simons and Walz 2006).

Following the initial discovery that defects in the renal cilium are associated with PKD, many other cystic kidney disease-related proteins (cystoproteins) have been localised to the renal cilium and/or the basal body (refer to Davenport and Yoder 2005, Hildebrandt and Otto 2005 for extensive reviews). *Lov-1* and *pkd-2*, the *Caenorhabditis elegans* homologues of *PKD1* and *PKD2*, were the first cystoproteins to be identified in the cilia and cell bodies of male specific sensory neurons (Barr *et al.* 2001). Mammalian PC1 and PC2 were subsequently localised to renal tubule epithelial cell primary cilia (Yoder *et al.* 2002), followed by many other cystoproteins, providing increasing evidence for the ciliary connection to cystic kidney disease (Table 1.14). Recently, hamartin was localised to the basal body of mouse embryonic

fibroblasts (MEFs), highlighting an intriguing link between TSC and primary cilia (Hartman *et al.* 2009).

Table 1.14 Cystoproteins localised to the primary cilium/basal body complex.

Gene (protein)	Genetic disease	Disease phenotype	Protein function	Ciliary expression
PKD1 (PC1)	ADPKD	Kidney, liver and pancreatic cysts, cardiac defects.	Mechanosensitive and G protein-coupled receptor.	Basal body and cilia
PKD2 (PC2)	ADPKD	Kidney, liver and pancreatic cysts, cardiac defects.	TRP-like non-selective cation channel permeable to Ca^{2+}. Involved in mechanosensation.	Cilia
PKHD1 (fibrocystin/ polyductin)	ARPKD	Kidney and liver cysts. Liver fibrosis.	Unknown. Transmembrane protein, perhaps mechanosensitive regulator?	Basal body and cilia
NPHP1 (nephrocystin)	Type I nephronophthisis (juvenile form)	Kidney cysts and fibrosis, liver fibrosis, growth retardation, retinal dystrophy.	Docking protein.	Cilia
NPHP2 / INVS (inversin)	Type II nephronophthisis (infantile form)	Kidney cysts and fibrosis, liver fibrosis.	Unknown. Interacts with nephrocystin.	Cilia
NPHP3 (nephrocystin-3)	Type III nephronophthisis (adolescent form)	Kidney cysts and fibrosis.	Unknown. Interacts with nephrocystin.	Cilia, retinal connecting cilium
NPHP4 (nephroretinin)	Type IV nephronophthisis (juvenile form)	Kidney cysts and fibrosis, growth retardation, retinitis pigmentosa.	Unknown. Interacts with nephrocystin.	Cilia
NPHP5 (nephrocystin-5)	Senior-Loken syndrome type I	Renal cysts, retinitis pigmentosa.	Unknown. Interacts with retinitis pigmentosa GTPase regulator and calmodulin within the photoreceptor cilia.	Cilia, retinal connecting cilium
OFD1 (OFD1)	Oral-facial-digital syndrome type1	Renal cysts, malformations in the oral cavity, face and digits, cognitive defects.	Unknown. Implicated in IFT and intracellular transport processes.	Basal body

Table 1.14 Cystoproteins localised to the primary cilium/basal body complex (continued).

BBS1-8 (BBS1-8)	Bardet-Biedl syndrome	Kidney cysts, obesity, anosmia, retinal dystrophy, *situs inversus*.	Several BBS proteins may be related to regulation of IFT and intracellular microtubule transport processes	Basal body and cilia
TSC1 (Hamartin)	TSC	Kidney cysts and AMLs, brain and skin lesions. Seizures.	Functions in the mTOR pathway when bound to tuberin.	Basal body
Tg737 (polaris)	Unknown	Mouse: kidney cysts resembling ARPKD, hydrocephalus, polydactyly, *situs inversus*.	IFT complex B protein.	Cilia and basal body
CYS1 (cystin)	Unknown	Mouse: similar to ARPKD. Renal cysts, congenital hepatic fibrosis, biliary dysgenesis	Unknown. May be associated with microtubule stabilisation and/or tubuloepithelial differentiation within the developing kidney and liver.	Cilia
NEK1 (Nek1/kat)	Unknown	Mouse: kidney cysts resembling ADPKD, facial dysmorphism, growth retardation, anaemia, male infertility.	NIMA kinase family member. Interacts with PKD proteins, cell-cycle regulation?	Basal body and cilia
NEK8 (Nek8/jck)	Unknown	Mouse: slowly progressive renal cysts resembling ARPKD.	NIMA kinase family member. Involved in cell-cycle regulation.	Basal body and cilia
KIF3a (Kif3a)	Unknown	Mouse: Kidney cysts, retinal dystrophy, *situs inversus*.	Subunit of the anterograde IFT motor protein kinesin II.	Cilia

BBS = Bardet-Biedl syndrome, *KIF3* = kinesin superfamily 3, *NEK* = NIMA-related kinase, NIMA = a cell-cycle regulated β-casein kinase encoded by *nimA* (*nim* = 'never in mitosis'), *NPHP* = nephronophthisis, *OFD1* = orofaciodigital syndrome 1, *PKHD1* = polycystic kidney and hepatic disease 1. Data and references obtained from Nauli and Zhou 2004, Hildebrandt and Otto 2006, Bisgrove and Yost 2006.

1.3.5 Pathogenic mechanisms

The pathogenic link between primary cilia localised cystoproteins and the renal cystic phenotype remains unknown. Nevertheless hypotheses have been proposed using knowledge of the mechanosensory function of primary cilia, the role of centrosomes in cell-cycle regulation and the multitude of proteins localised to the primary cilia/basal body complex. As previously mentioned (section 1.3.3), Ca^{2+} influx following flow mediated bending of the primary cilium is believed to mediate subcellular activities such as expression of STAT6/P100 activated target genes involved in cell growth regulation (Low *et al.* 2006). Defects/absence of primary cilia, restricted fluid flow or lack of sensory proteins such as PC1 and PC2 can lead to incorrect activation of the pathway and potential uncontrolled cell growth (Low *et al.* 2006, Nauli *et al.* 2003).

1.3.5.1 Cilia and cell-cycle regulation

Recent data has further highlighted the possibility that ciliary proteins may play a more direct role in cell-cycle regulation (reviewed in Pan and Snell 2007). The cilium is assembled during the G0 phase of the cell-cycle and originates from the basal body, which emerges from one of the two centrioles that together constitute the centrosome. Entry into the cell-cycle is preceded by cilia disassembly and resorption, at which point the basal body converts back into a centriole which then duplicates to form two centrosomes that form the poles of the mitotic spindle apparatus. Once the cell has exited mitosis, the centrosomes migrate towards the apical membrane where the mother centriole gives rise to the basal body, followed by cilia assembly. This close association between primary cilia and the centrosome/basal body led to hypotheses that the cilium is involved in cell-cycle regulation. It is thought that the presence of a primary cilium prevents the cell from entering mitosis until it is disassembled, freeing up the centrioles for cell division, however, a direct molecular link between cilia and the cell-cycle remains elusive (Quarmby and Parker 2005).

Recently, data has suggested that IFT proteins may play a role in regulating cell proliferation. IFT88/polaris has been found to localise to the

centrioles throughout the cell-cycle (Robert *et al.* 2007). Overexpression of IFT88/polaris interferes with G1-S transition, whereas depletion of the protein causes cilium disappearance and cell-cycle progression to the S and G2/M phases with an increase in proliferation (Robert *et al.* 2007). A reduced level of IFT27 also appears to effect cell-cycle control, resulting in cell growth inhibition and incomplete or asymmetrical cytokinesis (Qin *et al.* 2007).

Members of a cell-cycle kinase family, the Nek kinases (or NIMA-related kinases), provide a link between ciliary function and cell-cycle control. Nek1, deficiency of which leads to ARPKD in mice (Table 1.14), has been found to interact with Kif3a and localises to the centrosome (Mahjoub *et al.* 2005, Surpili *et al.* 2003). Targeted knockdown of Nek8 in zebrafish causes pronephric cysts and *Nek8* mutant mice have juvenile cystic kidney (JCK) disease (Upadhya *et al.* 2000, Liu *et al.* 2002). Nek8 localises to primary cilia during interphase and is undetectable during mitosis (Mahjoub *et al.* 2005). Cell cycle progression has been found to be affected in a cell line with a kinase domain mutation of Nek8 (Bowers and Boylan 2004). These observations provide interesting insight into the connection between primary cilia, cell-cycle kinases and control of the cell-cycle.

Another link between cilia and the cell-cycle is inversin, encoded by the gene *INVS*, mutations of which cause Type II nephronophthisis characterised by cystic kidneys and *situs inversus* (Table 1.14) (Otto *et al.* 2003). Inversin interacts with the anaphase-promoting complex protein APC2 which regulates cell cycle progression by selectively degrading checkpoint proteins such as cyclin B (Morgan *et al.* 2002, Nürnberger *et al.* 2002). Inversin has been found to have a cell-cycle dependent dynamic pattern of expression during mitosis, localising to primary cilia, basal bodies, the nucleus, and the cell-cell borders during interphase and to the spindle poles during mitosis (Morgan *et al.* 2002, Nürnberger *et al.* 2002). As the centrosomes are shared by mitotic spindles and cilia, it has been proposed that they integrate cilia-sensed signals into cellular pathways that affect proliferation and differentiation (Simons and Walz 2006).

1.3.5.2 Cilia and Wnt signalling

Successful development of the mammalian kidney is dependent upon many signalling pathways, with the Wnt signalling pathway being particularly important in the induction of the metanephric mesenchyme to form S- and comma-shaped epithelial tubes that are precursors of proximal parts of the nephron including the glomerulus (Simons and Walz 2006). For example, Wnt-4 and Wnt-11 have both been found to be important in the early stages of renal development during the mesenchymal to epithelial transdifferentiation stage and in regulating proliferation and ureteric bud branching, respectively (Stark *et al.* 1994, Majumdar *et al.* 2003).

As previously mentioned, there are two branches of the Wnt signalling pathway, the canonical β-catenin dependent Wnt pathway (described in section 1.2.8.3.3) and the non-canonical (PCP) Wnt pathway. Dishevelled is located at a decisive branch point, and either activates the canonical Wnt pathway, or the PCP pathway (Nelson and Nusse 2004). Evidence suggests that uncontrolled canonical Wnt signalling during renal development causes PKD, as demonstrated by transgenic overexpression of an activated form of β-catenin in mice which present with increased proliferation and apoptotic rates in cystic epithelia, and a delay in tubular maturation (Saadi-Kheddouci 2001).

A similar renal phenotype has also been found in the *inv/inv* mouse model of nephronophthisis type II, providing a tantalising link between Wnt signalling, cystic kidney disease (a primary feature of the disease) and primary cilia (inversin is localised to this organelle) (Guo *et al.* 2004, Simons *et al.* 2005). The potential role of inversin in Wnt signalling was recently studied in *Xenopus* and zebrafish (Simons *et al.* 2005). Inversin was found to directly interact with Dishevelled (Dsh) and regulate its stability by targeting cytoplasmic Dsh for degradation. This cytoplasmic localisation of Dsh is essential for canonical Wnt signalling where Dsh moves between different subcellular compartments, including the nucleus, cytoplasm and plasma membrane (Itoh *et al.* 2005, Wallingford and Habas 2005). In contrast, within the PCP pathway, Dsh has to be tightly associated with the plasma

membrane (Wallingford and Habas 2005). Inversin was found to not target membrane-bound Dsh pools, indicating that it may negatively regulate the canonical Wnt signalling pathway while promoting PCP signalling. Consistent with this proposed role in PCP signalling, inversin is required for convergent extension movements in gastrulating *Xenopus laevis* embryos and elongation of animal cap explants, both regulated by PCP signalling. In zebrafish, structurally related Diversin ameliorates pronephric cysts caused by the absence of inversin, implying that an inhibition of canonical Wnt signalling is required for normal renal development (Simons *et al.* 2005). Overall, this data suggests that cyst formation in the absence of inversin is caused by unopposed canonical Wnt signalling during permissive periods of renal development. The reversal of cyst formation by Diversin suggests that inversin has an essential role in PCP signalling by permitting the accumulation of Dsh at the plasma membrane (Simons *et al.* 2005).

Perhaps the most important question these results raise is how is the switch between canonical Wnt signalling and PCP signalling regulated? This is where the mechanosensory properties of primary cilia become important, with hypotheses suggesting that the initiation of fluid flow through a newly developed tubule, exposing tubular epithelial cells to shear stress for the first time and thus bending of their primary cilia, may affect the expression of inversin (Simons *et al.* 2005). Indeed, a flow rate equivalent to urine flow upregulated expression of inversin, accompanied by a reduction in β-catenin levels, in inner medullary collecting duct (IMCD) cells (Simons *et al.* 2005). Investigators have therefore speculated that urine flow terminates canonical Wnt signalling to facilitate β-catenin independent Wnt pathways, perhaps to endow tubular epithelial cells with the spatial information important to maintain correct tubular structure such as a constant tubule diameter (Simons *et al.* 2005).

1.3.5.2.1 PCP signalling

The PCP pathway was first discovered and is best understood in the fruit fly *Drosophila melanogaster*, particularly in the wing and the eye (Simons and Mlodzik 2008). PCP is the organisation of cells within the plane

of the epithelium, and is perpendicular to the apical-basal axis (Bacallao and McNeill 2009). An excellent example of this planar orientation is the organisation of actin-based hairs in the Drosophila wing, where a single hair extends from the distal section of each cell and points distally (Simons and Walz 2006). Planar organisation of ommatidia in the fly eye is another key example of PCP, with ommatidia in the dorsal half of the eye pointing dorsally, and those in the ventral half pointing ventrally (Bacallao and McNeill 2009). Ommatidia consist of eight photoreceptor cells and additional accessory cells arranged in a trapezoidal shape and when mutations in PCP genes occur, planar organisation is lost and ommatidia become randomly orientated (Bacallao and McNeill 2009). Prominent vertebrate examples of PCP signalling include neural tube closure, body hair orientation and the organisation of stereocilia bundles in the organ of Corti in the inner ear (Simons and Walz 2006). A role for PCP in the kidney has also been suggested, where it is believed to govern the orientation of cell division in renal tubule epithelial cells, thus maintaining a constant tubule diameter as the tubule grows (Germino 2005) (this is one of the main subjects of this thesis and will be discussed in more detail in chapter 6).

Genetic and biochemical data, based on characterisation of mutant phenotypes in *Drosophila*, has revealed three evolutionarily conserved groups of PCP genes that work together to coordinate PCP establishment (extensively reviewed in Bacallao and McNeill 2009, Simons and Mlodzik 2008). The first major group is known as the "upstream group" and includes *four-jointed* (*fj*), *Dachsous* (*Ds*), *Atrophin* (*atro*), *Widerborst* (*Wdb*) and *Fat* (*Ft*). These genes are involved in the first steps of establishing the direction of polarity and dictate a global planar polarity stemming from an initial long-range signal (Karner *et al.* 2006). This global planar polarity then biases the asymmetric sub-cellular localisation of the "core proteins" along the proximal/distal axis of the cell (Karner *et al.* 2006). The core group includes the genes *frizzled* (*fz*), *dishevelled* (*dsh*), *prickle* (*pk*), *Vang Gogh* (*Vang*)/*strabismus* (*stbm*), *flamingo* (*fmi*) and *diego* (*dgo*) (Bacallao and McNeill 2009). Dsh, dgo and fz are localised to the distal side of the cell whilst pk and Vang are proximally located. Fmi localises to both proximal and distal

sides of the cell. These genes are involved in establishing the planar polarity of individual cells (Karner *et al.* 2006). Downstream of the core proteins are the PCP effector genes which encode proteins that convert the PCP signal into a physical remodelling of cells (Bacallao and McNeill 2009). These genes are often tissue specific, for example, *inturned*, *fuzzy*, *fritz* and *multiple wing hair* only regulate PCP in the wing, while *nemo* and *unpaired* only regulate PCP in the eye (Bacallao and McNeill 2009). All core PCP proteins are located apically, suggesting that their function requires apical/basal polarity (Djiane *et al.* 2005). Indeed recent studies in *Drosophila* have found a direct molecular link between apical/basal determinants and Fz1-mediated PCP establishment. Work by Djiane *et al.* (2005) found that the Crumbs complex protein dPatj binds Fz1 and recruits aPKC, which in turn phosphorylates Fz1 and inhibits its function. The Crumbs complex is a vital component in the establishment of apical/basal polarity and cooperates with the Par complex in the formation of tight junctions (Karner *et al.* 2006). Although these results indicate an interaction between apical/basal polarity components and PCP components, the precise interplay of these two pathways remains poorly understood.

1.4 Aims

The aims of this project were:

- To investigate potential phenotypic interactions of hamartin and tuberin with PC1 by cross-breeding *Tsc1*$^{+/-}$, *Tsc2*$^{+/-}$ and *Pkd1*$^{+/-}$ mouse models.
- To understand the role of activation of the mTOR pathway in the initiation of renal cystogenesis in TSC and ADPKD using the above mentioned mouse models.
- To examine the integrity of primary cilia in pre-cystic renal tubules and renal cysts from TSC and ADPKD mouse models.
- To investigate the role of PCP in the pathogenesis of TSC and ADPKD by examining the mitotic orientation of pre-cystic renal tubule epithelial cells in *Tsc1*$^{+/-}$, *Tsc2*$^{+/-}$ and *Pkd1*$^{+/-}$ mouse models.

CHAPTER TWO: Materials and methods

2.1 Suppliers

The names and locations of all suppliers whose products were used in this study are listed below:

ABGene (Surrey, UK)
Applied Biosystems (Cheshire, UK)
Bibby Sterling (Staffordshire, UK)
Bioquote (Yorkshire, UK)
Bio-Rad Laboratories Ltd (Hertfordshire, UK)
Bright Instrument Co Ltd (Cambridgeshire, UK)
Carl Zeiss Vision (Hallbergmoos, Germany)
Cell Signalling Technologies (Danvers, MA, USA)
Chemicon International (Now part of Millipore)
DAKO (Cambridgeshire, UK)
EMScope (Kent, UK)
Eurogentec (Hampshire, UK)
Fisher Scientific (Leicestershire, UK)
GE Healthcare (Buckinghamshire, UK)
Genetic Research Instrumentation (GRI) (Essex, UK)
InterFocus Ltd (Cambridgeshire, UK)
Invitrogen Life Technologies (Strathclyde, UK)
JEOL (Tokyo, Japan)
Labtech International Ltd (East Sussex, UK)
Leica Microsystems (Heidelburg, Germany)
Millipore (Hertfordshire, UK)
Motic (Suffolk, UK)
MWG-Biotech (Buckinghamshire, UK)
New England Biolabs (Hertfordshire, UK)
Nikon (Surrey, UK)
Olympus Optical (London, UK)
Qiagen (West Sussex, UK)

Raymond A Lamb Ltd (East Sussex, UK)
Roche Biochemicals (East Sussex, UK)
Santa Cruz Biotechnologies (Santa Cruz, CA, USA)
Sigma-Aldrich (Dorset, UK)
Soft Imaging System GmbH (Münster, Germany)
Starlabs (Buckinghamshire, UK)
TAAB Laboratory and Microscopy (Berkshire, UK)
Thermo Electron Corporation (Middlesex, UK)
Vector Laboratories (Peterborough, UK)
VWR International Ltd (Dorset, UK)

2.2 Materials

2.2.1 Chemicals

Chemicals of analytical grade were supplied by Sigma-Aldrich or Fisher Scientific unless otherwise stated.

2.2.2 Histology

Accu-Edge low profile microtome blades, processing cassettes, paraffin wax and cork disks were purchased from Raymond A Lamb Ltd. Superfrost slides, 22x50mm cover slips, dibutyl phthalate and xylene (DPX) mountant, xylene, formaldehyde, optimum cutting temperature (OCT) embedding compound, haematoxylin and eosin (H&E), hydrogen peroxide and isopentane were purchased from VWR International Ltd. Poly-L-lysine and mineral oil were obtained from Sigma-Aldrich. Ethanol was purchased from VWR International Ltd.

2.2.3 Nucleic acid extraction and purification

QIAamp DNA mini kits, QIAamp DNA micro kits and proteinase K were supplied by Qiagen. Isopropanol was purchased from VWR International Ltd.

2.2.4 Oligonucleotides

HPSF purified oligonucleotide primers were purchased from either MWG-Biotech or Eurogentec and diluted to 100pM in sterile water for stock solutions.

2.2.5 PCR

AmpliTaq Gold DNA polymerase and 10X PCR buffer were purchased from Applied Biosystems. Deoxynucleotidetriphosphates (dNTPs) were from GE Healthcare.

2.2.6 PCR purification

Exonuclease I was purchased from New England Biolabs and shrimp alkaline phosphatase was from GE Healthcare.

2.2.7 Electrophoresis

Multipurpose agarose was obtained from Roche Biochemicals. 1kb DNA ladder was supplied by Invitrogen Life Technologies.

2.2.8 Sequencing and fluorescent product sizing

BigDye® Terminator v3.1 Cycle Sequencing Kit and POP6 polymer were purchased from Applied Biosystems. Montage SEQ_{96} sequencing reaction clean-up kits were purchased from Millipore.

2.2.9 Antibodies

Cell Signalling Technologies supplied the anti-phospho-S6 ribosomal protein ($Ser^{240/244}$) and anti-phospho-histone H3 (Ser^{10}) antibodies. Rhodamine conjugated goat anti-rabbit IgG (H+L) and fluorescein conjugated chicken anti-goat IgG (H+L) were purchased from Chemicon International/Millipore. Tamm-Horsfall glycoprotein (THP) was obtained from Santa Cruz Biotechnologies.

2.2.10 Immunohistochemistry

The rabbit VECTASTAIN ELITE ABC horseradish peroxidase kit and 3,3'-diaminobenzidine (DAB) peroxidase substrate kit were supplied by Vector Laboratories. Bovine albumin fraction V was purchased from VWR International Ltd. Cytomation wax pens were supplied by DAKO.

2.2.11 Immunofluorescence

Fluorescein *Lotus tetragonolobus* lectin (LTL), fluorescein *Dolichos biflorus* agglutinin (DBA) and goat serum were purchased from Vector Laboratories. ProLong® Gold antifade reagent with DAPI was obtained from Invitrogen Life Technologies. Sigma-Aldrich supplied the Triton X-100.

2.2.12 Scanning electron microscopy (SEM)

Phosphate buffered saline (PBS) for perfusion fixation was purchased from Sigma-Aldrich. TAAB Laboratory and Microscopy supplied the 70% vacuum distilled glutaraldehyde, 16% methanol-free formaldehyde, aluminium stubs, carbon paint and hexamethyldisilazane (HMDS).

2.3 Equipment

2.3.1 Plastics

Sterile tips for Gilson pipettes were purchased from Starlabs. Bioquote supplied 0.6ml, 1.5ml and 2.0ml plastic eppendorf tubes. Thermo Life Sciences supplied thermo fast 96 well PCR plates. ABGene provided 0.2ml thermo strip tubes, adhesive PCR film and thermo fast 96 well detection plates. Sterile universal tubes were purchased from Bibby Sterling.

2.3.2 Histology

InterFocus Ltd supplied tweezers and scissors for mouse dissection. Fixed tissue was processed using a Thermo Shandon Citadel 2000 tissue processor and embedded using a Raymond A Lamb Ltd wax embedder. Paraffin sections were cut on a Leica RM2235 microtome and stained with H&E on a Thermo Shandon Varistain Gemini. Frozen sections were cut on a cryostat, and a sledge microtome with freezing stage was used to cut un-embedded fixed tissue, all supplied by Bright Instrument Co Ltd. H&E and immunohistochemistry samples were viewed using an Olympus BX51 BF light microscope or a Motic B3 professional series light microscope.

2.3.3 Immunohistochemistry and immunofluorescence

Raymond A Lamb Ltd provided plastic slide racks, cardboard slide holders and Coplin jars. Immunofluorescent samples were viewed using an

Olympus BX51 BF microscope with mercury lamp attached or a Leica TCS SP2 AOBS spectral confocal laser scanning microscope.

2.3.4 DNA quantification and thermocycling

DNA concentration was measured using a NanoDrop 8-Sample Spectrophotometer purchased from Labtech International. Thermocycling of single tubes was carried out in a DNA thermal cycler 480 from Applied Biosystems. Thermocycling of 96-well plates and strip tubes was carried out in a PTC-225 Peltier thermal cycler from GRI.

2.3.5 Electrophoresis

Agarose gel electrophoresis was carried out using Horizon 11.14 gel tanks from Invitrogen Life Technologies or a 96-well gel apparatus from ABGene. Bio-Rad Laboratories Ltd supplied the power packs. Capillary gel electrophoresis of fluorescent sequencing or PCR products was performed on an ABI 3100 Genetic analyser purchased from Applied Biosystems.

2.3.6 SEM

Dehydrated aluminium stub mounted samples were sputter coated with gold using an EMScope vacuum coater. Prepared tissues were viewed in a JEOL 840A SEM.

2.3.7 Photography

Macroscopic pictures were recorded using a Nikon Coolpix 4500. Agarose gels were photographed using a Gel Doc 2000 ultraviolet (UV) transilluminator from Bio-Rad laboratories Ltd and printed using the Mitsubishi P91 video processor with high-density thermal paper. Micrographs were acquired using a Zeiss Axiocam digital camera purchased from Carl Zeiss Vision.

2.3.8 Software

Fluorescent images were analysed using AxioVision software from Carl Zeiss Vision. AnalySIS software from Soft Imaging System GmbH was used to measure cilia in SEM micrographs. Fluorescent confocal images were

analysed using Leica Confocal Software. Statistics and graphing was carried out using Minitab 15, Microsoft Excel and SPSS 16.

2.4 General solutions

- 1XTAE (0.4M Tris-acetate, 10mM EDTA, pH 8.0)
- 1XTBS (0.15M NaCl, 0.005M Tris, pH 7.6)
- Tail buffer (50mM Tris, 100mM EDTA, 100mM NaCl, 1%SDS, pH 8)
- 1XTBS/0.3% Triton X-100 (For 1L-100ml 10XTBS, 900ml dH_2O, 3ml Triton X-100)
- 10mM sodium citrate buffer (For 1L-2.94g sodium citrate trisodium salt dehydrate, 1L dH_2O, pH 6)
- 10% formal saline (For 1L-100ml 38% w/w formaldehyde, 900ml dH_2O, 9g NaCl)
- Phosphate buffered 4% formaldehyde/0.2% glutaraldehyde (PBFG)
  - Make up buffer solution of 0.167M Na_2HPO_4 and 3.35% sucrose (pH 7.4).
  - Add 10% formaldehyde (prepared from 16% methanol-free stock solution) in a 40:60 ratio with the buffer. This will produce a 4% formaldehyde in 100mM buffer + 2% sucrose solution. The solution will go cloudy and needs to be filtered through a fine paper filter.
  - Add glutaraldehyde (70% vacuum distilled) to 0.2% (2.857ml/L).
  - Aliquot and store at -30°C.

2.5 Methods

2.5.1 Animal husbandry

All procedures with animals were carried out in accordance with Home Office guidelines. Mice were housed in filter top cages and received filtered food and water. Cages were kept at an ambient temperature of 22ºC and maintained on a 12 hour light :12 hour dark cycle (7:30 hours to 19:30 hours). Mice were tagged using microchips and tail tips were cut for genotyping using a local anaesthetic. Mice were killed by cervical dislocation.

2.5.2 Necropsy analysis

Necropsy analysis included macroscopic examination of the brain, heart, lungs, kidneys, liver, spleen and uterus (in females) in all animals. Photos were taken of macroscopic lesions. Organs were longitudinally bisected, half was fixed and processed into paraffin wax and the other half was snap frozen. Longitudinally bisected kidneys and cochlea taken for SEM analysis were fixed and then transferred to 1XTBS.

2.5.3 Histology

2.5.3.1 Tissue fixation and paraffin embedding

Fixation is used to preserve tissue morphology by creating strong cross-links between the tissue proteins. Formaldehyde based fixative penetrates the tissue rapidly due to its small molecules and is therefore used for immersion fixation.

Fresh tissue was immersed in 10% formal saline overnight at room temperature and then transferred into 1XTBS. Fixed tissue was placed into the processor for a period of 1 hour in each of the following solutions; 70% ethanol, 90% ethanol, 100% ethanol, followed by 2 hours in 100% ethanol x2, followed by 1 hour in xylene, followed by 1.5 hours in xylene x2, and finally 3 hours in paraffin wax x2. Tissues were embedded cut side down and stored at room temperature. Paraffin sections were routinely sectioned at 4µm and floated onto poly-L-lysine treated glass slides. Sections were dried onto slides overnight at 45°C and stored at room temperature.

2.5.3.2 Freezing and sectioning tissue

Tissue was placed onto cork disks and covered with OCT embedding medium. Disks were dropped into liquid nitrogen-cooled isopentane until frozen, and stored in cryotubes at -70°C. This technique was used as liquid nitrogen-cooled isopentane provides more efficient heat transfer, therefore reducing ice crystal formation, compared to freezing in liquid nitrogen alone. Frozen sections were routinely sectioned at 10µm on a Bright cryostat and

placed onto glass slides. Sections were air-dried at room temperature for 2 hours and stored at -20°C.

2.5.3.3 Perfusion fixation and cochlea fixation for SEM

Perfusion fixation was used for SEM to ensure excellent morphology was preserved, such as open renal tubules for cilia viewing. By using a mixture of formaldehyde and glutaraldehyde, the rapid penetration of formaldehyde to initiate structural stabilization of the tissue, could be combined with the thorough cross-linking brought about by the more slowly penetrating glutaraldehyde.

Immediately following cervical dislocation the rib cage was removed to expose the heart and lungs. The right oracle was cut open to allow blood, PBS and fixative to drain out as it is syringed through the body. The left ventricle was then cut open and a large blunt needle and syringe used to pump 40ml of PBS through the body, followed by 50ml of PBFG. The kidneys were removed, longitudinally bisected, post-fixed for 24hrs in PBFG, and infiltrated with 2.3M sucrose in tris buffered saline (TBS). Kidneys were frozen and the tubule lumens exposed by sectioning with a freezing stage sledge microtome.

For the organ of Corti, cochleas encased in the temporal bone were dissected from 4 week old mice, perfused through the oval window with PBFG and immersed in PBFG overnight at 4°C. The temporal bone and vestibular and tectorial membranes were then removed and the cochleas placed in PBFG fixative overnight and transferred to 1XTBS. For SEM of E8.5 embryos, embryos were removed from their extra-embryonic membranes and fixed in PBFG overnight.

2.5.3.4 Haematoxylin and eosin staining

H&E staining reveals the architecture of a tissue. Haematoxylin stains the nucleus blue whereas eosin stains basic components of the cell and extracellular matrix, such as proteins, pink. Paraffin sections were stained with

H&E by immersion in the following: xylene (1 minute) x3, 100% ethanol (1 minute) x2, 70% ethanol (1 minute), Meyer's haematoxylin (5 minutes), running water (1 minute), eosin (2 minutes), running water (1 minute), 70% ethanol (1 minute), 100% ethanol (1 minute) x2, xylene (1 minute) x2. Sections were mounted with DPX.

2.5.4 Nucleic acid extraction

2.5.4.1 DNA extraction from tail tips

For the purpose of mouse genotyping, DNA was extracted from 3mm tail tips that had been immediately frozen after cutting. Tail tips were placed in 2ml eppendorf tubes with 500µl of tail buffer and 20µl of proteinase K (20mg/ml), which degrades ribonucleases and other proteins, and incubated overnight at 65°C. In the morning the samples were vortexed and if not fully digested an extra 20µl of proteinase K was added and vortexed. Once digested, 250µl of 6M supersaturated NaCl was added to the lysate to cause proteins and carbohydrates to precipitate while DNA remains in solution. The mixture was vortexed until a milky solution was obtained, and centrifuged at 13,000 rpm for 10 minutes. Without disturbing the salt pellet, the supernatant was collected into a fresh 1.5ml eppendorf and 500µl of isopropanol was added to precipitate the DNA. The tube was manually inverted until a DNA precipitate could be seen. Eppendorfs were left overnight at -20°C to aid precipitation, when required. The DNA precipitate was then separated by centrifugation at 13,000 rpm for 5 minutes. The supernatant was removed and the DNA pellet washed in 150µl of 70% ethanol. Finally, the pellet was air-dried for 15 minutes to remove any remaining ethanol and re-suspended in 30-50µl of DNAase-free water overnight at 35°C. Samples were stored at -20°C.

2.5.4.2 DNA extraction from fresh and frozen tissue

DNA was extracted from fresh and frozen tissue using the QIAamp DNA mini kit according to the manufacturers' instructions. Using this technique, DNA binds to a silica-gel membrane in the presence of a high salt medium. Contaminants are removed by washing the membrane with various buffers. Small pieces of tissue, up to 25mg, were incubated overnight at 65°C

with 180µl of Buffer ATL (contents a trade secret (CTS)) and 20µl of proteinase K. Once the tissue was completely lysed, 200µl of Buffer AL (CTS) was added and incubated for 10 minutes at 70°C. Two hundred micro litres of 100% ethanol was added and the solution applied to a QIAamp silica gel based Spin Column and centrifuged at 8,000 rpm for 1 minute. The filtrate was discarded and the column was transferred to a clean collection tube, 500µl of Buffer AW1 (CTS) added and re-centrifuged at 8,000 rpm for 1 minute. The filtrate was again discarded before a second wash was carried out using 500µl of Buffer AW2 (CTS) and the column was re-centrifuged at 13,000 rpm for 3 minutes followed by an extra 1 minute spin to remove any residual buffer. DNA was eluted in 200µl of DNAase free water by incubating for 1 minute at room temperature and finally centrifuging at 8,000 rpm for 1 minute. Samples were stored at -20°C.

2.5.4.3 DNA extraction from paraffin embedded tissue

DNA was extracted from paraffin embedded tissue using the QIAamp DNA mini kit. Three 4µm thick sections of tissue were placed into an eppendorf tube and incubated overnight at 65°C with 180µl Buffer ATL (CTS) and 20µl of proteinase K. Once the wax had melted and the tissue had lysed, 200µl of Buffer AL (CTS) was added and incubated for 10 minutes at 70°C. Two hundred micro litres of 100% ethanol was added and the solution was left at 25°C for at least 3 hours to allow the wax to set on top of the sample. A pipette tip was used to pierce through the wax and obtain the solution underneath, which was then applied to a QIAamp Spin Column and centrifuged at 8,000 rpm for 1 minute. The filtrate was discarded and the column was transferred to a clean collection tube, 500µl of Buffer AW1 (CTS) added and re-centrifuged at 8,000 rpm for 1 minute. The filtrate was again discarded before a second wash was carried out using 500µl of Buffer AW2 (CTS) and the column was re-centrifuged at 13,000 rpm for 3 minutes followed by an extra 1 minute spin to remove any residual buffer. DNA was eluted in ~100µl of DNAase free water by incubating for 1 minute at room temperature and finally centrifuging at 8,000 rpm for 1 minute. Samples were stored at -20°C.

2.5.5 Nucleic acid quantification

UV spectrophotometry at wavelengths of 260nm and 280nm was used to determine DNA concentrations. This allowed the amount of DNA to be quantified and the protein concentration to be established. An absorption ratio of 1.8 at 260nm:280nm indicates high sample purity.

2.5.6 Oligonucleotide primer design

Primers between 18-23 nucleotides in length were designed using Primer 3 (Rozen and Skaletsky 2000) and the following criteria where possible:

- Repetitive motifs and predicted dimerisation or secondary structure formation avoided.
- Four bases (A, T, C, G) represented in equal proportions.
- Melting temperatures of the primer pairs within 2°C of each other.

2.5.7 Polymerase chain reaction (PCR)

An *in vitro* cycling technique known as the polymerase chain reaction was used to amplify specific DNA sequences. Heat stable polymerase synthesises a complementary strand of DNA from template DNA between two oligonucleotides designed from two regions of known sequence. Multiple cycles (20-40) of temperature changes are used to carry out this reaction, with each PCR cycle comprised of a high temperature denaturation step to generate single stranded template DNA, followed by a cooler annealing step to bind the primers to the single stranded DNA and finally an extension step where the polymerase carries out the synthesis of the new complementary strand.

Standard conditions for PCR included 25ng of template DNA, 2µl of 10x reaction buffer (100mM TrisHCl, pH8.3, 500mM KCl, 15nM $MgCl_2$, 0.01% w/v gelatin), 0.25mM dNTPs, 25pmol of each primer, and 0.5Units (U) of AmpliTaq Gold DNA polymerase in a total reaction volume of 20µl. Reactions in tubes were scaled up to a 50µl total volume and overlaid with mineral oil. Standard cycling conditions were 94°C for 10-12 minutes, followed by 35

cycles of 52°C-60°C for 1 minute, 72°C for 1-2 minutes and 94°C for 1 minute. There was a final elongation step of 72°C for 12 minutes.

2.5.8 Agarose gel electrophoresis

DNA fragments are separated according to their size with smaller DNA fragments travelling further through the gel than larger fragments. The higher the gel concentration, the better the separation is for small DNA fragments due to the smaller gel pore size. Standard grade agarose is sufficient to separate fragments of 200bp-30Kb in size. Agarose gels of 1-2% w/v concentration were prepared using 1xTAE buffer and 0.05µg/ml ethidium bromide which incorporates into the DNA and allows visualisation under ultra-violet light. Ten micro litres of PCR sample was mixed with 2µl of loading dye (15% w/v ficol, 10mM Tris pH 8, 1mM EDTA, 0.2% orange G), loaded into the well of a gel and electrophoresis performed in 1xTAE buffer at 100 volts. A 1kb DNA ladder was used to allow fragment sizing. DNA was visualised under UV at a wavelength of 300nm and photographed using the Gel Doc 2000 system.

2.5.9 PCR purification

To prepare PCR products for cycle sequencing, the ExoSAP method was used to eliminate any unused dNTPs and primers. This involves the use of hydrolytic enzymes Exonuclease I (Exo) and Shrimp Alkaline Phosphatase (SAP) to degrade residual single-stranded primers and hydrolyse remaining dNTPs respectively. Fifteen micro litres of PCR product was purified by the addition of 5U Exo I and 0.5U SAP. The sample was incubated at 37°C for 1 hour followed by denaturation at 80°C for 15 minutes.

2.5.10 ABI cycle sequencing

ABI cycle sequencing uses the chain termination method developed by Sanger and Coulson (1977). In addition to dNTPs, fluorescently labelled chain terminating 2',3' ddNTPs are incorporated into the newly synthesised DNA strand. DNA polymerase cannot extend the growing DNA chain past the ddNTP, due to the lack of a hydroxyl group at the 3' position of the deoxyribose sugar, and so the reaction is terminated at this specific base. As

a result, single-stranded DNA strands are formed that differ in length by one nucleotide. In automated sequencing the reaction can take place in a single tube because each ddNTP is labelled with a different fluorphore. The ABI sequencer can then identify the position of the fluorescent bases by passing the single-stranded DNAs through a capillary gel, with smaller fragments migrating fastest through the polymer and through the laser beam first. The emitted wavelength is detected and used to determine the ddNTP incorporated at a particular position.

Purified PCR products were sequenced using a BigDye® Terminator v3.1 Cycle Sequencing Kit. A total reaction volume of 10µl was used containing 2µl of purified PCR product, 0.25pmol of primers, 0.75µl of terminator ready reaction mix (labelled A, C, G and T dye terminators, dNTPs, AmpliTaq DNA polymerase FS, $MgCl_2$ and Tris-HCl buffer, pH 9.0) and 2µl BigDye terminator sequencing buffer. Cycling parameters were 96°C for 1 minute followed by 25 cycles of 96°C for 10 seconds, 50°C for 5 seconds and 60°C for 4 minutes. Purification of sequencing products was performed using Montage SEQ_{96} sequencing reaction clean up kits. Twenty micro litres of injection fluid was added to sequencing reactions and transferred into the micro well filter plate. The samples were drawn through the plate using a vacuum pump (20 inches Hg) until the wells were empty. Two additional washes with injection fluid (25µl) were performed using the vacuum pump. Purified sequencing products were re-suspended in 25µl of injection fluid by shaking for 10 minutes. Samples were run on an ABI 3100 Genetic Analyser and sequence data viewed on Sequencher version 4.2.

2.5.11 Immunohistochemistry

The avidin-biotin complex (ABC) method was used for immunohistochemistry (IHC) procedures. This is an indirect IHC method which utilises the unique properties of the large glycoprotein avidin and the vitamin biotin which have an extremely high affinity for one another. Biotin can in turn be conjugated to a variety of biological molecules such as antibodies, whilst avidin can be labelled with peroxidase or fluorescein. The technique involves three main steps: application of unlabelled primary antibody,

application of biotinylated secondary antibody and application of a complex of avidin-biotin peroxidase. The peroxidase is then developed by DAB or other substrates to produce a coloured end product. The main advantage of this method is the amplification of the original antibody signal due to avidin having four binding sites for biotin, therefore amplifying the signal many fold.

Four micron thick kidney and liver paraffin sections were deparaffinised and rehydrated by immersing in xylene x2, 100% ethanol x2, 70% ethanol, 50% ethanol and water for 5 minutes each. For antigen retrieval, sections were boiled in 10 mM citrate buffer (pH 6.0) for 10 minutes and rinsed in running tap water. Endogenous peroxidase activity was blocked with 0.3% hydrogen peroxide for 30 minutes followed by two 1XTBS washes for 5 minutes. Immunostaining was performed in a humidity chamber using the rabbit VECTASTAIN ELITE ABC horseradish peroxidase kit. Sections were encircled with a wax ring and blocked in goat normal serum for 20 minutes. Primary antibodies were applied and incubated overnight at 4°C, followed by two 5 minute 1XTBS washes. A biotinylated secondary antibody was applied and incubated for 30 minutes followed by two 5 minute 1XTBS washes. Avidin-biotin complex (ABC) was incubated for 30 minutes followed by two 5 minute 1XTBS washes. Sections were developed using DAB, counterstained in Gills haematoxylin for 30 seconds, and blued in tap water. Sections were finally dehydrated by immersing in 50% ethanol, 70% ethanol and 100% ethanol x2 (all 5 minutes each), cleared in xylene for 10 minutes, mounted with DPX and air dried. Slides were viewed on an Olympus BX51 microscope. All incubations were at room temperature unless otherwise stated.

2.5.12 Double immunofluorescence staining

2.5.12.1 Double staining with primary antibody and lectins

Four micron thick kidney paraffin sections were deparaffinised and rehydrated as described above. For antigen retrieval, sections were boiled in 10 mM citrate buffer (pH 6.0) for 10 minutes, rinsed in running tap water and immersed in 1XTBS for 5 minutes. Immunofluorescence was performed in a humidity chamber covered in tin foil to keep the contents in darkness.

Sections were encircled with a wax ring and blocked in goat normal serum for 30 minutes. Primary antibodies were applied and incubated overnight at 4°C, followed by two 5 minute 1XTBS washes. A fluorescent secondary antibody was applied in combination with a fluorescent lectin, and both incubated for 1 hour in the dark, followed by two 5 minute 1XTBS washes. Sections were finally mounted with one drop of ProLong® Gold antifade reagent with DAPI and allowed to cure overnight in the dark. Once cured, the edges of the coverslip were sealed with clear nail varnish and the slides viewed immediately on an Olympus BX51 microscope. Finally, slides were stored at 4°C in the dark. All incubations were at room temperature unless otherwise stated.

2.5.12.2 Double staining with two primary antibodies

Four micron thick kidney paraffin sections were deparaffinised and rehydrated as described above. Antigen retrieval was carried out as described above followed by blocking in two 5 minute 1XTBS/0.6% bovine serum albumin (BSA) washes. Immunofluorescence was performed in a humidity chamber covered in tin foil to keep the contents in darkness. Sections were encircled with a wax ring, primary antibodies applied and incubated overnight at 4°C, followed by two 5 minute 1XTBS/0.6% BSA washes. The first fluorescent secondary antibody was applied and incubated for 1 hour in the dark, followed by two 5 minute 1XTBS/0.6% BSA washes. The second fluorescent secondary antibody was then applied and incubated for 1 hour in the dark, followed by two 5 minute 1XTBS/0.6% BSA washes. Sections were finally mounted with one drop of ProLong® Gold antifade reagent with DAPI and allowed to cure overnight in the dark. Once cured, the edges of the coverslip were sealed with clear nail varnish and the slides viewed immediately on an Olympus BX51 microscope. Finally, slides were stored at 4°C in the dark. All incubations were at room temperature unless otherwise stated.

2.5.12.3 Confocal immunofluorescence

Thirty micron thick kidney sections were stained as detailed in sections 2.5.12.1 and 2.5.12.2. Samples were imaged using a Leica TCS SP2 AOBS spectral confocal laser scanning microscope under x40 and x63 oil immersion objective lenses using appropriate excitation and emission settings for sequential recordings of fluorescence used. Z-stacks of optical sections (512 x 512 pixels) were taken through the tissue depth at a step size of 0.4μm and these were used to create Maximum intensity-type 3D reconstructions using Leica Confocal Software.

2.5.13 Scanning electron microscopy

All tissues for SEM were processed using the hexamethyldisilazane (HMDS) method (Nation 1983). This method was used as it does not shrink or distort the tissue upon air drying ensuring excellent surface detail is preserved and also it requires less time compared to the critical point drying procedure.

Samples were washed twice in dH_2O for 10 minutes each, followed by dehydration in 50%, 70%, 90% and 100% ethanol x2 for 15 minutes each. Samples were finally dehydrated in three 10 minute immersions in HMDS and allowed to air dry in a perspex cabinet with silica gel crystals to prevent moisture re-entering the samples. The specimens were then mounted on aluminium stubs using carbon paint, sputter coated with gold using an EMScope vacuum coater and viewed at 5kV using a JEOL 840A scanning electron microscope.

2.6 Bioinformatic tools

Genbank (http://www.ncbi.nih.gov/Genbank/) accession numbers for the genes analysed in this project are as follows:

Tsc1 (*Mus musculus*) NM_022887

Tsc2 (*Mus musculus*) NM_011647

Pkd1 (*Mus musculus*) NM_013630

BLAST searches were carried out against DNA sequences from Genbank (http://www.ncbi.nlm.nih.gov/BLAST/).

CHAPTER THREE: Investigating the role of mTOR activation in *Tsc*-associated renal cystogenesis

3.1 Introduction

Many lesions from patients with TSC exhibit activation of mTOR and clinical trials are underway for the treatment of these tumours using mTOR inhibitors (Bissler *et al.* 2008, Davies *et al.* 2008). Interestingly, the mTOR inhibitor rapamycin, has been shown to have no effect on a number of microscopic precursor kidney lesions that develop in a rat model of *Tsc2*-inactivation (Kenerson *et al.* 2005). Furthermore, data from a recent study in a conventional $Tsc2^{+/-}$ mouse model found that rapamycin treatment was not effective in young mice (under 6 months of age) with early disease and a mild cystic phenotype, and no significant difference in tumour burden was found when compared to untreated mice (Messina *et al.* 2007). Together, these results suggest that many TSC-associated renal tumours initially develop via an mTOR-independent pathway.

Here, we investigated the apparent rapamycin-insensitive pathway that may be involved in *Tsc*-associated renal cyst formation by studying renal lesions from $Tsc1^{+/-}$ (Wilson *et al.* 2005), $Tsc2^{+/-}$ mice (Onda *et al.* 1999) and $Tsc1^{+/-}Tsc2^{+/-}$ mice.

3.2 Materials and methods

3.2.1 DNA extraction and PCR genotyping

DNA was extracted from tail tips using NaCl/ isopropanol extraction methods (chapter 2, section 2.5.4.1). PCR genotyping of DNA from tail tips was performed by amplification of the wild-type and mutant alleles for *Tsc1* and *Tsc2* using the following primers in a 35 cycle PCR reaction with AmpliTaq gold DNA polymerase (Applied Biosystems). *Tsc1* wild-type allele: exon8F 5'-TGCCTGGAAGCCCAGGAAGGT-3' and exon8R 5'-CTGCAGGGCCCATGGTGGTT-3' (183bp product), *Tsc1* mutant allele: Tsc1HETF 5'-CGTTGGCTACCCGTGATATT-3' and Tsc1HETR 5'-CCAATGGGCTCATTACTCTCA-3' (268bp product). *Tsc2* wild-type allele:

Tsc2genF 5'-AATCGCATCCGAATGATAGG-3' and Tsc2WTR 5'-GTTTAATGGGCCCTGGATCT-3' (~900bp product), *Tsc2* mutant allele, Tsc2genF and Tsc2HETR 5'-GGATGATCTGGACGAAGAGC-3' (658bp product). Products were analysed on 2% agarose gels. Some genotyping assistance was provided by Carol Guy and Rebecca Harris.

3.2.2 Animal care, necropsy and pathology

All procedures with animals were carried out in accordance with Home Office guidelines as previously described (chapter 2, section 2.5.1). *Tsc1*$^{+/-}$ mice on a Balb/c background (Wilson *et al.* 2005) were crossed with *Tsc2*$^{+/-}$ mice on a Balb/c background (Onda *et al.* 1999) to produce *Tsc1*$^{+/-}$, *Tsc2*$^{+/-}$, *Tsc1*$^{+/-}$*Tsc2*$^{+/-}$ and wild-type progeny. Kidneys from 5 mice of each genotype were analysed at 6-7 and 11-12 months of age. Half of each kidney was snap frozen in liquid nitrogen-cooled isopentane and the other half was processed into paraffin wax and sectioned at 4μm. To estimate the average number of microscopically visible kidney lesions per mouse, five representative sections ~200μm apart from each half kidney were stained with H&E and inspected on an Olympus BX51 BF light microscope. Lesions crossing more than one section were only counted once and the total number of lesions were doubled and divided by 5 (5 mice per genotype) to generate a mean number per mouse in each genotype.

3.2.3 Immunohistochemistry

Immunohistochemistry of kidney paraffin sections from *Tsc1*$^{+/-}$, *Tsc2*$^{+/-}$, *Tsc1*$^{+/-}$*Tsc2*$^{+/-}$ and wild-type mice was performed as previously described (chapter 2, section 2.5.11) using the rabbit VECTASTAIN ELITE ABC horseradish peroxidase kit (Vector Laboratories), anti-phospho-S6 ribosomal protein (Ser$^{240/244}$, 1:400 dilution) and goat anti-rabbit biotinylated secondary antibody. Renal lesions were identified after H&E staining and adjacent sections were stained with anti-pS6 (5 mice per genotype were used). Staining was scored as either present or absent by an observer blinded to genotype.

3.2.4 Statistics

Lesion counts were compared using 2-sample T-tests and the Mann-Whitney confidence interval test. Numbers of lesions that stained for pS6 were compared using the Chi-squared test or Fisher's exact test.

3.3 Results

3.3.1 Designing *Tsc1* primers

The knockout construct in our *Tsc1*$^{+/-}$ mice was previously designed by our laboratory (Wilson *et al.* 2005, Figure 3.1) and contains a $(TAG)_3$/IRES-*lacz*-polyA/*loxP*/MC1*neo*-polyA/*loxP* reporter/positive selection cassette which replaces half of exon 6 and all of exons 7 and 8. Previous primers used for the genotyping of *Tsc1*$^{+/-}$ mice were located within a neomycin resistance cassette (*neo*); however, due to the use of other mouse models containing *neo* cassettes in this study, new primers were designed that were specific to the *Tsc1* mutant allele. A set of primers for the wild-type allele (exon8F and exon8R) were designed in exon 8 and primers to identify the mutant allele were designed at the 3' end of the construct with the forward primer (Tsc1HETF) lying within *neo* and the reverse primer (Tsc1HETR) located just outside the construct ~1000bp upstream from exon 9, therefore ensuring these primers were *Tsc1* allele specific. Genotyping results are shown in Figure 3.1.

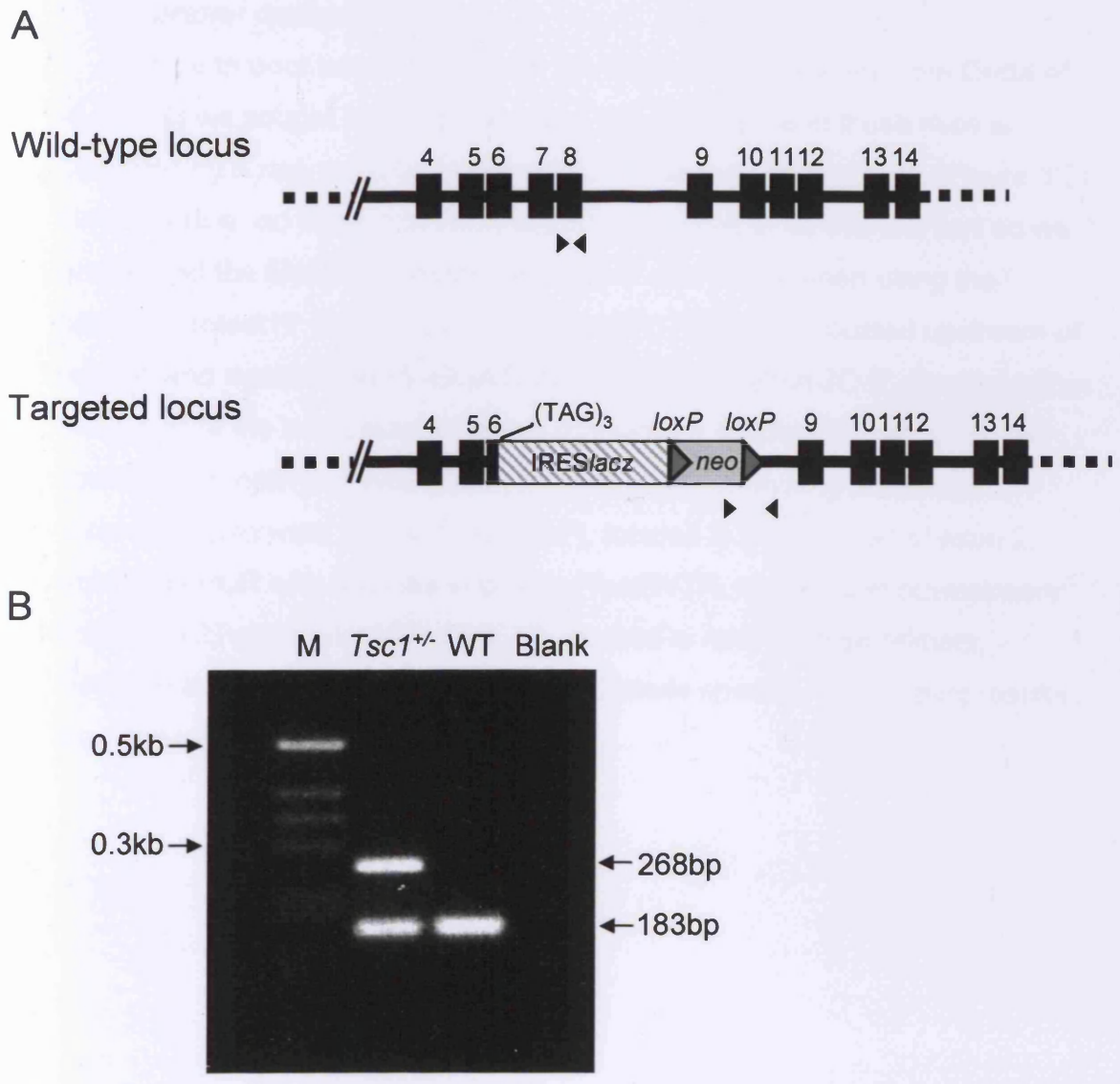

Figure 3.1 Targeted *Tsc1* locus and PCR genotyping results. (**A**) Schematic illustration of the wild-type *Tsc1* locus (upper panel) and the targeted locus (lower panel). Using homologous recombination, a $(TAG)_3$/IRES-*lacz*-polyA/*loxP*/MC1*neo*-polyA/*loxP* reporter/positive selection cassette was inserted into *Tsc1*. The targeted locus contains the reporter/ positive selection cassette inserted into exon 6 of *Tsc1* and introduces stop codons (TAG_3) into all three reading frames of the *Tsc1* coding sequence. The targeting event also simultaneously deletes the 3' part of exon 6 and all of exons 7 and 8 of *Tsc1*. Exons are shown as numbered black rectangles, introns as a thick black line, and flanking genomic regions as a thick dashed line. The reporter/selection cassette is shown as a large light grey striped rectangle (IRES-*lacz* component) and a large filled light grey rectangle (MC1*neo*-polyA component), with dark grey triangles indicating *loxP* sites. The genotyping primers are shown as black triangles. (**B**) PCR analysis with genotyping primers. *Tsc1*$^{+/-}$ mice contain both the wild-type fragment (183bp) and the mutant fragment (268bp). Wild-type mice contain only the wild-type fragment. M = marker, WT = wild-type.

3.3.2 Sequencing of the targeting cassette in *Tsc2*$^{+/-}$ mice and primer design

Due to poor amplification with the original *Tsc2* primers from Onda *et* al. (1999) we sought to design our own. The *Tsc2* gene in these mice is disrupted by a *neo* cassette inserted into the second coding exon (Figure 3.2). Unfortunately, no sequence information was available for this loci and so we sequenced the first half of exon 2 and the 5' end of the insert using the primers neotest1F (5'-ACCGGTCACCCATTCTTCTG-3', located upstream of exon 2) and neotest1bR (5'-GGATGATCTGGACGAAGAGC-3', located within the 5' end of the *neo* cassette) which produced a sequence from which we could design new genotyping primers. The new genotyping primer set consists of a forward primer (Tsc2genF), located in the first half of exon 2, which can PCR with both the wild-type (Tsc2WTR, located just downstream from exon 2) and mutant (Tsc2HETR, located in *neo*) reverse primers, therefore ensuring these primers are *Tsc2* allele specific. Genotyping results are shown in Figure 3.2.

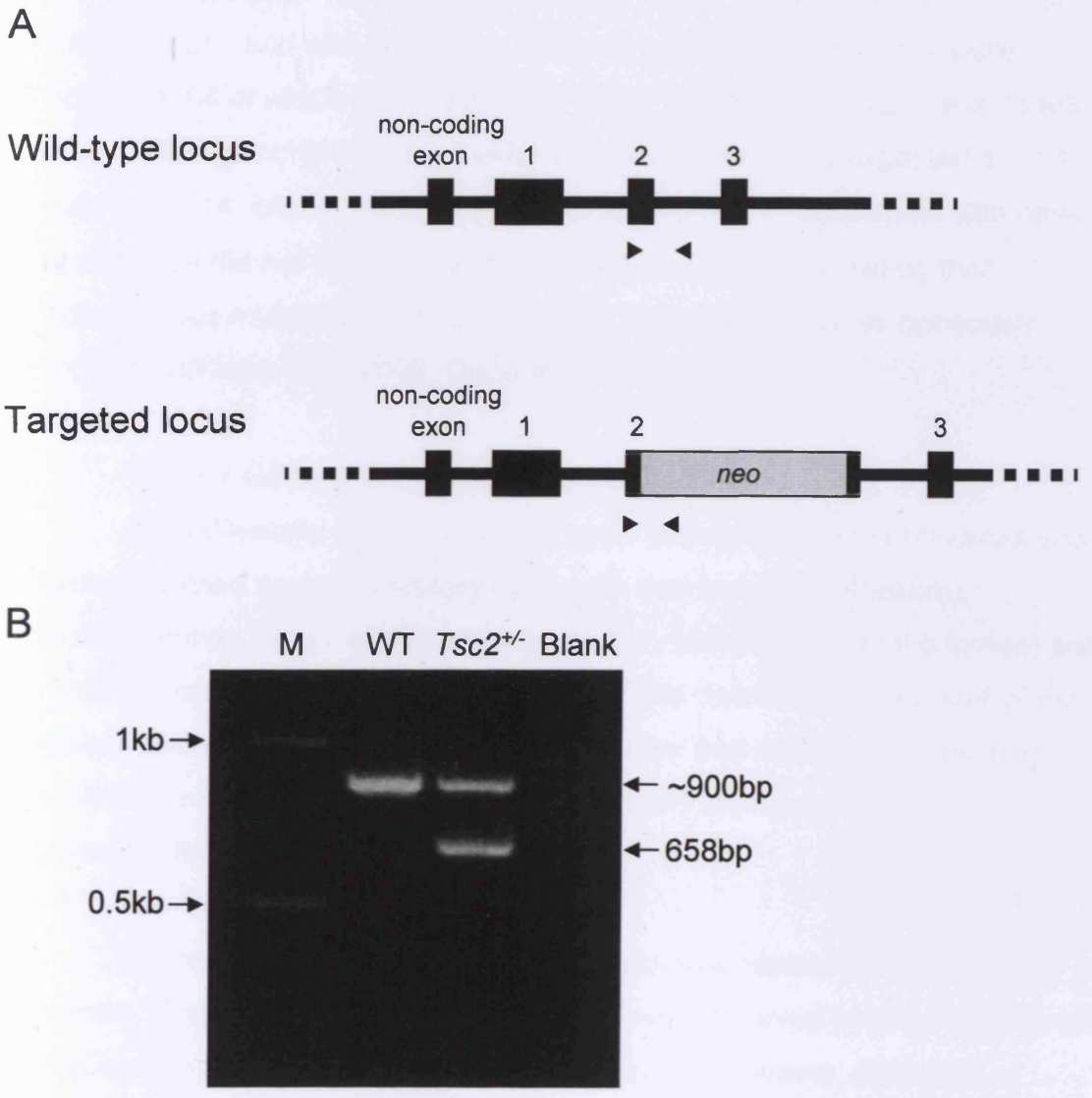

Figure 3.2 Targeted *Tsc2* locus and PCR genotyping results. (**A**) Schematic illustration of the wild-type *Tsc2* locus (upper panel) and the targeted locus (lower panel). Using homologous recombination, a neomycin (*neo*) resistance cassette was inserted into the second coding exon of *Tsc2*. Exons are shown as numbered black rectangles, introns as a thick black line, and flanking genomic regions as a thick dashed line. The *neo* resistance cassette is shown as a large light grey rectangle. The genotyping primers are shown as black triangles. The same forward primer is used for each reverse primer. (**B**) PCR analysis of genotyping primers. $Tsc2^{+/-}$ mice contain both the wild-type fragment (~900bp) and the mutant fragment (658bp). Wild-type mice contain only the wild-type fragment. M = marker, WT = wild-type.

3.3.3 Renal pathology

We crossed *Tsc1*$^{+/-}$ mice with *Tsc2*$^{+/-}$ mice to generate *Tsc1*$^{+/-}$, *Tsc2*$^{+/-}$, *Tsc1*$^{+/-}$*Tsc2*$^{+/-}$ and wild-type mice. From 17 crosses, 261 progeny were obtained, 64 of which were *Tsc1*$^{+/-}$, 67 *Tsc2*$^{+/-}$, 55 *Tsc1*$^{+/-}$ *Tsc2*$^{+/-}$ and 75 wild-type. These genotypes did not differ significantly from the expected 1:1:1:1 ratio (χ^2=3.14, critical value of χ^2=7.815 at *P*=0.05). In agreement with other studies, we did not find any *Tsc1*$^{-/-}$ or *Tsc2*$^{-/-}$ live pups, indicating that homozygous mutations in these mice are embryonic lethal as previously reported (Wilson *et al.* 2005, Onda *et al.* 1999).

3.3.3.1 General lesion observations

Renal lesions varied from pure cysts through to solid carcinomas and were classified as cysts (solitary cysts with one layer of epithelium), cystadenomas (cysts with branching papillary projections into the lumen) and renal cell carcinomas (RCCs) (Figure 3.3). The distribution in the size of the lesions, with simple cysts tending to be smaller and more numerous than cystadenomas and RCCs, supported the theory that these lesions progress from cyst through to RCC (Table 3.1).

No renal lesions were observed in wild-type littermates under 18 months of age. At 6-7 months, renal cysts were observed in all genotypes and RCCs were absent (Table 3.1). By 11-12 months however, 40% (2/5) of *Tsc1*$^{+/-}$, 80% (4/5) of *Tsc2*$^{+/-}$ and 100% (5/5) of *Tsc1*$^{+/-}$*Tsc2*$^{+/-}$ mice developed RCCs supporting a progression of early cystic lesions through to RCC with age.

3.3.3.2 Comparison of renal lesions from Tsc1$^{+/-}$ *and Tsc2*$^{+/-}$ *mice*

At 6-7 months, the number of renal lesions from *Tsc1*$^{+/-}$ and *Tsc2*$^{+/-}$ mice was almost identical at an average of 12.4 and 12.8 lesions per mouse respectively (*P*=0.957), however, at 11-12 months, we observed significantly more renal lesions in *Tsc2*$^{+/-}$ mice compared to age matched *Tsc1*$^{+/-}$ mice on the same genetic background (39.2 and 22.8 lesions per mouse respectively, *P*=0.04) (Table 3.1).

When examining the types of renal lesions, we found very little difference in the number of renal cysts in *Tsc1*$^{+/-}$ and *Tsc2*$^{+/-}$ mice at 6-7 months (5.6 and 7.6 lesions per mouse respectively), however by 11-12 months *Tsc2*$^{+/-}$ mice had significantly more cysts compared to *Tsc1*$^{+/-}$ mice (27.2 and 15.2 lesions per mouse respectively, P=0.038) (Table 3.1).

3.3.3.3 Comparison of renal lesions from Tsc1$^{+/-}$*Tsc2*$^{+/-}$ *mice and single heterozygote littermates*

In *Tsc1*$^{+/-}$*Tsc2*$^{+/-}$ mice at both 6 months and 11-12 months the total number of renal lesions was approximately the sum of the single heterozygotes at 24.8 and 58.4 lesions per mouse respectively (Table 3.1) highlighting a simple additive affect when both *Tsc1* and *Tsc2* are knocked out.

Table 3.1 Average number and histological classification of microscopic renal lesions in *Tsc1*$^{+/-}$, *Tsc2*$^{+/-}$ and *Tsc1*$^{+/-}$*Tsc2*$^{+/-}$ mice.

Age	Genotype	Cyst	Cystadenoma	Renal cell carcinoma	Total lesions
6-7 months	*Tsc1*$^{+/-}$	5.6	6.8	0	**12.4**$^{*\ \#}$
	Tsc2$^{+/-}$	7.6	5.2	0	**12.8**$^{*\ \dagger}$
	Tsc1$^{+/-}$*Tsc2*$^{+/-}$	15.6	9.2	0	**24.8**$^{\#\ \dagger}$
11-12 months	*Tsc1*$^{+/-}$	15.2	6.4	1.2	**22.8**$^{\Diamond\ +}$
	Tsc2$^{+/-}$	27.2	9.6	2.4	**39.2**$^{\Diamond\ \square}$
	Tsc1$^{+/-}$*Tsc2*$^{+/-}$	32.8	18.8	6.8	**58.4**$^{+\ \square}$

Numbers based on the analyses of five sections (~200μm apart) from half kidneys of five mice from each of the above genotypes in each age group.
$^{*}P$=0.96, $^{\#}P$=0.09, $^{\dagger}P$=0.1, $^{\Diamond}P$=0.035, ^{+}P=0.003, $^{\square}P$=0.09

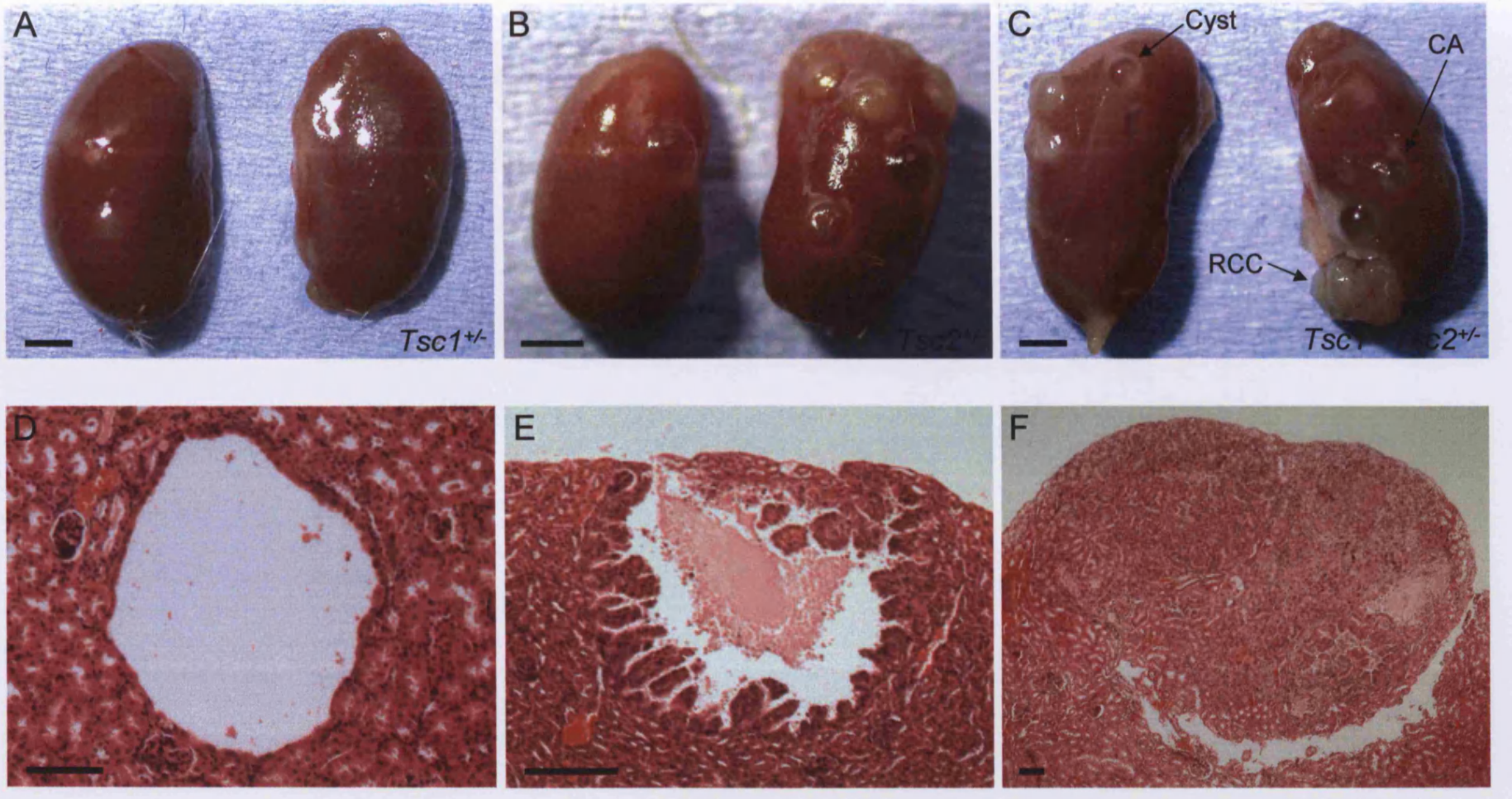

Figure 3.3 Macroscopic and microscopic analysis of renal lesions from *Tsc1*$^{+/-}$, *Tsc2*$^{+/-}$ and *Tsc1*$^{+/-}$*Tsc2*$^{+/-}$ mice. Macroscopic renal lesions could be seen on kidneys from 11-12 month old *Tsc1*$^{+/-}$ (**A**), *Tsc2*$^{+/-}$ (**B**) and *Tsc1*$^{+/-}$*Tsc2*$^{+/-}$ (**C**) mice. Significantly more renal lesions were found in 11-12 month old *Tsc2*$^{+/-}$ mice as compared to age matched *Tsc1*$^{+/-}$ mice on the same genetic background (P=0.04). Examples of macroscopic cysts, cystadenomas (CAs) and RCCs are indicated in panel **C**. Microscopic view of a cyst (**D**) with a single layer of cuboidal cells, a cystadenoma (**E**) with branching papillae projections beginning to fill the lumen and a solid renal cell carcinoma (**F**). Scale bars: **A**, **B** and **C**; 2mm, **D**; 100μm, **E**; 0.2mm, **F**; 0.1mm.

3.3.4 pS6 immunohistochemistry

We tested for activation of the mTOR pathway by staining renal lesions for the presence of pS6. We found that 33% (17/52) of cysts from *Tsc1*$^{+/-}$ mice, 46% (31/68) of cysts from *Tsc2*$^{+/-}$ mice and 32% (27/84) of those from *Tsc1*$^{+/-}$*Tsc2*$^{+/-}$ mice, failed to stain for pS6, whereas most advanced lesions (cystadenomas and RCCs) from these mice did stain (32/37, 87%, P=0.039, 35/42, 83%, P=0.002 and 71/75, 95%, P<0.001, respectively) (Table 3.2, Figure 3.4). There was no significant difference in pS6 staining patterns between the genotypes.

We determined the pattern of pS6 activation throughout individual renal cysts from *Tsc1*$^{+/-}$ mice by staining consecutive serial sections. Seventeen out of 26 (65%) cysts studied in this way showed consistently strong pS6 staining and the remaining 9 (35%) showed consistently little or no staining, in every serial section (Figure 3.5). Three of the cysts with little or no pS6 staining had some sections in which single cells displayed strong positivity (e.g. in Figure 3.5 C and D); however, this pattern was also seen in some normal tubular epithelial cells.

Table 3.2 Phosphorylated-S6 analysis of renal lesions from *Tsc1*$^{+/-}$, *Tsc2*$^{+/-}$ and *Tsc1*$^{+/-}$*Tsc2*$^{+/-}$ mice.

Genotype	Lesion type	Number pS6 positive
Tsc1$^{+/-}$	Cyst	35/52 (67%)*
	Cystadenoma	29/34 (85%)* [a]
	RCC	3/3 (100%)
Tsc2$^{+/-}$	Cyst	37/68 (54%)#
	Cystadenoma	29/36 (81%)# [a]
	RCC	6/6 (100%)
Tsc1$^{+/-}$*Tsc2*$^{+/-}$	Cyst	57/84 (68%)†
	Cystadenoma	57/61 (93%)† [a]
	RCC	14/14 (100%)

Numbers based on the analyses of five sections (~200μm apart) from half kidneys of five mice from each of the above genotypes.
[a] cystadenoma and RCC values combined, *P=0.039, #P=0.002, †P<0.001

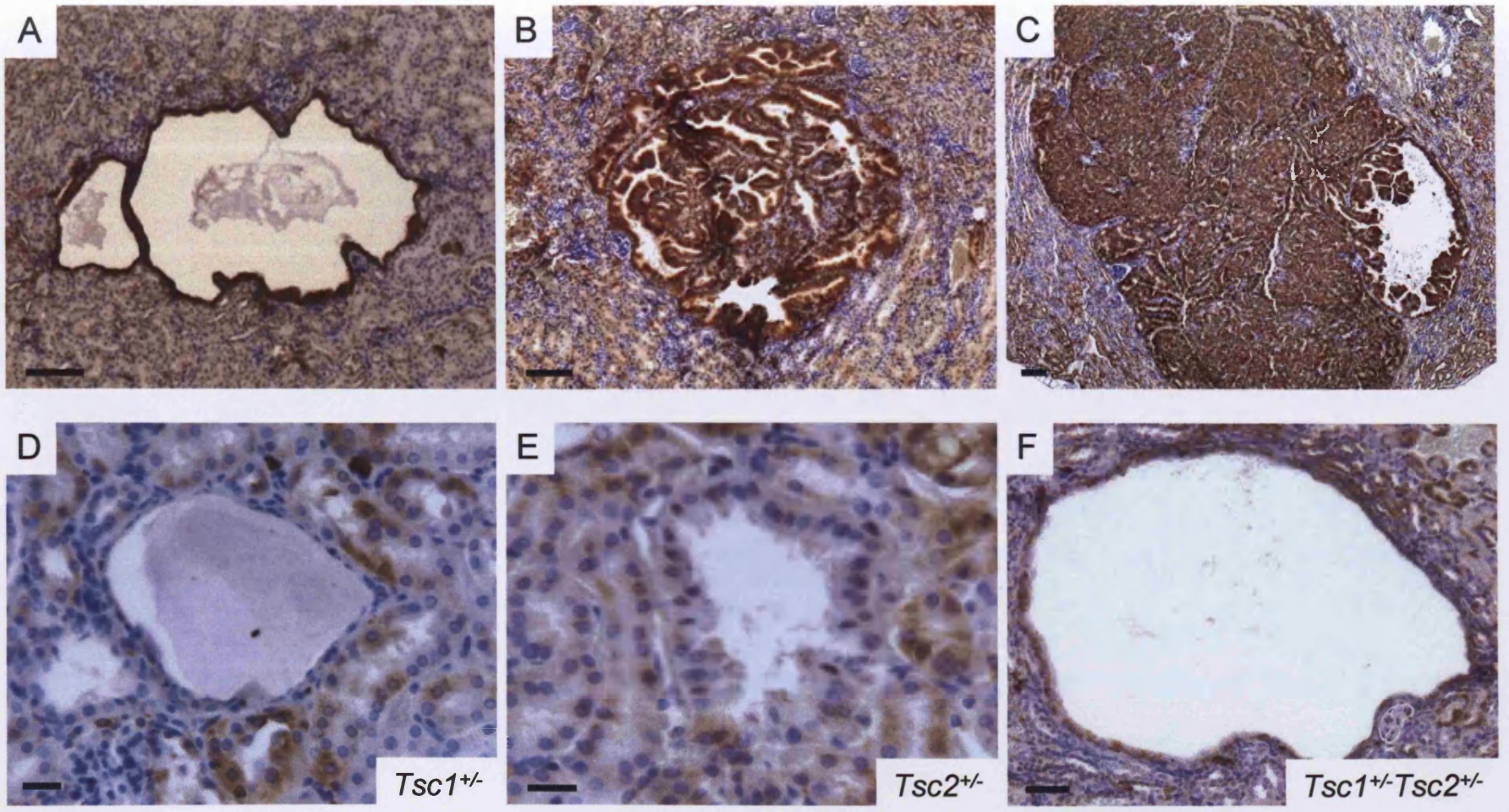

Figure 3.4 Immunohistochemistry analysis of murine renal lesions from *Tsc1*$^{+/-}$, *Tsc2*$^{+/-}$ and *Tsc1*$^{+/-}$*Tsc2*$^{+/-}$ mice using an anti-pS6 antibody. Intense (brown) staining is found in some cysts (**A**) and the vast majority of cystadenomas (**B**) and RCCs (**C**). A significant proportion of cysts from *Tsc1*$^{+/-}$ (**D**), *Tsc2*$^{+/-}$ (**E**), and *Tsc1*$^{+/-}$*Tsc2*$^{+/-}$ (**F**) mice showed little or no staining. Note: other lesions present in other parts of sections shown in **D-F** stained for pS6 (data not shown), confirming that the antibody worked successfully. Scale bars: **A-C**; 0.1mm, **D** & **E**; 20μm, **F**; 50μm.

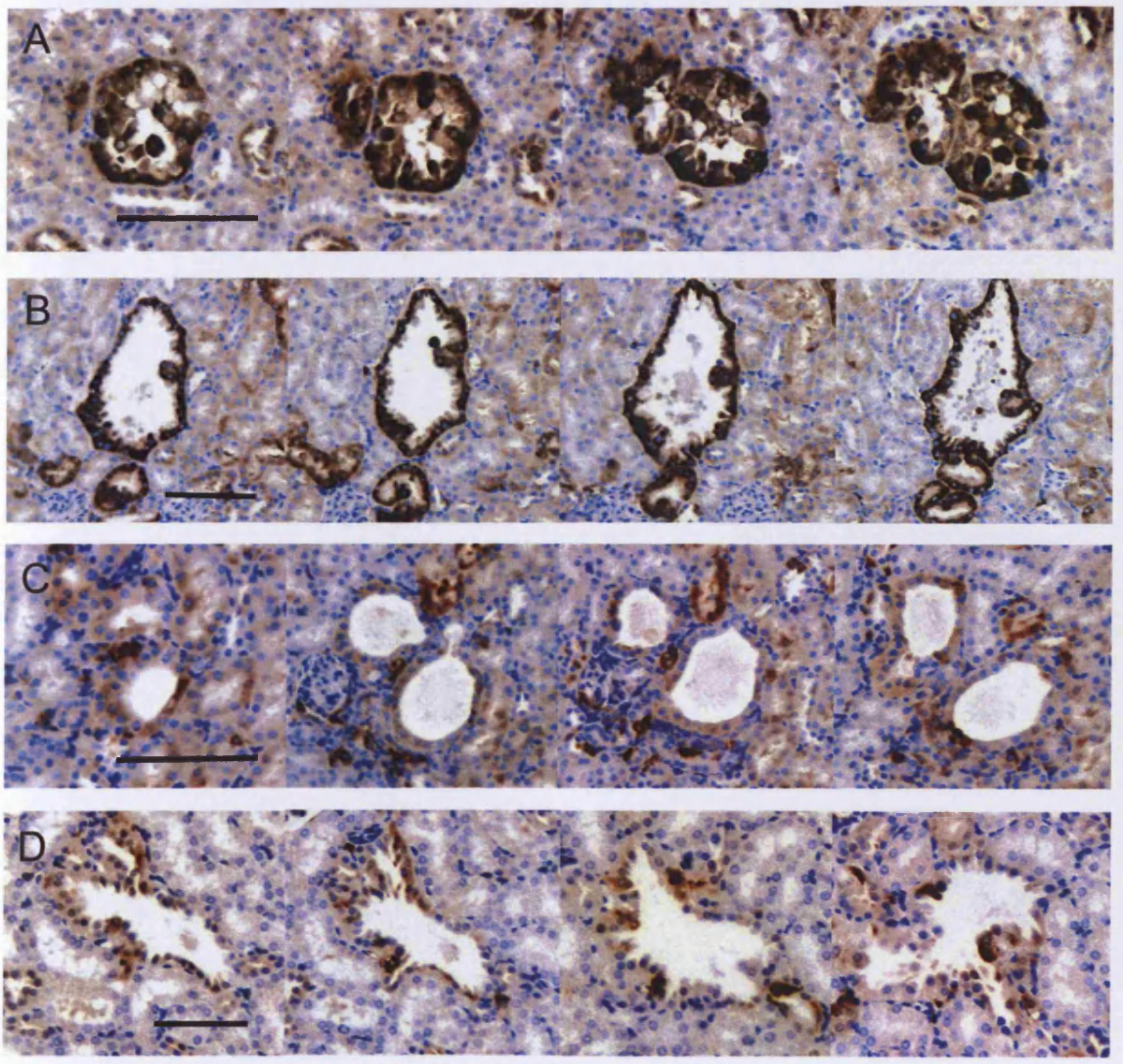

Figure 3.5 IHC of consecutive serial sections of renal cysts from *Tsc1*$^{+/-}$ mice using a pS6 antibody to show the pattern of pS6 staining throughout the cyst. Examples of serial sections through cysts that consistently either stained (**A**, **B**), or, that did not stain strongly (**C**, **D**). Note: other lesions present in other parts of sections shown in **C** and **D** stained for pS6 (data not shown), confirming that the antibody worked successfully. Scale bars: 100μm.

3.4 Discussion

3.4.1 *Tsc2*$^{+/-}$ mice have a more severe renal phenotype compared to *Tsc1*$^{+/-}$ mice

Genotype/phenotype correlation studies in patients with TSC have revealed that a more severe phenotype, including a higher rate of renal and skin lesions and mental retardation (matched by similar differences in brain radiographic findings such as tubers and SENs), is apparent in those with a *TSC2* mutation compared to those with a *TSC1* mutation (Jones *et al.* 1999, Dabora *et al.* 2001, Sancak *et al.* 2005, Au *et al.* 2007). Interestingly, Dabora *et al.* (2001) found that renal cystic disease occurred at similar rates in patients with sporadic *TSC2* compared to those with sporadic *TSC1* (25% vs. 16% respectively), however the patients with *TSC1* mutations who had renal cysts were on average older than patients with *TSC2* mutations who had renal cysts (26.3 vs. 13.8 years old respectively). There was however a higher frequency of grade 2-4 renal cystic disease (>2 small (<2cm) cysts up to classic polycystic kidney disease (multiple cysts with renal enlargement)) in patients with *TSC2* mutations (19% vs. 0%) as compared to those with *TSC1* mutations. Renal AMLs were also seen at a higher frequency and were more severe in patients with *TSC2* mutations compared to those with *TSC1* mutations. Two further studies found that renal AMLs and renal cysts were less frequent in patients with a *TSC1* mutation compared to patients with a *TSC2* mutation of a similar age (Sancak *et al.* 2005, Au *et al.* 2007). In agreement with these findings, we found that *Tsc2*$^{+/-}$ mice at 11-12 months had significantly more renal lesions than *Tsc1*$^{+/-}$ mice, in particular, significantly more cysts were found in *Tsc2*$^{+/-}$ mice compared to *Tsc1*$^{+/-}$ mice at this age. Unlike the genotype/phenotype correlations carried out by Dabora *et al.*, we controlled for age by only comparing mice of a similar age. Age is an important factor as in the younger mice where cysts are fewer in number, no difference was found in the number of renal lesions present in *Tsc1*$^{+/-}$ and *Tsc2*$^{+/-}$ mice.

Our data is the first to demonstrate a genotype/phenotype correlation in rodent models of TSC that resembles the difference observed between *TSC1* and *TSC2* associated disease in humans. At least two hypotheses have been

suggested to explain why *TSC2* associated disease is more severe than *TSC1* disease (Dabora *et al.* 2001). Firstly, it is possible that second-hit events (following Knudson's two-hit model) occur more often in *TSC2* than in *TSC1*, possibly due to the larger gene size and mutational spectrum of *TSC2* and the more complex structure. Secondly, it is proposed that complete loss of tuberin has different effects in cells compared with the loss of hamartin. An interaction between tuberin and hamartin may be necessary for their function in the mTOR pathway; however independent functions of the proteins may also be vital to the cell as indicated by the different binding domains present in each protein (Krymskaya 2003, Rosner *et al.* 2008, chapter 1, section 1.1.8.4).

3.4.2 Differing phenotypes between Tsc rodent models and patients with TSC

Although the phenotype of $Tsc1^{+/-}$ and $Tsc2^{+/-}$ rodent models may differ from patients with TSC, there are similarities, for example, in humans and rodents, tumours develop at a high frequency with a slow growth rate and malignancies occurring only rarely (Cheadle *et al.* 2000). Similarities in the TSC renal phenotype also exist between humans and rodents. In $Tsc1^{+/-}$ and $Tsc2^{+/-}$ mouse models, cysts, cystadenomas and RCCs are the most common renal lesions. Renal cysts are also a common feature in patients with TSC, and, although the occurrence of RCC in these patients is unusual, an association is recognised (Henske 2004) with studies suggesting that as with the rodent models, RCCs in humans arise from dysplastic renal cyst epithelial cells (Al-Saleem *et al.* 1998).

Perhaps the most striking difference between $Tsc1^{+/-}$ and $Tsc2^{+/-}$ mouse models and patients with TSC is the absence of brain lesions and renal AMLs in mouse models. This is perhaps surprising given the occurrence of cerebral pathology in approximately 90% and renal AMLs in approximately 80% of patients with TSC (Gomez *et al.* 1999). Thus a mutation of the same gene can cause phenotypic variation between species. These differences may simply reflect the much smaller size and cell number of mice compared to humans (Cheadle *et al.* 2000). Longevity differences may also be responsible; indeed,

the prevalence of renal AMLs in patients with TSC is positively correlated with age, whereas cysts are the commoner lesion in childhood (Cook *et al.* 1996). It is also possible that the progenitor cells which give rise to human brain lesions have different mechanisms of tuberin/hamartin regulated growth and differentiation compared to mouse brain precursor cells (Cheadle *et al.* 2000).

3.4.3 Combined loss of *Tsc1* and *Tsc2* results in an additive effect on phenotype

Studies in humans and mice indicate that loss of *TSC2* can lead to a more severe phenotype compared to loss of *TSC1*; however, the effect of heterozygosity of both *TSC1* and *TSC2* in the same organism has not been studied. We attempted to investigate this using our mouse models and found what appears to be an additive affect on renal lesion number. In $Tsc1^{+/-}Tsc2^{+/-}$ mice at both 6 months and 11-12 months the number of renal lesions was approximately the sum of the single heterozygotes. These findings are consistent with hamartin and tuberin functioning as a complex in the same pathway. Combined haploinsufficiency of hamartin and tuberin and/or an increase in the target of second (somatic) hits (due to the availability of two genes now containing germline mutations) could be responsible for the additive increase in renal lesions in $Tsc1^{+/-}Tsc2^{+/-}$ mice.

3.4.4 Activation of the mTOR pathway is not essential for cyst formation

Since the discovery that *TSC1* and *TSC2* inhibit the function of mTOR through Rheb (Inoki *et al.* 2002, Tee *et al.* 2002), most research into TSC has focussed on the mTOR pathway. Clinical trials of the mTOR inhibitor rapamycin are currently underway, with promising results on advanced lesions such as AMLs in humans (Bissler *et al.* 2008, Davies *et al.* 2008); however its effects on early precursor lesions such as cysts remain unclear. We found little or no activation of the mTOR pathway in 33% of cysts from $Tsc1^{+/-}$ mice, 46% of cysts from $Tsc2^{+/-}$ mice and 32% of cysts from $Tsc1^{+/-}$ $Tsc2^{+/-}$ mice whereas almost all advanced lesions did exhibit mTOR activation. This is in support of previous work on $Tsc1^{+/-}$ mice where 37% (20/54) of cysts showed little or no pS6 staining, compared with only 7%

(7/98) of advanced lesions (P<0.001) (Wilson *et al.* 2006). To ensure the pS6 staining in one section of a cyst was representative of the entire cyst we carried out serial sectioning which encompassed entire cysts and found that negative or positive staining was consistent throughout a cyst. This data indicates that cysts are clonal and that our pS6 staining technique gave a valid representation of the entire cystic structure and phenotype.

Our data, together with the data from Kenerson *et al.* (2005) and Messina *et al.* (2007), suggest that many TSC-associated renal tumours initially develop via an mTOR-independent pathway. Therefore, although rapamycin may help control TSC-associated tumour development, it may not prevent tumour initiation. Further work into the mechanism of cyst initiation in TSC may eventually provide new therapeutic targets to prevent lesions from forming, and will be focussed on throughout this thesis.

3.4.5 Somatic *Tsc1* mutations are not abundant in renal cysts from *Tsc1*$^{+/-}$ mice

Our laboratory has previously shown that renal cyst formation may occur without the need of a somatic mutation in *Tsc1*$^{+/-}$ mice (Wilson *et al.* 2006). DNA was extracted from 19 renal cysts, 49 renal cystadenomas and 65 RCCs from *Tsc1*$^{+/-}$ mice using laser capture microdissection (LCM). LOH analyses and direct sequencing of the entire *Tsc1* ORF were used to identify somatic *Tsc1* mutations in DNA from these lesions. Interestingly, somatic *Tsc1* mutations were not found in 68.4% (13/19) of cysts compared to only 20.4% (10/49) of cystadenomas and 20.0% (13/65) of RCCs, demonstrating significantly fewer second hits in cysts as compared to cystadenomas (P=0.0003) and RCCs (P=0.0001). It would be informative if we could identify whether cysts with no somatic mutation also stain negative for pS6 therefore indicating a possible mTOR independent/haploinsufficient pathway of cystogenesis in these mice. Unfortunately, there were a number of reasons why we were unable to undertake both mutation analysis and IHC on the same cysts. Firstly, the small size of cysts makes LCM and extraction of sufficient amounts of DNA difficult. Secondly, pS6 staining was not successful in frozen tissue. Thirdly, DNA extracted from paraffin embedded tissue was

not reliable in LOH assays and finally, immunohistochemical staining of paraffin and frozen tissue hinders DNA extraction. Therefore, paraffin embedded pS6 stained cysts could not be used for DNA extraction and frozen cysts could not be stained for pS6.

Interestingly, second hits at *Tsc1* and activation of the mTOR pathway were found in the vast majority of more advanced renal tumours (Wilson *et al.* 2006) suggesting that these are important steps in the latter stages of *Tsc*-associated renal tumourigenesis.

CHAPTER FOUR: Investigating the relationship between hamartin, tuberin and PC1

4.1 Introduction

Cysts are the second most common renal lesion in patients with TSC, occurring in up to 47% of affected adults (Rosser *et al.* 2006). In TSC mouse models, renal cysts show 100% penetrance and appear to be the earliest renal lesions, later progressing into cystadenomas and RCC (chapter 3, section 3.3.2). The event or events that initiate cyst formation are unknown, but could reveal new targets for preventative therapies.

One of the most common inherited human cystic diseases is ADPKD, characterised by progressive development of multiple fluid filled cysts in the kidney (Boucher *et al.* 2004). Approximately 5% of patients with TSC also have a very severe form of PKD, normally due to an inherited contiguous deletion which spans both *TSC2* and *PKD1* (which lie adjacent to one another on chromosome 16p13.3) (Brook-Carter *et al.* 1994). The severity of this disease suggests that tuberin and PC1 may co-operate at a cellular level which markedly accelerates the disease process in such patients. Indeed, an interaction between tuberin and PC1 at the functional level has been reported (Kleymenova *et al.* 2001). Using the Eker rat model, Kleymenova *et al.* found that tuberin is required for membrane localisation of PC1 and in tuberin-deficient cells, PC1 is unable to exit the Golgi where it remains sequestered until expression of exogenous tuberin reinstates appropriate PC1 localisation. The authors concluded that tuberin is required for appropriate intracellular trafficking and localisation of PC1 to the lateral domain of the cell membrane. Recently, Shillingford *et al.* (2006) showed that the cytoplasmic tail of PC1 interacts with tuberin and the mTOR pathway is inappropriately activated in cyst-lining epithelial cells in human ADPKD patients and mouse models.

Here, we attempted to understand the mechanism of renal cyst formation in TSC and ADPKD by crossing our $Tsc1^{+/-}$ and $Tsc2^{+/-}$ mice with a mouse model of ADPKD1 which has exons 17-21 replaced with a promoterless cassette ($Pkd1^{del17\text{-}21\beta geo}$ mouse model, hereafter termed

Pkd1$^{+/-}$) (Boulter *et al.* 2001). We also sought whether the human *TSC2/PKD1* contiguous deletion phenotype could be recapitulated in *Tsc1*$^{+/-}$*Pkd1*$^{+/-}$ and *Tsc2*$^{+/-}$*Pkd1*$^{+/-}$ mice. The role of mTOR activation was also investigated in a more severe *Pkd1*-deficiency model known as the *Pkd1*^{nl} mouse model (Lantinga-van Leeuwen *et al.* 2004).

4.2 Materials and methods

4.2.1 DNA extraction and PCR genotyping

DNA was extracted from tail tips as previously described (chapter 2, section 2.5.4.1). PCR genotyping of DNA from tail tips was performed by amplification of the wild-type and mutant alleles for *Pkd1* using the following primers in a 35 cycle PCR reaction with AmpliTaq gold DNA polymerase (Applied Biosystems). *Pkd1* wild-type allele: Pkd1WTF 5'-GCTCGCACTTTCAGCAATAAGAC-3' and Pkd1WTR 5'-CAGGATTTCCACTGGGTTCT-3' (661bp product), *Pkd1* mutant allele, Pkd1NEOF 5'-AGCGTTGGCTACCCGTGATATTG-3' and Pkd1EXON21R 5'-GTCTCCGTGATGTTCTTACGCATT-3' (731bp product). *Tsc1* and *Tsc2* were genotyped as previously described in chapter 3, section 3.2.1. Products were analysed on 2% agarose gels. Some genotyping assistance was provided by Carol Guy and Rebecca Harris. Genotyping for *Pkd1*$^{nl/nl}$ mice was carried out as previously described (Lantinga-van Leeuwen *et al.* 2004).

4.2.2 Animal care, necropsy and pathology

Tsc1$^{+/-}$ (Wilson *et al.* 2005) and *Tsc2*$^{+/-}$ mice (Onda *et al.* 1999) were crossed with *Pkd1*$^{+/-}$ mice (on a 129/Sv background) (Boulter *et al.* 2001) to produce *Tsc1*$^{+/-}$, *Tsc2*$^{+/-}$, *Pkd1*$^{+/-}$, *Tsc1*$^{+/-}$*Pkd1*$^{+/-}$, *Tsc2*$^{+/-}$*Pkd1*$^{+/-}$ and wild-type progeny. Kidneys and livers from 5 mice of each genotype were analysed at 6-7, 9-12 and 15-18 months of age. Tissue processing and lesion examination was carried out as described in chapter 3, section 3.3.2. Four micron thick *Pkd1*$^{nl/nl}$ paraffin embedded kidney sections were provided by Richard Sandford (Department of Medical Genetics, University of Cambridge, UK) from mice acquired from Dorien Peters (Leiden University Medical Centre, The Netherlands).

Mice from the above crosses were also examined at weaning (between 3-4 weeks of age) for the presence of PKD. Over 200 mice from the *Tsc1*$^{+/-}$ and *Pkd1*$^{+/-}$ crosses and over 200 mice from the *Tsc2*$^{+/-}$ and *Pkd1*$^{+/-}$ crosses were examined macroscopically following cervical dislocation. Kidneys with PKD were removed, processed and examined as described above.

4.2.3 Immunohistochemistry

Immunohistochemistry of kidney and liver paraffin sections from 5 mice from each genotype was performed as previously described (chapter 2, section 2.5.11) and analysed as described in chapter 3, section 3.2.3. Kidneys with a PKD phenotype from mice at weaning were also examined for pS6. In addition, pS6 staining was performed on kidney sections (two from each mouse) from three *Pkd1*$^{nl/nl}$ mice and one wild-type mouse. Statistics were performed as described in chapter 3, section 3.2.4.

4.3 Results

4.3.1 Sequencing of *Pkd1* insert and primer design

The *Pkd1* gene in our *Pkd1*$^{+/-}$ mice is disrupted by a promoterless cassette containing a donor *engrailed-2* intron and splice acceptor site, an internal ribosome entry site (IRES) coupled to a *lacZ-neomycin*^{R} fusion gene (*βgeo*) and a simian virus 40 polyadenylation site (Figure 4.1). Boulter *et al.* (2001) state that this cassette deletes a 1.5kb *Hin*dIII–*Xba*I fragment which contains exons 17–21. We therefore sought to sequence part of this cassette to enable us to design new allele specific primers for genotyping of our mice.

Analysis of the *Pkd1* gene sequence revealed that the *XbaI* restriction site was situated ~40bp upstream from exon 21, indicating that exon 21 was not actually deleted by the cassette. To confirm this we designed reverse primers in exon 21 (exon21R 5'-GTCTCCGTGATGTTCTTACGCATT-3') and exon 22 (exon22R 5'-AGCATCTTCTTCAGGCAGGA-3') which we then used in separate reactions with a primer designed within the *neo* sequence of the cassette (neoF 5'- AGCGTTGGCTACCCGTGATATTG-3', 731bp and 1608bp respectively). Both sets of primers showed clear bands, indicating that exon 21 and exon 22 were still present in the mutant allele and subsequent sequencing of these fragments generated sufficient sequence to design new genotyping primers (Figure 4.1). The wild-type forward (Pkd1WTF) and reverse (Pkd1WTR) primers are situated in exons 18 and 20 respectively, as these were deleted by the construct in mutant alleles, whilst the mutant forward primer (Pkd1NEOF) is situated in the *neo* cassette with the corresponding reverse primer (Pkd1EXON21R) in exon 21, thus ensuring *Pkd1* mutant allele specific amplification.

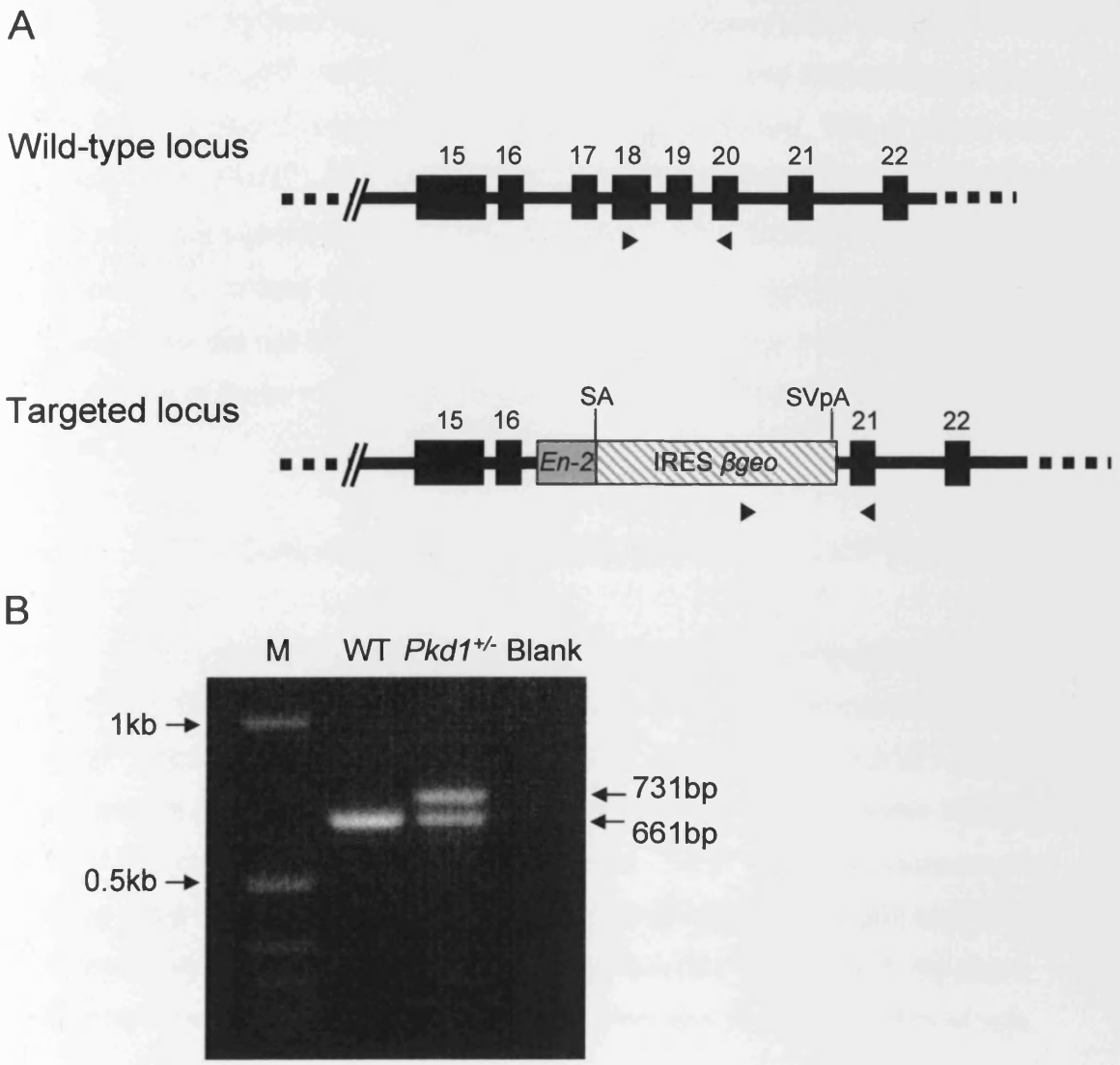

Figure 4.1 Targeted *Pkd1* locus and PCR genotyping results. (**A**) Schematic illustration of the wild-type *Pkd1* locus (upper panel) and the targeted locus (lower panel). Using homologous recombination, *Pkd1* exons 17–20 were replaced with a *lacZ-neomycin* fusion gene (βgeo) located downstream of an *engrailed-2* gene donor intron (En-2), splice acceptor site (SA) and an IRES, and upstream of a simian virus 40 polyadenylation signal (SVpA). Exons are shown as numbered black rectangles, introns as a thick black line, and flanking genomic regions as a thick dashed line. The fusion gene is shown as a large light grey striped rectangle (IRES-*βgeo* component) upstream of a filled light grey rectangle (*engrailed-2* gene donor intron component). The genotyping primers are shown as black triangles. (**B**) PCR analysis of genotyping primers. *Pkd1*$^{+/-}$ mice contain both the wild-type fragment (661bp) and the mutant fragment (731bp). Wild-type mice contain only the wild-type fragment. M = marker, WT = wild-type.

4.3.2 Renal pathology

From 36 *Tsc1*$^{+/-}$ x *Pkd1*$^{+/-}$ crosses, 629 progeny were obtained, 152 of which were *Tsc1*$^{+/-}$, 164 *Pkd1*$^{+/-}$, 147 *Tsc1*$^{+/-}$*Pkd1*$^{+/-}$ and 166 wild-type. From 33 *Tsc2*$^{+/-}$ x *Pkd1*$^{+/-}$ crosses, 631 progeny were obtained, 166 of which were *Tsc2*$^{+/-}$, 161 *Pkd1*$^{+/-}$, 142 *Tsc2*$^{+/-}$*Pkd1*$^{+/-}$ and 162 wild-type. These genotypes did not differ significantly from the expected 1:1:1:1 ratio (χ^2=1.62 and 2.19 respectively, critical value of χ^2=7.815 at *P*=0.05). In agreement with other studies, we did not find any *Pkd1*$^{-/-}$ live pups, indicating that homozygous mutations in these mice are embryonic lethal as previously reported (Boulter *et al.* 2001).

4.3.2.1 Comparison of renal lesions from Pkd1$^{+/-}$*, Tsc1*$^{+/-}$ *and Tsc2*$^{+/-}$ *mice*

No cysts were observed in *Pkd1*$^{+/-}$ mice at 6-7 months of age. At both 9-12 and 15-18 months of age, low numbers of renal cysts were observed in *Pkd1*$^{+/-}$ mice from both crosses ranging from an average of 1.2 to 7.6 lesions per mouse (Tables 4.1 and 4.2). No cystadenomas or RCCs were observed in *Pkd1*$^{+/-}$ mice. At 6-7, 9-12 and 15-18 months, *Tsc2*$^{+/-}$ mice had consistently more renal lesions compared to *Tsc1*$^{+/-}$ mice (*P*=0.012, *P*=0.031 and *P*=0.004 respectively), consistent with our results presented in chapter 3. No renal lesions were observed in wild-type littermates less than 18 months of age.

4.3.2.2 Comparison of renal lesions from compound heterozygotes and single heterozygote littermates

We failed to find any *Tsc1*$^{+/-}$ *Pkd1*$^{+/-}$ mice with a gross PKD phenotype between 6-18 months of age. At 6-7 months renal lesion numbers were very low in both *Tsc1*$^{+/-}$ mice and *Tsc1*$^{+/-}$ *Pkd1*$^{+/-}$ mice respectively (4 and 8.4 lesions per mouse respectively, *P*=0.12). We found that at 9-12 months, *Tsc1*$^{+/-}$*Pkd1*$^{+/-}$ mice had significantly more renal lesions (32 lesions per mouse) compared to either *Pkd1*$^{+/-}$ (5.2 lesions per mouse, *P*=0.01) or *Tsc1*$^{+/-}$ (10 lesions per mouse, *P*=0.01) mice (Table 4.1, Figure 4.2). In terms of the type of lesion, *Tsc1*$^{+/-}$ *Pkd1*$^{+/-}$ mice had significantly more cysts and cystadenomas as compared to either *Pkd1*$^{+/-}$ (*P*=0.02 and *P*<0.01,

respectively) or *Tsc1*$^{+/-}$ mice (*P*=0.01 and *P*=0.009, respectively) (Table 4.1). By 15-18 months, no significant difference was observed in the total number of renal lesions from *Tsc1*$^{+/-}$ *Pkd1*$^{+/-}$ mice (28.8 lesions per mouse) compared to *Tsc1*$^{+/-}$ mice (19.2 lesions per mouse).

A gross PKD phenotype was not observed in any *Tsc2*$^{+/-}$ *Pkd1*$^{+/-}$ mice between the ages of 6-18 months. Interestingly, whereas the number of renal lesions in *Tsc2*$^{+/-}$ mice steadily rose from 6-7 months to 15-18 months, the number of lesions in *Tsc2*$^{+/-}$ *Pkd1*$^{+/-}$ mice at 6-7 months was considerably higher at 90.4 lesions per mouse, compared to 53.2 lesions per mouse at 9-12 months (Table 4.2). At 9-12 months, the number of renal lesions from *Tsc2*$^{+/-}$ *Pkd1*$^{+/-}$ and *Tsc2*$^{+/-}$ mice were similar at 53.2 and 59.6 respectively, however, when the types of these lesions were examined, the *Tsc2*$^{+/-}$ *Pkd1*$^{+/-}$ mice had double the number of cystadenomas and significantly more RCCs compared to *Tsc2*$^{+/-}$ mice (*P*=0.03) (Table 4.2). We also found that *Tsc2*$^{+/-}$ *Pkd1*$^{+/-}$ mice had more renal lesions (228.8 lesions per mouse), that were more advanced, as compared to *Tsc2*$^{+/-}$ mice (152 lesions per mouse) at 15-18 months (*P*=0.03) (Table 4.2, Figure 4.3).

Finally, significantly more renal lesions were observed in *Tsc2*$^{+/-}$ *Pkd1*$^{+/-}$ mice compared to *Tsc1*$^{+/-}$ *Pkd1*$^{+/-}$ mice at 6-7 and 15-18 months of age (*P*=0.03 and *P*=0.001 respectively).

Table 4.1 Average number and histological classification of microscopic renal lesions in *Tsc1*$^{+/-}$, *Pkd1*$^{+/-}$ and *Tsc1*$^{+/-}$*Pkd1*$^{+/-}$ mice.

Age	Genotype	Cyst	Cystadenoma	RCC	Total lesions
6-7 months	*Tsc1*$^{+/-}$	3.2	0.8	0	**4***
	Pkd1$^{+/-}$	0	0	0	**0**
	Tsc1$^{+/-}$*Pkd1*$^{+/-}$	7.2	1.2	0	**8.4***
9-12 months	*Tsc1*$^{+/-}$	8.4	1.2	0.4	**10**$^{\# \dagger}$
	Pkd1$^{+/-}$	5.2	0	0	**5.2**$^{\# \diamond}$
	Tsc1$^{+/-}$*Pkd1*$^{+/-}$	21.2	10	0.8	**32**$^{\dagger \diamond}$
15-18 months	*Tsc1*$^{+/-}$	10.4	7.6	1.2	**19.2**$^{+ \ddagger}$
	Pkd1$^{+/-}$	1.2	0	0	**1.2**$^{+ \pm}$
	Tsc1$^{+/-}$*Pkd1*$^{+/-}$	12.4	13.2	3.2	**28.8**$^{\ddagger \pm}$

Numbers based on the analyses of five sections (~200μm apart) from half kidneys of five mice from each of the above genotypes in each age group.
*P=0.12, $^{\#}P$=0.34, $^{\dagger}P$=0.01, $^{\diamond}P$<0.001, ^{+}P=0.01, $^{\ddagger}P$=0.2, $^{\pm}P$<0.001

Table 4.2 Average number and histological classification of microscopic renal lesions in *Tsc2*$^{+/-}$, *Pkd1*$^{+/-}$ and *Tsc2*$^{+/-}$*Pkd1*$^{+/-}$ mice.

Age	Genotype	Cyst	Cystadenoma	RCC	Total lesions
6-7 months	*Tsc2*$^{+/-}$	21.2	2	0.4	**23.6***
	Pkd1$^{+/-}$	0	0	0	**0**
	Tsc2$^{+/-}$*Pkd1*$^{+/-}$	88.4	2	0	**90.4***
9-12 months	*Tsc2*$^{+/-}$	49.2	9.6	0.8	**59.6**$^{\# \dagger}$
	Pkd1$^{+/-}$	7.6	0	0	**7.6**$^{\# \diamond}$
	Tsc2$^{+/-}$*Pkd1*$^{+/-}$	30	19.2	4	**53.2**$^{\dagger \diamond}$
15-18 months	*Tsc2*$^{+/-}$	126.4	20	5.6	**152**$^{+ \ddagger}$
	Pkd1$^{+/-}$	3.6	0	0	**3.6**$^{+ \pm}$
	Tsc2$^{+/-}$*Pkd1*$^{+/-}$	157.2	56.4	15.2	**228.8**$^{\ddagger \pm}$

Numbers based on the analyses of five sections (~200μm apart) from half kidneys of five mice from each of the above genotypes in each age group.
*P=0.4, $^{\#}P$=0.01, $^{\dagger}P$=0.83, $^{\diamond}P$=0.016, ^{+}P=0.01, $^{\ddagger}P$=0.4, $^{\pm}P$=0.001

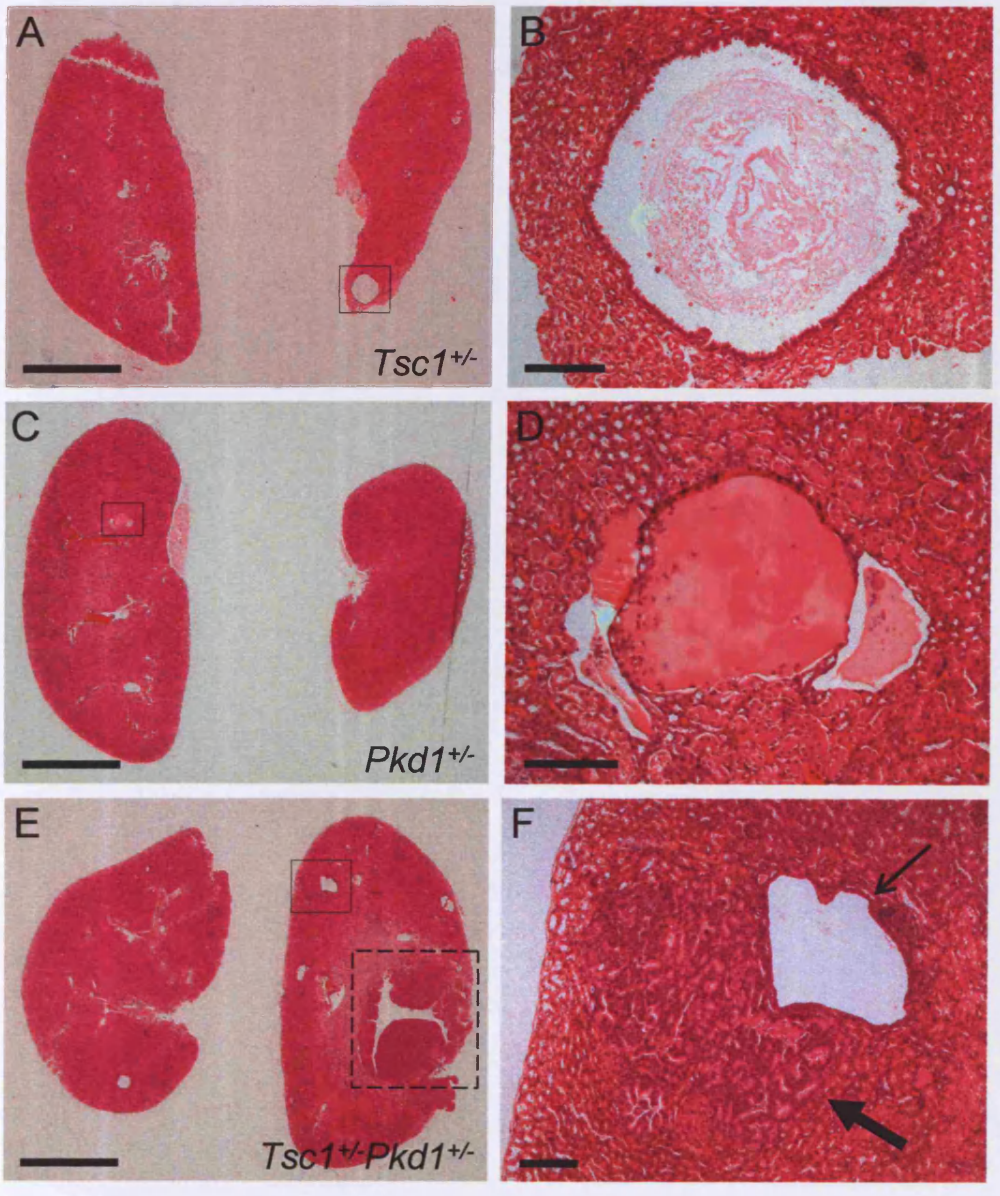

Figure 4.2 Microscopic analysis of renal lesions from *Tsc1*$^{+/-}$, *Pkd1*$^{+/-}$ and *Tsc1*$^{+/-}$*Pkd1*$^{+/-}$ mice at 9-12 months of age. (**A**) Kidneys from a *Tsc1*$^{+/-}$ mouse with a cyst boxed and enlarged in **B**. (**B**) Cyst lined with a single layer of cuboidal epithelial cells. (**C**) Kidneys from a *Pkd1*$^{+/-}$ mouse with a cyst (boxed and enlarged in **D**). (**D**) Fluid filled cyst from a *Pkd1*$^{+/-}$ mouse kidney. (**E**) Kidneys from a *Tsc1*$^{+/-}$ *Pkd1*$^{+/-}$ mouse with a large RCC highlighted by a dashed box; solid line boxed region (enlarged in **F**) shows a cystadenoma (large filled arrow) and an adjacent cyst (thin arrow). Significantly more renal lesions were found in *Tsc1*$^{+/-}$*Pkd1*$^{+/-}$ mice compared to either *Tsc1*$^{+/-}$ or *Pkd1*$^{+/-}$ mice (P=0.01 for both). Scale bars: **A**, **C** and **E**; 2mm, **B**, **D** and **F**; 200μm.

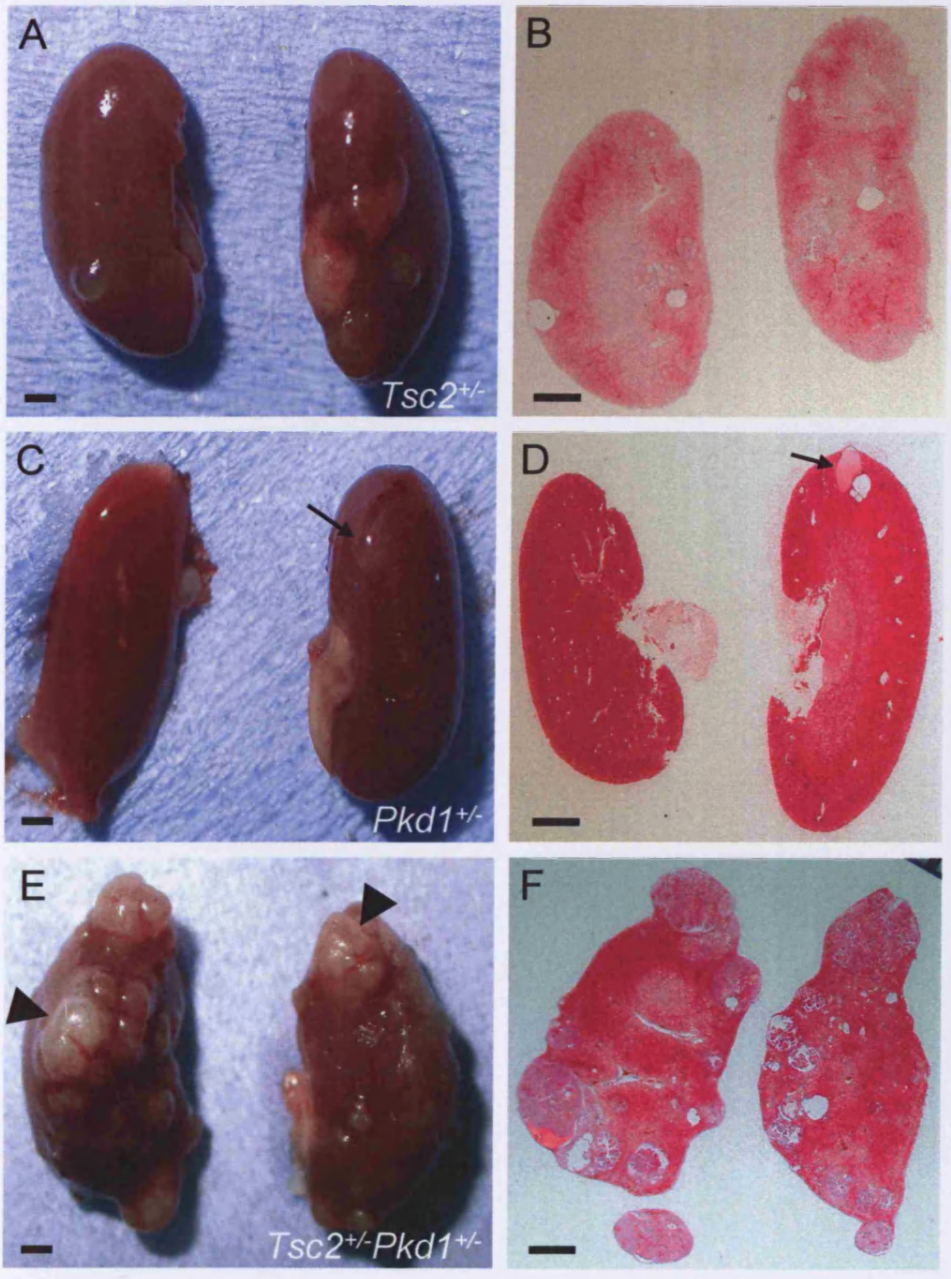

Figure 4.3 Macroscopic and microscopic analysis of renal lesions from *Tsc2*$^{+/-}$, *Pkd1*$^{+/-}$ and *Tsc2*$^{+/-}$*Pkd1*$^{+/-}$ mice at 15-18 months of age. (**A**, **B**) Macroscopic view and H&E section of kidneys from a *Tsc2*$^{+/-}$ mouse showing cysts, cystadenoma and RCC. (**C**, **D**) Macroscopic view and H&E section of kidneys from a *Pkd1*$^{+/-}$ mouse showing a cyst (arrows). (**E**, **F**) Macroscopic view and H&E section of kidneys from a *Tsc2*$^{+/-}$*Pkd1*$^{+/-}$ mouse showing many RCCs (examples indicated by arrow heads) as well as cysts and cystadenomas. Scale bar: 2mm.

4.3.3 Extra-renal pathology

Liver cysts were found in approximately 20-40% of *Pkd1*$^{+/-}$, *Tsc1*$^{+/-}$*Pkd1*$^{+/-}$ and *Tsc2*$^{+/-}$*Pkd1*$^{+/-}$ mice over 15 months of age. No liver cysts were found in wild-type, *Tsc1*$^{+/-}$ or *Tsc2*$^{+/-}$ mice. Macroscopically, liver cysts ranged in size from 0.3-3cm in diameter (Figure 4.4). The very large liver cysts (over 1 inch) tended to be found in mice over 20 months of age. Microscopically, all liver cysts were lined with a single layer of epithelium and had no papillary projections (Figure 4.4).

4.3.4 pS6 immunohistochemistry

We tested for activation of the mTOR pathway by staining cells for the presence of pS6.

4.3.4.1 pS6 staining in renal and liver cysts from Pkd1$^{+/-}$ *mice and renal cysts from Pkd1*$^{nl/nl}$ *mice*

We examined 42 renal cysts and 10 liver cysts from *Pkd1*$^{+/-}$ mice and failed to identify any cysts that stained for pS6 (Table 4.3, Figures 4.4 and 4.5). Although we did observe some renal cysts that stained for pS6 from the *Pkd1*$^{nl/nl}$ mice, we found that significantly less small cysts (<50μm) stained (56%, 168/300) compared to large cysts (>200μm) (85%, 93/110; P<0.001) (Table 4.4, Figure 4.5).

4.3.4.2 pS6 staining in renal lesions and liver cysts from compound heterozygous mice

We found that 47% (27/58) of renal cysts from *Tsc1*$^{+/-}$*Pkd1*$^{+/-}$ mice failed to stain for pS6, whereas 93% (26/28) of advanced lesions (cystadenomas and RCCs) from these mice did stain (P<0.001), and similarly, in *Tsc2*$^{+/-}$*Pkd1*$^{+/-}$ mice, significantly fewer renal cysts stained for pS6 as compared to advanced lesions (128/163 vs. 42/42, P<0.001) (Table 4.3, Figure 4.5). We also examined 8 liver cysts from *Tsc1*$^{+/-}$*Pkd1*$^{+/-}$ mice and 7 from *Tsc2*$^{+/-}$*Pkd1*$^{+/-}$ mice and failed to find any that stained for pS6 (Figure 4.4).

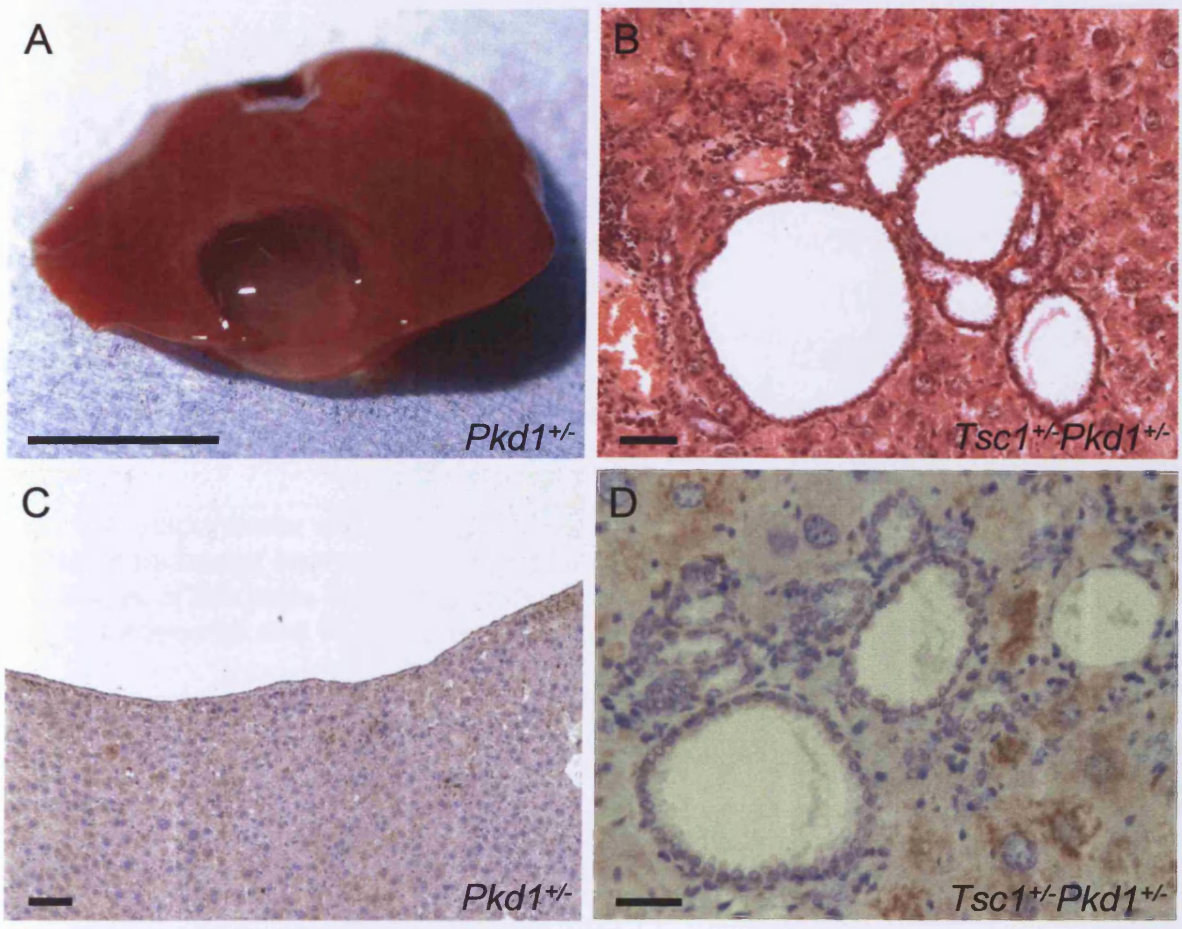

Figure 4.4 H&E and immunohistochemistry analysis of murine liver lesions using anti-pS6. (**A**) Large liver cyst from a *Pkd1*$^{+/-}$ mouse. (**B**) Section through a focal multi-cystic region found in the liver of a *Tsc1*$^{+/-}$*Pkd1*$^{+/-}$ mouse. Cyst are lined with a single layer of cuboidal epithelial cells. (**C**, **D**) Corresponding pS6 staining of cysts in **A** and **B**. No staining was seen in any liver cysts. Scale bars: **A**; 5mm, **B** & **D**; 50μm, **C**; 0.1mm.

Table 4.3 pS6 analysis of renal lesions from *Pkd1*$^{+/-}$, *Tsc1*$^{+/-}$*Pkd1*$^{+/-}$ and *Tsc2*$^{+/-}$*Pkd1*$^{+/-}$ mice.

Genotype	Lesion type	Number pS6 positive
Pkd1$^{+/-}$	Cyst	0/30 (0%)
	Cystadenoma	n/a
	RCC	n/a
Tsc1$^{+/-}$*Pkd1*$^{+/-}$	Cyst	31/58 (53%)*
	Cystadenoma	24/26 (92%)* [a]
	RCC	2/2 (100%)
Tsc2$^{+/-}$*Pkd1*$^{+/-}$	Cyst	128/163 (78%)#
	Cystadenoma	40/40 (100%)# [a]
	RCC	2/2 (100%)

n/a, cystadenomas and RCCs were not found in *Pkd1*$^{+/-}$ mice.
Numbers based on the analyses of five sections (~200μm apart) from half kidneys of five mice from each of the above genotypes.
[a] cystadenoma and RCC values combined, *P<0.001, #P<0.001

Table 4.4 pS6 analysis of renal lesions from *Pkd1*$^{nl/nl}$ mice.

Mouse	pS6 +ve cysts <50μm diameter	pS6 +ve cysts >200μm diameter	Total cysts pS6 +ve
WT	n/a	n/a	n/a
Pkd1$^{nl/nl}$ 1	55/100 (55%)	12/14 (86%)	147/250 (59%)
Pkd1$^{nl/nl}$ 2	55/100 (55%)	35/41 (85%)	621/848 (73%)
Pkd1$^{nl/nl}$ 3	58/100 (58%)	46/55 (84%)	1065/1340 (80%)

n/a, no cysts were present for scoring.
Numbers based on the analyses of one section from half kidneys of each of the above mice.
Significantly less small cysts (<50μm) stained positive for pS6 (56%, 168/300) compared to large cysts (>200μm) (85%, 93/110; P<0.001).

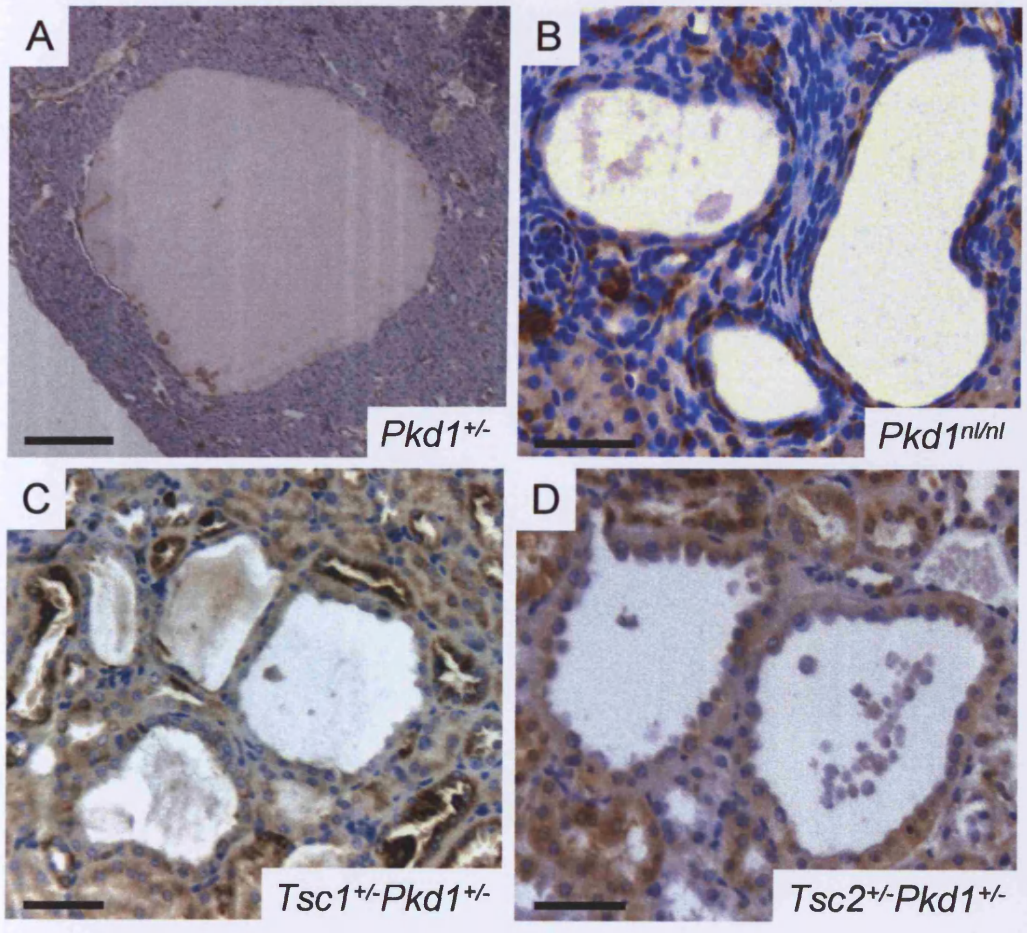

Figure 4.5 Immunohistochemistry analysis of murine renal lesions using anti-pS6. Examples of cysts from *Pkd1*$^{+/-}$ (**A**), *Pkd1*$^{nl/nl}$ (**B**), *Tsc1*$^{+/-}$*Pkd1*$^{+/-}$ (**C**) and *Tsc2*$^{+/-}$*Pkd1*$^{+/-}$ (**D**) mice that did not stain for pS6. Scale bars: (**A**) 0.2mm, (**B**-**D**) 50µm.

4.3.5 Study of mice with early onset PKD

We failed to find any mice in the previous *Tsc1*$^{+/-}$*Pkd1*$^{+/-}$ and *Tsc2*$^{+/-}$ *Pkd1*$^{+/-}$ studies that recapitulated the contiguous gene syndrome phenotype of early onset severe PKD. We reasoned that mice with early onset PKD may have died before the age of 6 months (the earliest age we previously examined) and so we therefore set up a breeding programme where mice were examined at weaning. In over 200 mice generated from *Tsc2*$^{+/-}$ x *Pkd1*$^{+/-}$ crosses we identified three mice with a polycystic renal phenotype (no extra-renal lesions were observed). Two of these mice were characterised as *Tsc2*$^{+/-}$ and one was a *Tsc2*$^{+/-}$*Pkd1*$^{+/-}$. No mice from over 200 offspring generated from *Tsc1*$^{+/-}$ x *Pkd1*$^{+/-}$ crosses were identified with PKD.

4.3.5.1 Renal pathology of mice with early onset PKD

PKD in the three mice was unilateral, with one normal kidney and one polycystic kidney (Figure 4.6). Macroscopically, the polycystic kidney appeared enlarged but maintained its reniform shape and had a smooth cortical surface with multiple cysts clearly visible under the surface. Upon longitudinal bisection, the cysts were distributed homogeneously throughout the cortical and medullary regions and ranged in size from <1mm to 5mm (Figure 4.6). Microscopically, the cysts differed in morphology with those from the two *Tsc2*$^{+/-}$ mice resembling TSC-associated cysts (Figure 4.2, panel B) lined with a single layer of cuboidal epithelial cells. Four cystadenomas were observed in one of the *Tsc2*$^{+/-}$ polycystic kidneys whilst five were observed in the other. Cysts from the *Tsc2*$^{+/-}$*Pkd1*$^{+/-}$ mouse with PKD were lined with a single layer of flattened looking epithelial cells similar to those observed in *Pkd1*$^{+/-}$ mice. No cystadenomas were observed in this mouse.

4.3.5.2 pS6 staining in polycystic kidneys from mice with early onset PKD

All kidney cysts and cystadenomas from the polycystic kidneys of the two *Tsc2*$^{+/-}$ mice stained positive for pS6 (Figure 4.7). In the *Tsc2*$^{+/-}$*Pkd1*$^{+/-}$ mouse with PKD, the majority of cysts were negative for pS6 except for a large cyst which showed pS6 staining within the single layer of epithelial cells and also closely surrounding cells (Figure 4.7).

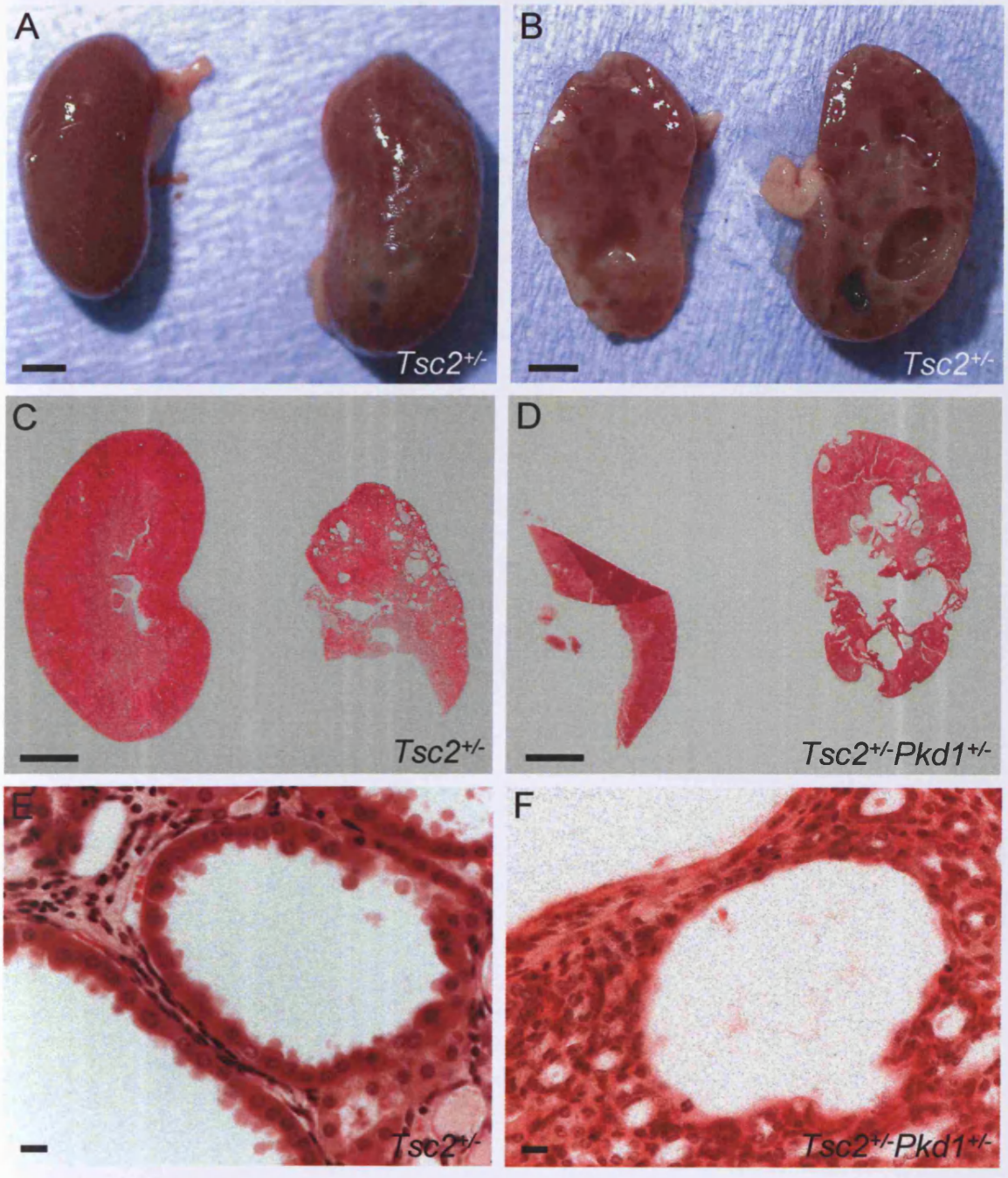

Figure 4.6 Macroscopic and microscopic images of polycystic kidneys from 3-4 week old mice with early onset PKD. (**A**) Macroscopic image showing the unilateral nature of the polycystic kidney phenotype with one normal looking kidney (on the left) and one polycystic kidney (on the right) both from the same mouse. (**B**) Macroscopic image of the polycystic kidney from (**A**) cut in half to reveal the internal cysts which are present throughout the cortex and medulla. (**C**, **D**) H&E images of the kidneys from *Tsc2*$^{+/-}$ and *Tsc2*$^{+/-}$*Pkd1*$^{+/-}$ mice with early onset PKD which show the normal architecture of one kidney and the polycystic architecture of the other. (**E**) Microscopic image of a cyst from a *Tsc2*$^{+/-}$ mouse with PKD showing a single layer of cuboidal epithelial cells in contrast to the *Tsc2*$^{+/-}$*Pkd1*$^{+/-}$ mouse with PKD (**F**) where the cyst lining epithelial cells are flattened in appearance. Scale bars: (**A**-**D**) 2mm, (**E**, **F**) 10μm.

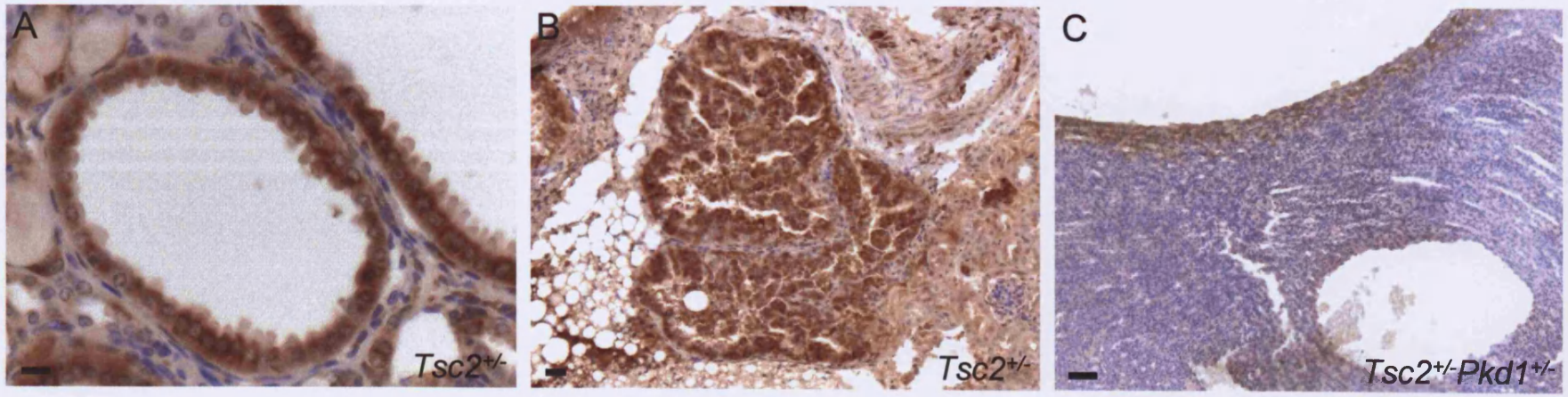

Figure 4.7 Immunohistochemistry analysis of polycystic kidneys from 3-4 week old mice with early onset PKD using anti-pS6. Cysts (**A**) and a cystadenoma (**B**) from a *Tsc2*$^{+/-}$ mouse with PKD showing strong staining for pS6. (**C**) Large cyst (top left) showing staining for pS6 and small cyst (bottom right) negative for pS6 from the *Tsc2*$^{+/-}$*Pkd1*$^{+/-}$ mouse with PKD. The majority of cysts in this mouse were negative for pS6. Scale bars: **A**; 10μm, **B**; 20μm, **C**; 40μm.

4.4 Discussion

4.4.1 Genetic interaction between *Tsc1*, *Tsc2* and *Pkd1*

A genetic interaction between *TSC2* and *PKD1* is suggested by the severe early onset PKD phenotype of the *TSC2/PKD1* contiguous gene deletion syndrome (Brook-Carter *et al.* 1994, Sampson *et al.* 1997). We bred $Tsc2^{+/-}$ mice with $Pkd1^{+/-}$ mice in an attempt to recapitulate this phenotype; however, although we found more renal lesions that were more advanced in $Tsc2^{+/-}Pkd1^{+/-}$ mice, this was not on the same scale as that seen in the contiguous gene syndrome. Severe PKD was not a common feature of these mice, which instead presented with an increased burden of a mixture of cysts, cystadenomas and RCC which progressed in severity with age.

Tuberin and hamartin physically interact to from a tumour suppressor complex (van Slegtenhorst *et al.* 1998, Tee *et al.* 2003) and it is therefore of interest to investigate whether a similar enhanced kidney phenotype is produced in $Tsc1^{+/-}Pkd1^{+/-}$ compound heterozygous mice. Severe PKD was not a phenotype of the $Tsc1^{+/-}Pkd1^{+/-}$ mice, however significantly more renal lesions (cysts, cystadenomas and RCCs) were found in these mice compared to their single heterozygote littermates.

This data, although different to the human *TSC2/PKD1* contiguous gene deletion syndrome, indicates that a genetic interaction exists between *Tsc1*, *Tsc2* and *Pkd1*. Although *TSC2* and *PKD1* lie immediately adjacent to each other on chromosome 16 in humans, *TSC1* lies separately on chromosome 9. In our mouse models, although *Tsc2* and *Pkd1* lie adjacent to each other on chromosome 17, the gene targeting constructs will lie in different alleles and *Tsc1* is located on chromosome 2. This suggests that *trans*-regulatory changes, perhaps in combination with *cis*-regulatory changes, may affect gene expression and play a role in disease severity.

4.4.1.1 Advanced renal lesions may obscure accurate lesion counting

The main underlying problem when using renal lesion number as a marker of disease severity is that advanced renal lesions (such as cystadenomas and RCCs) tend to be much larger than the earlier renal cysts

and invade much of the kidney, obscuring the smaller more numerous cysts (Wilson *et al.* 2005). Where 10 small cysts may once have been, a RCC may later infiltrate that space, thus making the overall renal lesion number lower, but the severity of the disease greater. This could explain some of the unusual renal lesion number results we observed, for example, between 6-7 months and 9-12 months of age, the overall lesion number in *Tsc2*$^{+/-}$*Pkd1*$^{+/-}$ mice actually decreased with age (although not significantly) from an average of 90.4 lesions per mouse to 53.2 lesions per mouse respectively. An explanation for this can be found when the types of these lesions are examined. Ninety eight percent (221/226) of lesions in the 6-7 month old mice are cysts, whereas in the 9-12 month old *Tsc2*$^{+/-}$*Pkd1*$^{+/-}$ mice only 56% (75/133) of the lesions are cysts, indicating that a significantly larger proportion of advanced lesions (cystadenomas and RCCs) are present in older mice ($P<0.001$).

Perhaps one slightly odd result that cannot be explained by the presence of large advanced lesions obscuring accurate lesion numbers is the small decrease in the number of renal cysts in *Pkd1*$^{+/-}$ mice as age increased from 9-12 months to 15-18 months (from an average of 5.2 to 1.2 lesions per mouse in *Pkd1*$^{+/-}$ mice from *Tsc1*$^{+/-}$ x *Pkd1*$^{+/-}$ crosses and from 7.6 to 3.6 lesions per mouse in *Pkd1*$^{+/-}$ mice from *Tsc2*$^{+/-}$ x *Pkd1*$^{+/-}$ crosses). Due to the small *n* value it is unclear whether this observation is a true representation of cyst regression in older animals, however a similar phenomenon was found by Jiang *et al.* when working on the conditional *Pkd1*^{L3} mouse model (Jiang *et al.* 2006). The authors observed cyst regression, linked to cyst epithelia apoptosis, in mice past the age of 30 days. They state infiltration of inflammatory cells, hypoxia and a general hostile environment for tubular cell survival as possible mechanisms for apoptosis in these cystic epithelial cells. Although this model is more severe than our *Pkd1*$^{+/-}$ mouse model, further lesion counting and terminal dUTP nick-end labelling (TUNEL) staining could reveal more about possible cyst regression in these mice.

4.4.2 Functional interaction between hamartin, tuberin and PC1

Another possible reason for the significant increase in lesion numbers and/or advancement of these lesions found in our compound heterozygous mice could be that second hits, due to the availability of two genes now containing germline mutations, are occurring more frequently and thus increasing the lesion burden. However, one would expect an additive increase in lesion numbers if this were the case, unlike the much greater increase in lesion numbers observed in our *Tsc1*$^{+/-}$*Pkd1*$^{+/-}$ and *Tsc2*$^{+/-}$*Pkd1*$^{+/-}$ mice. Many studies have also found that second hits are not apparent in all TSC and ADPKD associated lesions (Wilson *et al.* 2006, Onda *et al.* 1999, Koptides *et al.* 2000).

Perhaps a combined drop in gene dosage levels could lead to a more than additive phenotype in *Tsc1*$^{+/-}$*Pkd1*$^{+/-}$ and *Tsc2*$^{+/-}$*Pkd1*$^{+/-}$ mice. The signalling pathways downstream from PC1, tuberin and hamartin may converge at some crucial point, with loss of an allele of each taking the gene dosage level below a critical threshold, thus accelerating disease initiation and progression. Indeed, when *Pkd1*$^{+/-}$ mice were bred with *Pkd2*$^{+/-}$ mice (Wu *et al.* 2002), cystic disease in the *trans*-heterozygous mice was notably more severe than that predicted by a simple additive effect in the single heterozygous mice. The authors state that their data suggest a modifier role for the '*trans*' polycystin gene in cystic kidney disease, and support a contribution from threshold effects to cyst formation and growth (Wu *et al.* 2002). As previously mentioned, tuberin and PC1 have been found to functionally and physically interact, with tuberin trafficking PC1 from the Golgi to the lateral cell membrane (Kleymenova *et al.* 2001) at which point PC1 has been suggested to assemble a complex with tuberin and mTOR through interaction with its cytoplasmic C-terminal tail (Shillingford *et al.* 2006, Mostov 2006). A combined reduction in each protein (tuberin and PC1) in *Tsc2*$^{+/-}$ *Pkd1*$^{+/-}$ mice may potentially lead to an even greater drop in the amount of functionally active protein, thus leading to a more severe disease phenotype. As hamartin and tuberin have been shown to form a tumour suppressor complex, the same may also apply to *Tsc1*$^{+/-}$*Pkd1*$^{+/-}$ mice.

4.4.3 A rare occurrence of mice with severe early onset PKD was observed

Interestingly, although extremely rare, we did observe 3 cases of PKD in mice from crosses between *Tsc2*$^{+/-}$ and *Pkd1*$^{+/-}$ mice. These cases stood out as the mice were only 3-4 weeks of age and displayed severe unilateral PKD. Upon genotyping we discovered that two of these mice were *Tsc2*$^{+/-}$ and the other was *Tsc2*$^{+/-}$*Pkd1*$^{+/-}$. This was surprising considering the contiguous gene syndrome involves a deletion that spans both *TSC2* and *PKD1*. The morphology of lesions from the *Tsc2*$^{+/-}$ and *Tsc2*$^{+/-}$*Pkd1*$^{+/-}$ mice with severe PKD differed, with those from *Tsc2*$^{+/-}$ mice resembling *Tsc*-associated cysts and cystadenomas, and those from *Tsc2*$^{+/-}$*Pkd1*$^{+/-}$ mice resembling cysts found in *Pkd1*$^{+/-}$ mice. Interestingly, similar to our *Tsc2*$^{+/-}$ mice with severe PKD, Cai *et al.* (2003) have identified three young Eker rats (<3 months of age) with PKD. Their observations were similar to ours with the polycystic kidneys containing cysts throughout the cortex and medulla and also cystadenomas and RCCs were present. Differences lay in the fact that PKD in the Eker rat was bilateral whereas in our *Tsc2*$^{+/-}$ mice with PKD it was unilateral. Also Cai *et al.* observed extra renal lesions in the spleen and uterus whereas we observed no extra-renal lesions. The authors found that affected cells from these rats had lost the wild-type *Tsc2* allele while retaining two copies of chromosome 10 containing the mutant *Tsc2* allele as well as two normal copies of *Pkd1*. Due to this, affected organs did not express tuberin, whereas unaffected organs such as the brain and liver did. Also, despite the presence of two normal copies of *Pkd1*, tuberin deficient cells had an apparent functional inactivation of PC1 due to the requirement of tuberin for intracellular trafficking of PC1 to the lateral cell membrane (Kleymenova *et al.* 2001). The authors state that the genetic data, bilateral nature of the kidney disease, and extent of involvement of the spleen and kidney indicate that, in affected animals, loss of the wild-type *Tsc2* allele occurred during embryogenesis, probably as a result of chromosome nondisjunction, with affected animals being mosaics for loss of *Tsc2* gene function. It is likely that a similar event has occurred in our *Tsc2*$^{+/-}$ mice with PKD considering the cystic phenotype was similar and we observed strong pS6 staining in all cysts suggesting biallelic inactivation of *Tsc2* and subsequent mTOR activation.

The major difference with our mice is that PKD was unilateral. This could indicate that loss of the wild-type allele may have occurred at a later stage in embryogenesis.

The PKD phenotype in our *Tsc2*$^{+/-}$*Pkd1*$^{+/-}$ mouse with PKD appears to be quite different to the *Tsc2*$^{+/-}$ mice with PKD with lesions resembling those found in *Pkd1*$^{+/-}$ mice and also a lack of activation of the mTOR pathway in almost all cysts. Without molecular data it is unclear what is occurring in this mouse, however, one could speculate that a second hit may have occurred in the wild-type *Pkd1* allele early in development, leading to severe early onset PKD in one of the kidneys with cysts resembling those found in *Pkd1*$^{+/-}$ mice. Interestingly, cysts resembling those found in both TSC and ADPKD have been found in patients with *TSC2/PK*D1 contiguous gene syndrome (Martignoni *et al.* 2002, Bisceglia *et al.* 2008). Perhaps one could speculate that the contiguous gene syndrome may arise through a variety of different second hits during development thus leading to slightly different mosaic phenotypes as observed in our mice with severe PKD. For example some patients, as with our *Tsc2*$^{+/-}$ mice and the Eker rats with PKD, may acquire a second hit in the wild-type *TSC2* allele during development, leading to PKD with cysts resembling those seen in TSC. Loss of the wild-type *TSC2* allele may lead to PC1 becoming sequestered in the Golgi, thus preventing its function in cell-cell and cell-matrix interactions at the lateral cell membrane (Cai *et al.* 2003). Therefore PKD may arise early in life with the severity of that seen in advanced stage ADPKD, but the phenotype of cysts seen in TSC (Sampson *et al.* 1997). Indeed, three cases of patients with multiple cysts in both kidneys and a large rearrangement in *TSC2* but no deletion in *PKD1* have been indentified (Sampson *et al.* 1997). Another mechanism may involve somatic mutations in both *TSC2* and *PKD1* during development. This could explain the presence of cysts with the appearance of those found in TSC and ADPKD in kidneys from patients with the contiguous deletion syndrome (Martignoni *et al.* 2002, Bisceglia *et al.* 2008). Finally, a third possibility could be somatic mutations occurring in *PKD1* during development giving rise to cysts with morphology similar to those found in ADPKD. This scenario may be occurring in our *Tsc2*$^{+/-}$*Pkd1*$^{+/-}$ mouse with PKD as the renal

cysts appear similar to those seen in the *Pkd1*$^{+/-}$ mice and also may occur in an mTOR independent manner as cysts were negative for pS6. Of interest, one of the large renal cysts present in our *Tsc2*$^{+/-}$*Pkd1*$^{+/-}$ mouse with PKD stained positive for pS6. One might speculate that a second hit in *Tsc2* may have occurred in this cyst leading to loss of tuberin and subsequent activation of the mTOR pathway. It would be extremely interesting if mTOR analyses were preformed on kidneys from patients with the contiguous gene syndrome to assess whether those cysts with a TSC appearance stain positive for mTOR activation and if those cysts with an ADPKD appearance stain negative. It is interesting to note that patients with the contiguous gene syndrome may develop AMLs later in life (personal correspondence with Julian Sampson regarding patients from his clinic). All three of the above scenarios could lead to this either through a somatic hit in *TSC2* during development, or a somatic hit in *TSC2* later in life in an individual cell.

In conclusion, it is unclear whether our three mice with PKD recapitulate the *TSC2/PKD1* contiguous gene syndrome due to a lack of molecular data from both sources. One can only speculate about the involvement of second hits in this phenotype, however, a study by Smulders *et al.* (2003) revealed a patient with contiguous deletion of both *TSC2* and *PKD1* who displayed no signs of infantile PKD. The authors found an absence of somatic mosaicism in this patient thus perhaps highlighting the need for an early somatic mutation during development in order for early onset PKD to arise. Hopefully future studies involving LOH and other mutation analyses will reveal the role of second hits in the *TSC2/PKD1* contiguous gene syndrome.

4.4.4 The role of mTOR activation in renal and hepatic cyst formation

We previously found that cysts, the earliest renal lesions present in *Tsc1*$^{+/-}$ and *Tsc2*$^{+/-}$ mouse models, showed significantly less pS6 staining compared to cystadenomas and RCCs. These results suggested that activation of the mTOR pathway may not be necessary for renal cyst formation in TSC. Conflicting evidence exists for the role of mTOR activation

in ADPKD (Shillingford *et al.* 2006, Hartman *et al.* 2009) and so we attempted to investigate activation of the mTOR pathway in our *Pkd1* mouse models.

4.4.4.1 Lack of mTOR activation in Pkd1$^{+/-}$ cysts

A possible functional interaction between PC1, tuberin and hamartin through the mTOR pathway was recently suggested by Shillingford *et al.* (2006). They found that the cytoplasmic tale of PC1 physically interacts with tuberin and mTOR and proposed that PC1, tuberin (and thus potentially hamartin) and mTOR form a protein complex in renal epithelial cells, the function of which is the down-regulation of mTOR activity under normal conditions. The authors also found that renal cysts from ADPKD patients and mouse models (*Orpk*-rescue, *Pkd1^{cond}* and myelin and lymphocyte protein over-expressing mice) stained positive for pS6 and phospho-mTOR. In contrast, we failed to identify pS6 staining in any renal or hepatic cysts from *Pkd1$^{+/-}$* mice indicating that mTOR was not active in these animals. Obvious reasons for this difference to the ADPKD samples lie in the fact that human ADPKD specimens represent advanced stage disease, whereas our mouse model represents a very mild cystic phenotype where early factors are in play, quite different to end stage disease factors. This could also be the reason why Shillingford *et al.* found pS6 staining in their mouse models as these also had a severe cystic phenotype reminiscent of late stage disease. We too examined a mouse model with severe renal cystic disease by 3 weeks of age (*Pkd1$^{nl/nl}$* mice) and found pS6 staining in a number of cysts, however, it appears that smaller cysts (<50μm diameter) display significantly less pS6 staining compared to larger cysts (>200μm diameter), suggesting that mTOR activation occurs later in the disease process. Recently, work by Hartman *et al.* (2009) showed that only a small proportion of cysts (30%) from patients with ADPKD had strong to moderate pS6 staining, with the other 70% showing weak or negative pS6 immunoreactivity. It is unclear if these results are in agreement with those from Shillingford *et al.* as these authors do not state the specific percentage of renal cysts from patients with ADPKD which stained positive or negative for pS6. It is however clear that in kidneys from patients with late stage ADPKD, a significant proportion of cysts do not show evidence of mTOR activation.

The role of mTOR activation has recently been investigated in hepatic cysts from patients with ADPKD who had received kidney transplants (Qian *et al.* 2008). The authors found a high level of p-mTOR and pS6 staining in liver cyst lining epithelial cells. In contrast, we found no evidence of pS6 staining in liver cysts from *Pkd1*$^{+/-}$ mice. As with our renal lesion data, we believe that this difference lies in the fact that human ADPKD specimens represent advanced stage disease, whereas our mouse model represents a mild cystic phenotype. It would be interesting to know if all liver cysts from these patients with ADPKD (*n*=2) were positive for p-mTOR and pS6, or if only a small proportion were positive (the authors to do not state any percentages).

We feel that our *Pkd1*$^{+/-}$ findings represent what occurs in early stage cystic disease. Our data suggests that early cyst formation in ADPKD does not involve the activation of mTOR, however, at later stages mTOR can become active and perhaps accelerate and progress the disease.

4.4.4.2 Activation of the mTOR pathway is not essential for cyst initiation in compound heterozygous mice

As with *Tsc1*$^{+/-}$ and *Tsc2*$^{+/-}$ mice, we found a significant proportion of renal cysts in both *Tsc1*$^{+/-}$*Pkd1*$^{+/-}$ and *Tsc2*$^{+/-}$*Pkd1*$^{+/-}$ mice were negative for pS6 compared to advanced lesions. Liver cysts, as in the *Pkd1*$^{+/-}$ mice, were also negative for pS6 in *Tsc1*$^{+/-}$*Pkd1*$^{+/-}$ and *Tsc2*$^{+/-}$*Pkd1*$^{+/-}$ mice. No liver cysts were observed in *Tsc1*$^{+/-}$ or *Tsc2*$^{+/-}$ mice indicating that these lesions are a phenotype of *Pkd1* heterozygosity. This data further supports our hypothesis that activation of the mTOR pathway is not the initiating mechanism of renal cystogenesis in TSC or ADPKD, but perhaps is one of the key events for disease progression.

4.4.4.3 Implications for rapamycin treatment

Clinical trials are currently underway for the treatment of TSC and ADPKD with the mTOR inhibitor rapamycin. Early results in TSC patients reveal a decrease in the size of AMLs (Bissler *et al.* 2008, Davies *et al.* 2008), however the effects on cysts have not been reported. Clinical trials for the use of rapamycin treatment in ADPKD patients are also underway with results

pending. A small retrospective study has been performed on advanced-stage ADPKD patients who had recently received a renal transplant without removal of the affected cystic kidneys (Shillingford *et al.* 2006). Rapamycin treatment is used in some of these patients as an immunosuppressant to prevent transplant rejection. At this advanced stage of disease a reduction in kidney volume was seen in the rapamycin group. This agrees with results from rapamycin treatment in two advanced mouse models of PKD (the *bpk* and *orpk*-rescue mouse models) in which the histological renal cystic index was significantly reduced in rapamycin treated mutant mice. Recently, a small retrospective study was carried out which measured the volumes of polycystic livers and kidneys in patients with ADPKD who had received kidney transplants and had participated in a randomised trial that compared a sirolimus-containing immunosuppression regimen to a tacrolimus-containing immunosuppression regimen (Qian *et al.* 2008). The investigators found that treatment with the sirolimus regimen was associated with an 11.9 ± 0.03% reduction in polycystic liver volume, whereas treatment with tacrolimus for a comparable duration was associated with a 14.1 ± 0.09% increase. They also noted a trend toward a greater reduction in kidney volume in the sirolimus group compared with the non-sirolimus group.

Despite all this data, studies of the efficacy of rapamycin in early cystic disease in TSC or ADPKD have not been carried out. Here we found that many of the earliest renal lesions from *Tsc1*$^{+/-}$, *Tsc2*$^{+/-}$, *Pkd1*$^{+/-}$, *Tsc1*$^{+/-}$*Pkd1*$^{+/-}$ and *Tsc2*$^{+/-}$*Pkd1*$^{+/-}$ mice did not exhibit activation of mTOR. Other investigators have also found that ~70% of cysts from patients with ADPKD had weak or absent pS6 staining (Hartman *et al.* 2009) whilst studies in the Eker rat reveal that rapamycin has no effect on the number of microscopic precursor lesions, (Kenerson *et al.* 2005). These data suggest that although mTOR inhibitors may be an effective treatment for the advanced stages of TSC and ADPKD associated kidney disease, they may have little effect in preventing initial cyst/tumour formation.

CHAPTER FIVE: Investigating primary cilia in TSC and ADPKD mouse models

5.1 Introduction

Defects in the structure and/or function of primary cilia may be involved in some of the earliest stages of cystic disease such as cell proliferation and tubular differentiation (Lin and Satlin 2004). Numerous proteins associated with cystic kidney disease have been localised to the renal primary cilium or basal body including the *ADPKD2* protein PC2 (Pazour *et al.* 2002, Yöder *et al.* 2002), the product of the human autosomal recessive *PKD* gene (*PKHD1*), fibrocystin (Ward *et al.* 2003), and polaris and cystin, which are mutated in two mouse models of PKD (Yoder *et al.* 2002). Mice with mutant polaris develop shortened cilia or no cilia in kidney epithelia (Pazour *et al.* 2000) and PCK rats (an orthologous model for *PKHD1*) (Ward *et al.* 2002) have cilia that are abnormal and shortened (Masyuk *et al.* 2003).

The proteins associated with TSC and ADPKD have been localised to the primary cilium. PC1 and PC2 can be found in the primary cilium where the two proteins interact to form a mechanosensory complex (Yoder *et al.* 2002). Hamartin has been localised to the centrosome/basal body complex (Astrinidis *et al.* 2006, Hartman *et al.* 2009) and tuberin interacts with PC1 (Shillingford *et al.* 2006), which could potentially localise the protein to the primary cilium.

Here, we studied the structure of primary cilia in pre-cystic renal tubule epithelial cells from wild-type, *Tsc1*$^{+/-}$, *Tsc2*$^{+/-}$, *Pkd1*$^{+/-}$, *Tsc1*$^{+/-}$*Pkd1*$^{+/-}$ and *Tsc2*$^{+/-}$*Pkd1*$^{+/-}$ mice at 3 months of age by SEM. We also examined primary cilia in cysts from these mice to assess potential differences between pre-cystic and cystic tubules. Defects in ciliary structure are often associated with disrupted IFT and so a general role for hamartin, tuberin and PC1 in this process was sought.

5.2 Materials and methods

5.2.1 Animal care, genotyping and tissue fixation

All procedures with animals, DNA extraction and genotyping were performed as previously described. *Tsc1*$^{+/-}$ and *Tsc2*$^{+/-}$ mice were crossed with *Pkd1*$^{+/-}$ mice to produce *Tsc1*$^{+/-}$, *Tsc1*$^{+/-}$*Pkd1*$^{+/-}$, *Tsc2*$^{+/-}$, *Tsc2*$^{+/-}$*Pkd1*$^{+/-}$, *Pkd1*$^{+/-}$ and wild-type progeny. Pre-cystic renal tubules were examined in three month old mice and cysts were examined in 15-18 month old mice following perfusion fixation with PBFG (chapter 2, section 2.5.3.3). Five mice from each genotype were used for both age groups. Fixed kidneys from 3 month old mice were sectioned to reveal open tubules (chapter 2, section 2.5.3.3) and cysts were removed from 15-18 month old fixed mouse kidneys.

For SEM analysis of E8.5 embryos, wild-type, *Tsc1*$^{+/-}$, *Tsc2*$^{+/-}$, *Tsc1*$^{-/-}$ and *Tsc2*$^{-/-}$ embryos were removed from their extra-embryonic membranes and fixed in PBFG overnight. For cardiac tube examination, E9.5 embryos were extracted and viewed under an Olympus BX51 microscope using a dark field filter. DNA was extracted from yolk sacs using the QIAamp DNA mini kit (chapter 2, section 2.5.4.2) and genotyping performed as described in sections 3.2.1 and 4.2.1.

5.2.2 SEM processing and analysis

All specimens were dehydrated using the HMDS method (Nation 1983, chapter 2, section 2.5.13), mounted on aluminium stubs using carbon paint, sputter coated with gold and viewed at 5kV in a JEOL 840A SEM. Kidney halves for tubule examination were mounted cut side facing up and cysts were mounted with the lumen facing up. AnalySIS software was used to measure primary and nodal cilia lengths.

5.2.3 Statistics

Primary cilia lengths were compared using 2-sample T-tests and the Mann-Whitney confidence interval test.

5.3 Results

5.3.1 Primary cilia in pre-cystic renal tubules

We examined collecting tubules as these displayed the best morphology with clearly visible primary cilia. The collecting tubule consists of two cell types: light cells, which possess a single central cilium, and dark cells which do not usually display a primary cilium but do possess thin folds called microplicae (Figure 5.1) (Kessel and Kardon 1979). These cells were clearly visible in our samples and enabled the accurate identification of collecting tubules.

Primary cilia from pre-cystic renal tubules displayed no abnormal morphology such as bulbous tips and appeared as solitary projections with no evidence of multiple cilia per cell. We found that primary cilia in pre-cystic renal tubule cells from *Tsc1*$^{+/-}$ and *Tsc2*$^{+/-}$ mice were 5% and 10% shorter, respectively, as compared to those from age-matched wild-type littermates (P=0.016 and P<0.001, respectively) (Table and Figure 5.1). We found that the lengths of primary cilia from pre-cystic renal tubule cells from *Pkd1*$^{+/-}$ mice were 5% longer than those found in wild-type animals (P=0.02) (Table 5.1). Interestingly, the lengths of primary cilia from pre-cystic tubule cells from *Tsc1*$^{+/-}$*Pkd1*$^{+/-}$ and *Tsc2*$^{+/-}$*Pkd1*$^{+/-}$ mice were also significantly longer than those found in *Tsc1*$^{+/-}$ and *Tsc2*$^{+/-}$ mice (P<0.001 for both) and wild-type mice (P<0.001 and P=0.043 respectively), and were of a similar length to those found in *Pkd1*$^{+/-}$ mice (P>0.12) (Table 5.1).

5.3.2 Primary cilia in renal cystic epithelia

As with the pre-cystic renal tubule cells, primary cilia from epithelial cells lining cysts had a normal morphology and no multiple cilia per cell were observed. We found that the lengths of primary cilia in epithelial cells lining cysts from *Tsc1*$^{+/-}$ and *Tsc2*$^{+/-}$ mice were ~200% longer than primary cilia from pre-cystic tubule cells from wild-type, *Tsc1*$^{+/-}$ or *Tsc2*$^{+/-}$ mice (P<0.001) (Table and Figure 5.1). Conversely, primary cilia from epithelial cells lining cysts from *Tsc1*$^{+/-}$*Pkd1*$^{+/-}$ and *Tsc2*$^{+/-}$*Pkd1*$^{+/-}$ mice were 34-39% shorter than those found in cysts from *Tsc1*$^{+/-}$ and *Tsc2*$^{+/-}$ mice (P<0.001 for both) (Table and Figure 5.1), but still remained significantly longer than those from pre-cystic tubule

cells from wild-type, *Tsc1*$^{+/-}$*Pkd1*$^{+/-}$ and *Tsc2*$^{+/-}$*Pkd1*$^{+/-}$ mice (P<0.001). No renal cysts were found from *Pkd1*$^{+/-}$ mice for SEM analysis.

Table 5.1 Measurements of primary cilia length (μm) from pre-cystic renal tubule cells and epithelial cells lining cysts.

Genotype	**Pre-cystic tubule cells** mean length (and SD)	**Epithelial cells lining cysts** mean length (and SD)
Wild-type	2.233 (0.449) n=205	n/a [a]
Tsc1$^{+/-}$	2.122 (0.537) n=126 P=0.016	5.157 (3.059) n=442 P<0.001
Tsc2$^{+/-}$	2.016 (0.410) n=255 P<0.001	5.091 (2.921) n=128 P<0.001
Pkd1$^{+/-}$	2.333 (0.399) n=285 P=0.02	n/a [b]
Tsc1$^{+/-}$*Pkd1*$^{+/-}$	2.389 (0.456) n=269 P<0.001	3.384 (1.404) n=157 P<0.001
Tsc2$^{+/-}$*Pkd1*$^{+/-}$	2.356 (0.589) n=261 P=0.043	3.091 (1.351) n=106 P<0.001

n/a, not applicable ([a]wild-type animals do not develop renal cysts and [b]no renal cysts were found from *Pkd1*$^{+/-}$ mice for SEM analysis). n values denote number of primary cilia measured from five mice of each genotype.
P values in table correspond to associated genotype cilia length compared to wild-type cilia length.

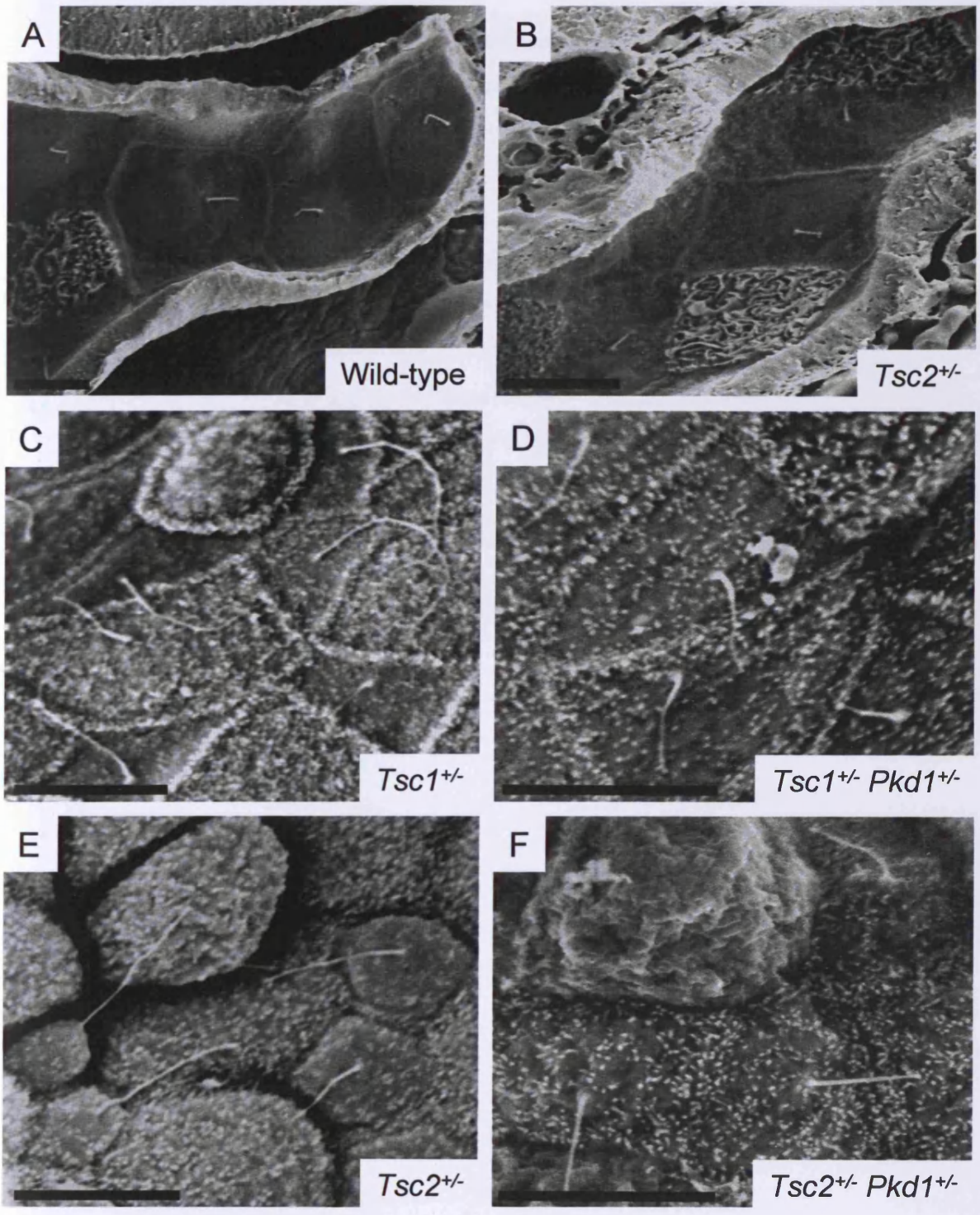

Figure 5.1 SEM examination of renal primary cilia in pre-cystic collecting tubule cells (**A**, **B**) and epithelial cells lining cysts (**C**-**F**). Primary cilia from pre-cystic cells from *Tsc2*$^{+/-}$ mice (**B**, mean length 2.016μm) were 10% shorter compared to those from wild-type littermates (**A**, mean 2.223μm, $P<0.001$). Primary cilia from epithelial cells lining cysts from (**C**) *Tsc1*$^{+/-}$ (mean 5.157μm) and (**E**) *Tsc2*$^{+/-}$ (mean 5.091μm) mice were >200% longer than primary cilia from pre-cystic tubule cells from wild type, *Tsc1*$^{+/-}$ or *Tsc2*$^{+/-}$ mice ($P<0.001$). *Pkd1*-haploinsufficiency significantly reduced the length of the primary cilia from epithelial cells lining cysts from *Tsc1*$^{+/-}$ or *Tsc2*$^{+/-}$ mice: (**D**) *Tsc1*$^{+/-}$ *Pkd1*$^{+/-}$ mice, mean 3.384μm, and, (**F**) *Tsc2*$^{+/-}$ *Pkd1*$^{+/-}$ mice, mean 3.091μm ($P<0.001$ for both). Scale bars: 5μm.

5.3.3 Examination of nodal cilia and cardiac tube position

We investigated whether hamartin and tuberin play a role in IFT and the active maintenance of cilia. Mice with mutations in proteins necessary for cilium formation often have an absence or malfunction in nodal cilia in E7.5-E8.5 embryos which prevents the generation of the leftward nodal flow of extra-embryonic fluid required for activation of the molecular signals in the left side of the body and, as a consequence, develop *situs inversus*. However, we failed to find any differences in nodal cilia from $Tsc1^{+/-}$, $Tsc1^{-/-}$, $Tsc2^{+/-}$, $Tsc2^{-/-}$ and wild-type embryos (Figure 5.2), nor did we, or others (Onda *et al.* 1999), find any evidence of *situs inversus* or defects in cardiac tube position (Figure 5.3).

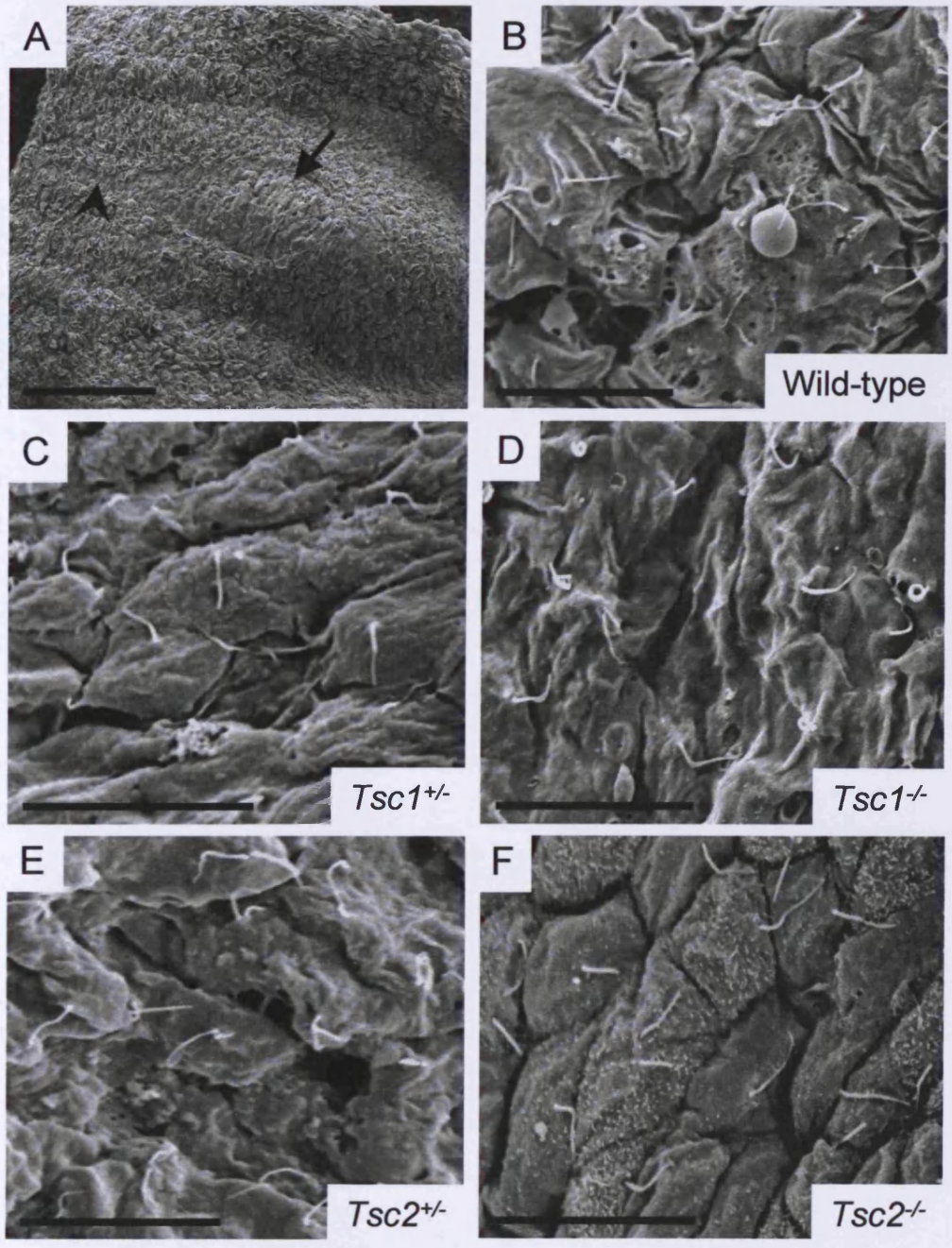

Figure 5.2 SEM examination of nodal cilia from E8.5 embryos. (**A**) Lower magnification view of the node region (arrow) and notochordal plate (arrow head). We observed no difference in the length or structure of nodal cilia from wild-type (**B**), *Tsc1*$^{+/-}$ (**C**), *Tsc1*$^{-/-}$ (**D**), *Tsc2*$^{+/-}$ (**E**) and *Tsc2*$^{-/-}$ (**F**) embryos. Scale bars: **A**; 100μm, **B-F**; 10μm.

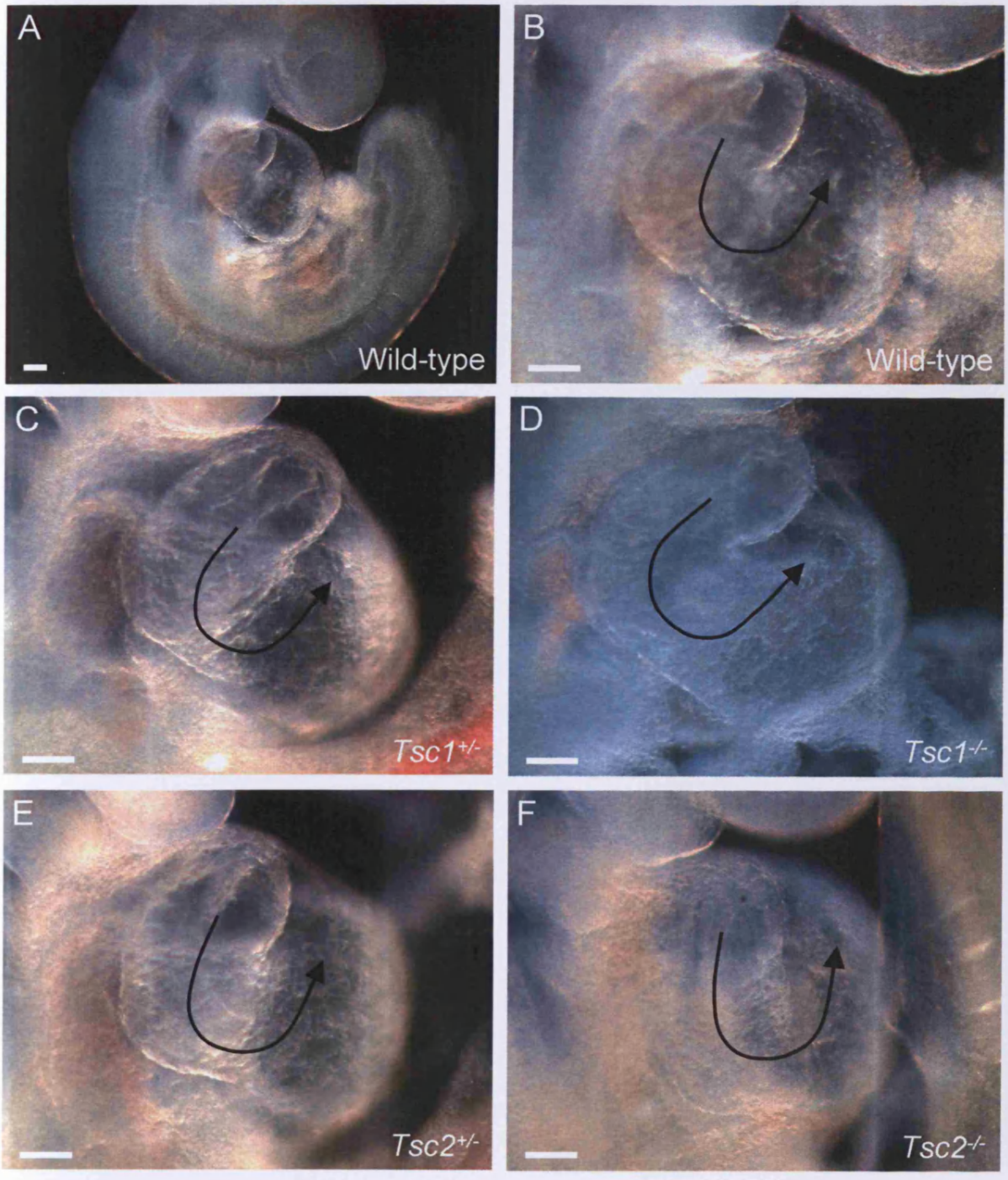

Figure 5.3 Microscopic examination of cardiac tube position in E9.5 mouse embryos. (**A**) Lower magnification view of a wild-type embryo showing the location of the cardiac tube with a higher magnification view (**B**) to show the direction of cardiac tube looping. We observed no difference in looping of the cardiac tube between wild-type (**B**), *Tsc1*$^{+/-}$ (**C**), *Tsc1*$^{-/-}$ (**D**), *Tsc2*$^{+/-}$ (**E**) and *Tsc2*$^{-/-}$ (**F**) embryos. Scale bars: 0.1mm.

5.4 Discussion

5.4.1 A possible role for hamartin, tuberin and PC1 in renal ciliogenesis

Defects in the structure or function of primary cilia are thought to underlie numerous disorders associated with cystic kidneys. Hartman *et al.* (2009) recently described a ciliary disruption in TSC with enhanced cilia development in *Tsc1* and *Tsc2* null mouse embryonic fibroblasts (MEFs) which manifests in an mTOR-independent mechanism. Normally, *Tsc1* and *Tsc2* null MEFs have difficulty growing and so in order to compensate for this, p53 is often knocked out (Kwiatkowski *et al.* 2002, Zhang *et al.* 2003). By silencing p53 expression, the protein's function as a cell cycle regulator is abolished, thus leading to uncontrolled cell growth and proliferation, effectively immortalising the cell. Of course, a major disadvantage of this approach is the multitude of other cellular processes that could potentially be affected by this silencing, for example, DNA repair and apoptosis (Sancar *et al.* 2004). By losing p53, the cell becomes genetically unstable and susceptible to mutations in other genes with no applicable mechanism to correct or eradicate these mutated cells (Sancar *et al.* 2004).

In our study, we found that hamartin, tuberin and PC1 all played a role in maintaining the length of primary cilia in pre-cystic renal tubule cells (those from $Tsc1^{+/-}$ and $Tsc2^{+/-}$ mice were 5-10% shorter and those from $Pkd1^{+/-}$ mice were 5% longer, compared to wild-type littermates). These data support a role for hamartin, tuberin and PC1 in renal ciliogenesis and suggest that cellular abnormalities exist in pre-cystic cells in a *Tsc1*-, *Tsc2*- or *Pkd1*-haploinsufficient state. Our $Tsc1^{+/-}$ and $Tsc2^{+/-}$ cilia data differ to those of Hartman *et al.* who found an increase in the number of ciliated cells and also an increase in the length of cilia in *Tsc1* and *Tsc2* null MEFs compared to wild-type cells. We found no difference in the number of ciliated cells between genotypes and found that cilia length decreased in $Tsc1^{+/-}$ and $Tsc2^{+/-}$ pre-cystic renal tubule cells compared to wild-types. There are a number of reasons why our data may differ from that of Hartman *et al.* The *Tsc1* null MEFs used were spontaneously immortalised and so it is unclear what else has been knocked during this process (Kwiatkowski *et al.* 2002). Also, as

previously mentioned, the *Tsc2* null MEFs had p53 knocked out which could have a variety of other effects on the cell which may contribute to an altered ciliary phenotype. Perhaps the biggest difference between our methods and those used by Hartman *et al.* is the fact that cilia formation was forcibly induced in the *Tsc1* and *Tsc2* null MEFs. To achieve this, three different conditions were used: cells were serum starved for 48-72 hours, cells were cultured with cell-to-cell contact inhibition in the presence of 10% foetal bovine serum (FBS) for 48 hours, or cells were grown logarithmically in the presence of 10% FBS at subconfluency for 24 hours. None of these conditions are a true representation of actual physiological conditions and tubular flow present in the renal tubule. We collected our cilia measurements from *in vivo* primary cilia which have been exposed to natural conditions found in renal tubules. Cell culture methods will always be faced with the problem of not recapitulating actual *in vivo* conditions and therefore results from these studies should be treated with caution.

Interestingly, we saw a large increase (~200%) in cilia length in cyst lining epithelial cells from $Tsc1^{+/-}$ and $Tsc2^{+/-}$ mice. All the cysts examined were >1mm in diameter and are therefore quite developed with a significant chance of having acquired a second hit (and so may be in a *Tsc1* or *Tsc2* null state). This brings our results more inline with those found by Hartman *et al.* and suggests that defects exist in pre-cystic renal tubule cells in which the primary cilia are shortened in length, however in large cysts which may have advanced and acquired second hits, primary cilia have significantly grown in length. Similar length differences have been reported in kidneys and cell cultures from mice with mutations in the renal cystic disease associated Bbs4 (Mokrzan *et al.* 2007) and Nek8 (Smith *et al.* 2006) proteins. Mokrzan *et al.* found that in cells cultured from $Bbs4^{-/-}$ mice, cilia were initially shorter, but surpassed the length of control cilia by 10 days, whilst Smith *et al.* found significant lengthening of primary cilia in cysts from *jck* (mutation in *Nek8*) mouse kidneys.

5.4.2 Do ciliary length differences have a pathophysiological effect?

It is clear from previous studies that loss of primary cilia has a detrimental effect to the cell, for example the reduction of flow mediated Ca^{2+} entry into the cell, and can lead to the formation of cysts (Nauli *et al.* 2003, Praetorius and Spring 2003, Lin *et al.* 2003). It is however unclear if differences in cilia length, particularly small variations in length as seen in our mice, result in a pathophysiological affect. Studies using the *orpk* mouse model of ARPKD have revealed that in *orpk* homozygous mutants, renal primary cilia are severely stunted (but still present) and when their sensitivity to flow was measured, the magnitude of the increase in intracellular Ca^{2+} concentration was reduced (Liu *et al.* 2005). Interestingly, a recent paper by Verghese *et al.* (2008) demonstrated a pattern of renal cilia length alterations in mice similar to our findings in pre-cystic renal tubule cells and renal cysts, with an initial shortening of cilia in the proximal tubule after ischaemic renal injury, followed by lengthening of cilia in both the proximal tubule and distal/collecting duct. It has been shown that longer cilia experience greater the shear forces and bending response to flow (Schwartz *et al.* 1997). Cilium lengthening is an energy-dependent process that uses kinesin- and dynein-based IFT. Verghese *et al.* therefore suggest that cilium lengthening during epithelial injury is likely to be a directed response, rather than the result of simple metabolic disruption. The authors propose that lengthening of the renal cilium increases their sensitivity to flow and other cilium detected factors that promote maintenance of the epithelial phenotype and may represent a compensatory response that counteracts dedifferentiation. This situation may also be occurring in renal cysts from our mouse models which showed a lengthening of primary cilia in *Tsc1*$^{+/-}$, *Tsc2*$^{+/-}$, *Tsc1*$^{+/-}$*Pkd1*$^{+/-}$ and *Tsc2*$^{+/-}$*Pkd1*$^{+/-}$ mice. Increasing primary cilia length in renal cysts may be the cells final attempt at detecting essential flow and ligand mediated physiological signals, however, unlike in an injured tubule where these factors may be more abundant, a cyst represents a very hostile environment with perhaps no flow and a variety of abnormal ligands which will not promote a normal epithelial phenotype.

5.4.3 Haploinsufficiency of *Pkd1* modulates the ciliary defect observed in *Tsc1*- and *Tsc2*-haploinsufficient mice

Cilia defects have previously not been found in *Pkd1* knockout cell lines and mouse models. Nauli *et al.* (2003) reported no difference in renal cilia length between wild-type embryonic kidney cells and embryonic kidney cells with biallelic mutations in *Pkd1* (obtained from kidneys from wild-type and $Pkd1^{del34/del34}$ embryos respectively), whilst Hartman *et al.* (2009) found no evidence of enhanced cilia development in $Pkd1^{-/-}$ MEFs. We have however showed that cilia are significantly longer in pre-cystic renal tubule cells from $Pkd1^{+/-}$ mice compared to those found in wild-type mice. Reasons for this discrepancy could be explained by the fact that these labs carried out their research on cells using artificial flow and growth conditions which can not accurately mimic *in vivo* conditions. Also they measured cilia length from immunofluorescent images which have limited resolution compared to SEM, therefore small differences in length (as seen in our studies) may not be picked up. Finally, $Pkd1^{-/-}$ MEFs were immortalised by knocking out p53 (Hartman *et al.* 2009). As previously mentioned this could lead to a variety of other pathways being affected in these cells and so may affect primary cilia data.

Interestingly, the lengths of primary cilia from pre-cystic tubule cells from $Tsc1^{+/-}Pkd1^{+/-}$ and $Tsc2^{+/-}Pkd1^{+/-}$ mice were significantly longer than those found in $Tsc1^{+/-}$ and $Tsc2^{+/-}$ mice and were of a similar length to those found in $Pkd1^{+/-}$ mice. Conversely, in epithelial cells lining cysts they were significantly shorter than those found in cysts from $Tsc1^{+/-}$ and $Tsc2^{+/-}$ mice. Although it is unclear why haploinsufficiency of *Pkd1* modulates the ciliary defect observed in *Tsc1*- and *Tsc2*-haploinsufficient mice, these data clearly support a functional relationship between PC1 and hamartin/tuberin within the renal primary cilium. Perhaps alterations in Ca^{2+} influx controlled by PC1 and PC2 override the effects of hamartin and tuberin, and thus lead to a compound heterozygous phenotype similar to that of *Pkd1* haploinsufficiency. This could perhaps be mediated by the calmodulin (CaM) binding domain present in the C-terminus of tuberin (Figure 1.3), which enables the binding of tuberin to the calcium-dependent intracellular signalling protein CaM (Noonan

et al. 2002). This binding domain is believed to overlap with a binding domain for oestrogen receptor α (ERα) and a functional nuclear localisation sequence (NLS) (York *et al.* 2006). Hamartin is often found in a complex with tuberin and so may also be affected by altered Ca^{2+} influx (due to haploinsufficiency of *Pkd1*) and subsequent CaM binding. Further work is needed to elucidate the effect of intracellular Ca^{2+} concentration on hamartin and tuberin, particularly in connection with flow induced primary cilia Ca^{2+} influx and altered levels of PC1.

5.4.4 No evidence for a direct role of hamartin, tuberin or PC1 in IFT

Left-right asymmetry is established early in embryonic life by the leftward flow of extraembryonic fluid across the node region generated by the beating of nodal cilia (Nonaka *et al.* 2005). Nodal cilia beat by twirling in a circle and are therefore situated toward the back of node cells and tilted toward the posterior of the embryo to ensure that extraembryonic fluid flows in a leftward direction (Nonaka *et al.* 2005). As previously mentioned, mice with mutations in proteins necessary for cilium formation often have an absence or malfunction in nodal cilia and, as a consequence, develop defects in cardiac tube position and abnormal expression of asymmetrical markers. Such models include mice with mutations in ciliary proteins such as kinesins (Marszalek *et al.* 1999), dyneins (Supp *et al.* 1999), and the IFT proteins IFT88 (encoded by *Ift88*, also known as *Polaris*) (Murcia *et al.* 2000, Hamada *et al.* 2002) and IFT172 (encoded by *Ift172*, also known as *Wim*) (Huangfu *et al.* 2003). We failed to find any differences in nodal cilia or cardiac tube position from $Tsc1^{+/-}$, $Tsc1^{-/-}$, $Tsc2^{+/-}$, $Tsc2^{-/-}$ and wild-type embryos, suggesting that IFT was not altered in these mice. Interestingly, a recent paper by DiBella *et al.* (2009) demonstrated left-right asymmetry defects in a *Tsc1* zebrafish morpholino. Knockdown of *Tsc1* resulted in an abnormal expression pattern of two asymmetry markers (*cmlc2* (cardiac myosin light chain 2) and *southpaw*) usually expressed on the left side of the embryo. Although our data indicates no obvious morphological defects in left-right asymmetry, perhaps subtle changes in asymmetry markers are present and should be investigated in further embryo studies. Overall, this data provides

no evidence for a direct role of hamartin and tuberin in IFT but suggests that perhaps the ciliary length differences found in our mouse models could be secondary to perturbation of an upstream pathway, perhaps the PCP pathway which primary cilia have been linked to (investigated in the next chapter).

CHAPTER SIX: Defects in cell polarity may underlie renal cystic disease in TSC and ADPKD

6.1 Introduction

Renal primary cilia project into the tubule lumen and monitor urinary flow via the mechanotransduction properties of PC1 and PC2 (Nauli *et al.* 2003). It is now emerging that many of the ciliary proteins are involved in maintenance of the canonical and noncanonical Wnt pathways. The ciliary protein inversin acts as a molecular switch from the canonical to the noncanonical/PCP Wnt signalling pathways by targeting cytoplasmic dishevelled (Dsh) for degradation (Simons *et al.* 2005). Notably Dsh is positioned at a crucial junction between the two arms of the Wnt pathway (Germino 2005). Furthermore, mutations in *Kif3a*, *Ift88* and *Ofd1*, that disrupt ciliogenesis, restricts the activity of the canonical Wnt pathway with loss of *Kif3a* causing constitutive phosphorylation of Dsh (Corbit *et al.* 2008). Interestingly, tuberin and hamartin associate with the GSK3/axin complex to promote β-catenin degradation and inhibit canonical Wnt-signalling (Mak *et al.* 2003) and tuberin also interacts with Dsh upon Wnt stimulation (Mak *et al.* 2005).

The lengthening of developing renal tubules is associated with the mitotic orientation of cells along the tubule axis, demonstrating intrinsic PCP (Fischer *et al.* 2006). During renal development, newly formed tubules undergo an intense proliferative phase and increase in length whilst maintaining a constant diameter (Simons and Walz 2006). Oriented cell division is thought to dictate the maintenance of this constant tubule diameter by ensuring cells divide in a direction parallel to the longitudinal axis of the tubule (Simons and Mlodzik 2008). If PCP is disrupted, cells may lose the ability to divide along the longitudinal tubule axis and may deviate from this axis, eventually leading to a dilated tubule and perhaps cyst formation (Figure 7.2) (Germino *et al.* 2005). Defects in oriented cell division during kidney tubule development have been found in mice with a renal-specific inactivation of *Tcf2*, a transcription factor essential for the expression of genes involved in

PKD, the PCK rat and *Kif3a* mutant mice (Fischer *et al.* 2006, Patel *et al.* 2008). Given that we observed a role for hamartin, tuberin and PC1 in maintaining the structure of the renal primary cilium (which others have linked to the PCP pathway); we hypothesised that these proteins may also play a role in maintaining tubule cell polarity.

The most distinct example of vertebrate PCP is the uniform orientation of stereociliary bundles in the organ of Corti. Stereociliary bundles consist of a single specialised primary cilium (the kinocilium) and multiple stereocilia situated at the apices of sensory hair cells in the mammalian auditory sensory organ (Wang *et al.* 2005). Mice with mutations in genes involved in Bardet-Biedl syndrome (BBS), a disorder associated with ciliary dysfunction, display PCP defects including open eyelids and disrupted cochlear stereociliary bundles (Ross *et al.* 2005). We examined our mouse models of TSC and ADPKD for misrotations of stereociliary bundles, one of the most prominent examples of PCP defects in the mammalian body.

6.2 Materials and methods

6.2.1 Animal care, genotyping and tissue preparation

All procedures with animals, DNA extraction and genotyping were carried out as previously described. Five mice from each genotype (wild-type, *Tsc1*$^{+/-}$, *Tsc2*$^{+/-}$, *Pkd1*$^{+/-}$, *Tsc1*$^{+/-}$*Pkd1*$^{+/-}$ and *Tsc2*$^{+/-}$*Pkd1*$^{+/-}$) were sacrificed at 48 hours, 10 days, 15 days and 20 days of age and embedded in paraffin wax as previously described.

For SEM analysis of cochlea, five mice from each genotype were culled at 4 weeks of age and cochlea extracted and fixed as described in chapter 2, section 2.5.3.3.

6.2.2 Immunofluorescence

For fluorescent microscopy, five 4µm thick sections were cut from each set of kidneys for each age group and stained as described in chapter 2, section 2.5.12. Anti-phospho-histone H3 (Ser^{10}) (anti-H3pS10, 1:50 dilution) and tetramethyl rhodamine isothiocyanate (TRITC) conjugated goat anti-rabbit

IgG (H+L) (1:300 dilution) were used to label the chromosomes of dividing cells in late anaphase and telophase. Sections were counterstained with either fluorescein isothiocyanate (FITC) *Lotus tetragonolobus* lectin (LTL, 1:100 dilution) for the proximal kidney tubule, FITC *Dolichos biflorus* agglutinin (DBA, 1:100 dilution) for the collecting duct or immunostained overnight at 4°C with anti-Tamm-Horsfall glycoprotein (THP, 1:150 dilution) followed by FITC conjugated chicken anti-goat IgG (H+L) (1:200 dilution) for the thick limb of the loop of Henle/distal convoluted tubule. Slides were examined using an Olympus BX51 microscope, images were acquired using a Zeiss Axiocam digital camera and analysed with AxioVision software. The orientation of cell division was determined by measuring the angle between the mitotic spindles of dividing cells and the longitudinal axis of the kidney tubules. Metaphase chromosomes were ignored to avoid the measurement of spindles that had not yet reached their definitive orientation.

For confocal microscopy, 30µm thick sections were cut from each set of kidneys for each age group and stained with anti-H3pS10 and THP as described above. Dividing pre-cystic cells from the loop of Henle/distal convoluted tubule were scanned as detailed in chapter 2, section 2.5.12.3 using excitation and emission settings for sequential recordings of FITC (Ex[max]: 494nm; Em[max]: 518nm) and TRITC (Ex[max]: 555nm; Em[max]: 580nm). Mitotic orientations were determined as described above.

6.2.3 SEM processing and analysis

Cochlea were dehydrated using the HMDS method (Nation 1983, chapter 2, section 2.5.13), mounted on aluminium stubs using carbon paint, sputter coated with gold and viewed at 5kV in a JEOL 840A SEM. AnalySIS software was used to view and record images.

6.2.4 Statistics

The distribution of mitotic angles between genotypes was compared using the chi-squared test.

6.3 Results

6.3.1 Mitotic orientation of pre-cystic renal tubule cells from 48 hour old mice

We sought defects in cell polarity in our mice by assessing the mitotic orientations of dividing pre-cystic cells from the proximal tubule, collecting duct and loop of Henle/distal convoluted tubule from mice at 48 hrs of age. For wild-type mice, we found that 78% of dividing cells from the proximal tubule, 82% from the collecting duct and 78% from the loop of Henle/distal convoluted tubule divided within 10° of the longitudinal axis (Figure 6.1), demonstrating that, in agreement with others (Fischer *et al.* 2006), oriented cell division is tightly regulated during tubule lengthening. In contrast, we found significant defects in the mitotic orientations of dividing cells from *Tsc1*$^{+/-}$, *Tsc2*$^{+/-}$ and *Pkd1*$^{+/-}$ mice. For *Tsc1*$^{+/-}$ mice, we found that 41% of dividing cells from the proximal tubule, 45% from the collecting duct and 53% from the loop of Henle/distal convoluted tubule divided within 10° of the longitudinal axis (P=0.002, 0.003 and 0.039, respectively, compared to wild-type), for *Tsc2*$^{+/-}$ mice, we found that 46% of dividing cells from the proximal tubule, 27% from the collecting duct and 44% from the loop of Henle/distal convoluted tubule divided within 10° of the longitudinal axis (P=0.003, <0.001 and 0.009, respectively, compared to wild-type) and for *Pkd1*$^{+/-}$ mice, we found that 61% of dividing cells from the proximal tubule, 47% from the collecting duct and 44% from the loop of Henle/distal convoluted tubule divided within 10° of the longitudinal axis (P=0.133, 0.001 and 0.002, respectively, compared to wild-type) (Figure 6.1). Within each genotype, we observed no significant difference between the mitotic orientations of dividing cells from the different tubule segments.

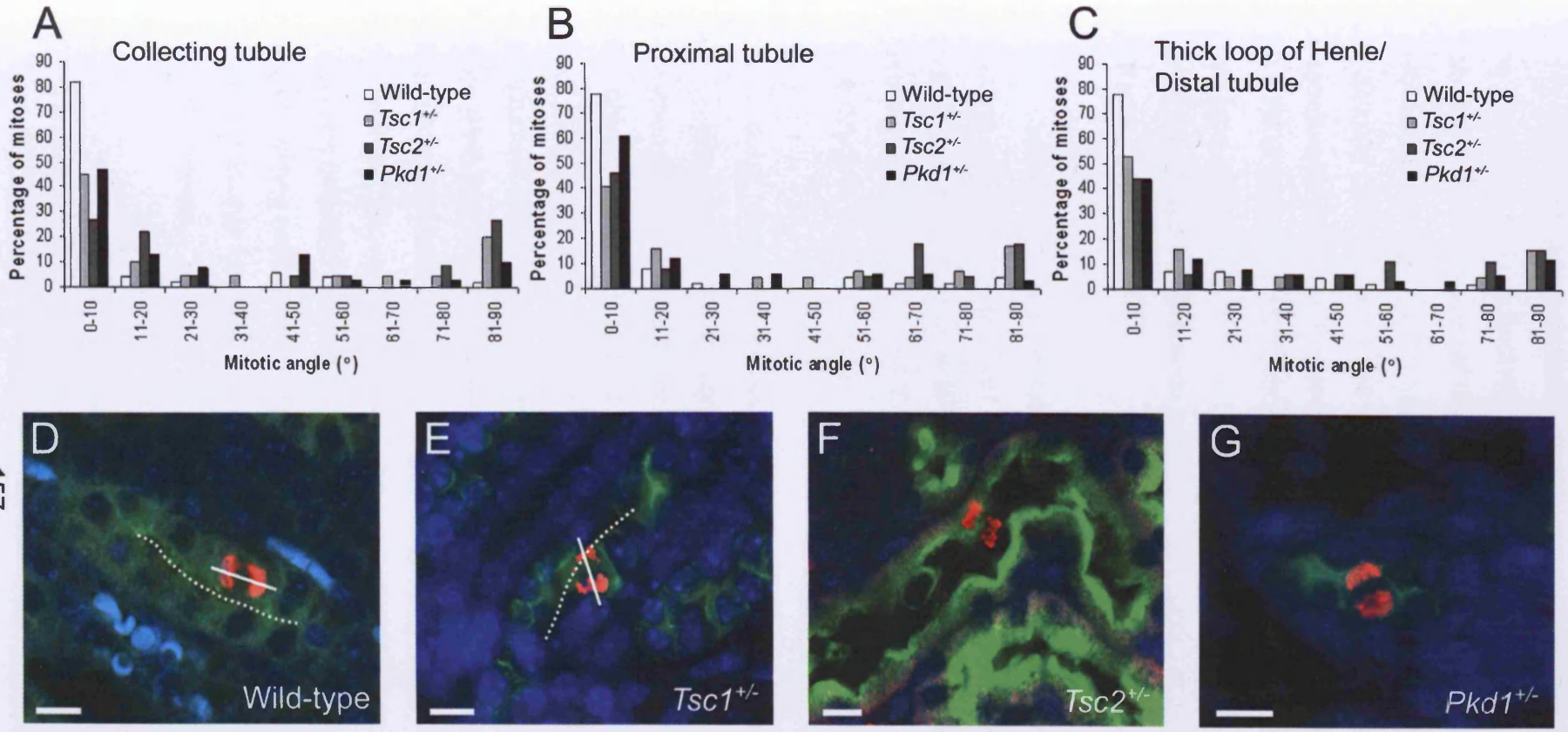

Figure 6.1 Mitotic orientations of dividing pre-cystic tubule cells from 2 day old mouse kidneys. Graphs showing the distribution of the mitotic angles from wild-type, *Tsc1*$^{+/-}$, *Tsc2*$^{+/-}$ and *Pkd1*$^{+/-}$ mice in the collecting tubule (**A**), proximal tubule (**B**) and loop of Henle/distal convoluted tubule (**C**). Fluorescent micrographs showing examples of the orientation of dividing cells in wild-type (**D**), *Tsc1*$^{+/-}$ (**E**), *Tsc2*$^{+/-}$ (**F**) and *Pkd1*$^{+/-}$ (**G**) mice using anti-H3pS10 to stain for dividing chromosomes (red), DBA, LTL or THP to stain for tubules (green) and DAPI for nuclear staining (blue). In wild-type mice, tubule cells predominantly divided in parallel with the longitudinal tubule axis whereas in *Tsc1*$^{+/-}$, *Tsc2*$^{+/-}$ and *Pkd1*$^{+/-}$ mice, the mitotic alignments were often distorted and in a plane perpendicular to the epithelial sheath. Examples of how mitotic angles were measured (**D**, **E**). Tubule lumens are indicated by a dashed white line and the direction of tubule cell division is indicated by a solid white line. Scale bars: 10μm.

We also observed that in *Tsc1*$^{+/-}$ mice, 21-30% of dividing cells from the proximal tubule, collecting duct and loop of Henle/distal convoluted tubule showed an 'extreme' dysregulation of mitotic orientation (with divisions between 60° and 90° to the tubule axis) and, similarly, in *Tsc2*$^{+/-}$ mice, 28-49% of dividing cells displayed this severe phenotype (Figure 6.1). Such dysregulation was less frequently observed in dividing cells from *Pkd1*$^{+/-}$ mice (9-21% of cells depending upon tubule segment) and was rarely observed in wild-type mice (2-8% of cells) ($P<0.05$ compared to both *Tsc1*$^{+/-}$ and *Tsc2*$^{+/-}$ cells). We found no difference between *Tsc1*- and *Tsc2*-associated polarity defects.

Interestingly, we did find significant differences in the orientations of dividing tubule cells from *Tsc1*$^{+/-}$ *Pkd1*$^{+/-}$ and *Tsc2*$^{+/-}$ *Pkd1*$^{+/-}$ mice as compared to their wild-type littermates ($P<0.04$), but did not observe any differences between *Tsc1*$^{+/-}$ *Pkd1*$^{+/-}$ and *Tsc2*$^{+/-}$ *Pkd1*$^{+/-}$ mice, or their corresponding single heterozygote *Tsc1*$^{+/-}$ or *Tsc2*$^{+/-}$ littermates ($P>0.1$) (Figure 6.2).

6.3.2 Confocal analysis of mitotic orientation in 48 hour old mice

We generated more comprehensive, three dimensional (3D) images of the aberrant mitotic orientations using confocal microscopy. In agreement with our previous results, we found that only 44%, 40% and 50% of dividing cells from *Tsc1*$^{+/-}$, *Tsc2*$^{+/-}$ and *Pkd1*$^{+/-}$ mice, respectively, divided within 10° of the longitudinal tubule axis, as compared to 80% of dividing cells from wild-type mice ($P=0.023$, $P=0.01$ and $P=0.037$, respectively) (Figure 6.3). We also found that 39% and 40% of dividing cells from *Tsc1*$^{+/-}$ and *Tsc2*$^{+/-}$ mice, respectively, showed an 'extreme' dysregulation of mitotic orientation (divisions between 60° and 90° to the tubule axis) and this was only found in 5% of dividing cells from wild-type mice ($P=0.01$ and $P=0.008$, respectively) (Figure 6.3). We found no difference between *Tsc1*- and *Tsc2*-associated polarity defects.

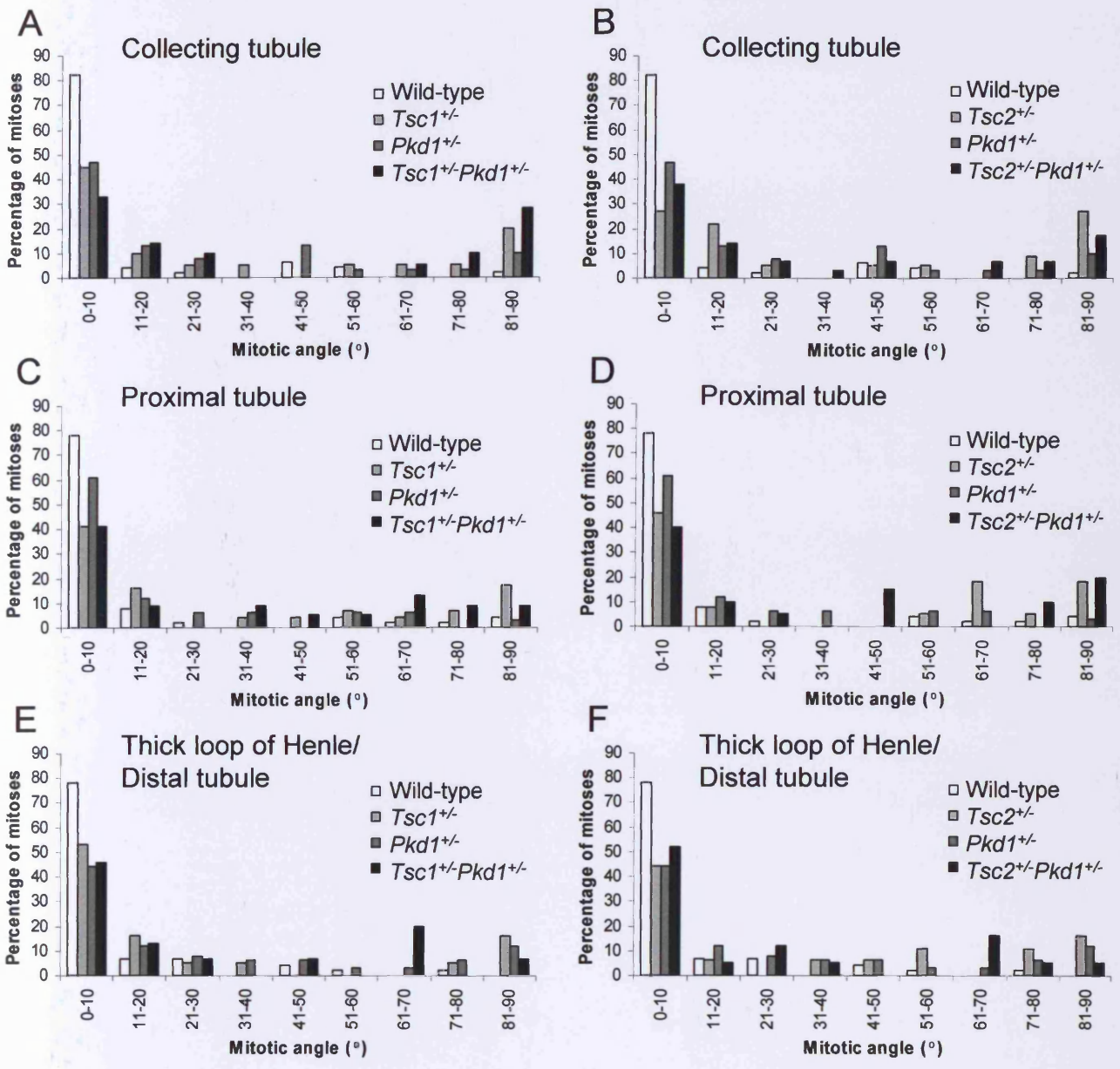

Figure 6.2 Mitotic orientations of dividing pre-cystic renal tubule cells from 2 day old *Tsc1*$^{+/-}$ *Pkd1*$^{+/-}$ and *Tsc2*$^{+/-}$ *Pkd1*$^{+/-}$ mice compared to respective littermates. Graphs showing the distribution of the mitotic angles from wild-type, *Tsc1*$^{+/-}$, *Tsc2*$^{+/-}$, *Pkd1*$^{+/-}$, *Tsc1*$^{+/-}$ *Pkd1*$^{+/-}$ and *Tsc2*$^{+/-}$ *Pkd1*$^{+/-}$ mice in the collecting tubule (**A**, **B**), proximal tubule (**C**, **D**) and loop of Henle/distal convoluted tubule (**E**, **F**). Aberrant mitotic orientations in *Tsc1*$^{+/-}$ *Pkd1*$^{+/-}$ and *Tsc2*$^{+/-}$ *Pkd1*$^{+/-}$ mice were similar to their corresponding single heterozygote *Tsc1*$^{+/-}$ or *Tsc2*$^{+/-}$ littermates.

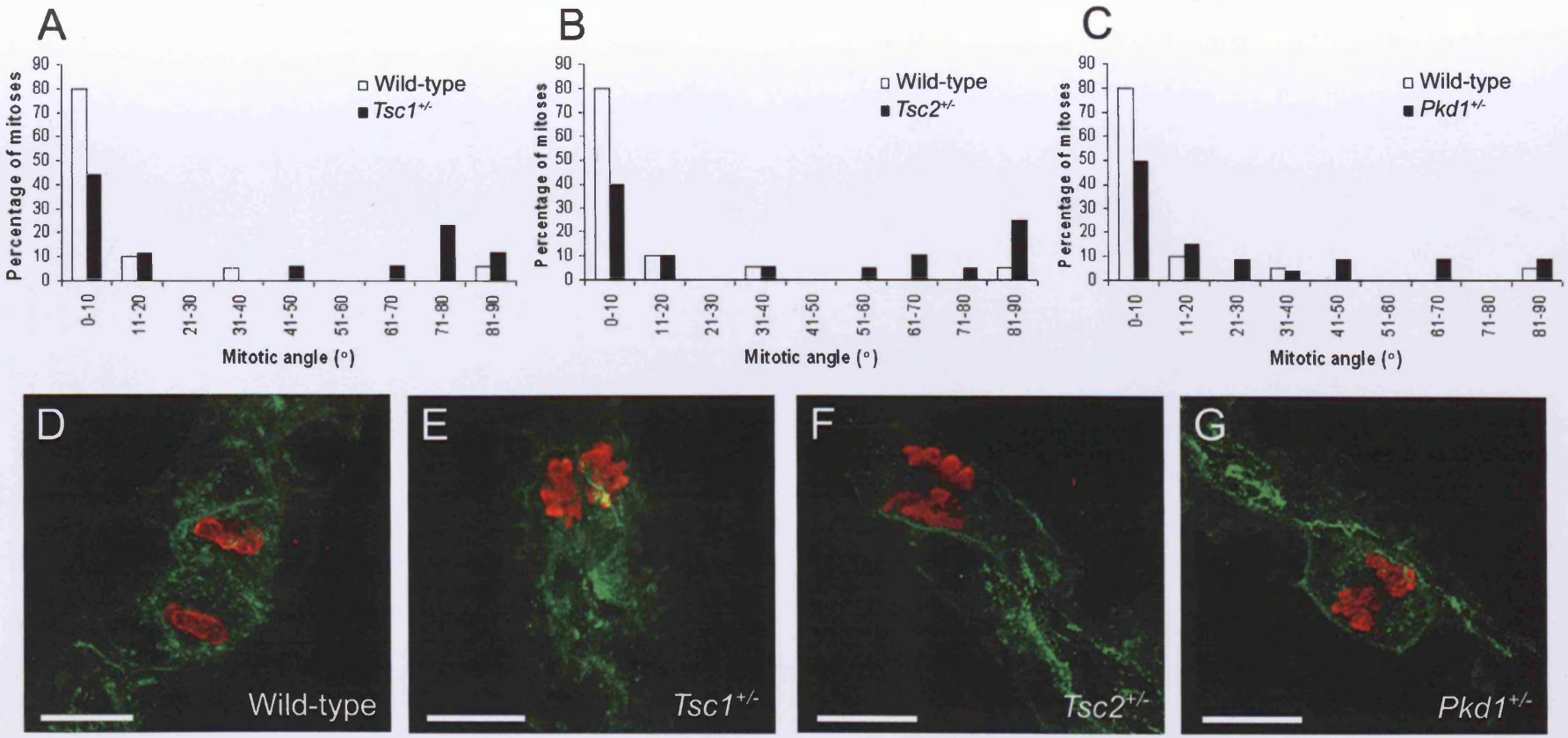

Figure 6.3 Three dimensional reconstruction of the mitotic orientations of dividing pre-cystic renal tubule cells using confocal microscopy. Graphs showing the distribution of the mitotic angles in *Tsc1*$^{+/-}$ (**A**), *Tsc2*$^{+/-}$ (**B**) and *Pkd1*$^{+/-}$ (**C**) mice (black bars) compared to wild-type littermates (white bars). Significantly fewer cells from *Tsc1*$^{+/-}$, *Tsc2*$^{+/-}$ and *Pkd1*$^{+/-}$ mice divided within 10° of the tubule axis compared to wild-type littermates ($P<0.038$). Confocal fluorescent micrographs showing examples of the orientation of dividing cells in wild-type (**D**), *Tsc1*$^{+/-}$ (**E**), *Tsc2*$^{+/-}$ (**F**) and *Pkd1*$^{+/-}$ (**G**) mice using anti-H3pS10 to stain for dividing chromosomes (red) and THP to stain for tubules (green). Scale bars: 10μm.

6.3.3 Mitotic orientation in pre-cystic renal tubule cells from 10 day old mice

We also studied dividing cells from mice at 10 days of age and observed identical results to our studies at 48 hrs of age, with significant differences in the mitotic orientations of dividing cells in all regions of the kidney tubule from *Tsc1*$^{+/-}$, *Tsc2*$^{+/-}$, *Pkd1*$^{+/-}$, *Tsc1*$^{+/-}$ *Pkd1*$^{+/-}$ and *Tsc2*$^{+/-}$ *Pkd1*$^{+/-}$ mice as compared to wild-type littermates ($P<0.05$ for each genotype) (Figure 6.4). By 15 days of age, the number of dividing tubule cells had dramatically reduced in all mice regardless of genotype and by 20 days of age, no dividing cells were observed indicating the completion of tubule development.

6.3.4 SEM analysis of stereociliary bundles in mouse cochlea

We addressed whether the observed defects in polarity were also present in extra-renal tissues from our mouse models. We analysed stereociliary bundles from *Tsc1*$^{+/-}$, *Tsc2*$^{+/-}$, *Pkd1*$^{+/-}$, *Tsc1*$^{+/-}$*Pkd1*$^{+/-}$ and *Tsc2*$^{+/-}$ *Pkd1*$^{+/-}$ mice by SEM to search for abnormalities in PCP, but found no differences between these animals and their wild-type littermates (Figures 6.5 and 6.6). The majority of stereociliary bundles in mice from all genotypes were of normal appearance and orientation (Figure 6.5). Rarely, abnormal looking structures such as misorientation, misalignment and absence (Figure 6.6) of stereociliary bundles were observed in all mice. Regardless of genotype, the overall structure of the cochlea also appeared regular with all turns of the cochlea (one and a half turns with a basal 'hook' region) normal in both structure and length.

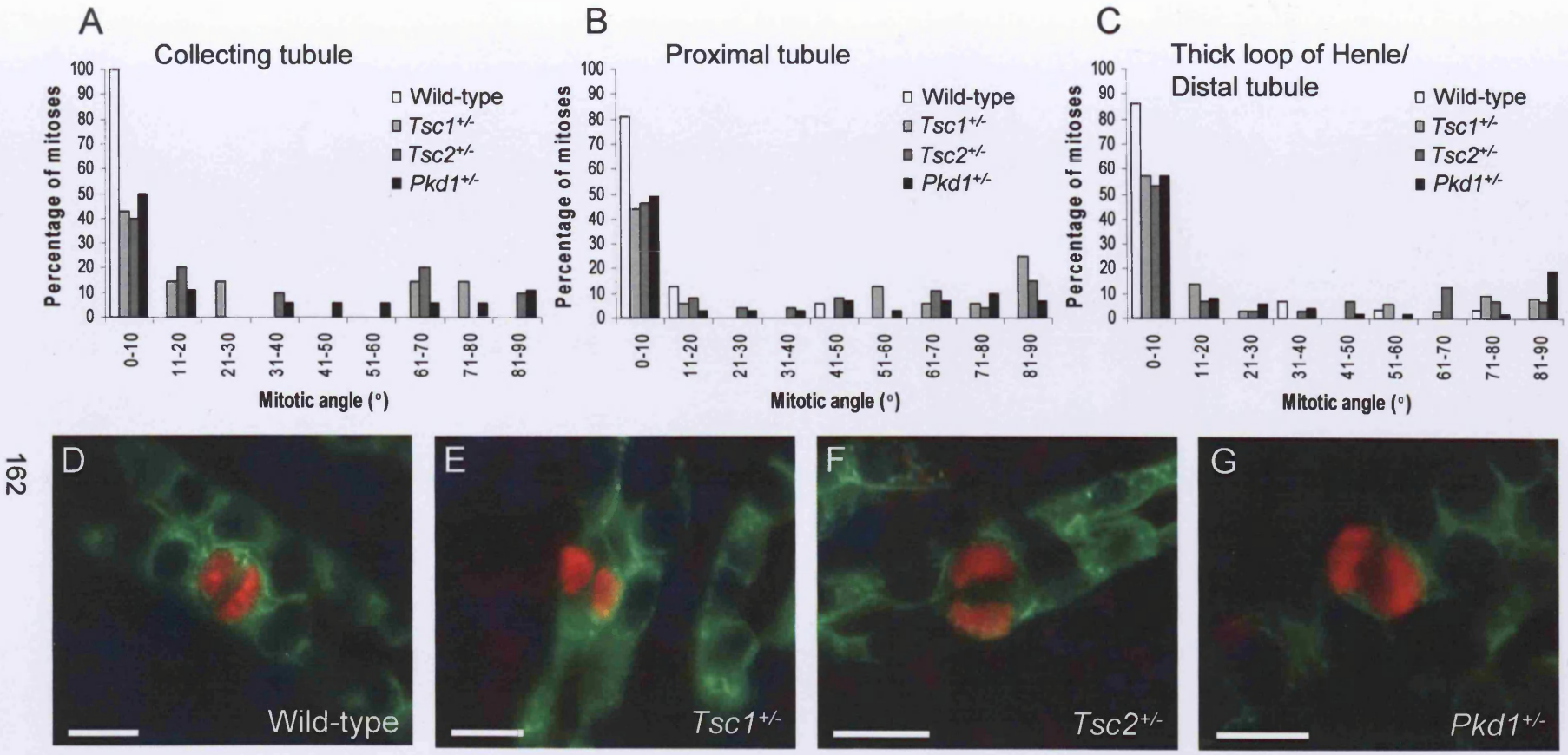

Figure 6.4 Mitotic orientations of dividing pre-cystic renal tubule cells from ten day old mouse kidneys. Graphs show the distribution of the mitotic angles from wild-type, *Tsc1*$^{+/-}$, *Tsc2*$^{+/-}$ and *Pkd1*$^{+/-}$ mice in the collecting tubule (**A**), proximal tubule (**B**) and thick loop of Henle/distal convoluted tubule (**C**). Fluorescent micrographs show examples of the orientation of dividing cells in wild-type (**D**), *Tsc1*$^{+/-}$ (**E**), *Tsc2*$^{+/-}$ (**F**) and *Pkd1*$^{+/-}$ (**G**) mice using anti-H3pS10 to stain for dividing chromosomes (red) and DBA, LTL or THP to stain for tubules (green). Scale bars: 10μm.

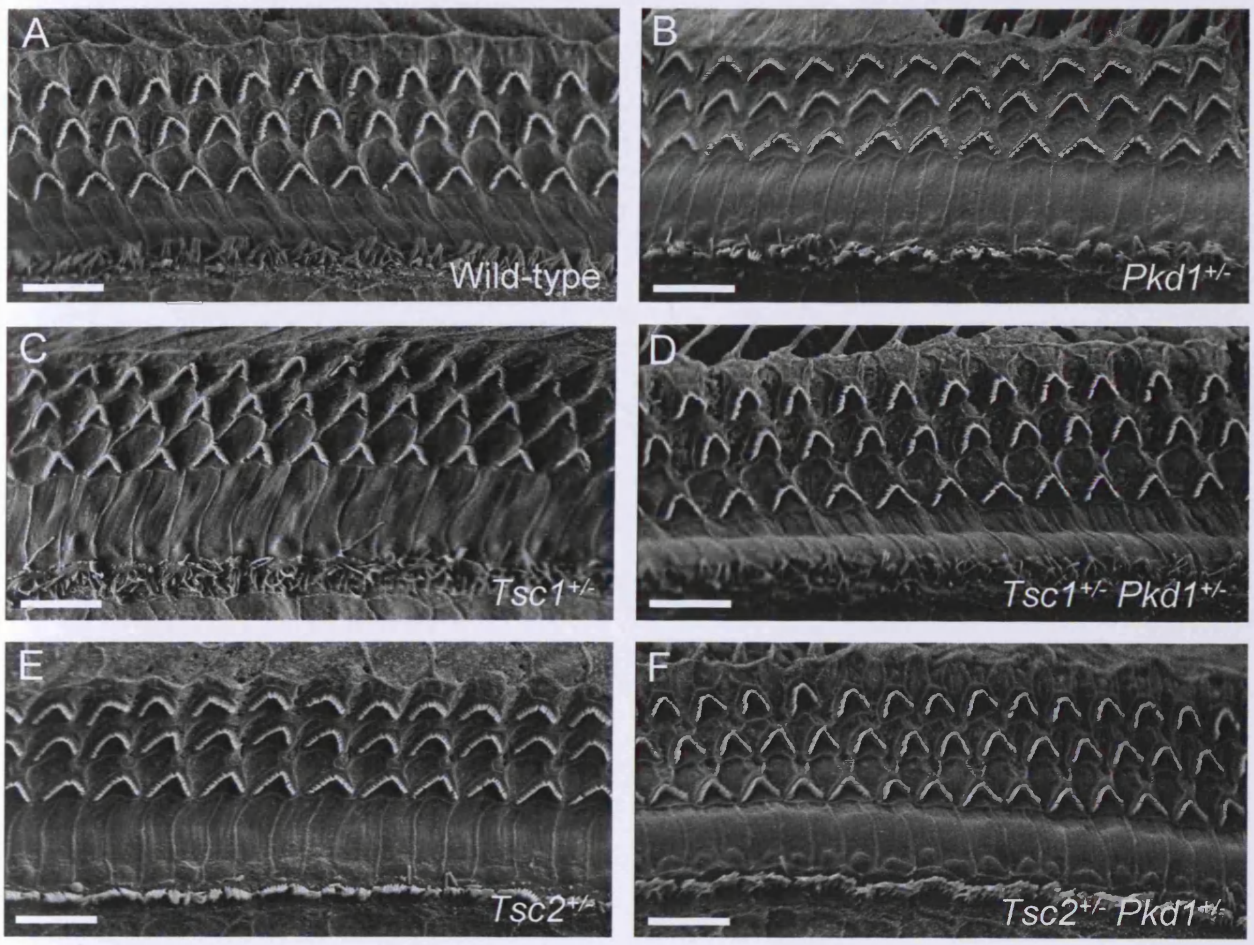

Figure 6.5 SEM examination of stereociliary bundles in the organ of Corti from wild-type (**A**), *Pkd1*$^{+/-}$ (**B**), *Tsc1*$^{+/-}$ (**C**), *Tsc1*$^{+/-}$*Pkd1*$^{+/-}$ (**D**), *Tsc2*$^{+/-}$ (**E**), and *Tsc2*$^{+/-}$*Pkd1*$^{+/-}$ (**F**) mice. In all animals, the outer hair cells were uniformly arranged in three rows, with a row of inner hair cells underneath. Scale bars: 10μm.

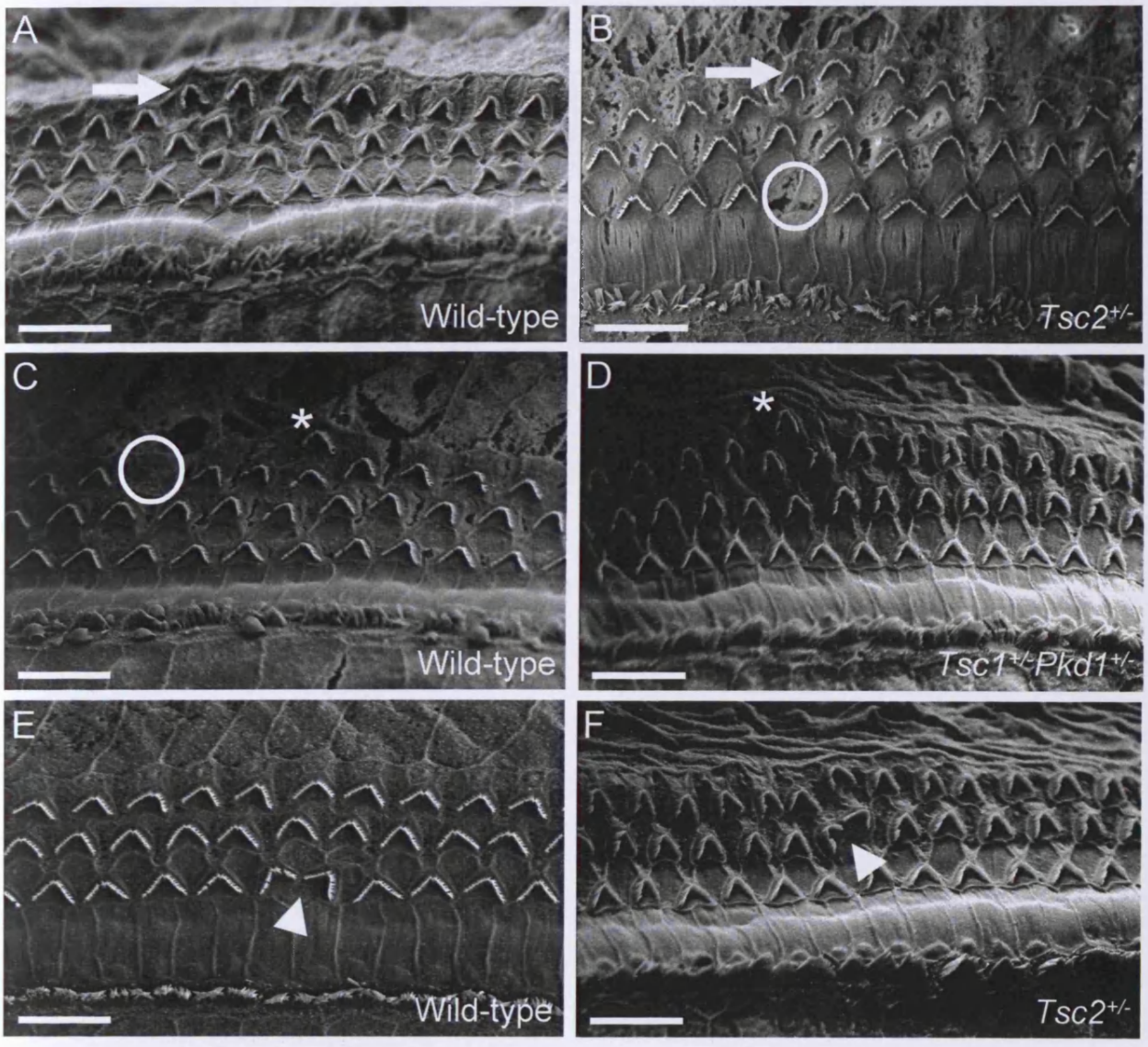

Figure 6.6 SEM micrographs of abnormal stereociliary bundles in the mouse organ of Corti found in both mutant and wild-type mice. Rarely, four rows of outer hair cells were observed rather than the normal three rows (arrows) (**A**, **B**). Stereociliary bundles were sometimes absent (circled areas), however this may be an artefact from dissection and/or processing of the tissues (**B**, **C**). Occasionally, stereociliary bundles can appear out of alignment from the rest of the row (asterix) (**C**, **D**). Mis-orientated stereociliary bundles were infrequently observed (arrow heads) (**E**, **F**). These organ of Corti abnormalities were found in both wild-type and heterozygous mice and so are not thought to represent a disease phenotype. Scales bars: 10μm.

6.4 Discussion

6.4.1 A novel role for hamartin and tuberin in cell polarity?

To date, PCP defects have not been examined in TSC- or ADPKD-associated renal disease. Fischer *et al.* (2006) recently reported defects in the mitotic orientation of dividing tubule epithelial cells during renal tubule elongation in a rat model of ARPKD. Similar to these findings, we found a high percentage of cells from *Tsc1*$^{+/-}$, *Tsc2*$^{+/-}$ and *Pkd1*$^{+/-}$ mouse models divided in a plane perpendicular to the longitudinal tubule axis demonstrating extreme dysregulation of mitotic orientation. This novel data suggests that defects in cell polarity underlie not just ADPKD but also TSC-associated renal cystic disease.

Interestingly, *Tsc1*$^{+/-}$*Pkd1*$^{+/-}$ and *Tsc2*$^{+/-}$*Pkd1*$^{+/-}$ mice showed similar mitotic orientation defects to their corresponding *Tsc1*$^{+/-}$ or *Tsc2*$^{+/-}$ littermates. It is unclear why haploinsufficiency of *Pkd1* does not appear to elicit a significant effect on mitotic orientation during tubule development as it does with lesion numbers or primary cilia length in older compound heterozygotes. Perhaps expression levels of PC1, hamartin and tuberin during development may provide an answer. Expression of PC1 is developmentally regulated, with high levels in developing mouse kidney, falling to a low level 2 weeks after birth (Geng *et al.* 1997). This drop in PC1 expression correlates with the dramatic drop in dividing tubule cells as tubule development and lengthening comes to an end approximately 2 weeks after birth. Tuberin levels also drop as age increases with a significant reduction in the rat kidney by day 15, falling to very low levels in adult life (12 weeks) (Murthy *et al.* 2001). Hamartin expression appears to fall dramatically by day 1 in the rat kidney, remaining at this low level through to adult life (Murthy *et al.* 2001). These differences in protein expression levels between the developing and adult kidneys may account for the differences in the effect of compound heterozygosity on mitotic orientation in early life and primary cilia length and lesion number in later life.

6.4.2 Apical/basal polarity may be altered in *Tsc1* and *Tsc2* haploinsufficient mice

Close examination of the misorientated tubule cells revealed that most of these cells were dividing in a plane perpendicular to the epithelial sheath, consistent with defects in apical/basal (A/B) polarity which occurs perpendicular to the PCP axis. While the apical localization of PCP determinants such as Frizzled (Fz1) is critical for their function, the link between A/B polarity and PCP is poorly understood. Djiane *et al.* (2005) have shown that dPatj, a member of the Crumbs complex which plays a key role in A/B polarity, binds to the cytoplasmic tail of Fz1 which recruits aPKC, which in turn phosphorylates and inhibits Fz1, thereby providing a direct link between A/B polarity and PCP. Accordingly, components of the aPKC complex and dPatj produce PCP defects in the *Drosophila* eye such as ommatidial misrotations (Djiane *et al.* 2005). Interestingly, tuberin has been found to directly interact with PATJ (Massey-Harroche *et al.* 2007) and *Drosophila* with mosaic *Tsc1* mutant cells in their eyes exhibit ommatidial misrotations (Tapon *et al.* 2001). This data suggests that tuberin may in some way influence the interaction between PATJ and Fz1, perhaps by stabilising the complex (Figure 6.7). Given that primary cilia are the most apical structures in a cell, this raises the possibility that the defects that we observed in primary cilium length may be secondary consequences of perturbed A/B polarity.

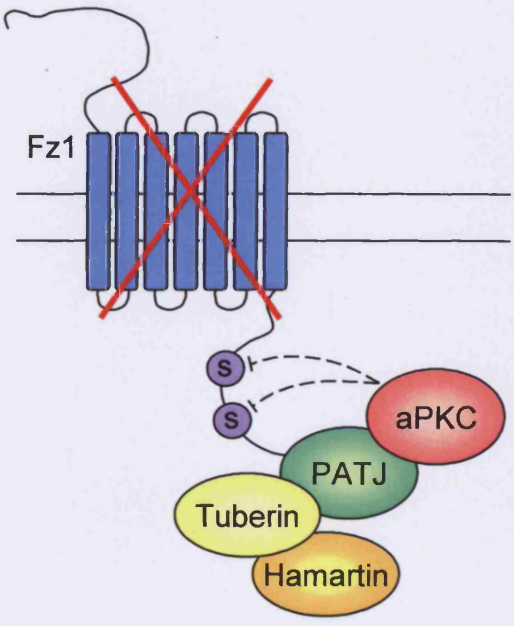

Figure 6.7 Model of the interaction between tuberin and PATJ and the possible effect on Fz1 activation. dPatJ binds directly to the Fz1 cytoplasmic tail and recruits aPKC which phophorylates Fz1 at Ser^{554} and Ser^{560} thus inhibiting the activity of Fz1 in cells where signalling should not be occurring. Tuberin interacts through its C-terminal domain with PATJ. The role of tuberin in this complex is unclear, however one could speculate that perhaps tuberin is required to stabilise the PATJ/Fz1/aPKC interaction. Hamartin co-precipitates with PATJ indicating the requirement of the functional hamartin/tuberin complex.

6.4.3 Stereocilia bundle abnormalities are occasionally observed in wild-type mice

Examination of the organ of Corti occasionally revealed an extra row of outer hair cells, missing bundles and misoriented stereocilia bundles in all genotypes, including wild-type mice. These findings in wild-type mice were surprising, however, personal correspondence with an expert in the field (Prof. Karen Steel) has revealed that these abnormalities do occasionally occur in wild-type mice, and are often dependent on background. Indeed, work by Hayashi *et al.* (2007) using a mouse model of fibroblast growth factor receptor-3 (FGFR3) deficiency (*Fgfr3*$^{-/-}$) to examine the role of FGFR3 in development of the organ of Corti, found an extra row of outer hair cells in *Fgfr3*$^{-/-}$ mice which had previously not been observed in an earlier analysis of *Fgfr3*-deficient mice. The authors suggest that this difference may be due to the different backgrounds of these mice.

6.4.4 Polarity defects may be tissue or cell-type specific

It has recently been shown by others that hamartin and tuberin play a role in neuronal polarity (Choi *et al.* 2008). Polarisation of the neuron is essential for the correct formation and function of dendrites and axons. Kishi *et al.* (2005) previously showed that SAD (synapses of amphids defective)-A and SAD-B, mammalian orthologues of SAD-1 kinase required for presynaptic differentiation in *C. elegans*, are required for neuronal polarisation in mice. Choi *et al.* (2008) found that cortical and hippocampal neurons deficient for *Tsc1/Tsc2* function form ectopic axons both *in vitro* and *in vivo*. They also revealed that inactivation of *Tsc1/Tsc2* promotes axonal growth via up-regulation of neuronal polarity SAD kinases, particularly SAD-A, which they also found to be elevated in cortical tubers of a TSC patient. The authors suggest that the Tsc/mTOR pathway may limit multiple axon formation and confine polarised growth within a single axon in the mammalian brain, and its deregulation likely contributes to the neurological symptoms commonly observed in patients with TSC. Here, we show a role for hamartin and tuberin in renal tubule cell polarity. Since we did not find any defects in the orientations of the stereociliary bundles from our mice, we suggest that hamartin, tuberin and PC1 are not 'classical' PCP proteins and that the

associated defects in polarity are tissue or cell-type specific. Such tissue specific PCP proteins (PCP effectors) are found in *Drosophila* where certain proteins regulate PCP in the wing while completely different proteins regulate PCP in the eye (chapter 1, section 1.3.5.2.1 and reviewed in Fanto and McNeill 2004). It is interesting to note that TSC patients have no known hearing impairment, but the majority do develop brain and kidney lesions (Gomez *et al.* 1999). Further investigation of polarity defects in other affected and unaffected organs may provide more insight into the tissue specificity of TSC polarity defects.

Interestingly, the work carried out by Choi *et al.* and our work on renal tubule epithelial cells suggests that the polarity defects observed may occur as a consequence of haploinsufficiency and not through a requirement for additional somatic mutations. Choi *et al.* (2008) showed that SAD-A levels are often notably increased in the giant cells of a cortical tuber from a patient with TSC. LOH of the wild-type *TSC1* or *TSC2* alleles in cortical tubers is rare (Henske *et al.* 1996, Niida *et al.* 2001) and indicates that the loss of one copy of *Tsc1* or *Tsc2* may be sufficient to significantly increase the amount of SAD and affect neuronal polarity and/or morphology (Wildonger *et al.* 2008). We observed polarity defects in renal tubule epithelial cells from mice as young as 2 days old. At this young age it is unlikely second hits have occurred and suggests that these defects are due to haploinsufficiency of *Tsc1* or *Tsc2*.

CHAPTER SEVEN: General discussion

7.1 Haploinsufficiency in TSC and ADPKD

We have shown that hamartin, tuberin and PC1 play a key role in maintaining renal tubule cell polarity during development. This early aberrant phenotype suggests that haploinsufficiency for *Tsc1*, *Tsc2* or *Pkd1* may have pathogenic consequences, a notion supported by other studies which have highlighted the importance of haploinsufficiency in TSC (Figure 7.1) and ADPKD.

7.1.1 Haploinsufficiency in TSC and other hamartoma syndromes

Microscopically normal renal tubule epithelial cells from germline *TSC* mutation carriers have significant differences in gene expression profiles compared to control cells (Stoyanova et al. 2004). *TSC* renal epithelial cells showed increased expression of transcripts for several factors involved in protein synthesis including eukaryotic translation initiation factor 3 and upregulation of several ribosomal protein genes (S6, S25, L6, L21). In addition HIF signalling was altered, as shown by increased expression of the HIF1α subunit, hypoxia-inducible protein 2 and hypoxia induced gene 1 (Stoyanova et al. 2004).

Work on rodent models of *Tsc* has provided more insight into the role of haploinsufficiency, particularly in pathogenic central nervous system manifestations. As previously mentioned, young Eker rats, which rarely harbour brain lesions early in life, exhibit enhanced episodic-like memory and enhanced responses to chemically-induced kindling (Waltereit *et al.* 2006). Goorden *et al.* (2007) reported that $Tsc1^{+/-}$ mice with no apparent cerebral pathology showed impaired learning in hippocampus-sensitive versions of learning tasks and also impaired social behaviour. Furthermore, Uhlmann *et al.* (2002) reported that grossly normal $Tsc1^{+/-}$ and $Tsc2^{+/-}$ mouse brains exhibit a 1.5 fold increase in the number of astrocytes in the hippocampus.

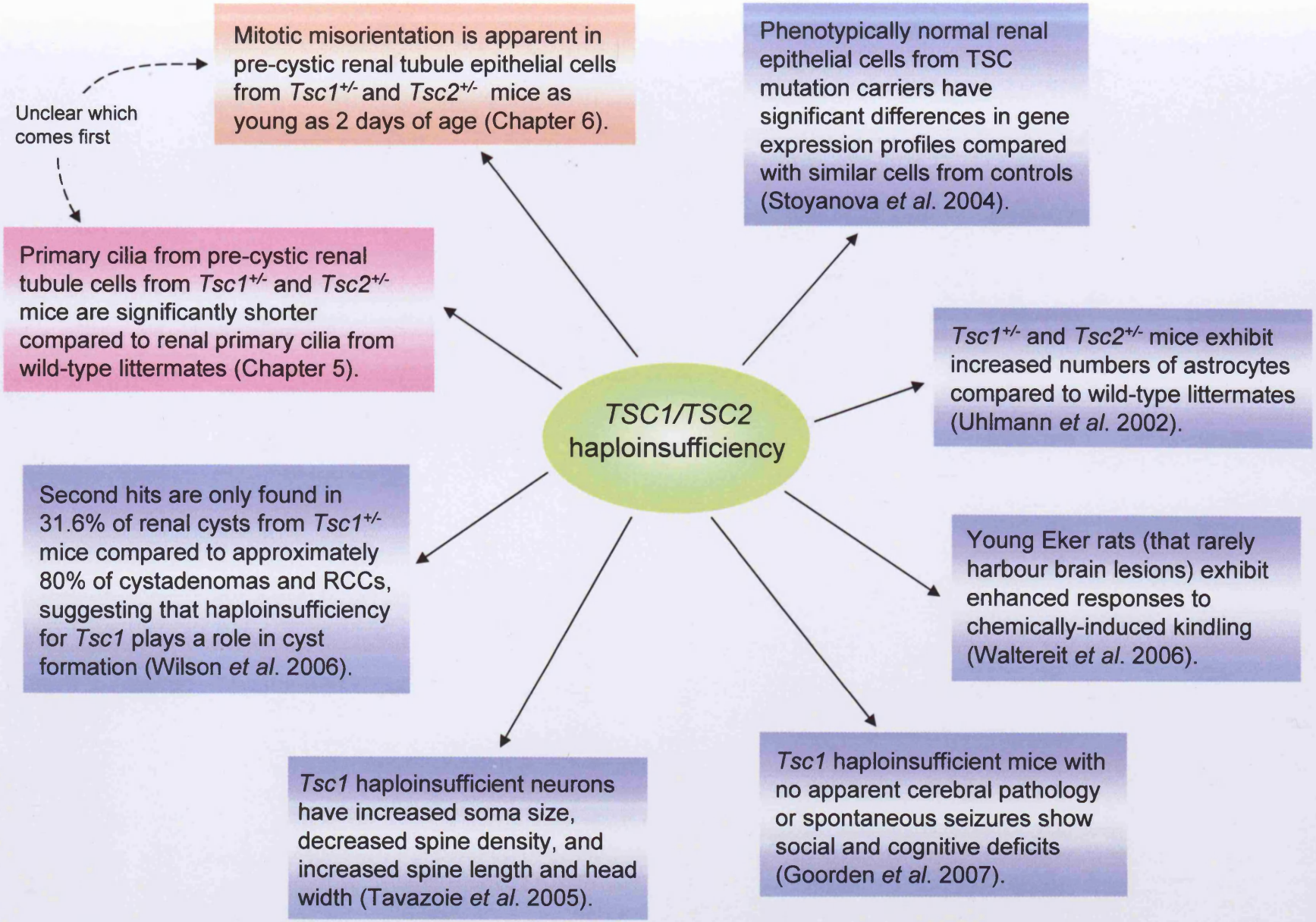

Figure 7.1 *Tsc1* and *Tsc2* haploinsufficiency effects.

Our laboratory has previously demonstrated a lack of *Tsc1* second hits in 68.4% of renal cysts compared to approximately 20% of advanced lesions (cystadenomas and RCCs) from *Tsc1*$^{+/-}$ mice. These results were obtained after LOH analyses and direct sequencing of the entire *Tsc1* ORF and suggest that haploinsufficiency for *Tsc1* may be sufficient to initiate cystogenesis. Our findings of mitotic orientation and primary cilia length defects in pre-cystic renal tubule epithelial cells may be some of the earliest events in cystogenesis and support the theory that haploinsufficiency of *Tsc1* or *Tsc2* is sufficient to elicit a pathogenic phenotype.

There is increasing evidence that haploinsufficiency in a variety of other hamartoma syndromes may be involved in tumour initiation. These diseases include Peutz-Jeghers syndrome (PJS), PTEN hamartoma syndromes and juvenile polyposis syndrome (JPS) (summarised in Table 7.1). In addition to the haploinsufficiency found in early cystic lesions from our studies in TSC and early lesions of other hamartoma syndromes, a common trend is observed that many advanced lesions display second hits in their corresponding wild-type gene. We have previously identified somatic *Tsc1* mutations in more than 80% of cystadenomas and RCCs from *Tsc1*$^{+/-}$ mice. Biallelic inactivation of the *Lkb1* gene (associated with PJS) has been found in advanced hepatocellular carcinomas in *Lkb1*$^{+/-}$ mice (Nakau *et al.* 2002) and Entius *et al.* (2001) found LOH of the *LKB1* wild-type allele in only 38% of benign hamartomatous polyps from PJS patients, in contrast to 100% of carcinomas. LOH of the *Smad4* allele (associated with JPS) has been detected in 40% of lesions from *Smad4*$^{+/-}$ mice up to 15 months, which increased to 64% in tumours from mice over 18 months (Alberici *et al.* 2006).

Our data suggests that although *Tsc1* haploinsufficiency may be an important step in the initiation of *Tsc*-associated renal tumourigenesis, biallelic inactivation of *Tsc1* is an important factor in the latter stages. Together, these results suggest a possible common mechanism of tumour initiation in hamartoma syndromes, whereby one hit initiates tumourigenesis, while a second hit promotes the progression to more advanced lesions.

Table 7.1 Examples of haploinsufficiency in other hamartoma syndromes.

Disease	Gene mutated	Haploinsufficiency effects
PJS	*LKB1/STK11*	▪ LOH of the *LKB1* wild-type allele found in only 19%-38% of tumours from PJS patients (Resta *et al.* 1998, Entius *et al.* 2001). ▪ Loss of only one copy of *Lkb1* is necessary to produce gastrointestinal polyps in *Lkb1*$^{+/-}$ mice (Miyoshi *et al.* 2002, Rossi *et al.* 2002, Jishage *et al.* 2002).
PTEN hamartoma syndromes	*PTEN*	▪ *PTEN* haploinsufficiency results in altered gene expression in subventricular zone precursor cells (Li *et al.* 2003a). ▪ Loss of the wild-type *Pten* allele does not occur in hyperplastic-dysplastic changes of the colon mucosa and polyps in the lower gastronintestinal tract in *Pten*$^{+/-}$ mice (Di Cristofano *et al.* 1998).
JPS	*SMAD4, BMPR1A*	▪ Only 9% of gastrointestinal polyps show LOH of the wild-type *SMAD4* allele (Howe *et al.* 1998). ▪ Early gastrointestinal lesions from *Smad4*$^{+/-}$ mice often do not display LOH of the *Smad4* wild-type allele (Xu *et al.* 2000, Alberici *et al.* 2005).

7.1.2 Haploinsufficiency in ADPKD

As previously discussed (chapter 1, section 1.2.7), second hits in *PKD1* or *PKD2* are only found in a proportion of cysts from patients with ADPKD, and both high and low gene dosage levels of *Pkd1* can lead to renal cystic disease in mouse models (Lantinga-van Leeuwen *et al.* 2004, Jiang *et al.* 2006, Pritchard *et al.* 2000, Thivierge *et al.* 2006). *Pkd1* haploinsufficiency has been found to be associated with increased pre-cystic renal tubule epithelial cell proliferation in *Pkd1* mutant mice compared to controls (Lantinga-van

Leeuwen *et al.* 2007). Ahrabi *et al.* (2007) studied a non-cystic *Pkd1*$^{+/-}$ mouse model and found that *Pkd1* haploinsufficiency is associated with a syndrome of inappropriate antidiuresis (reduction of urinary volume) reflecting decreased intracellular Ca^{2+} concentration, decreased activity of RhoA and inappropriate expression of arginine vasopressin in the brain. Haploinsufficiency of *Pkd2* has also been found to elicit a pathogenic phenotype, with *Pkd2*$^{+/-}$ mice displaying an enhanced level of intracranial vascular abnormalities when induced to develop hypertension, possibly due to significant alteration of intracellular Ca^{2+} homeostasis (Qian *et al.* 2003b). Chang *et al.* (2006) have also found an increased proliferative index in non-cystic tubules from *Pkd2* mutant mice 5-10 times higher than that of normal control tissue. Similarly, the proliferative index of non-cystic tubules in kidneys from patients with ADPKD was 40 times higher than corresponding controls, suggesting that an increase in cell proliferation is an early event preceding cyst formation and can result from haploinsufficiency at *PKD2* (Chang *et al.* 2006).

We found ciliary length defects and misoriented mitotic orientations in pre-cystic renal tubule epithelial cells from *Pkd1*$^{+/-}$ mice. In combination with the above studies, a clear case for haploinsufficiency at *Pkd1* or *Pkd2* causing pre-cystic abnormalities is suggested. An increase in proliferation is highlighted as a necessary step towards cystogenesis in ADPKD and, in combination with misoriented renal tubule epithelial cell divisions, a mechanism for cystogenesis can be envisaged (Figure 7.2). This model may also apply to TSC, as discussed in the next section.

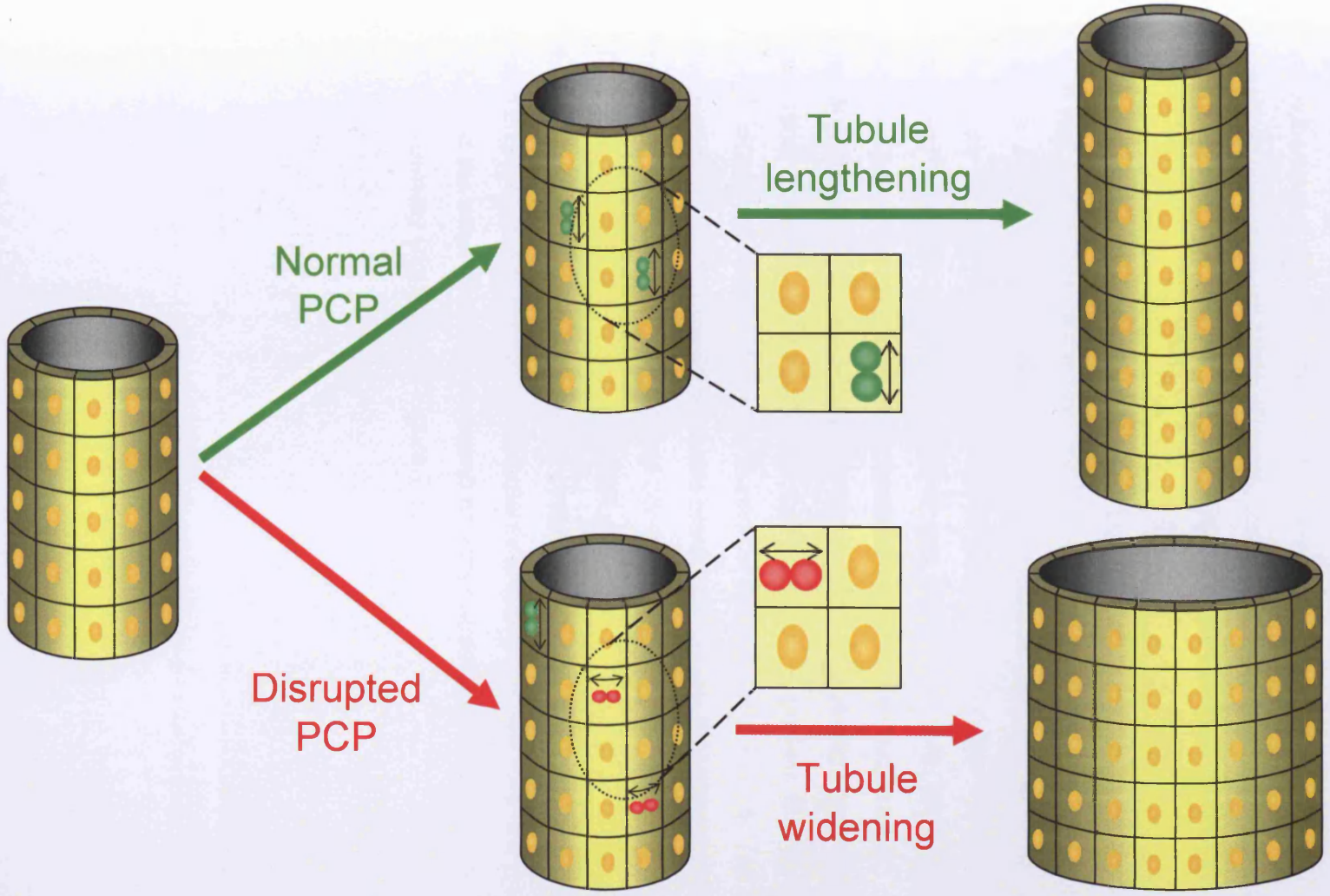

Figure 7.2 Planar cell polarity (PCP) and tubular morphogenesis. During renal development, newly formed tubules undergo an intense proliferative phase and increase in length whilst maintaining a constant diameter. In order for this to occur, tubular epithelial cells must be correctly orientated along the longitudinal tubule axis, a process which is controlled by PCP. If PCP is disrupted, cells may lose the ability to divide along the longitudinal tubule axis and may deviate from this axis, eventually leading to a dilated tubule, one of the first stages of cyst formation.

7.2 Mechanisms of cyst formation

Our results suggest that dysregulation of the A/B polarity (and consequently PCP) pathway initiates renal cystic disease in TSC and ADPKD, and subsequent activation of mTOR promotes cyst expansion (in PKD) and tumour progression (in TSC). Several issues still require further investigation. Firstly, although we demonstrated aberrant polarity in tubule cells from *Tsc1*$^{+/-}$, *Tsc2*$^{+/-}$ and *Pkd1*$^{+/-}$ mice at both 2 and 10 days of age, these animals ultimately develop tubules that are structurally indistinguishable from wild-type mice and, in the case of the TSC models, do not develop cysts for many months. Although we have identified dilated tubules (which may result from aberrantly dividing tubule cells and subsequently develop into cysts) in *Tsc1*$^{+/-}$ and *Tsc2*$^{+/-}$ mice as early as 1 month of age, these were rare. We therefore propose that other events, such as cessation of fluid flow, enhanced proliferation and defective apoptosis may also be required to trigger cyst formation. Secondly, we hypothesise, but have not yet proven, that activation of mTOR occurs after somatic inactivation of the wild-type *Tsc1* or *Tsc2* allele. In support of this hypothesis, we have previously shown that somatic *Tsc1* mutations are infrequent in cysts but common in advanced lesions from *Tsc1*$^{+/-}$ mice, a similar pattern to mTOR activation (Wilson *et al.* 2006). We therefore propose a model whereby cystogenesis may occur via two distinct routes; one involving defective A/B polarity and/or PCP (left side of Figure 7.3), and the other involving a second hit with subsequent activation of the mTOR pathway (right side of Figure 7.3).

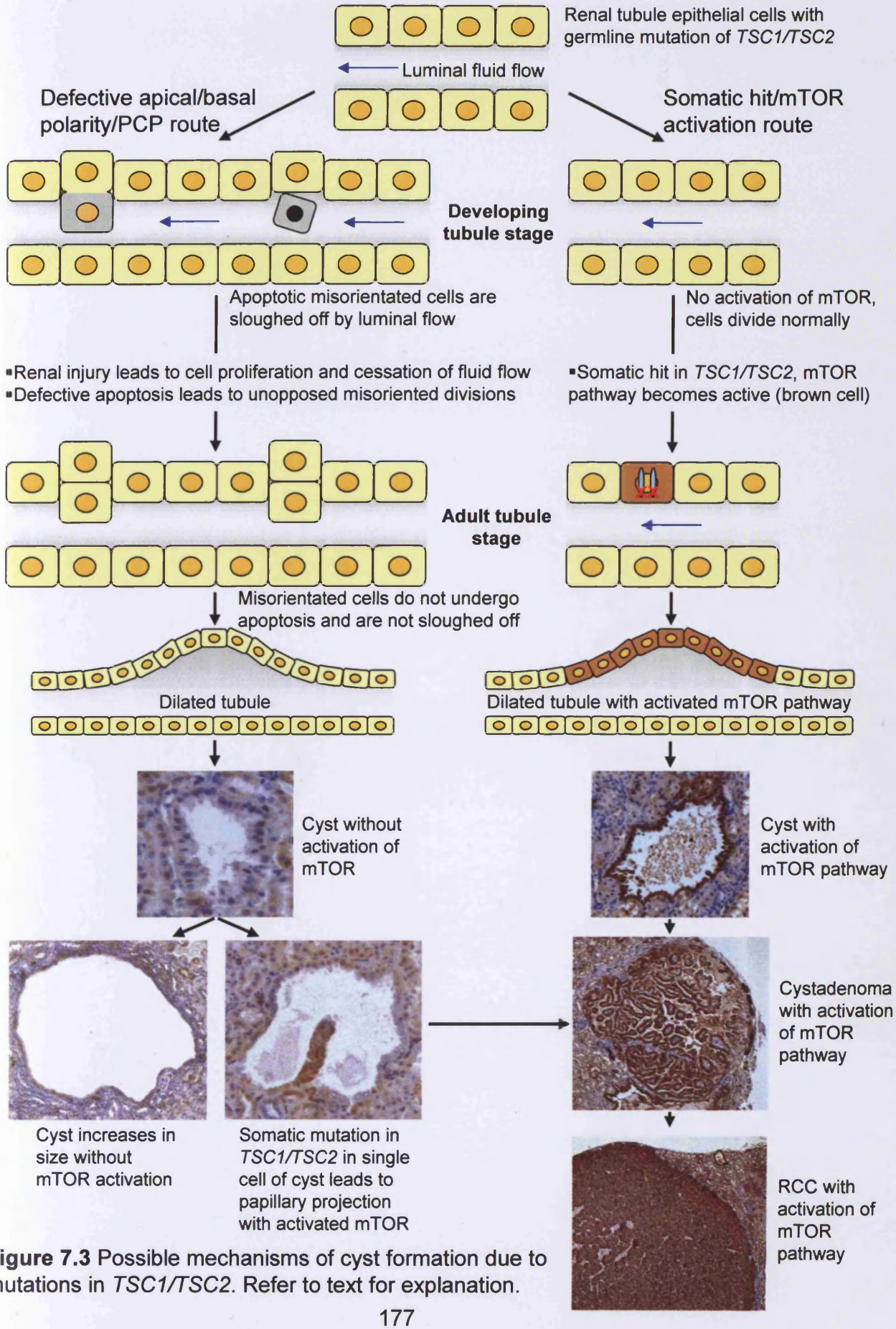

Figure 7.3 Possible mechanisms of cyst formation due to mutations in *TSC1/TSC2*. Refer to text for explanation.

7.2.1 Renal cystogenesis as a consequence of defective polarity

Our results suggest that haploinsufficiency for *Tsc1*, *Tsc2* or *Pkd1* in pre-cystic renal tubule epithelial cells can result in misoriented mitotic divisions during renal development. However, during this intense proliferative phase, why do we not observe a multitude of dilated tubules? One explanation may involve cellular apoptosis and subsequent sloughing off of apoptotic bodies by luminal fluid flow. It has previously been shown that when displaced from the extracellular matrix, epithelial and endothelial cells undergo apoptosis (Frisch and Francis 1994, Meredith *et al.* 1993). This action is suggested to be an important protective measure for the organism, preventing detached cells from reattaching to new matrices and growing dysplastically (Frisch and Ruoslahti 1997). This scenario may also be occurring inside developing kidneys. The daughter cell of a misoriented dividing tubule cell may protrude out from the epithelial cell layer and into the lumen where it is no longer in contact with the extracellular matrix, and must therefore undergo apoptosis. Interestingly, when examining our mouse kidneys for misoriented dividing tubule epithelial cells, misoriented cells that had completed or almost completed cytokinesis were not observed, indicating that the mispositioned daughter cell had been removed, leaving behind one normal looking cell. Due to constant flow of urine through the renal tubules, apoptotic bodies may easily be sloughed off and swept away, therefore leaving no sign of the mispositioned cell. This scenario may explain why dilated tubules were not a feature of 2-10 day old developing mouse kidneys as aberrant mitotic divisions usually undergo apoptosis. We propose that this situation may change as age increases and other pathogenic events take place as described below.

7.2.1.1 Renal injury in adult kidneys leads to cell proliferation and cystogenesis

Previous studies have shown that the severity of renal cystic disease is dependent upon the stage of development at which the gene in question is inactivated. Patel *et al.* (2008) found that kidney-specific inactivation of *Kif3a* in newborn mice (beginning at P2) resulted in the loss of primary cilia and the rapid formation of kidney cysts; however, kidney-specific inactivation of *Kif3a*

in adult mice caused no histological abnormalities up to 4 weeks after tamoxifen administration, despite loss of primary cilia (Patel *et al.* 2008). Similar results have been found in *Pkd1* mouse models. Lantinga-van Leeuwen *et al.* (2007) found that timing of *Pkd1* gene disruption has a major effect on the severity of cyst development with adult mice showing a mild cystic phenotype one month after tamoxifen-induced disruption of the *Pkd1* gene, compared to rapid and massive cyst formation observed in newborn mice. More recently, Takakura *et al.* (2008) showed that inactivation of *Pkd1* in one week old developing kidneys led to rapid, widespread cyst formation, however, when *Pkd1* was inactivated in 5 week old mice, only focal and slow progression of PKD was observed. These studies suggest that the formation of kidney cysts is dependent on elevations in the basal rate of cell proliferation in renal tubules (Patel *et al.* 2008). Cell proliferation is markedly decreased in the adult kidney following the intense proliferative phase observed during kidney development in newborn mice. Patel *et al.* (2008) found that in newborn mice, in which inactivation of *Kif3a* produced multiple kidney cysts, 0.99% of the renal tubule epithelial cells were undergoing mitosis, whereas in adult mice that did not develop kidney cysts, only 0.06% of the cells were undergoing mitosis. Additional evidence supporting the role of cell proliferation as a prerequisite to cyst formation has been shown in *Kif3a* and *Pkd1* knockout mice following acute kidney injury. Renal regeneration following ischaemic/reperfusion injury (IRI) (caused by clamping the left renal pedicle followed by release of the clamp) is primarily mediated by proliferation of surviving tubular epithelial cells. Patel *et al.* (2008) and Takakura *et al.* (2009) found that following renal IRI, *Kif3a* mutant mice and *Pkd1* mutant mice respectively, developed cysts in the injured kidney whilst no cyst formation was observed in the uninjured contralateral kidney. These results indicate that renal injury and/or tubular regeneration trigger cystogenesis in adult *Kif3a* and *Pkd1* mutant mice and support the hypothesis that cell proliferation stimulates cyst formation (Patel *et al.* 2008).

Following acute kidney injury, the surviving renal tubular cells transiently lose epithelial characteristics, similar to that seen in epithelial cells lining renal cysts (Patel *et al.* 2008). However, unlike the injured kidney where re-establishment of the differentiated epithelial state marks recovery, cystic kidney epithelial cells remain persistently dedifferentiated (Patel *et al.* 2008). Based on these observations, it is possible that progression of cystic disease may result from failure to switch off the normal renal injury induced repair programme due to failure of complete recovery after kidney injury (Takakura *et al.* 2009). Instead, they continue to proliferate, resulting in cyst formation. This theory may explain the focal nature of cyst formation in patients with TSC and ADPKD, and individual differences in exposure to factors that cause subclinical kidney injury and tubular regeneration may contribute to the variability in cyst formation between patients.

7.2.1.2 Apoptosis defects may lead to unopposed misoriented renal tubule epithelial cell divisions

Renal tubule epithelial cells with the potential to divide in an aberrant mitotic orientation which have lain in a quiescent state since completion of renal development, may begin to undergo mitosis again as a consequence of renal injury induced cellular proliferation. However, as in the developing tubule, these misoriented cells may undergo apoptosis and be sloughed off by tubular fluid flow (Frisch and Ruoslahti 1997). We propose that somatic mutations or dysregulation of apoptotic genes in the adult kidney, such as those in the BCL2 family of genes, may cause defective apoptosis, thus allowing misoriented mitotic division to continue unopposed. Indeed, *bcl-2* is known to enhance lymphoid cell survival by interfering with apoptotic cell death (Kamada *et al.* 1995). Perhaps upregulation of this gene may prolong survival of misoriented dividing renal tubule epithelial cells. Other members of the BCL2 family are pro-apoptotic, such as Bax, a Bcl2-like protein that binds to and antagonises the protective effect of Bcl2, rendering cells more susceptible to death (Ortiz *et al.* 2000). Inactivating mutations in this gene may render misoriented dividing cells immune to apoptosis. Studies to elucidate the expression levels of the BCL2 proteins, and other apoptotic

proteins, in early and late stages of TSC and ADPKD will provide vital insight into the role of apoptosis in the early stages of cyst formation.

In conclusion, results from recent studies suggest that in humans with ADPKD, subclinical injury may be an important factor determining disease progression in adults. Renal injury is known to effect fluid flow rate through renal tubules and can often lead to cessation of fluid flow (Weimbs 2007). This may result in the reduction of sloughing off of misoriented dividing renal tubule epithelial cells. We propose that cellular proliferation and aberrant fluid flow caused by renal injury, in combination with defective apoptosis, lead to unopposed misoriented cell division in epithelial cells with defective A/B polarity (as observed in our *Tsc1*$^{+/-}$, *Tsc2*$^{+/-}$ and *Pkd1*$^{+/-}$ mice). This combination of events may then lead to tubular dilation and subsequent formation of cysts in both TSC and ADPKD. Preventing kidney injury and targeting the developmental pathways reactivated in kidneys undergoing repair represent important areas of possible intervention in cystic disease.

7.2.2 Renal cystogenesis as a consequence of somatic mutation and activation of the mTOR pathway

Renal cyst formation in TSC may also occur by a second mechanism (somatic hit/mTOR activation route in Figure 7.3) involving a second hit in *TSC1* or *TSC2* and subsequent activation of the mTOR pathway. We have previously shown that somatic *Tsc1* mutations and mTOR activation are common in advanced lesions from *Tsc1*$^{+/-}$ mice (Wilson *et al.* 2006), suggesting that activation of the mTOR pathway may occur after somatic inactivation of the wild-type *Tsc1* or *Tsc2* allele. Since we did find a small proportion of cysts with somatic *Tsc1* mutations and some with mTOR activation, we propose that a proportion of cysts in *Tsc1*$^{+/-}$ and *Tsc2*$^{+/-}$ mice form through somatic inactivation of *Tsc1* or *Tsc2*, causing activation of the mTOR pathway and subsequent mTOR dependent proliferation leading to renal tubule dilation and eventual formation of cysts. These mTOR positive cysts then advance through to cystadenomas and RCCs.

Interestingly, some cysts which may have formed through the defective A/B polarity/PCP route could possibly also progress to cystadenomas and RCCs. We occasionally observed cysts with a single pS6 positive papillae projection in *Tsc1*$^{+/-}$ and *Tsc2*$^{+/-}$ mice (Figure 7.3). We propose that these cysts have arisen through defective polarity and have eventually acquired a second hit in *Tsc1* or *Tsc2* in a single cell of the cystic epithelium, leading to mTOR activation and subsequent formation of a papillae projection. This cyst may then progress through to a full cystadenoma and eventually RCC.

Much work is needed to validate the model illustrated in Figure 7.3; however, it does serve to explain many inconsistencies from previous studies, such as why is cyst formation focal? Why is there a delay between aberrant mitotic orientation during renal development and cyst formation in adulthood? Why are second hits not found in all cysts? Why is mTOR not active in all cysts? Further studies are therefore warranted to unravel the exact relationship between hamartin, tuberin and PC1, and their role in cell polarity and cystogenesis. Once more is known about this complex pathway, potential new therapeutic targets could come to light for the treatment and perhaps prevention of TSC and PKD.

7.3 The complex relationship between primary cilia and canonical and noncanonical Wnt signalling

The precise relationship between primary cilia and Wnt signalling remains unclear despite recent research. Defects in primary cilia structure and/or function have been shown to affect Wnt signalling and, conversely, Wnt pathway proteins facilitate cilia formation (Figures 7.4 and 7.5). As previously discussed in chapter 1 (section 1.3.5.2), some of the earliest indications that primary cilia may be involved in PCP signalling came from studies on the nephronophthisis type II gene *inversin* (Simons *et al.* 2008). The authors found that inversin targets cytoplasmic Dsh (essential for canonical Wnt signalling) for degradation indicating that this ciliary protein may negatively regulate the canonical Wnt pathway while promoting PCP signalling (Figure 7.4). Data has now emerged showing that nephrocystin-3

(NPHP3, encoded by *NPHP3*), also localised to the primary cilium/basal body, directly interacts with inversin and can inhibit canonical Wnt signalling similar to inversin (Bergmann *et al.* 2008) (Figure 7.4). Work in *X. laevis* has revealed that NPHP3 deficiency leads to convergent extension defects suggesting a role for this protein in PCP pathway activation (Bergmann *et al.* 2008). Taken together, these results indicate a similar role for both inversin and NPHP3 in the control of the switch between canonical and noncanonical Wnt signalling (Bergmann *et al.* 2008).

7.3.1 Primary cilia defects affect PCP signalling

Ift88, a component of the IFT complex, is essential for normal ciliogenesis in *Chlamydomonas* and mice (Qin *et al.* 2001, Pazour *et al.* 2000). Studies in mice have revealed loss of *Ift88* results in stereociliary bundle misrotations and a genetic interaction with the core PCP gene *Vangl2* was suggested in compound *Ift88* and *Vangl2* mutant mice during PCP regulation in the organ of Corti (Jones *et al.* 2007) (Figure 7.4). To determine whether the requirement for *Ift88* is dependent on cilia, and to support a role for cilia in PCP regulation, Jones *et al.* examined a *Kif3a* ciliary mouse mutant. These mice displayed similar defective PCP phenotypes to those observed in *Ift88* mutant mice, suggesting a general requirement for the ciliary axoneme and/or basal body in the regulation of bundle orientation in the organ of Corti (Jones *et al.* 2007).

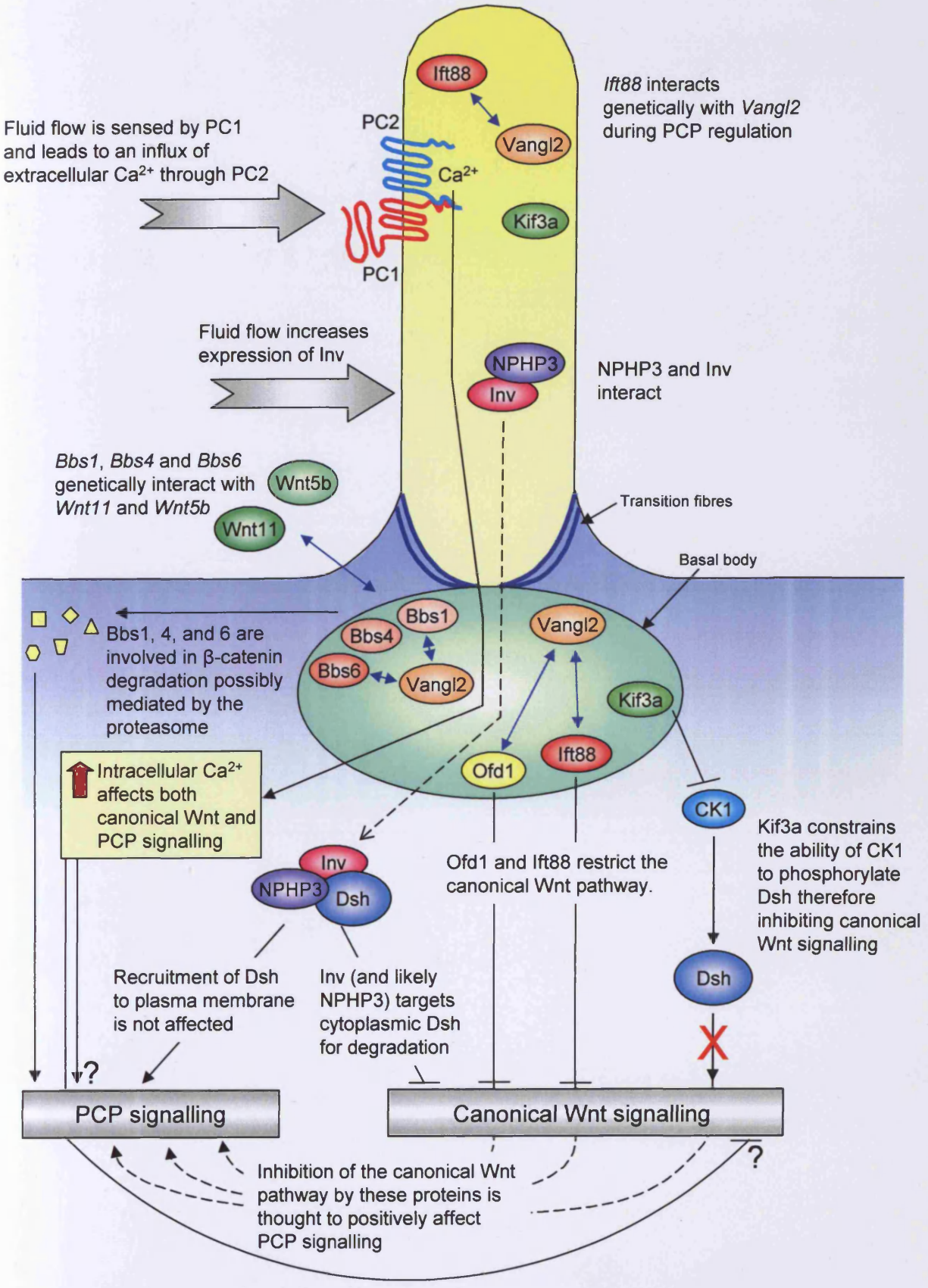

Figure 7.4 The potential regulation of PCP by ciliary proteins and the putative role of PC1 and PC2.

Primary cilia are also required for the maintenance of PCP in the mammalian kidney. Patel *et al.* (2008) found misoriented mitotic spindles in dividing pre-cystic renal tubule epithelial cells from *Kif3a* mutant mouse kidneys. This study indicates that primary cilia are required for the maintenance of PCP in the mammalian kidney and the loss of cilia produces aberrant PCP prior to cyst formation (Patel *et al.* 2008). A possible mechanism whereby Kif3a could regulate PCP may involve phosphorylation of Dsh. By disrupting ciliogenesis either through culture conditions or mutations in *Kif3a*, *Ift88* or a basal body component (*Ofd1*), Corbit *et al.* (2008) showed that the primary cilium restricts the activity of the canonical Wnt pathway (Figure 7.4). It was found that Kif3a may achieve this by constraining the ability of casein kinase I (CK1) to phosphorylate Dsh with loss of Kif3a resulting in uncontrolled phosphorylation of Dsh by CK1 leading to hyper-responsiveness of the downstream pathway (Corbit *et al.* 2008) (Figure 7.4). The authors state that these findings indicate a critical role for primary cilia in the Wnt pathway by restricting the magnitude of the canonical response (Corbit *et al.* 2008).

7.3.1.1 Ciliary localised cystic kidney disease proteins and PCP

Substantial evidence exists for the role of primary cilia in PKD cystogenesis (chapter 1, section 1.3.4) and now a link between some cystic kidney diseases and PCP is beginning to emerge. We found abnormalities in renal tubule primary cilia length and mitotic orientations in our *Pkd1*$^{+/-}$ mice; however, the link between these two phenotypes is unclear, particularly which is a cause and which is a consequence. Studies in other renal cystic diseases indicate that defects in PCP may occur as a consequence of aberrant ciliogenesis.

BBS is a pleiotropic disorder characterised by obesity, age-related retinal dystrophy, polydactyly, reproductive tract abnormalities, cognitive impairment and renal cystic disease (Ross *et al.* 2005). To date, mutations in 12 genes have been identified; *BBS1*, *BBS2*, *BBS3* (also called *ARL6*), *BBS4*, *BBS5*, *BBS6* (also called *MKKS*), *BBS7*, *BBS8* (also called *TTC8*), *BBS9* (also called *B1*), *BBS10*, *BBS11* (also called *TRIM32*) and *BBS12* (Tobin and

Beales 2007). So far, BBS1-8 have been localised to the primary cilium/basal body, suggesting that the BBS phenotype is due to a defect in the assembly or function of cilia or basal bodies (Tobin and Beales 2007). Ross *et al.* (2005) showed that *Bbs1*, *Bbs4* and *Bbs6* null mice display anterior neural tube and stereociliary bundle orientation defects, with mice heterozygous for both *Vangl2* and *Bbs1* or *Bbs6* displaying more severe PCP defects compared to single heterozygote littermates suggesting a genetic interaction between the *Bbs* genes and *Vangl2* (Ross *et al.* 2005). A tempting functional link between the Bbs proteins and Vangl2 was suggested when Vangl2 showed strong expression around the base of the cilium (Ross *et al.* 2005). Recently Gerdes *et al.* (2007) found that *Bbs1*, *Bbs4* and *Bbs6* genetically interact with Wnt genes involved in non-canonical Wnt signalling: *Wnt11* and *Wnt5b*, with suppression of *Bbs1*, *Bbs4* and *Bbs6* resulting in stabilisation of β-catenin with concomitant upregulation of TCF-dependent transcription (Figure 7.4). This was found to be dependent upon the cilium and IFT as confirmed by suppression of KIF3A. The observation of excessive β-catenin, primarily in the cytoplasm, suggested to Gerdes *et al.* that deficiencies existed in β-catenin clearance. Indeed suppression of *BBS4* was found to lead to defective proteasomal targeting and degradation of β-catenin. The proteasome is known to be enriched in the pericentriolar region surrounding centrioles (and therefore the basal body) leading the authors to speculate that the transmission of PCP or other Wnt signals from the cilium is likely to be interpreted at the pericentriolar region which then dictates a range of decisions mediated by the pericentriolar material, including proteasomal degradation and phosphorylation and dephosphorylation events (Gerdes *et al.* 2007).

Similar to the BBS proteins, OFD1, the protein involved in oral-facial-digital type I (OFD1) syndrome, has been localised to the basal body (Ferrante *et al.* 2009). OFD1 is a male-lethal X-linked dominant developmental disorder characterised by malformations of the face, oral cavity and digits, and, in 15% of cases, polycystic kidneys. Recent studies in zebrafish have revealed a role for Ofd1 in convergent extension, a conclusion supported by the finding that Ofd1 downregulation enhanced the phenotype of

embryos that were also disrupted for *Wnt11* or *Vangl2*, two important PCP proteins (Ferrante *et al.* 2009). The authors suggest that as for inversin, Ofd1 might influence the switch from the canonical Wnt pathway to the PCP pathway possibly as an indirect result of a requirement for Ofd1 in normal ciliary structure and function or a direct interaction with Wnt signalling components (Ferrante *et al.* 2009). Indeed, recent work by Corbit *et al.* (2008) has shown that *Ofd1* null mouse embryonic stem cells lack cilia and are hyper-responsive to Wnt ligand resulting in exaggerated β-catenin signalling (Figure 7.4).

It appears from these studies that much of the communication between ciliary localised proteins and PCP signalling occurs via the basal body. Defective proteasomal targeting and degradation of β-catenin can lead to PCP defects, thus implicating the pericentriolar region surrounding centrioles in the transmission of PCP and other Wnt signals from the cilium leading to a range of cellular effects (Gerdes *et al.* 2007). The indication that the basal body may be the key organelle linking ciliary cues with PCP signalling is perhaps unsurprising considering the basal body, in combination with the transition zone, is thought to function as a filter for the cilium, regulating the molecules that can pass into or out of the cilium (Bisgrove and Yost 2006). Perhaps insufficient signals from a defective primary cilium could be intercepted at the basal body and subsequently passed onto proteins involved in Wnt signalling such as Vangl2 and Dsh leading to aberrant PCP. It is tempting to speculate that a lack of PC1 (due to mutations in *PKD1*) in the ciliary axoneme could lead to decreased levels of Ca^{2+} reaching the basal body which could therefore lead to inadequate signals to the PCP pathway, thus resulting in the polarity defects we observed in our mice (Figure 7.4). Ca^{2+} release has been shown to influence PCP signalling and plays an important role in both canonical Wnt and PCP signalling (Slusarski and Pelegri 2007). As previously mentioned, lengthening of the primary cilium, as seen in pre-cystic renal tubule epithelial cells from *Pkd1*$^{+/-}$ mice, could be the cells attempt in compensating for insufficient Ca^{2+} signalling, however this rescue response is inadequate and cannot correct the defective signalling thus leading to aberrant mitotic orientations due to defective PCP signalling.

The studies discussed above have led us to speculate that aberrant mitotic orientation in *Pkd1*$^{+/-}$ mice may occur as a consequence of insufficient extracellular Ca^{2+} entry into the cell with subsequent compensatory ciliary lengthening. Evidence also exists for the role of PCP influencing ciliogenesis. Certain PCP proteins have been localised to the primary cilium. As previously mentioned, Vangl2, a core PCP protein, has been observed in the base of the cilium in mouse IMCD3 kidney epithelial cells (Ross *et al.* 2005) (Figure 7.5). One of the key "upstream" PCP proteins, Fat4, has been localised to the primary cilium in MDCK cells (Saburi *et al.* 2008) (Figure 7.5). It is unclear if these proteins are involved in maintenance of ciliary structure as no alterations in cilia number or size have been found in *Fat4*$^{-/-}$ mouse kidneys (Saburi *et al.* 2008). Research is lacking in the role of Vangl2 and Fat4 in IFT and other ciliary functions and could provide exciting insights into the relationship between PCP signalling and cilia functions.

7.3.2 Regulation of ciliogenesis by PCP proteins

Polarity defects were evident in our *Tsc1*$^{+/-}$ and *Tsc2*$^{+/-}$ mice as demonstrated by the misorientation of dividing renal tubule epithelial cells. These aberrant divisions appeared to be occurring perpendicular to the plane of the epithelium, suggesting defects in A/B polarity. Indeed, tuberin has been found to interact with PATJ (Massey-Harroche *et al.* 2007) a scaffold member of the Crumbs complex which also includes Crumbs (CRB) and protein associated with Lin seven 1 (PALS1). Interestingly, an isoform of CRB3 (CRB3-CLPI) has been localised to the primary cilium and knockdown of CRB3-CLPI leads to loss of cilia in MDCK cells (Fan *et al.* 2007), providing a link between A/B polarity and ciliogenesis (Figure 7.5). A functional link between dPatJ, aPKC and Fz1 has also been demonstrated with subsequent inhibition of Fz1 and PCP signalling defects (Djiane *et al.* 2005). We proposed that the tuberin/hamartin complex functions in this model through its interaction with PATJ and therefore mutations affecting hamartin or tuberin could potentially lead to defective PCP signalling (Figure 7.5). Recent research has in fact shown that knockdown of various PCP genes can cause ciliogenesis defects.

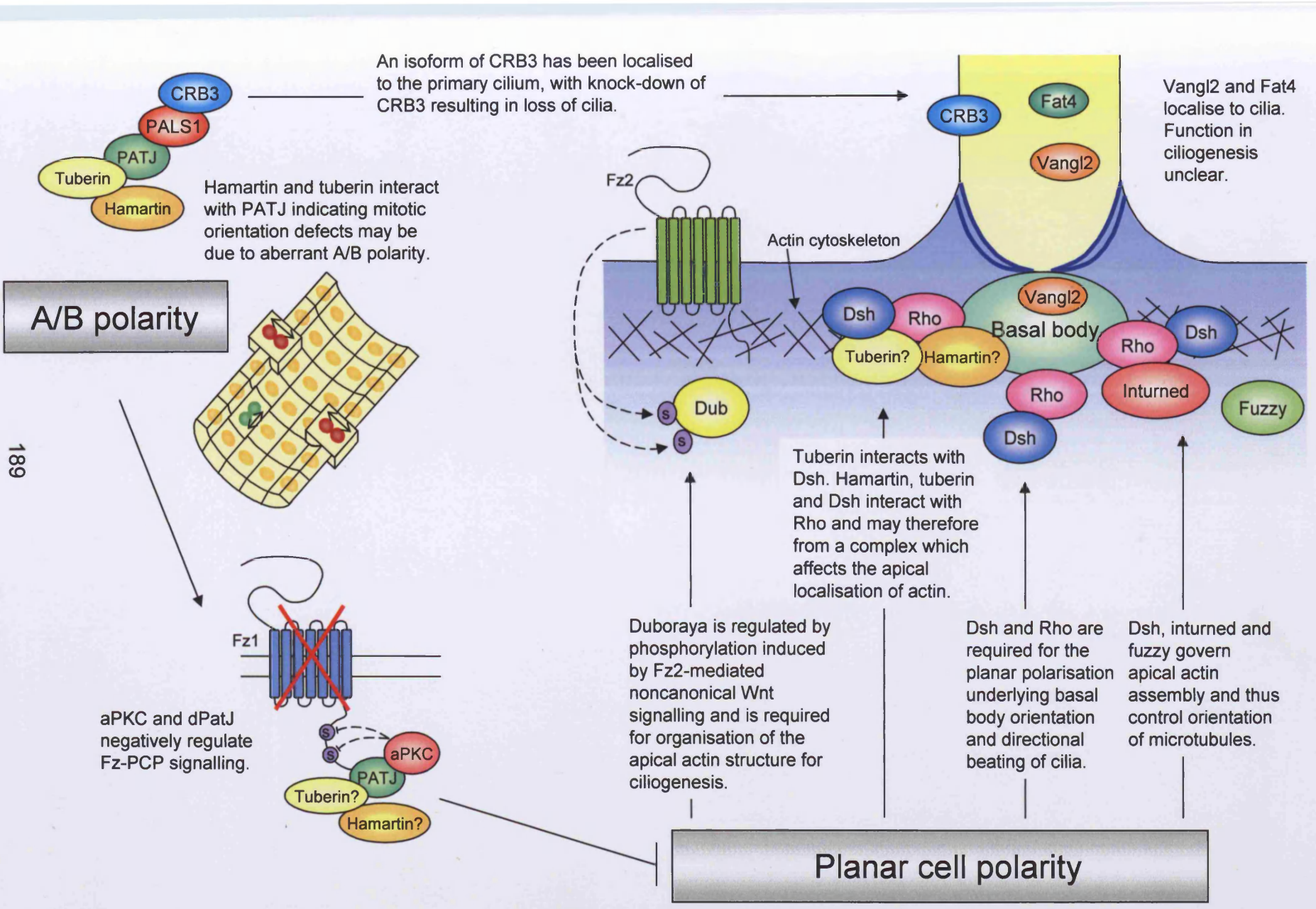

Figure 7.5 The potential regulation of ciliogenesis by A/B polarity and PCP, and the putative roles of hamartin and tuberin.

The PCP effector proteins inturned and fuzzy have been shown to be necessary for ciliogenesis in *X. laevis* embryos (Park *et al.* 2006). Examination of *inturned* and *fuzzy X. laevis* morphants (embryos injected with inturned and fuzzy morpholinos respectively) revealed that defective ciliogenesis was due to a lack of organisation of microtubules into apically projecting cilia (Park *et al.* 2006). Instead, a dense mesh of microtubules was observed parallel to and below the apical cell surface in morphants. The spatial ordering of elongating ciliary microtubules is determined by the ciliary basal apparatus whose orientation and position is controlled by the actin cytoskeleton (Park *et al.* 2006). In *inturned* and *fuzzy* morphants, the apical actin meshwork of ciliated epidermal cells is less dense than in controls suggesting that inturned and fuzzy control ciliogenesis by governing the organisation of the apical actin cytoskeleton in ciliated cells, which in turn is required for the orientation of elongating ciliary microtubules (Park *et al.* 2006) (Figure 7.5). These defects in the actin cytoskeleton were further investigated by Park *et al.* (2008) using the *X. laevis* mucociliary epithelium. The ciliated cells of mucuciliary epithelia are covered in dozens of large cilia which beat directionally to clear mucus away. Knockdown of Dsh proteins (Dsh1, Dsh2 and Dsh3 using morpholinos) resulted in ciliogenesis defects, mislocalisation of microtubules and a failure to accumulate apically localised actin, resulting in the inability of basal bodies to reach the apical surface. The authors therefore suggest that the ciliogenesis defects in Dsh morphants (and presumably inturned and fuzzy morphants) stem from a failure of basal body docking rather than from a failure of cilia assembly (Park *et al.* 2008). Dsh, together with inturned was also found to mediate Rho activation and together these proteins governed apical docking (Figure 7.5). Once docked, basal bodies were found to require Dsh and Rho for the planar polarisation underlying basal body orientation and directional beating of cilia (Park *et al.* 2008).

Actin organisation and ciliogenesis has also been linked to a protein called duboraya (dub) which is regulated by Frizzled-2 (Fz2)-mediated phosphorylation events (Oishi *et al.* 2006). Dub is encoded by the zebrafish gene *duboraya* (*dub*) and is similar to mammalian CapZIP, a putative

phosphorylation-dependent cytoskeletal regulatory molecule (Oishi *et al.* 2006). Zebrafish *dub* morphants were found to have fewer and shorter primary cilia present in both the Kupffer's vesicle (functions as an embryonic organ of asymmetry equivalent to the mammalian ventral node) and renal primary cilia. Convergent extension defects were also present indicating that dub function may depend on PCP signalling. In fact, dub was found to functionally interact with Fz2, a protein involved in PCP signalling, and authors proposed a model in which dub phosphorylation, induced by Fz2-mediated PCP signalling, regulates cilia formation and left-right patterning. Similar to *inturned*, *fuzzy* and *Dsh* morphants, actin assembly at the apical surface of Kupffer's vesicle cells and renal epithelial cells was found to be disorganised in dub morphants, suggesting that dub regulates primary cilia formation by organising the apical actin structure (Figure 7.5). These findings in *inturned*, *fuzzy*, *Dsh* and *dub* morphant embryos highlight the role PCP signalling plays in ciliogenesis, a role that is conveyed through the actin cytoskeleton.

We found that primary cilia from pre-cystic renal tubule epithelial cells in *Tsc1*$^{+/-}$ and *Tsc2*$^{+/-}$ mouse kidneys were significantly shorter than those in wild-type littermates. This finding is similar, although not to the same severity, to those in PCP morphant embryos as described above. Interestingly, both hamartin and tuberin have been shown to interact with Rho (Lamb *et al.* 2000, Astrinidis *et al.* 2002, Goncharova *et al.* 2004), a known regulator of the actin cytoskeleton, which is required for the apical localisation of actin and subsequent successful ciliogenesis (in combination with Dsh and inturned as described above). Hamartin is localised to the basal body and has been found to activate Rho (similar to Dsh) and regulate focal adhesion and stress fibre formation via an interaction with the ezrin-radixin-moesin family of cytoskeletal proteins (Lamb *et al.* 2000). The interaction between tuberin and Rho remains unclear with different groups suggesting that it inhibits and also activates Rho (Astrinidis *et al.* 2002, Goncharova *et al.* 2004). Interestingly, tuberin has been found to associate with Dsh (Mak *et al.* 2005), suggesting that perhaps tuberin, hamartin, Rho and Dsh may form a complex involved in successful localisation of the actin cytoskeleton to the apical cell surface with subsequent

basal body docking (Figure 7.5). The exact role of hamartin and tuberin in the apical localisation of actin and its subsequent effects on ciliogenesis remains to be examined, but could potentially explain the length defects observed in *Tsc1*$^{+/-}$ and *Tsc2*$^{+/-}$ pre-cystic renal tubule epithelial cell primary cilia.

In conclusion, our results highlight a novel role for hamartin, tuberin and PC1 in renal tubule epithelial cell polarity. The precise mechanism of this role remains unclear, as does the interaction between primary cilia and PCP. It is of key importance that A/B and/or PCP defects are undoubtedly some of the earliest pathogenic mechanisms in disease initiation. Further research into this area will no doubt reveal other diseases with similar pathogenic mechanisms, and, hopefully soon, potential therapeutic targets will provide strategies to prevent disease initiation.

Publications resulting from this work

Bonnet, C. S., Aldred, M., von Ruhland, C., Harris, R., Sandford, R. and Cheadle, J. P. (2009) Defects in cell polarity underlie TSC and ADPKD-associated cystogenesis. *Hum Mol Genet.*, Mar 25. [Epub ahead of print]

Wilson, C., Bonnet, C., Guy, C., Idziaszczyk, S., Colley, J., Humphreys, V., Maynard, J., Sampson, J. R. and Cheadle, J. P. (2006) *Tsc1* haploinsufficiency without mammalian target of rapamycin activation is sufficient for renal cyst formation in *Tsc1*$^{+/-}$ mice. *Cancer Res.*, 66: 7934-7938.

References

Ahrabi, A. K., Terryn, S., Valenti, G., Caron, N., Serradeil-Le Gal, C., Raufaste, D., Nielsen, S., Horie, S., Verbavatz, J. M. and Devuyst, O. (2007) *PKD1* haploinsufficiency causes a syndrome of inappropriate antidiuresis in mice. *J Am Soc Nephrol.*, 18: 1740-1753.

Aicher, L. D., Campbell, J. S. and Yeung, R. S. (2001) Tuberin phosphorylation regulates its interaction with hamartin. Two proteins involved in tuberous sclerosis. *J Biol Chem.*, 276: 21017-21021.

Alberici, P., Jagmohan-Changur, S., De Pater, E., Van Der Valk, M., Smits, R., Hohenstein, P. and Fodde, R. (2006) *Smad4* haploinsufficiency in mouse models for intestinal cancer. *Oncogene*, 25: 1841-1851.

Al-Saleem, T., Wessner, L. L., Scheithauer, B. W., Patterson, K., Roach, E. S., Dreyer, S. J., Fujikawa, K., Bjornsson, J., Bernstein, J. and Henske, E. P. (1998) Malignant tumours of the kidney, brain and soft tissues in children and young adults with the tuberous sclerosis complex. *Cancer*, 83: 2208-2216.

Anyatonwu, G. I. and Ehrlich, B. E. (2005) Organic cation permeation through the channel formed by polycystin-2. *J Biol Chem.*, 280: 29488-29493.

Ariza, M., Alvarez, V., Marín, R., Aguado, S., López-Larrea, C., Alvarez, J., Menéndez, M. J. and Coto, E. (1997) A family with a milder form of adult dominant polycystic kidney disease not linked to the *PKD1* (16p) or *PKD2* (4q) genes. *J Med Genet.*, 34: 587-589.

Astrinidis, A., Cash, T. P., Hunter, D. S., Walker, C. L., Chernoff, J., and Henske, E. P. (2002) Tuberin, the tuberous sclerosis complex 2 tumor suppressor gene product, regulates Rho activation, cell adhesion and migration. *Oncogene.*, 21: 8470-8476.

Astrinidis, A., Senapedis, W., Coleman, T. R. and Henske, E. P. (2003) Cell cycle-regulated phosphorylation of hamartin, the product of the tuberous sclerosis complex 1 gene, by cyclin-dependent kinase 1/cyclin B. *J Biol Chem.*, 278: 51372-51379.

Astrinidis, A. and Henske, E. P. (2005) Tuberous sclerosis complex: linking growth and energy signalling pathways with human disease. *Oncogene*, 24: 7475-7481.

Astrinidis, A., Senapedis, W. and Henske, E. P. (2006) Hamartin, the tuberous sclerosis complex 1 gene product, interacts with polo-like kinase 1 in a phosphorylation-dependent manner. *Hum Mol Genet.*, 15: 287-297.

Au, K. S., Rodriguez, J. A., Rodriguez, E. Jr., Dobyns, W. B., Delgado, M. R. and Northrup, H. (1997) Mutations and polymorphisms in the tuberous sclerosis complex gene on chromosome 16. *Hum Mutat.*, 9: 23–29.

Au, K. S., Williams, A. T., Roach, E. S., Batchelor, L., Sparagana, S. P., Delgado, M. R., Wheless, J. W., Baumgartner, J. E., Roa, B. B., Wilson, C. M., *et al.* (2007) Genotype/phenotype correlation in 325 individuals referred for a diagnosis of tuberous sclerosis complex in the United States. *Genet Med.*, 9: 88-100.

Avni, F. E., Guissard, G., Hall, M., Janssen, F., DeMaertelaer, V. and Rypens, F. (2002) Hereditary polycystic kidney diseases in children: changing sonographic patterns through childhood. *Pediatr Radiol.*, 32: 169-174.

Bacallao, R. L. and McNeill, H. (2009) Cystic kidney diseases and planar cell polarity signaling. *Clin Genet.*, 75: 107-117.

Barr, M. M., DeModena, J., Braun, D., Nguyen, C. Q., Hall, D. H. and Sternberg, P. W. (2001) The Caenorhabditis elegans autosomal dominant polycystic kidney disease gene homologs lov-1 and pkd-2 act in the same pathway. *Curr Biol.* 11: 1341-1346.

Bateman, A. and Sandford, R. (1999) The PLAT domain: a new piece in the PKD1 puzzle. *Curr. Biol.* 9: R588–R590.

Bénit, P., Bonnefont, J. P., Kara Mostefa, A., Francannet, C., Munnich, A. and Ray, P. F. (2001) Denaturing high-performance liquid chromatography (DHPLC)-based prenatal diagnosis for tuberous sclerosis. *Prenat Diagn.*, 21: 279-283.

Benvenuto, G., Li, S., Brown, S. J., Braverman, R., Vass, W. C., Cheadle, J. P., Halley, D. J., Sampson, J. R., Wienecke, R. and DeClue, J. E. (2000) The tuberous sclerosis-1 (*TSC1*) gene product hamartin suppresses cell growth and augments the expression of the TSC2 product tuberin by inhibiting its ubiquitination. *Oncogene*, 19: 6306-6316.

Berg, H. (1913) Vererbung der tuberösen skerose durch zwei bzw. Drei Generationon. *Z Ges Neurol Psychiatri.*, 19: 528-539.

Bergmann, C., Fliegauf, M., Brüchle, N. O., Frank, V., Olbrich, H., Kirschner, J., Schermer, B., Schmedding, I., Kispert, A., Kränzlin, B., *et al.* (2008) Loss of nephrocystin-3 function can cause embryonic lethality, Meckel-Gruber-like syndrome, situs inversus, and renal-hepatic-pancreatic dysplasia. *Am J Hum Genet.*, 82: 959-970.

Bernstein, J. and Robbins, T. O. (1991) Renal involvement in tuberous sclerosis. *Ann N Y Acad Sci.*, 615: 36-49.

Bisceglia, M., Galliani, C., Carosi, I., Simeone, A. and Ben-Dor, D. (2008) Tuberous Sclerosis Complex With Polycystic Kidney Disease of the Adult Type: The TSC2/ADPKD1 Contiguous Gene Syndrome. *Int J Surg Pathol.*, 16: 375-385.

Bisgrove, B. W. and Yost, H. J. (2006) The roles of cilia in developmental disorders and disease. *Development*, 133: 4131-4143.

Bissler, J. J., McCormack, F. X., Young, L. R., Elwing, J. M., Chuck, G., Leonard, J. M., Schmithorst, V. J., Laor, T., Brody, A. S., Bean, J., *et al.* (2008) Sirolimus for angiomyolipoma in tuberous sclerosis complex or lymphangioleiomyomatosis. *N Engl J Med.*, 358: 140-151.

Bjornsson, J., Short, M. P., Kwiatkowski, D. J. and Henske, E. P. (1996) Tuberous sclerosis-associated renal cell carcinoma. Clinical, pathological and genetic features. *Am J Pathol.*, 149:1201-1208.

Blacque, O. E., Reardon, M. J., Li, C., McCarthy, J., Mahjoub, M. R., Ansley, S. J., Badano, J. L., Mah, A. K., Beales, P. L., Davidson, W. S., *et al.* (2004) Loss of C. elegans BBS-7 and BBS-8 protein function results in cilia defects and compromised intraflagellar transport. *Genes Dev.*, 18: 1630-1642.

Boucher, C. and Sandford, R. (2004) Autosomal dominant polycystic kidney disease (ADPKD, MIM 173900, *PKD1* and *PKD2* genes, protein products known as polycystin-1 and polycystin-2). *Eur J Hum Genet.*, 12: 347-354.

Boulter, C., Mulroy, S., Webb, S., Fleming, S., Brindle, K. and Sandford, R. (2001) Cardiovascular, skeletal, and renal defects in mice with a targeted disruption of the *Pkd1* gene. *Proc. Natl. Acad. Sci. USA*, 98: 12174-12179.

Bourneville, D. M. (1880) Sclérose tubéreuse des circonvolutions cérébrales: idiotie et épilepsie hémiplégique. *Arch Neurol. (Paris)*, 1: 81-91.

Bowers, A. J. and Boylan, J. F. (2004) Nek8, a NIMA family kinase member, is overexpressed in primary human breast tumors. *Gene*, 328: 135-142.

Brasier, J. L. and Henske, E. P. (1997) Loss of the polycystic kidney disease (*PKD1*) region of chromosome 16p13 in renal cyst cells supports a loss-of-function model for cyst pathogenesis. *J Clin Invest.*, 99: 194-199.

Breysem, L., Nijs, E., Proesmans, W. and Smet, M. H. (2002) Tuberous sclerosis with cystic renal disease and multifocal renal cell carcinoma in a baby girl. *Pediatr Radiol.*, 32:677-680.

Brook-Carter, P. T., Peral, B., Ward, C. J., Thompson, P., Hughes, J., Maheshwar, M. M., Nellist, M., Gamble, V., Harris, P. C. and Sampson, J. R. (1994) Deletion of the *TSC2* and *PKD1* genes associated with severe infantile polycystic kidney disease- a contiguous gene syndrome. *Nat. Genet.*, 8: 328-332.

Cai, S., Everitt, J. I., Kugo, H., Cook, J., Kleymenova, E. and Walker, C. L. (2003) Polycystic kidney disease as a result of loss of the tuberous sclerosis 2 tumor suppressor gene during development. *Am J Pathol.*, 162: 457-468.

Cai, Y., Maeda, Y., Cedzich, A., Torres, V. E., Wu, G., Hayashi, T., Mochizuki, T., Park, J. H., Witzgall, R. and Somlo, S. (1999) Identification and characterization of polycystin-2, the *PKD2* gene product. *J Biol Chem.*, 274: 28557-28565.

Carbonara, C., Longa, L., Grosso, E., Borrone, C., Garre, M., Brisigotti, M. and Migone, N. (1994) 9q34 loss of heterozygosity in a tuberous sclerosis astrocytoma suggests a growth suppressor-like activity also for the *TSC1* gene. *Hum Mol Genet.*, 3: 1829-1832.

Casper, K. A., Donnelly, L. F., Chen, B. and Bissler, J. J. (2002) Tuberous sclerosis complex: renal imaging findings. *Radiology*, 225: 451-456.

Chang, M. Y., Parker, E., Ibrahim, S., Shortland, J. R., Nahas, M. E., Haylor, J. L. and Ong, A. C. M. (2006) Haploinsufficiency of *Pkd2* is associated with increased tubular cell proliferation and interstitial fibrosis in two murine *Pkd2* models. *Nephrol Dial Transplant*, 21: 2078-2084.

Chapman, A. B., Rubinstein, D., Hughes, R., Stears, J. C., Earnest, M. P., Johnson, A. M., Gabow, P. A. and Kaehny, W. D. (1992) Intracranial aneurysms in autosomal dominant polycystic kidney disease. *N Engl J Med.*, 327: 916-920.

Chapman, A. B. (2007) Autosomal dominant polycystic kidney disease: time for a change? *J Am Soc Nephrol.*, 18: 1399-1407.

Chauvet, V., Tian, X., Husson, H., Grimm, D. H., Wang, T., Hiesberger, T., Igarashi, P., Bennett, A. M., Ibraghimov-Beskrovnaya, O., Somlo, S. and Caplan, M. J. (2004) Mechanical stimuli induce cleavage and nuclear translocation of the polycystin-1 C terminus. *J Clin Invest.*, 114: 1433-1443.

Cheadle, J. P., Reeve, M. P., Sampson, J. R. and Kwiatkowski, D. J. (2000) Molecular genetic advances in tuberous sclerosis. *Hum Genet.*, 107: 97-114.

Choi, Y. J., Di Nardo, A., Kramvis, I., Meikle, L., Kwiatkowski, D. J., Sahin, M. and He, X. (2008) Tuberous sclerosis complex proteins control axon formation. *Genes Dev.*, 22: 2485-2495.

Clevers, H. (2006) Wnt/beta-catenin signaling in development and disease. *Cell*, 127: 469-480.

Cook, J. A., Oliver, K., Mueller, R. F. and Sampson, J. (1996) A cross sectional study of renal involvement in tuberous sclerosis. *J Med Genet.*, 33: 480-484.

Corbit, K.C., Shyer, A. E., Dowdle, W. E., Gaulden, J., Singla, V., Chen, M. H., Chuang, P. T. and Reiter, J. F. (2008) Kif3a constrains beta-catenin-dependent Wnt signalling through dual ciliary and non-ciliary mechanisms. *Nat. Cell Biol.*, 10: 70-76.

Dabora, S. L., Jozwiak, S., Franz, D. N., Roberts, P. S., Nieto, A., Chung, J., Choy, Y., Reeve, M. P., Thiele, E., Egelhoff, J. C., *et al.* (2001) Mutational analysis in a cohort of 224 tuberous sclerosis patients indicates increased severity of *TSC2*, compared with *TSC1*, disease in multiple organs. *Am J Hum Genet.*, 68: 64-80.

Dalgaard, O. Z. (1957) Bilateral polycystic disease of the kidneys; a follow-up of two hundred and eighty-four patients and their families. *Acta Med Scand Suppl.*, 328: 1-255.

Daoust, M. C., Reynolds, D. M., Bichet, D. G. and Somlo, S. (1995) Evidence for a third genetic locus for autosomal dominant polycystic kidney disease. *Genomics*, 25: 733-736.

Davenport, J. R. and Yoder, B. K. (2005) An incredible decade for the primary cilium: a look at a once-forgotten organelle. *Am J Physiol Renal Physiol.*, 289: F1159-F1169.

Davies, D. M., Johnson, S. R., Tattersfield, A. E., Kingswood, J. C., Cox, J. A., McCartney, D. L., Doyle, T., Elmslie, F., Saggar, A., de Vries, P. J. and Sampson, J. R. (2008) Sirolimus therapy in tuberous sclerosis or sporadic lymphangioleiomyomatosis. *N Engl J Med.*, 358: 200-203.

Dawson, J. (1954) Pulmonary tuberous sclerosis and its relation to other forms of the disease. *Q J Med.*, 23: 113-145.

de Almeida, S., de Almeida, E., Peters, D., Pinto, J. R., Távora, I., Lavinha, J., Breuning, M. and Prata, M. M. (1995) Autosomal dominant polycystic kidney disease: evidence for the existence of a third locus in a Portuguese family. *Hum Genet.*, 96: 83-88.

Delmas, P., Nomura, H., Li, X., Lakkis, M., Luo, Y., Segal, Y., Fernández-Fernández, J. M., Harris, P., Frischauf, A. M., Brown, D. A. and Zhou, J. (2002) Constitutive activation of G-proteins by polycystin-1 is antagonized by polycystin-2. *J Biol Chem.*, 277: 11276-11283.

Delmas, P., Padilla, F., Osorio, N., Coste, B., Raoux, M. and Crest, M. (2004) Polycystins, calcium signalling, and human diseases. *Biochem Biophys Res Commun.*, 322: 1374-1383.

Devlin, L. A., Shepherd, C. H., Crawford, H. and Morrison, P. J. (2006) Tuberous sclerosis complex: clinical features, diagnosis, and prevalence within Northern Ireland. *Dev Med Child Neurol.*, 48: 495-499.

Di Cristofano, A., Pesce, B., Cordon-Cardo, C. and Pandolfi, P. P. (1998) Pten is essential for embryonic development and tumour suppression. *Nat Genet.*, 19: 348-355.

Djiane, A., Yogev, S. and Mlodzik, M. (2005) The apical determinants aPKC and dPatj regulate Frizzled-dependent planar cell polarity in the Drosophila eye. *Cell*, 121: 621-631.

Ecder, T. and Schrier, R. W. (2001) Hypertension in autosomal-dominant polycystic kidney disease: early occurrence and unique aspects. *J Am Soc Nephrol.*, 12: 194-200.

Eisenmann, D. M. (2005) Wnt signaling. *WormBook.* Jun 25: 1-17.

Eker, R. (1954) Familial renal adenomas in Wistar rats. *Acta Pathol Microbiol Scand.*, 34: 554-562.

Eker, R., Mossige, J., Johannessen, J. V. and Aars, H. (1981) Hereditary renal adenomas and adenocarcinomas in rats. *Diagn Histopathol.*, 4: 99-110.

Eley, L., Yates, L. M. and Goodship, J. A. (2005) Cilia and disease. *Curr Opin Genet Dev.*, 15: 308-314.

Entius, M. M., Keller, J. J., Westerman, A. M., van Rees, B. P., van Velthuysen, M. L., de Goeij, A. F., Wilson, J. H., Giardiello, F. M., Offerhaus, G. J. (2001) Molecular genetic alterations in hamartomatous polyps and carcinomas of patients with Peutz-Jeghers syndrome. *J Clin Pathol.*, 54: 126-131.

Ewalt, D. H., Sheffield, E., Sparagana, S. P., Delgado, M. R. and Roach, E. S. (1998) Renal lesion growth in children with tuberous sclerosis complex. *J Urol.*, 160: 141-145.

Fan, S., Fogg, V., Wang, Q., Chen, X. W., Liu, C. J. and Margolis, B. (2007) A novel Crumbs3 isoform regulates cell division and ciliogenesis via importin beta interactions. *J Cell Biol.*, 178: 387-398.

Fanto, M. and McNeill, H. (2004) Planar polarity from flies to vertebrates. *J Cell Sci.*, 117: 527-533.

Fawcett, D. W. and Porter, K. R. (1954) A study of the fine structure of ciliated epithelia. *J Morphol.*, 94: 221-282.

Ferrante, M. I., Zullo, A., Barra, A., Bimonte, S., Messaddeq, N., Studer, M., Dollé, P. and Franco, B. (2006) Oral-facial-digital type I protein is required for primary cilia formation and left-right axis specification. *Nat Genet.*, 38: 112-117.

Ferrante, M. I., Romio, L., Castro, S., Collins, J. E., Goulding, D. A., Stemple, D. L., Woolf, A. S. and Wilson, S. W. (2009) Convergent extension movements and ciliary function are mediated by *ofd1*, a zebrafish orthologue of the human oral-facial-digital type 1 syndrome gene. *Hum Mol Genet.*, 18: 289-303.

Fick, G. M., Johnson, A. M., Hammond, W. S. and Gabow, P. A. (1995) Causes of death in autosomal dominant polycystic kidney disease. *J Am Soc Nephrol.*, 5: 2048-2056.

Fingar, D. C. and Blenis, J. (2004) Target of rapamycin (TOR): an integrator of nutrient and growth factor signals and coordinator of cell growth and cell cycle progression. *Oncogene*, 23: 3151-3171.

Fischer, E., Legue, E., Doyen, A., Nato, F., Nicolas, J. F., Torres, V., Yaniv, M. and Pontoglio, M. (2006) Defective planar cell polarity in polycystic kidney disease. *Nat Genet.*, 38: 21-23.

Flaherty, L., Bryda, E. C., Collins, D., Rudofsky, U. and Montogomery, J. C. (1995) New mouse model for polycystic kidney disease with both recessive and dominant gene effects. *Kidney Int.*, 47: 552-558.

Fliegauf, M., Benzing, T. and Omran, H. (2007) When cilia go bad: cilia defects and ciliopathies. *Nat Rev Mol Cell Biol.*, 8: 880-893.

Foggensteiner, L., Bevan, A. P., Thomas, R., Coleman, N., Boulter, C., Bradley, J., Ibraghimov-Beskrovnaya, O., Klinger, K. and Sandford, R. (2000) Cellular and subcellular distribution of polycystin-2, the protein product of the PKD2 gene. *J Am Soc Nephrol.*, 11: 814-827.

Franz, D. N., Leonard, J., Tudor, C., Chuck, G., Care, M., Sethuraman, G., Dinopoulos, A., Thomas, G. and Crone, K. R. (2006) Raoamycin causes regression of astrocytomas in tuberous sclerosis complex. *Ann Neurol.*, 59: 490-498.

Frisch, S. M. and Francis, H. (1994) Disruption of epithelial cell-matrix interactions induces apoptosis. *J Cell Biol.*, 124: 619-626.

Frisch, S. M. and Ruoslahti, E. (1997) Integrins and anoikis. *Curr Opin Cell Biol.*, 9: 701-706.

Fry, J. L. Jr., Koch, W. E., Jennette, J. C., McFarland, E., Fried, F. A. and Mandell, J. (1985) A genetically determined murine model of infantile polycystic kidney disease. *J Urol.*, 134: 828-833.

Fryer, A. E., Chalmers, A. H., Connor, J. M., Fraser, I., Povey, S., Yates, A. D., Yates, J. R. and Osborne, J. P. (1987) Evidence that the gene for tuberous sclerosis is on chromosome 9. *Lancet*, 1: 659-661.

Gabow, P. A., Johnson, A. M., Kaehny, W. D., Manco-Johnson, M. L., Duley, I. T. and Everson, G. T. (1990) Risk factors for the development of hepatic cysts in autosomal dominant polycystic kidney disease. *Hepatology*, 11: 1033-1037.

Gabow, P. A. (1993) Autosomal dominant polycystic kidney disease. *N Engl J Med.*, 329: 332-342.

Gao, X. and Pan, D. (2001) TSC1 and TSC2 tumor suppressors antagonize insulin signalling in cell growth. *Genes Dev.*, 15: 1383-1392.

Geng, L., Segal, Y., Peissel, B., Deng, N., Pei, Y., Carone, F., Rennke, H. G., Glücksmann-Kuis, A. M., Schneider, M. C., Ericsson, M. *et al.* (1996) Identification and localization of polycystin, the *PKD1* gene product. *J Clin Invest.*, 98: 2674-2682.

Geng, L., Segal, Y., Pavlova, A., Barros, E. J., Lohning, C., Lu, W., Nigam, S. K., Frischauf, A. M., Reeders, S. T. and Zhou, J. (1997) Distribution and developmentally regulated expression of murine polycystin. *Am J Physiol.*, 272: F451-F459.

Geng, L., Okuhara, D., Yu, Z., Tian, X., Cai, Y., Shibazaki, S. and Somlo, S. (2006) Polycystin-2 traffics to cilia independently of polycystin-1 by using an N-terminal RVxP motif. *J Cell Sci.*, 119: 1383-1395.

Gerdes, J. M., Liu, Y., Zaghloul, N. A., Leitch, C. C., Lawson, S. S., Kato, M., Beachy, P. A., Beales, P. L., DeMartino, G. N., Fisher, S., Badano, J. L. and Katsanis, N. (2007) Disruption of the basal body compromises proteasomal function and perturbs intracellular Wnt response. *Nat Genet.*, 39: 1350-1360.

Germino, G. G., Weinstat-Saslow, D., Himmelbauer, H., Gillespie, G. A. J., Somlo, S., Wirth, B., Barton, N., Harris, K. L., Frischauf, A. M. and Reeders, S. T. (1992) The gene for Autosomal dominant polycystic kidney disease lies in a 750-kb CpG-rich region. *Genomics*, 13: 144-151.

Germino, G. G. (2005) Linking cilia to Wnts. *Nat Genet.*, 37: 455-457.

Gilbert, J. R., Kandt, R. S. Lennon, F., Gardner, R. J. M., Roses, A. D. and Pericak-Vance, M. A. (1993) Linkage and cross-over analysis in tuberous sclerosis (TSC). *Am J Hum Genet.*, 53: A1004.

Gingras, A. C., Raught, B., Gygi, S. P., Niedzwiecka, A., Miron, M., Burley, S. K., Polakiewicz, R. D., Wyslouch-Cieszynska, A., Aebersold, R. and Sonenberg, N. (2001) Hierarchical phosphorylation of the translation inhibitor 4E-BP1. *Genes Dev.*, 15: 2852-2864.

Gomez, M. R. (1979) *Tuberous sclerosis*. Raven Press, Ltd., New York.

Gomez, M. R. (1988) *Tuberous sclerosis, Second Edition*. Raven Press, Ltd., New York.

Gomez, M. R., Sampson, J. R. & Whittemore, V. H. (1999) *The Tuberous sclerosis complex*. Oxford University press, Oxford, UK.

Goncharova, E., Goncharov, D., Noonan, D. and Krymskaya, V. P. (2004) TSC2 modulates actin cytoskeleton and focal adhesion through TSC1-binding domain and the Rac1 GTPase. *J Cell Biol.*, 167: 1171-1182.

Goorden, S. M., van Woerden, G. M., van der Weerd, L., Cheadle, J. P. and Elgersma, Y. (2007) Cognitive deficits in *Tsc1+/-* mice in the absence of cerebral lesions and seizures. *Ann Neurol.*, 62: 648-655.

Green, A. J., Smith, M. and Yates, J. (1994) Loss of heterozygosity on chromosome 16p13.3 in hamartomas from tuberous sclerosis patients. *Nature Genet.*, 6: 193-196.

Grimm, D. H., Cai, Y., Chauvet, V., Rajendran, V., Zeltner, R., Geng, L., Avner, E. D., Sweeney, W., Somlo, S. and Caplan, M. J. (2003) Polycystin-1 distribution is modulated by polycystin-2 expression in mammalian cells. *J Biol Chem.*, 278: 36786-36793.

Guay-Woodford, L. M., Muecher, G., Hopkins, S. D., Avner, E. D., Germino, G. G., Guillot, A. P., Herrin, J., Holleman, R., Irons, D. A., Primack, W., *et al.* (1995) The severe perinatal form of autosomal recessive polycystic kidney disease maps to chromosome 6p21.1-p12: implications for genetic counselling. *Am J Hum Genet.*, 56: 1101-1107.

Guay-Woodford, L. M. (2003) Murine models of polycystic kidney disease: molecular and therapeutic insights. *Am J Physiol Renal Physiol.*, 285: F1034-F1049.

Gunther, M. and Penrose, L. S. (1935) The genetics of epiloia. *J Genet.*, 31:413-430.

Guo, N., Hawkins, C. and Nathans, J. (2004) Frizzled6 controls hair patterning in mice. *Proc Natl Acad Sci U S A*, 101: 9277-9281.

Habas, R. and Dawid, I. B. (2005) Dishevelled and Wnt signaling: is the nucleus the final frontier? *J Biol.*, 4: 2. Epub

Haddad, L. A., Smith, N., Bowser, M., Niida, Y., Murthy, V., Gonzalez-Agosti, C. and Ramesh, V. (2002) The TSC1 tumor suppressor hamartin interacts with neurofilament-L and possibly functions as a novel integrator of the neuronal cytoskeleton. *J Biol Chem.*, 277: 44180-44186.

Haimo, L. T. and Rosenbaum, J. L. (1981) Cilia, flagella and microtubules. *J Cell Biol.*, 91: 125s-130s.

Haines, J. L., Short, M. P., Kwiatkowski, D. J., Jewell, A., Andermann, E., Bejjani, B., Yang, C., Guselle, J. F. and Amos, J. A. (1991) Localisation of one gene for tuberous sclerosis within 9q32-9q34, and further evidence for heterogeneity. *Am J Hum Genet.*, 49: 764-772.

Hamada, H., Meno, C., Watanabe, D. and Saijoh, Y. (2002) Establishment of vertebrate left-right asymmetry. *Nat Rev Genet.*, 3: 103-113.

Hanaoka, K., Qian, F., Boletta, A., Bhunia, A. K., Piontek, K., Tsiokas, L., Sukhatme, V. P., Guggino, W. B. and Germino, G. G. (2000) Co-assembly of polycystin-1 and -2 produces unique cation-permeable currents. *Nature*, 408: 990-994.

Harris, P. C., Barton, N. J., Higgs, D. R., Reeders, S. T. and Wilkie, A. O. M. (1990)A long-range restriction map between the α-globin complex and a marker closely linked to the polycystic kidney disease 1 (*PKD1*) locus. *Genomics*, 7: 195-206.

Harris, P. C., Thomas, S., Ratcliffe, P. J., Breuning, M. H., Coto, E. and Lopez-Larrea, C. (1991) Rapid genetic analysis of families with polycystic kidney disease 1 by means of a microsatellite marker. *Lancet*, 338: 1484-1487.

Hartman, T. R., Liu, D., Zilfou, J. T., Robb, V., Morrison, T., Watnick, T. and Henske, E. P. (2009) The tuberous sclerosis proteins regulate formation of the primary cilium via a rapamycin-insensitive and polycystin 1-independent pathway. *Hum Mol Genet.*, 18: 151-163.

Hateboer, N., v Dijk, M. A., Bogdanova, N., Coto, E., Saggar-Malik, A. K., San Millan, J. L., Torra, R., Breuning, M. and Ravine, D. (1999) Comparison of phenotypes of polycystic kidney disease types 1 and 2. European PKD1-PKD2 Study Group. *Lancet*, 353: 103-107.

Hayashi, T., Cunningham, D. and Bermingham-McDonogh, O. (2007) Loss of Fgfr3 leads to excess hair cell development in the mouse organ of Corti. *Dev Dyn.*, 236: 525-533.

Henske, E. P., Scheithauer, B. W., Short, M. P., Wollmann, R., Nahmias, J., Hornigold, N., van Slegtenhorst, M., Welsh, C. T. and Kwiatkowski, D. J. (1996) Allelic loss is frequent in tuberous sclerosis kidney lesions but rare in brain lesions. *Am J Hum Genet.*, 59: 400-406.

Henske, E. P. (2005) Tuberous sclerosis and the kidney: from mesenchyme to epithelium, and beyond. *Pediatr Nephrol.*, 20: 854-857.

Herry, I., Neukirch, C., Debray, M. P., Mignon, F. and Crestani, B. (2007) Dramatic effect of sirolimus on renal angiomyolipomas in a patient with tuberous sclerosis complex. *Eur J Intern Med.*, 18: 76-77.

Hildebrandt, F. and Otto, E. (2005) Cilia and centrosomes: a unifying pathogenic concept for cystic kidney disease? *Nat Rev Genet.*, 6: 928-940.

Hino, O., Klein-Szanto, A. J., Freed, J. J., Testa, J. R., Brown, D. Q., Vilensky, M., Yeung, R. S., Tartof, K. D. and Knudson, A. G. (1993a) Spontaneous and radiation-induced renal tumors in the Eker rat model of dominantly inherited cancer. *Proc Natl Acad Sci U S A*, 90: 327-331.

Hino, O., Mitani, H., Nishizawa, M., Katsuyama, H., Kobayashi, E. and Hirayama, Y. (1993b) A novel renal cell carcinoma susceptibility gene maps on chromosome 10 in the Eker rat. *Jpn J Cancer Res.*, 84: 1106-1109.

Hino, O., Kobayashi, T., Tsuchiya, H., Kikuchi, Y., Kobayashi, E., Mitani, H. and Hirayama, Y. (1994) The predisposing gene of the Eker rat inherited cancer syndrome is tightly linked to the tuberous sclerosis (*TSC2*) gene. *Biochem Biophys Res Commun.*, 203: 1302-1308.

Hodges, A. K., Li, S., Maynard, J., Parry, L., Braverman, R., Cheadle, J. P., DeClue, J. E. and Sampson, J. R. (2001) Pathological mutations in *TSC1* and *TSC2* disrupt the interaction between hamartin and tuberin. *Hum Mol Genet.*, 10: 2899-2905.

Hornigold, N., van Slegtenhorst, M., Nahmias, J., Ekong, R., Rousseaux, S., Hermans, C., Halley, D., Povey, S. and Wolfe, J. (1997) A 1.7-Megabase Sequence-Ready Cosmid Contig Covering the TSC1 Candidate Region in 9q34. *Genomics*, 41: 385-389.

Hou, X., Mrug, M., Yoder, B. K., Lefkowitz, E. J., Kremmidiotis, G., D'Eustachio, P., Beier, D. R. and Guay-Woodford, L. M. (2002) Cystin, a novel cilia-associated protein, is disrupted in the cpk mouse model of polycystic kidney disease. *J Clin Invest.*, 109: 533-540.

Howe, J. R., Roth, S., Ringold, J. C., Summers, R. W., Järvinen, H. J., Sistonen, P., Tomlinson, I. P., Houlston, R. S., Bevan, S., Mitros, F. A., Stone, E. M. and Aaltonen, L. A. (1998) Mutations in the SMAD4/DPC4 gene in juvenile polyposis. *Science*, 280: 1086-1088.

Huan, Y. and van Adelsberg, J. (1999) Polycystin-1, the *PKD1* gene product, is in a complex containing E-cadherin and the catenins. *J Clin Invest.*, 104: 1459-1468.

Huang, J. and Manning, B. D. (2008) The TSC1-TSC2 complex: a molecular switchboard controlling cell growth. *Biochem J.*, 412: 179-190.

Huangfu, D., Liu, A., Rakeman, A. S., Murcia, N. S., Niswander, L. and Anderson, K. V. (2003) Hedgehog signalling in the mouse requires intraflagellar transport proteins. *Nature*, 426: 83-87.

Hughes, J., Ward, C. J., Peral, B., Aspinwall, R., Clark, K., San Millán, J. L., Gamble, V. and Harris, P. C. (1995) The polycystic kidney disease 1 (*PKD1*) gene encodes a novel protein with multiple cell recognition domains. *Nat Genet.*, 10: 151-160.

Ibraghimov-Beskrovnaya, O., Bukanov, N. O., Donohue, L. C., Dackowski, W. R., Klinger, K. W. and Landes, G. M. (2000) Strong homophilic interactions of the Ig-like domains of polycystin-1, the protein product of an autosomal dominant polycystic kidney disease gene, *PKD1. Hum Mol Genet.*, 9: 1641-1649.

Ibraghimov-Beskrovnaya, O. and Bukanov, N. (2008) Polycystic kidney diseases: from molecular discoveries to targeted strategies. *Cell Mol Life Sci.*, 65: 605-619.

Iglesias, C. G., Torres, V. E., Offord, K. P., Holley, K. E., Beard, C. M. and Kurland, L. T. (1983) Epidemiology of adult polycystic kidney disease, Olmsted County, Minnesota: 1935-1980. *Am J Kidney Dis.*, 2: 630-639.

Inoki, K., Li, Y., Zhu, T., Wu, J., and Guan, K.L. (2002) *TSC2* is phosphorylated and inhibited by Akt and suppresses mTOR signalling. *Nat. Cell Biol.*, 4, 648–657.

Inoki, K., Zhu, T. and Guan, K. L. (2003) TSC2 mediates cellular energy response to control cell growth and survival. *Cell*, 115: 577-590.

Inoki, K., Corradetti, M. N. and Guan, K. (2005) Dysregulation of the TSC-mTOR pathway in human disease. *Nature Genet.*, 37: 19-24.

Itoh, K., Brott, B. K., Bae, G. U., Ratcliffe, M. J. and Sokol, S. Y. (2005) Nuclear localization is required for Dishevelled function in Wnt/beta-catenin signaling. *J Biol.*, 4: 3.

Ito, N. and Rubin, G. M. (1999) Gigas, a Drosophila homolog of tuberous sclerosis gene product-2, regulates the cell cycle. *Cell*, 96: 529-539.

Jacinto, E., Loewith, R., Schmidt, A., Lin, S., Rüegg, M. A., Hall, A. and Hall, M. N. (2004) Mammalian TOR complex 2 controls the actin cytoskeleton and is rapamycin insensitive. *Nat Cell Biol.*, 6: 1122-1128.

Jacob, H. J. and Kwitek, A. E. (2002) Rat genetics: attaching physiology and pharmacology to the genome. *Nat Rev Genet.*, 3: 33-42.

Jiang, S. T., Chiou, Y. Y., Wang, E., Lin, H. K., Lin, Y. T., Chi, Y. C., Wang, C. K., Tang, M. J. and Li, H. (2006) Defining a link with autosomal-dominant polycystic kidney disease in mice with congenitally low expression of *Pkd1*. *Am J Pathol.*, 168: 205-220.

Jishage, K., Nezu, J., Kawase, Y., Iwata, T., Watanabe, M., Miyoshi, A., Ose, A., Habu, K., Kake, T., Kamada, N., *et al.* (2002) Role of Lkb1, the causative gene of Peutz-Jegher's syndrome, in embryogenesis and polyposis. *Proc Natl Acad Sci U S A.*, 99: 8903-8908.

Johnson, M. W., Kerfoot, C., Bushnell, T., Li, M. and Vinters, H. V. (2001) Hamartin and tuberin expression in human tissues. *Mod Pathol.*, 14: 202-210.

Jones, A. C., Shyamsundar, M. M., Thomas, M. W., Maynard, J., Idziaszczyk, S., Tomkins, S., Sampson, J. R. and Cheadle, J. P. (1999) Comprehensive mutation analysis of *TSC1* and *TSC2*-and phenotypic correlations in 150 families with tuberous sclerosis. *Am J Hum Genet.*, 64: 1305-1315.

Jones, A. C., Sampson, J. R., Hoogendoorn, B., Cohen, D. and Cheadle, J. P. (2000) Application and evaluation of denaturing HPLC for molecular genetic analysis in tuberous sclerosis. *Hum Genet.*, 106: 663-668.

Jones, C., Roper, V. C., Foucher, I., Qian, D., Banizs, B., Petit, C., Yoder, B. K. and Chen, P. (2007) Ciliary proteins link basal body polarization to planar cell polarity regulation. *Nat Genet.*, 40: 69-77.

Kamada, S., Shimono, A., Shinto, Y., Tsujimura, T., Takahashi, T., Noda, T., Kitamura, Y., Kondoh, H. and Tsujimoto, Y. (1995) *bcl-2* deficiency in mice leads to pleiotropic abnormalities: accelerated lymphoid cell death in thymus and spleen, polycystic kidney, hair hypopigmentation, and distorted small intestine. *Cancer Res.*, 55: 354-359.

Kandt, R. S., Haines, J. L., Smith, M., Northrup, H., Gardner, R. J., Short, M. P., Dumars, K., Roach, E. S., Steingold, S., Wall, S., *et al.* (1992) Linkage of an important gene locus for tuberous sclerosis to a chromosome 16 marker for polycystic kidney disease. *Nature Genet.*, 2: 37-41.

Karner, C., Wharton, K. A. and Carroll, T. J. (2006) Apical-basal polarity, Wnt signaling and vertebrate organogenesis. *Semin Cell Dev Biol.*, 17: 214-222.

Keith, D. S., Torres, V. E., King, B. F., Zincki, H. and Farrow, G. M. (1994) Renal cell carcinoma in autosomal dominant polycystic kidney disease. *J Am Soc Nephrol.*, 4: 1661-1669.

Kenerson, H., Dundon, T. A. and Yeung, R. S. (2005) Effects of Rapamycin in the Eker rat model of tuberous sclerosis complex. *Pediatr Res.*, 57: 67-75.

Kessel, R. G. and Kardon, R. H. (1979) Tissues and Organs: a text-atlas of scanning electron microscopy. Bartlett, A. C. and Johnson, D. (eds.), W. H. Freeman and Company, USA.

Kim, E., Arnould, T., Sellin, L. K., Benzing, T., Fan, M. J., Grüning, W., Sokol, S. Y., Drummond, I. and Walz, G. (1999) The polycystic kidney disease 1 gene product modulates Wnt signaling. *J Biol Chem.*, 274: 4947-4953.

Kimberling, W. J., Fain, P. R., Kenyon, J. B., Goldgar, D., Sujansky, E. and Gabow, P. A. (1988) Linkage heterogeneity of autosomal dominant polycystic kidney disease. *N Engl J Med.*, 319: 913-918.

Kimberling, W. J., Kumar, S., Gabow, P. A., Kenyon, J. B., Connolly, C. J. and Somlo, S. (1993) Autosomal dominant polycystic kidney disease: localization of the second gene to chromosome 4q13-q23. *Genomics*, 18: 467-472.

Kirpicznik, J. (1910) Ein fall von Tuberoser Sklerose und gleichzeitigen multiplen Nierengeschwulsten. *Virchows Arch f Path Anat.*, 202: 358.

Kishi, M., Pan, Y. A., Crump, J. G. and Sanes, J. R. (2005) Mammalian SAD kinases are required for neuronal polarization. *Science*, 307: 929-932.

Kleymenova, E., Ibraghimov-Beskrovnaya, O., Kugoh, H., Everitt, J., Xu, H., Kiguchi, K., Landes, G., Harris, P. and Walker, C. (2001) Tuberin-dependent membrane localization of polycystin-1: a functional link between polycystic kidney disease and the *TSC2* tumor suppressor gene. *Mol Cell.*, 7: 823-832.

Kobayashi, T., Urakami, S., Hirayama, Y., Yamamoto, T., Nishizawa, M., Takahara, T., Kubo, Y. and Hino, O. (1997) Intragenic *Tsc2* somatic mutations as Knudson's second hit in spontaneous and chemically induced renal carcinomas in the Eker rat model. *Jpn J Cancer Res.*, 88: 254-261.

Koptides, M., Hadjimichael, C., Koupepidou, P., Pierides, A. and Constantinou Deltas, C. (1999) Germinal and somatic mutations in the *PKD2* gene of renal cysts in autosomal dominant polycystic kidney disease. *Hum Mol Genet.*, 8: 509-513.

Koptides, M., Mean, R., Demetriou, K., Pierides, A. and Deltas, C. C. (2000) Genetic evidence for a trans-heterozygous model for cystogenesis in autosomal dominant polycystic kidney disease. *Hum Mol Genet.*, 9: 447-452.

Kozminski, K. G., Johnson, K. A., Forscher, P. and Rosenbaum, J. L. (1993) A motility in the eukaryotic flagellum unrelated to flagellar beating. *Proc Natl Acad Sci U S A*, 90: 5519-5523.

Knudson, A. G. Jr. (1971) Mutation and cancer: statistical study of retinoblastoma. *Proc Natl Acad Sci.*, 68: 820-823.

Kobayashi, T., Hirayama, Y., Kobayashi, E., Kubo, Y. and Hino, O. (1995) A germline insertion in the tuberous sclerosis (*Tsc2*) gene gives rise to the Eker rat model of dominantly inherited cancer. *Nat Genet.*, 9: 70-74.

Kobayashi, T., Urakami, S., Cheadle, J. P. Aspinwall, R., Harris, P., Sampson, J. R. and Hino, O. (1997) Identification of a leader exon and a core promoter for the rat tuberous sclerosis 2 (*Tsc2*) gene and structural comparison with the human homolog. *Mamm Genome*, 8: 554-558.

Kobayashi, T., Minowa, O., Kuno, J., Mitani, H., Hino, O. and Noda, T. (1999) Renal carcinogenesis, hepatic hemangiomatosis, and embryonic lethality caused by a germ-line *Tsc2* mutation in mice. *Cancer Res.*, 59: 1206-1211.

Kobayashi, T., Minowa, O., Sugitani, Y., Takai, S., Mitani, H., Kobayashi, E., Noda, T. and Hino, O. (2001) A germ-line *Tsc1* mutation causes tumour development and embryonic lethality that are similar, but not identical to, those caused by *Tsc2* mutation in mice. *Proc Natl Acad Sci U S A.*, 98: 8762-8767.

Kobayashi, N., Rivas-Carrillo, J. D., Soto-Gutierrez, A., Fukazawa, T., Chen, Y., Navarro-Alvarez, N. and Tanaka, N. (2005) Gene delivery to embryonic stem cells. *Birth Defects Res C Embryo Today*, 75: 10-18.

Kobe, B. and Deisenhofer, J. (1994) The leucine-rich repeat: a versatile binding motif. *Trends Biochem Sci.*, 19: 415-421.

Koulen, P., Cai, Y., Geng, L., Maeda, Y., Nishimura, S., Witzgall, R., Ehrlich, B. E. and Somlo, S. (2002) Polycystin-2 is an intracellular calcium release channel. *Nat Cell Biol.*, 4: 191-197.

Kozlowski, P., Bissler, J., Pei, Y. and Kwiatkowski, D. J. (2007) Analysis of *PKD1* for genomic deletion by multiplex ligation-dependent probe assay: absence of hot spots. *Genomics*, 91: 203-208.

Krymskaya, V. P. (2003) Tumour suppressors hamartin and tuberin: intracellular signalling. *Cell Signal.*, 15: 729-739.

Kubo, Y., Kikuchi, Y., Mitani, H., Kobayashi, E., Kobayashi, T. and Hino, O. (1995) Allelic loss at the tuberous sclerosis (*Tsc2*) gene locus in spontaneous uterine leiomyosarcomas and pituitary adenomas in the Eker rat model. *Jpn J Cancer Res.*, 86: 828-832.

Kwiatkowski, D., Armour, J., Bale, A., Fountain, J., Goudie, D., Haines, J., Knowles, M., Pilz, A., Slaugenhaupt, S. and Povey, S. (1993) Report and abstracts of the Second International Workshop on Human Chromosome 9 Mapping. *Cytogenet Cell Genet.*, 64: 93-121.

Kwiatkowski, D. J., Zhang, H., Bandura, J. L., Heiberger, K. M., Glogauer, M., el-Hashemite, N. and Onda, H. (2002) A mouse model of *TSC1* reveals sex-dependent lethality from liver haemangioma, and up-regulation of p70S6 kinase activity in Tsc1 null cells. *Hum Mol Genet.*, 11: 525-534.

Laas, M. W., Spiegel, M., Jauch, A., Hahn, G., Rupprecht, E., Vogelberg, C., Bartsch, O. and Huebner, A. (2004) Tuberous sclerosis and polycystic kidney disease in a 3-month-old infant. *Pediatr Nephrol.*, 19: 602-608.

Lagos, J. C. and Gomez, M. R. (1967) Tuberous sclerosis: reappraisal of a clinical entity. *Mayo Clin Proc.*, 42: 26-49.

Lakshmanan, J. and Eysselein, V. (1993) Hereditary error in epidermal growth factor prohormone metabolism in a rat model of autosomal dominant polycystic kidney disease. *Biochem Biophys Res Commun.*, 197: 1083-1093.

Lamb, R. F., Roy, C., Diefenbach, T. J., Vinters, H. V. Johnson, M. W., Jay, D. G. and Hall, A. (2000) The *TSC1* tumour suppressor hamartin regulates cell adhesion through ERM proteins and the GTPase Rho. *Nat Cell Biol.*, 2: 281-287.

Lantinga-van Leeuwen, I. S., Dauwerse, J. G., Baelde, H. J., Leonhard, W. N., van de Wal, A., Ward, C. J., Verbeek, S., Deruiter, M. C., Breuning, M. H., de Heer, E. and Peters, D. J. (2004) Lowering of *Pkd1* expression is sufficient to cause polycystic kidney disease. *Hum Mol Genet.*, 13: 3069-3077.

Lantinga-van Leeuwen, I. S., Leonhard, W. N., van der Wal, A., Breuning, M. H., de Heer, E. and Peters, D. J. (2007) Kidney-specific inactivation of the Pkd1 gene induces rapid cyst formation in developing kidneys and a slow onset of disease in adult mice. *Hum Mol Genet.*, 16: 3188-3196.

Le, N. H., van der Bent, P., Huls, G., van de Wetering, M., Loghman-Adham, M., Ong, A. C., Calvet, J. P., Clevers, H., Breuning, M. H., van Dam, H. and Peters, D. J. (2004) Aberrant polycystin-1 expression results in modification of activator protein-1 activity, whereas Wnt signaling remains unaffected. *J Biol Chem.*, 279: 27472-27481.

Lee, D. F., Kuo, H. P., Chen, C. T., Hsu, J. M., Chou, C. K., Wei, Y., Sun, H. L., Li, L. Y., Ping, B., Huang, W. C. *et al.* (2007) IKK beta suppression of TSC1 links inflammation and tumor angiogenesis via the mTOR pathway. *Cell*, 130: 440-455.

Lendvay, T. S. and Marshall, F. F. (2003) The tuberous sclerosis complex and its highly variable manifestations. *J Urol.*, 169: 1635-1642.

Li, H. P., Geng, L., Burrow, C. R. and Wilson, P. D. (1999) Identification of phosphorylation sites in the PKD1-encoded protein C-terminal domain. *Biochem Biophys Res Commun.*, 259: 356-363.

Li, L., He, F., Litofsky, N. S., Recht, L. D. and Ross, A. H. (2003a) Profiling of genes expressed by PTEN haploinsufficient neural precursor cells. *Mol Cell Neurosci.*, 24: 1051-1061.

Li, Y., Inoki, K., Vacratsis, P. and Guan, K. L. (2003b) The p38 and MK2 kinase cascade phosphorylates tuberin, the tuberous sclerosis 2 gene product, and enhances its interaction with 14-3-3. *J Biol Chem.*, 278: 13663-13671.

Lin, F., Hiesberger, T., Cordes, K., Sinclair, A. M., Goldstein, L. S., Somlo, S. and Igarashi, P. (2003) Kidney-specific inactivation of the KIF3A subunit of kinesin-II inhibits renal ciliogenesis and produces polycystic kidney disease. *Proc Natl Acad Sci U S A*, 100: 5286-5291.

Lin, F. and Satlin, L. M. (2004) Polycystic kidney disease: the cilium as a common pathway in cystogenesis. *Curr Opin Pediatr.*, 16: 171-176.

Liu, S., Lu, W., Obara, T., Kuida, S., Lehoczky, J., Dewar, K., Drummond, I. A. and Beier, D. R. (2002) A defect in a novel Nek-family kinase causes cystic kidney disease in the mouse and in zebrafish. *Development*, 129: 5839-5846.

Liu, W., Murcia, N. S., Duan, Y., Weinbaum, S., Yoder, B. K., Schwiebert, E. and Satlin, L. M. (2005) Mechanoregulation of intracellular Ca^{2+} concentration is attenuated in collecting duct of monocilium-impaired *orpk* mice. *Am J Physiol Renal Physiol.*, 289: F978-F988.

Loghman-Adham, M., Soto, C. E., Inagami, T. and Cassis, L. (2004) The intrarenal renin-angiotensin system in autosomal dominant polycystic kidney disease. *Am J Physiol Renal Physiol.* 287: F775-F788.

Lou, D., Griffith, N. and Noonan, D. J. (2001) The tuberous sclerosis 2 gene product can localize to nuclei in a phosphorylation-dependent manner. *Mol Cell Biol Res Commun.*, 4: 374-380.

Low, S. H., Vasanth, S., Larson, C. H., Mukherjee, S., Sharma, N., Kinter, M. T., Kane, M. E., Obara, T. and Weimbs, T. (2006) Polycystin-1, STAT6, and P100 function in a pathway that transduces ciliary mechanosensation and is activated in polycystic kidney disease. *Dev Cell.*, 10: 57-69.

Luo, Y., Vassilev, P. M., Li, X., Kawanabe, Y. and Zhou, J. (2003) Native polycystin 2 functions as a plasma membrane Ca2+-permeable cation channel in renal epithelia. *Mol Cell Biol.*, 23: 2600-2607.

Ma, L., Chen, Z., Erdjument-Bromage, H., Tempst, P. and Pandolfi, P. P. (2005) Phosphorylation and functional inactivation of TSC2 by Erk implications for tuberous sclerosis and cancer pathogenesis. *Cell*, 121: 179-193.

Magistroni, R., He, N., Wang, K., Andrew, R., Johnson, A., Gabow, P., Dicks, E., Parfrey, P., Torra, R., San-Millan, J. L., *et al.* (2003) Genotype-renal function correlation in type 2 autosomal dominant polycystic kidney disease. *J Am Soc Nephrol.*, 14: 1164-1174.

Maheshwar, M. M., Cheadle, J. P., Jones, A. C., Myring, J., Fryer, A. E., Harris, P. C. and Sampson, J. R. (1997) The GAP-related domain of tuberin, the product of the *TSC2* gene, is a target for missense mutations in tuberous sclerosis. *Hum Mol Genet.*, 6: 1991-1996.

Mahjoub, M. R., Trapp, M. L. and Quarmby, L. M. (2005) NIMA-related kinases defective in murine models of polycystic kidney diseases localize to primary cilia and centrosomes. *J Am Soc Nephrol.*, 16: 3485-3489.

Majumdar, A., Vainio, S., Kispert, A., McMahon, J. and McMahon, A. P. (2003) Wnt11 and Ret/Gdnf pathways cooperate in regulating ureteric branching during metanephric kidney development. *Development*, 130: 3175-3185.

Mak, B.C., Takemaru, K., Kenerson, H. L., Moon, R. T. and Yeung, R. S. (2003) The tuberin-hamartin complex negatively regulates beta-catenin signalling activity. *J. Biol. Chem.*, 278: 5947-5951.

Mak, B. C., Kenerson, H. L., Aicher, L. D., Barnes, E. A. and Yeung, R. S. (2005) Aberrant beta-catenin signalling in tuberous sclerosis. *Am J Pathol.*, 167: 107-116.

Malhas, A. N., Abuknesha, R. A. and Price, R. G. (2002) Interaction of the leucine-rich repeats of polycystin-1 with extracellular matrix proteins: possible role in cell proliferation. *J Am Soc Nephrol.*, 13: 19-26.

Manning, B. D., Tee, A. R., Logsdon, M. N., Blenis, J. and Cantley, L. C. (2002) Identification of the tuberous sclerosis complex-2 tumor suppressor gene product tuberin as a target of the phosphoinositide 3-kinase/akt pathway. *Mol Cell.*, 10: 151-162.

Manning, B. D. (2004) Balancing Akt with S6K: implications for both metabolic diseases and tumorigenesis. *J Cell Biol.*, 167: 399-403.

Marszalek, J. R., Ruiz-Lozano, P., Roberts, E., Chien, K. R. and Goldstein, L. S. (1999) Situs inversus and embryonic ciliary morphogenesis defects in mouse mutants lacking the KIF3A subunit of kinesin-II. *Proc Natl Acad Sci U S A*, 96: 5043-5048.

Martignoni, G., Bonetti, F., Pea, M., Tardanico, R., Brunelli, M. and Eble, J. N. (2002) Renal disease in adults with TSC2/PKD1 contiguous gene syndrome. *Am J Surg Pathol.*, 26: 198-205.

Massey-Harroche, D., Delgrossi, M. H., Lane-Guermonprez, L., Arsanto, J. P., Borg, J. P., Billaud, M. and Le Bivic, A. (2007) Evidence for a molecular link between the tuberous sclerosis complex and the Crumbs complex. *Hum Mol Genet.*, 16: 529-536.

Masyuk, T. V., Huang, B. Q., Ward, C. J., Masyuk, A. I., Yuan, D., Splinter, P. L., Punyashthiti, R., Ritman, E. L., Torres, V. E., Harris, P. C. *et al.* (2003) Defects in cholangiocyte fibrocystin expression and ciliary structure in the PCK rat. *Gastroenterology*, 125: 1303-1310.

Matsumoto, S., Bandyopadhyay, A., Kwiatkowski, D. J., Maitra, U. and Matsumoto, T. (2002) Role of the Tsc1-Tsc2 complex in signalling and transport across the cell membrane in the fission yeast Schizosaccharomyces pombe. *Genetics*, 161: 1053-1063.

Menezes, L. F. and Onuchic, L. F. (2006) Molecular and cellular pathogenesis of autosomal recessive polycystic kidney disease. *Braz J Med Biol Res.*, 39: 1537-1548.

Menini, A. (1999) Calcium signalling and regulation in olfactory neurons. *Curr Opin Neurobiol.*, 9: 419-426.

Meredith, J. E. Jr., Fazeli, B. and Schwartz, M. A. (1993) The extracellular matrix as a cell survival factor. *Mol Biol Cell.*, 4: 953-961.

Messina, M. P., Rauktys, A., Lee, L. and Dabora, S. L. (2007) Tuberous sclerosis preclinical studies: timing of treatment, combination of a rapamycin analog (CCI-779) and interferon-gamma, and comparison of rapamycin to CCI-779. *BMC Pharmacol.*, 7: 14.

Miyoshi, H., Nakau, M., Ishikawa, T. O., Seldin, M. F., Oshima, M., Taketo, M. M. (2002) Gastrointestinal hamartomatous polyposis in *Lkb1* heterozygous knockout mice. *Cancer Res.*, 62: 2261-2266.

Mizuguchi, M., Takashima, S., Yamanouchi, H., Nakazato, Y., Mitani, H. and Hino, O. (2000) Novel cerebral lesions in the Eker rat model of tuberous sclerosis: cortical tuber and anaplastic ganglioglioma. *J Neuropathol Exp Neurol.*, 59: 188-196.

Mochizuki, T., Wu, G., Hayashi, T., Xenophontos, S. L., Veldhuisen, B., Saris, J. J., Reynolds, D. M., Cai, Y., Gabow, P. A., Pierides, A., *et al.* (1996) *PKD2*, a gene for polycystic kidney disease that encodes an integral membrane protein. *Science*, 272: 1339-1342.

Mokrzan, E. M., Lewis, J. S. and Mykytyn, K. (2007) Differences in renal tubule primary cilia length in a mouse model of Bardet-Biedl syndrome. *Nephron Exp Nephrol.*, 106: e88-e96.

Moolten, S. E. (1942) Hamartial nature of the tuberous sclerosis complex and its bearing on the tumour problem: report of one case with tumour anomaly of the kidney and adenoma sebaceum. *Arch Intern Med.*, 69: 589-623.

Morgan, D., Eley, L., Sayer, J., Strachan, T., Yates, L. M., Craighead, A. S. and Goodship, J. A. (2002) Expression analyses and interaction with the anaphase promoting complex protein Apc2 suggest a role for inversin in primary cilia and involvement in the cell cycle. *Hum Mol Genet.*, 11: 3345-3350.

Mostov, K. E. (2006) mTOR is out of control in polycystic kidney disease. *Proc Natl Acad Sci U S A*, 103: 5247-5248.

Moy, G. W., Mendoza, L. M., Schulz, J. R., Swanson, W. J., Glabe, C. G. and Vacquier, V. D. (1996) The sea urchin sperm receptor for egg jelly is a modular protein with extensive homology to the human polycystic kidney disease protein, PKD1. *J Cell Biol.*, 133: 809-817.

Moyer, J. H., Lee-Tischler, M. J., Kwon, H. Y., Schrick, J. J., Avner, E. D., Sweeney, W. E., Godfrey, V. L., Cacheiro, N. L., Wilkinson, J. E. and Woychik, R. P. (1994) Candidate gene associated with a mutation causing recessive polycystic kidney disease in mice. *Science*, 264: 1329-1333.

Murcia, N. S., Richards, W. G., Yoder, B. K., Mucenski, M. L., Dunlap, J. R. and Woychik, R. P. (2000) The Oak Ridge Polycystic Kidney (*orpk*) disease gene is required for left-right axis determination. *Development*, 127: 2347-2355.

Murthy, V., Stemmer-Rachamimov, A. O., Haddad, L. A., Roy, J. E., Cutone, A. N., Beauchamp, R. L., Smith, N., Louis, D. N. and Ramesh, V. (2001) Developmental expression of the tuberous sclerosis proteins tuberin and hamartin. *Acta Neuropathol.*, 101: 202-210.

Nakase, Y., Fukuda, K., Chikashige, Y., Tsutsumi, C., Morita, D., Kawamoto, S., Ohnuki, M., Hiraoka, Y. and Matsumoto, T. (2006) A defect in protein farnesylation suppresses a loss of Schizosaccharomyces pombe *tsc2+*, a homolog of the human gene predisposing to tuberous sclerosis complex. *Genetics*, 173: 569-578.

Nakau, M., Miyoshi, H., Seldin, M. F., Imamura, M., Oshima, M. and Taketo, M. M. (2002) Hepatocellular carcinoma caused by loss of heterozygosity in *Lkb1* gene knockout mice. *Cancer Res.*, 62: 4549-4553.

Nascimento, A. B., Mitchell, D. G., Zhang, X. M., Kamishima, T., Parker, L. and Holland, G. A. (2001) Rapid MR imaging detection of renal cysts: age-based standards. *Radiology.*, 221: 628-632.

Nation, J. L. (1983) A new method using hexamethyldisilazane for preparation of soft insect tissues for scanning electron microscopy. *Stain Technol.*, 58: 347-351.

Nauli, S. M., Alenghat, F. J., Luo, Y., Williams, E., Vassilev, P., Li, X., Elia, A. E., Lu, W., Brown, E. M., Quinn, S. J., Ingber, D. E. and Zhou, J. (2003) Polycystins 1 and 2 mediate mechanosensation in the primary cilium of kidney cells. *Nat Genet.*, 33: 129-137.

Nauli, S. M. and Zhou, J. (2004) Polycystins and mechanosensation in renal and nodal cilia. *Bioessays*, 26: 844-856.

Nauta, J., Ozawa, Y., Sweeney, W. E. Jr., Rutledge, J. C. and Avner, E. D. (1993) Renal and biliary abnormalities in a new murine model of autosomal recessive polycystic kidney disease. *Pediatr Nephrol.*, 7: 163-172.

Nellist, M., Brook-Carter, P. T., Connor, J. M. Kwiatkowski, D. J., Johnson, P. and Sampson, J. R. (1993) Identification of markers flanking the tuberous sclerosis locus on chromosome 9 (TSC1). *J Med Genet.*, 30: 224-227.

Nellist, M., van Slegtenhorst, M. A., Goedbloed, M., van den Ouweland, A. M., Halley, D. J. and van der Sluijs, P. (1999) Characterization of the cytosolic tuberin-hamartin complex. Tuberin is a cytosolic chaperone for hamartin. *J Biol Chem.*, 274: 35647-35652.

Nellist, M., Verhaaf, B., Goedbloed, M. A., Reuser, A. J., van den Ouweland, A. M., and Halley, D. J. (2001) *TSC2* missense mutations inhibit tuberin phosphorylation and prevent formation of the tuberin-hamartin complex. *Hum Mol Genet.*, 10: 2889-2898.

Nelson, W. J. and Nusse, R. (2004) Convergence of Wnt, beta-catenin, and cadherin pathways. *Science*, 303: 1483-1487.

Nevin, N. C. and Pearce, W. G. (1968) Diagnostic and genetical aspects of tuberous sclerosis. *J Med Genet.*, 5: 273-280.

Niida, Y., Stemmer-Rachamimov, A. O., Logrip, M., Tapon, D., Perez, R., Kwiatkowski, D. J., Sims, K., MacCollin, M., Louis, D. N. and Ramesh, V. (2001) Survey of somatic mutations in tuberous sclerosis complex (TSC) hamartomas suggests different genetic mechanisms for pathogenesis of TSC lesions. *Am J Hum Genet.*, 69: 493-503.

Nonaka, S., Yoshiba, S., Watanabe, D., Ikeuchi, S., Goto, T., Marshall, W. F. and Hamada, H. (2005) De novo formation of left-right asymmetry by posterior tilt of nodal cilia. *PLoS Biol.*, 3: e268.

Noonan, D. J., Lou, D., Griffith, N. and Vanaman, T. C. (2002) A calmodulin binding site in the tuberous sclerosis 2 gene product is essential for regulation of transcription events and is altered by mutations linked to tuberous sclerosis and lymphangioleiomyomatosis. *Arch Biochem Biophys.*, 398: 132-140.

Northrup, H., Kwiatkowski, D. J., Roach, E. S., Dobyns, W. B., Lewis, R. A., Herman, G. E., Rodriguez, E. Jr., Daiger, S. P. and Blanton, S. H. (1992) Evidence for genetic heterogeneity in tuberous sclerosis: one locus on chromosome 9 and at least one locus elsewhere. *Am J Hum Genet.*, 51: 709-720.

Nürnberger, J., Bacallao, R. L. and Phillips, C. L. (2002) Inversin forms a complex with catenins and N-cadherin in polarized epithelial cells. *Mol Biol Cell*, 13: 3096-3106.

Oishi, I., Kawakami, Y., Raya, A., Callol-Massot, C. and Izpisúa Belmonte, J. C. (2006) Regulation of primary cilia formation and left-right patterning in zebrafish by a noncanonical Wnt signaling mediator, duboraya. *Nat Genet.*, 38: 1316-1322.

Okimoto, K., Kouchi, M., Kikawa, E., Toyosawa, K., Koujitani, T., Tanaka, K., Matsuoka, N., Sakurai, J. and Hino, O. (2000) A novel "Nihon" rat model of a Mendelian dominantly inherited renal cell carcinoma. *Jpn J Cancer Res.*, 91: 1096-1099.

Onda, H., Lueck, A., Marks, P. W., Warren, H. B. and Kwiatkowski, D. J. (1999) *Tsc2(+/-)* mice develop tumors in multiple sites that express gelsolin and are influenced by genetic background. *J Clin Invest.*, 104: 687-695.

Ong, A. C. and Harris, P. C. (1997) Molecular basis of renal cyst formation--one hit or two? *Lancet*, 349: 1039-1040.

Ong, A. C., Ward, C. J., Butler, R. J., Biddolph, S., Bowker, C., Torra, R., Pei, Y. and Harris, P. C. (1999a) Coordinate expression of the autosomal dominant polycystic kidney disease proteins, polycystin-2 and polycystin-1, in normal and cystic tissue. *Am J Pathol.*, 154: 1721-1729.

Ong, A. C., Harris, P. C., Davies, D. R., Pritchard, L., Rossetti, S., Biddolph, S., Vaux, D. J., Migone, N. and Ward, C. J. (1999b) Polycystin-1 expression in PKD1, early-onset PKD1, and TSC2/PKD1 cystic tissue. *Kidney Int.*, 56: 1324-1333.

Onuchic, L. F., Furu, L., Nagasawa, Y., Hou, X., Eggermann, T., Ren, Z., Bergmann, C., Senderek, J., Esquivel, E., Zeltner, R., *et al.* (2002) *PKHD1*, the polycystic kidney and hepatic disease 1 gene, encodes a novel large protein containing multiple immunoglobulin-like plexin-transcription-factor domains and parallel beta-helix 1 repeats. *Am J Hum Genet.*, 70: 1305-1317.

Ortiz, A., Lorz, C., Catalán, M. P., Danoff, T. M., Yamasaki, Y., Egido, J. and Neilson, E. G. (2000) Expression of apoptosis regulatory proteins in tubular epithelium stressed in culture or following acute renal failure. *Kidney Int.*, 57: 969-981.

Otto, E. A., Schermer, B., Obara, T., O'Toole, J. F., Hiller, K. S., Mueller, A. M., Ruf, R. G., Hoefele, J., Beekmann, F., Landau, D., *et al.* (2003) Mutations in *INVS* encoding inversin cause nephronophthisis type 2, linking renal cystic disease to the function of primary cilia and left-right axis determination. *Nat Genet.*, 34: 413-420.

Pagliuca, A., Gallo, P., De Luca, P. and Lania, L. (2000) Class A helix-loop-helix proteins are positive regulators of several cyclin-dependent kinase inhibitors' promoter activity and negatively affect cell growth. *Cancer Res.*, 60: 1376–1382.

Pan, J. and Snell, W. (2007) The primary cilium: keeper of the key to cell division. *Cell*, 129: 1255-1257.

Park, T. J., Haigo, S. L. and Wallingford, J. B. (2006) Ciliogenesis defects in embryos lacking inturned or fuzzy function are associated with failure of planar cell polarity and Hedgehog signaling. *Nat Genet.*, 38: 303-311.

Park, T. J., Mitchell, B. J., Abitua, P. B., Kintner, C. and Wallingford, J. B. (2008) Dishevelled controls apical docking and planar polarization of basal bodies in ciliated epithelial cells. *Nat Genet.*, 40: 871-879.

Parnell, S. C., Magenheimer, B. S., Maser, R. L., Rankin, C. A., Smine, A., Okamoto, T. and Calvet, J. P. (1998) The polycystic kidney disease-1 protein, polycystin-1, binds and activates heterotrimeric G-proteins in vitro. *Biochem Biophys Res Commun.*, 251: 625-631.

Parnell, S. C., Magenheimer, B. S., Maser, R. L. and Calvet, J. P. (1999) Identification of the major site of in vitro PKA phosphorylation in the polycystin-1 C-terminal cytosolic domain. *Biochem Biophys Res Commun.*, 259: 539-543.

Parry, L., Maynard, J. H., Patel, A., Clifford, S. C., Morrissey, C., Maher, E. R., Cheadle, J. P. and Sampson, J. R. (2001) Analysis of the *TSC1* and *TSC2* genes in sporadic renal cell carcinomas. *Br J Cancer*, 85: 1226-1230.

Patel, V., Li, L., Cobo-Stark, P., Shao, X., Somlo, S., Lin, F. and Igarashi, P. (2008) Acute kidney injury and aberrant planar cell polarity induce cyst formation in mice lacking renal cilia. *Hum Mol Genet.*, 17: 1578-1590.

Paterson, A. D. and Pei, Y. (1998) Is there a third gene for autosomal dominant polycystic kidney disease? *Kidney Int.*, 54: 1759-1761.

Paterson, A. D. and Pei, Y. (1999) *PKD3*-to be or not to be? *Nephrol Dial Transplant*, 14: 2965-2966.

Paulson, G. W. and Lyle, C. B. (1966) Tuberous sclerosis. *Dev Med Child Neurol.*, 8: 571-586.

Pazour, G. J., Dickert, B. L., Vucica, Y., Seeley, E. S., Rosenbaum, J. L., Witman, G. B., and Cole, D. G. (2000) Chlamydomonas *IFT88* and its mouse homologue, polycystic kidney disease gene *tg737*, are required for assembly of cilia and flagella. *J. Cell Biol.*, 151: 709-718.

Pazour, G. J., San Agustin, J. T., Follit, J. A., Rosenbaum, J. L., and Witman, G. B. (2002) Polycystin-2 localizes to kidney cilia and the ciliary level is elevated in orpk mice with polycystic kidney disease. *Curr. Biol.*, 12: R378-380.

Pei, Y., Watnick, T., He, N., Wang, K., Liang, Y., Parfrey, P., Germino, G. and St George-Hyslop, P. (1999) Somatic *PKD2* mutations in individual kidney and liver cysts support a "two-hit" model of cystogenesis in type 2 autosomal dominant polycystic kidney disease. *J Am Soc Nephrol.*, 10: 1524-1529.

Pei, Y. (2001) A "two-hit" model of cystogenesis in autosomal dominant polycystic kidney disease? *Trends Mol Med.*, 7: 151-156.

Pei, Y., Paterson, A. D., Wang, K. R., He, N., Hefferton, D., Watnick, T., Germino, G. G., Parfrey, P., Somlo, S. and St George-Hyslop, P. (2001) Bilineal disease and trans-heterozygotes in autosomal dominant polycystic kidney disease. *Am J Hum Genet.*, 68: 355-363.

Pei, Y. (2006) Diagnostic approach in autosomal dominant polycystic kidney disease. *Clin J Am Soc Nephrol.*, 1: 1108-1114.

Peral, B., San Millán, J. L., Hernández, C., Valero, A., Lathrop, G. M., Beckmann, J. S. and Moreno, F. (1993) Estimating locus heterogeneity in autosomal dominant polycystic kidney disease (ADPKD) in the Spanish population. *J Med Genet.*, 30: 910-913.

Peters, D. J. and Sandkuijl, L. A. (1992) Genetic heterogeneity of polycystic kidney disease in Europe. *Contrib Nephrol.*, 97: 128-139.

Peters, D. J., Spruit, L., Saris, J. J., Ravine, D., Sandkuijl, L. A., Fossdal, R., Boersma, J., van Eijk, R., Nørby, S., Constantinou-Deltas, C. D., *et al.* (1993) Chromosome 4 localization of a second gene for autosomal dominant polycystic kidney disease. *Nat Genet.*, 5: 359-362.

Peters, D. J. and Breuning, M. H. (2001) Autosomal dominant polycystic kidney disease: modification of disease progression. *Lancet*, 358: 1439-1444.

Piedimonte, L. R., Wailes, I. K. and Weiner, H. L. (2006) Tuberous sclerosis complex: molecular pathogenesis and animal models. *Neurosurg Focus*, 20: E4.

Piontek, K. B., Huso, D. L., Grinberg, A., Liu, L., Bedja, D., Zhao, H., Gabrielson, K., Qian, F., Mei, C., Westphal, H. and Germino, G. G. (2004) A functional floxed allele of *Pkd1* that can be conditionally inactivated in vivo. *J Am Soc Nephrol.*, 15: 3035-3043.

Pitiot, G., Waksman, G., Bragado-Nilsson, E., Jobert, S., Cornelis, F. and Mallet, J. (1994) Linkage analysis places the *TSC1* gene distal to D9S10. *Ann Hum Genet.*, 58: 232-233.

Plank, T. L., Yeung, R. S. and Henske, E. P. (1998) Hamartin, the product of the tuberous sclerosis 1 (*TSC1*) gene, interacts with tuberin and appears to be localized to cytoplasmic vesicles. *Cancer Res.*, 58: 4766-4770.

Plank, T. L., Logginidou, H., Klein-Szanto, A. and Henske, E. P. (1999) The expression of hamartin, the product of the *TSC1* gene, in normal human tissues and in TSC1- and TSC2-linked angiomyolipomas. *Mod Pathol.*, 12: 539-545.

Potter, C. J., Huang, H. and Xu, T. (2001) Drosophila Tsc1 functions with Tsc2 to antagonize insulin signalling in regulating cell growth, cell proliferation, and organ size. *Cell*, 105: 357-368.

Potter, C. J., Pedraza, L. G. and Xu, T. (2002) Akt regulates growth by directly phosphorylating Tsc2. *Nat Cell Biol.*, 4: 658-665.

Povey, S., Armour, J., Farndon, P., Haines, J. L., Knowles, M., Olopade, F., Pilz, A., White, J. A., Members of the Utah Genome Centre Genetic Marker and Mapping Group, and Kwiatkowski, D. J. (1994) Report on the Third International Workshop on Chromosome 9. *Ann Hum Genet.*, 58: 177-250.

Praetorius, H. A. and Spring, K. R. (2001) Bending the MDCK cell primary cilium increases intracellular calcium. *J Membr Biol.*, 184: 71-79.

Praetorius, H. A. and Spring, K. R. (2003) Removal of the MDCK cell primary cilium abolishes flow sensing. *J Membr Biol.*, 191: 69-76.

Preminger, G. M., Koch, W. E., Fried, F. A., McFarland, E., Murphy, E. D. and Mandell, J. (1982) Murine congenital polycystic kidney disease: a model for studying development of cystic disease. *J Urol.*, 127: 556-560.

Pritchard, L., Sloane-Stanley, J. A., Sharpe, J. A., Aspinwall, R., Lu, W., Buckle, V., Strmecki, L., Walker, D., Ward, C. J., Alpers, C. E. *et al.* (2000) A human *PKD1* transgene generates functional polycystin-1 in mice and is associated with a cystic phenotype. *Hum Mol Genet.*, 9: 2617-2627.

Qian, F., Watnick, T. J., Onuchic, L. F. and Germino, G. G. (1996) The molecular basis of focal cyst formation in human autosomal dominant polycystic kidney disease type 1. *Cell*, 87: 979-987.

Qian, F., Germino, F. J., Cai, Y., Zhang, X., Somlo, S. and Germino, G. G. (1997) PKD1 interacts with PKD2 through a probable coiled-coil domain. *Nat Genet.*, 16: 179-183.

Qian, F., Boletta, A., Bhunia, A. K., Xu, H., Liu, L., Ahrabi, A. K., Watnick, T. J., Zhou, F. and Germino, G. G. (2002) Cleavage of polycystin-1 requires the receptor for egg jelly domain and is disrupted by human autosomal-dominant polycystic kidney disease 1-associated mutations. *Proc Natl Acad Sci U S A*, 99: 16981-16986.

Qian, Q., Li, A., King, B. F., Kamath, P. S., Lager, D. J., Huston, J. 3rd, Shub, C., Davila, S., Somlo, S. and Torres, V. E. (2003a) Clinical profile of autosomal dominant polycystic liver disease. *Hepatology*, 37: 164-171.

Qian, Q., Hunter, L. W., Li, M., Marin-Padilla, M., Prakash, Y. S., Somlo, S., Harris, P. C., Torres, V. E. and Sieck, G. C. (2003b) *Pkd2* haploinsufficiency alters intracellular calcium regulation in vascular smooth muscle cells. *Hum Mol Genet.*, 12: 1875-1880.

Qian, Q., Du, H., King, B. F., Kumar, S., Dean, P. G., Cosio, F. G. and Torres, V. E. (2008) Sirolimus reduces polycystic liver volume in ADPKD patients. *J Am Soc Nephrol.*, 19: 631-638.

Qin, H., Rosenbaum, J. L. and Barr, M. M. (2001) An autosomal recessive polycystic kidney disease gene homolog is involved in intraflagellar transport in C. elegans ciliated sensory neurons. *Curr Biol.*, 11: 457-461.

Qin, H., Wang, Z., Diener, D. and Rosenbaum, J. (2007) Intraflagellar transport protein 27 is a small G protein involved in cell-cycle control. *Curr Biol.*, 17: 193-202.

Quarmby, L. M. and Parker, J. D. (2005) Cilia and the cell cycle? *J Cell Biol.*, 169: 707-710.

Quon, K. C. and Berns, A. (2001) Haplo-insufficiency? Let me count the ways. *Genes Dev.*, 15: 2917-2921.

Rauktys, A., Lee, N., Lee, L. and Dabora, S. L. (2008) Topical rapamycin inhibits tuberous sclerosis tumour growth in a nude mouse model. *BMC Dermatol.*, 8: 1.

Ravine, D., Walker, R. G., Gibson, R. N., Forrest, S. M., Richards, R. I., Friend, K., Sheffield, L. J., Kincaid-Smith, P. and Danks, D. M. (1992) Phenotype and genotype heterogeneity in autosomal dominant polycystic kidney disease. *Lancet*, 340: 1330-1333.

Ravine, D., Gibson, R. N., Walker, R. G., Sheffield, L. J., Kincaid-Smith, P. and Danks, D. M. (1994) Evaluation of ultrasonographic diagnostic criteria for autosomal dominant polycystic kidney disease 1. *Lancet.*, 343: 824-827.

Reeders, S. T., Breuning, M. H., Davies, K. E., Nicholls, R. D., Jarman, A. P., Higgs, D. R., Pearson, P. L. and Weatherall, D. J. (1985) A highly polymorphic DNA marker linked to adult polycystic kidney disease on chromosome 16. *Nature*, 317: 542-544.

Reeders, S. T. (1992) Multilocus polycystic disease. *Nat Genet.*, 1: 235-237.

Resta, N., Simone, C., Mareni, C., Montera, M., Gentile, M., Susca, F., Gristina, R., Pozzi, S., Bertario, L., Bufo, P. *et al.* (1998) *STK11* mutations in Peutz-Jeghers syndrome and sporadic colon cancer. *Cancer Res.*, 58: 4799-4801.

Rinkel, G. J., Djibuti, M., Algra, A. and van Gijn, J. (1998) Prevalence and risk of rupture of intracranial aneurysms: a systematic review. *Stroke*, 29: 251-256.

Roach, E. S., Gomez, M. R. and Northrup, H. (1998) Tuberous sclerosis complex consensus conference: revised clinical diagnostic criteria. *J Child Neurol.*, 13: 624-628.

Roach, E. S. and Sparagana, S. P. (2004) Diagnosis of tuberous sclerosis complex. *J Child Neurol.*, 19: 643-649.

Robert, A., Margall-Ducos, G., Guidotti, J. E., Brégerie, O., Celati, C., Bréchot, C. and Desdouets, C. (2007) The intraflagellar transport component IFT88/polaris is a centrosomal protein regulating G1-S transition in non-ciliated cells. *J Cell Sci.*, 120: 628-637.

Robertson, F. M., Cendron, M., Klauber, G. T. and Harris, B. H. (1996) Renal cell carcinoma in association with tuberous sclerosis in children. *J Pediatr Surg.*, 31:729-730.

Romeo, G., Devoto, M., Costa, G., Roncuzzi, L., Catizone, L., Zucchelli, P., Germino, G. G., Keith, T., Weatherall, D. J. and Reeders, S. T. (1988) A second genetic locus for autosomal dominant polycystic kidney disease. *Lancet*, 2: 8-11.

Rosner, M., Hanneder, M., Siegel, N., Valli, A. and Hengstschläger, M. (2008) The tuberous sclerosis gene products hamartin and tuberin are multifunctional proteins with a wide spectrum of interacting partners. *Mutat Res.*, 658: 234-246.

Ross, A. T. and Dickerson, W. W. (1943) Tuberous sclerosis. *Arch Neurol Psychiatry*, 50: 233-257.

Ross, A. J., May-Simera, H., Eichers, E. R., Kai, M., Hill, J., Jagger, D. J., Leitch, C. C., Chapple, J. P., Munro, P. M., Fisher, S., *et al.* (2005) Disruption of Bardet-Biedl syndrome ciliary proteins perturbs planar cell polarity in vertebrates. *Nat Genet.*, 37: 1135-1140.

Rosser, T., Panigrahy, A. and McClintock, W. (2006) The diverse clinical manifestations of tuberous sclerosis complex: a review. *Semin Pediatr Neurol.*, 13: 27-36.

Rossetti, S., Strmecki, L., Gamble, V., Burton, S., Sneddon, V., Peral, B., Roy, S., Bakkaloglu, A., Komel, R., Winearls, C. G. and Harris, P. C. (2001) Mutation analysis of the entire *PKD1* gene: genetic and diagnostic implications. *Am J Hum Genet.*, 68: 46-63.

Rossetti, S., Burton, S., Strmecki, L., Pond, G. R., San Millán, J. L., Zerres, K., Barratt, T. M., Ozen, S., Torres, V. E., Bergstralh, E. J., *et al.* (2002a) The position of the polycystic kidney disease 1 (*PKD1*) gene mutation correlates with the severity of renal disease. *J Am Soc Nephrol.*, 13: 1230-1237.

Rossetti, S., Chauveau, D., Walker, D., Saggar-Malik, A., Winearls, C. G., Torres, V. E. and Harris, P. C. (2002b) A complete mutation screen of the ADPKD genes by DHPLC. *Kidney Int.*, 61: 1588-1599.

Rossetti, S., Chauveau, D., Kubly, V., Slezak, J. M., Saggar-Malik, A. K., Pei, Y., Ong, A. C., Stewart, F., Watson, M. L., Bergstralh, E. J., *et al.* (2003) Association of mutation position in polycystic kidney disease 1 (*PKD1*) gene and development of a vascular phenotype. *Lancet*, 361: 2196-2201.

Rossetti, S., Consugar, M. B., Chapman, A. B., Torres, V. E., Guay-Woodford, L. M., Grantham, J. J., Bennett, W. M., Meyers, C. M., Walker, D. L., Bae, K., *et al.* (2007) Comprehensive molecular diagnostics in autosomal dominant polycystic kidney disease. *J Am Soc Nephrol.*, 18: 2143-2160.

Rossetti, S. and Harris, P. C. (2007) Genotype-phenotype correlations in autosomal dominant and autosomal recessive polycystic kidney disease. *J Am Soc Nephrol.*, 18: 1374-1380.

Rossi, D. J., Ylikorkala, A., Korsisaari, N., Salovaara, R., Luukko, K., Launonen, V., Henkemeyer, M., Ristimaki, A., Aaltonen, L. A. and Makela, T. P. (2002) Induction of cyclooxygenase-2 in a mouse model of Peutz-Jeghers polyposis. *Proc Natl Acad Sci U S A.*, 99: 12327-12332.

Roux, P. P., Ballif, B. A., Anjum, R., Gygi, S. P. and Blenis, J. (2004) Tumor-promoting phorbol esters and activated Ras inactivate the tuberous sclerosis tumor suppressor complex via p90 ribosomal S6 kinase. *Proc Natl Acad Sci U S A.*, 101: 13489-13494.

Rozen, S. and Skaletsky, H. (2000) Primer3 on the WWW for general users and for biologist programmers. *Methods Mol Biol.*, 132: 365-386.

Ruggieri, P. M., Poulos, N., Masaryk, T. J., Ross, J. S., Obuchowski, N. A., Awad, I. A., Braun, W. E., Nally, J., Lewin, J. S. and Modic, M. T. (1994) Occult intracranial aneurysms in polycystic kidney disease: screening with MR angiography. *Radiology*, 191: 33-39.

Saadi-Kheddouci, S., Berrebi, D., Romagnolo, B., Cluzeaud, F., Peuchmaur, M., Kahn, A., Vandewalle, A. and Perret, C. (2001) Early development of polycystic kidney disease in transgenic mice expressing an activated mutant of the beta-catenin gene. *Oncogene*, 20: 5972-5981.

Saburi, S., Hester, I., Fischer, E., Pontoglio, M., Eremina, V., Gessler, M., Quaggin, S. E., Harrison, R., Mount, R. and McNeill, H. (2008) Loss of *Fat4* disrupts PCP signaling and oriented cell division and leads to cystic kidney disease. *Nat Genet.*, 40: 1010-1015.

Salomon, R., Saunier, S. and Niaudet, P. (2008) Nephronophthisis. *Pediatr Nephrol.* Jul 8. [Epub ahead of print].

Sampson, J. R., Yates, J. R. W., Pirrit, L. A. Fleury, P., Winship, I., Beighton, P. and Connor, J. M. (1989) Evidence for genetic heterogeneity in tuberous sclerosis. *J Med Genet.*, 26: 511-516.

Sampson, J. R., Maheshwar, M. M., Aspinwall, R., Thompson, P., Cheadle, J. P., Ravine, D., Roy, S., Haan, E., Bernstein, J. and Harris, P. C. (1997) Renal cystic disease in tuberous sclerosis: role of the polycystic kidney disease 1 gene. *Am J Hum Genet.*, 61: 843-851.

Sancak, O., Nellist, M., Goedbloed, M., Elfferich, P., Wouters, C., Maat-Kievit, A., Zonnenberg, B., Verhoef, S., Halley, D. and van den Ouweland, A. (2005) Mutational analysis of the *TSC1* and *TSC2* genes in a diagnostic setting: genotype-phenotype correlations and comparison of diagnostic DNA techniques in tuberous sclerosis complex. *Eur J Hum Genet.*, 13: 731-741.

Sancar, A., Lindsey-Boltz, L. A., Unsal-Kaçmaz, K. and Linn, S. (2004) Molecular mechanisms of mammalian DNA repair and the DNA damage checkpoints. *Annu Rev Biochem.*, 73: 39-85.

Sandford, R., Mulroy, S. and Foggensteiner, L. (1999) The polycystins: a novel class of membrane-associated proteins involved in renal cystic disease. *Cell Mol Life Sci.*, 56: 567-579.

Sanger, F., Nicklen, S. and Coulson, A. R. (1977) DNA sequencing with chain-terminating inhibitors. *Proc Natl Acad Sci U S A*, 74: 5463-7.

Santarosa, M. and Ashworth, A. (2004) Haploinsufficiency for tumour suppressor genes: when you don't need to go all the way. *Biochim Biophys Acta.*, 1654: 105-122.

Sarbassov, D. D., Guertin, D. A., Ali, S. M. and Sabatini, D. M. (2005) Phosphorylation and regulation of Akt/PKB by the rictor-mTOR complex. *Science*, 307: 1098-1101.

Saucedo, L. J., Gao, X., Chiarelli, D. A., Li, L., Pan, D. and Edgar, B. A. (2003) Rheb promotes cell growth as a component of the insulin/TOR signalling network. *Nat Cell Biol.*, 5: 566-571.

Scheffers, M. S., van der Bent, P., Prins, F., Spruit, L., Breuning, M. H., Litvinov, S. V., de Heer, E. and Peters, D. J. (2000) Polycystin-1, the product of the polycystic kidney disease 1 gene, co-localizes with desmosomes in MDCK cells. *Hum Mol Genet.*, 9: 2743-2750.

Scholey, J. M. (2003) Intraflagellar transport. *Annu Rev Cell Dev Biol.*, 19: 423-443.

Schrier, R., McFann, K., Johnson, A., Chapman, A., Edelstein, C., Brosnahan, G., Ecder, T. and Tison, L. (2002) Cardiac and renal effects of standard versus rigorous blood pressure control in autosomal dominant polycystic kidney disease: Results of a seven-year prospective randomized study. *J Am Soc Nephrol.*, 13: 1733-1739.

Schwartz, E. A., Leonard, M. L., Bizios, R. and Bowser, S. S. (1997) Analysis and modelling of the primary cilium bending response to fluid shear. *Am J Physiol.*, 272: F132-F138.

Sehgal, S. N., Baker, H. and Vézina, C. (1975) Rapamycin (AY-22,989), a new antifungal antibiotic. II. Fermentation, isolation and characterization. *J Antibiot (Tokyo)*, 28: 727-732.

Shepherd, C. W., Beard, C. M., Gomez, M. R. Kurland, J. T. and Whisnant, J. P. (1991a) Tuberous sclerosis complex in Olmsted County, Minnesota, 1950-1989. *Arch Neurol.*, 48: 400-401.

Shepherd, C. W., Gomez, M. R., Lie, J. T. and Crowson, C. S. (1991b) Causes of death in patients with tuberous sclerosis. *Mayo Clin Proc.*, 66: 792-796.

Shillingford, J. M., Murcia, N. S., Larson, C. H., Low, S. H., Hedgepeth, R., Brown, N., Flask, C. A., Novick, A. C., Goldfarb, D. A., Kramer-Zucker, A. *et al.* (2006) The mTOR pathway is regulated by polycystin-1, and its inhibition reverses renal cystogenesis in polycystic kidney disease. *Proc Natl Acad Sci U S A*, 103: 5466-5471.

Simons, M., Gloy, J., Ganner, A., Bullerkotte, A., Bashkurov, M., Krönig, C., Schermer, B., Benzing, T., Cabello, O. A., Jenny, A., *et al.* (2005) Inversin, the gene product mutated in nephronophthisis type II, functions as a molecular switch between Wnt signalling pathways. *Nat. Genet.*, 37: 537-543.

Simons, M. and Walz, G. (2006) Polycystic kidney disease: cell division without a c(l)ue? *Kidney Int.*, 70: 854-864.

Simons, M. and Mlodzik, M. (2008) Planar cell polarity signalling: from fly development to human disease. *Annu Rev Genet.*, 42: 517-540.

Singer, K. (1971) Genetic aspects of tuberous sclerosis in a Chinese population. *Am J Hum Genet.*, 23: 33-40.

Singla, V. and Reiter, J. F. (2006) The primary cilium as the cell's antenna: signalling at a sensory organelle. *Science*, 313: 629-633.

Sloboda, R. D. (2005) Intraflagellar transport and the flagellar tip complex. *J. Cell Biochem.*, 94: 266-272.

Sloboda, R. D. and Rosenbaum, J. L. (2007) Making sense of cilia and flagella. *J Cell Biol.*, 179: 575-582.

Slusarski, D. C. and Pelegri, F. (2007) Calcium signaling in vertebrate embryonic patterning and morphogenesis. *Dev Biol.*, 307: 1-13.

Smalley, S. L., Tanguay, P. E., Smith, M. and Gutierrez, G. (1992) Autism and tuberous sclerosis. *J Autism Dev Disord.*, 22: 339-355.

Smith, L. A., Bukanov, N. O., Husson, H., Russo, R. J., Barry, T. C., Taylor, A. L., Beier, D. R. and Ibraghimov-Beskrovnaya, O. (2006) Development of polycystic kidney disease in juvenile cystic kidney mice: insights into pathogenesis, ciliary abnormalities, and common features with human disease. *J Am Soc Nephrol.*, 17: 2821-2831.

Smulders, Y. M., Eussen, B. H., Verhoef, S. and Wouters, C. H. (2003) Large deletion causing the TSC2-PKD1 contiguous gene syndrome without infantile polycystic disease. *J Med Genet.*, 40: E17.

Somlo, S., Wirth, B., Germino, G. G. Weinstat-Saslow, D., Gillespie, G. A. J., Himmelbauer, H., Steevens, L., Coucke, P., Willems, P., Bachner, L., *et al.* (1992) Fine genetic localisation of the gene for Autosomal dominant polycystic kidney disease (PKD1) with respect to physically mapped markers. *Genomics*, 13: 152-158.

Stark, K., Vainio, S., Vassileva, G. and McMahon, A. P. (1994) Epithelial transformation of metanephric mesenchyme in the developing kidney regulated by Wnt-4. *Nature*, 372: 679-683.

Stevenson, A. C. and Fischer, O. D. (1956) Frequency of epiloia in Northern Ireland. *Br J Prev Soc Med.*, 10: 134-135.

Stoyanova, R., Clapper, M. L., Bellacosa, A., Henske, E. P., Testa, J. R., Ross, E. A., Yeung, A. T., Nicolas, E., Tsichlis, N., Li, Y. S., *et al.* (2004) Altered gene expression in phenotypically normal renal cells from carriers of tumor suppressor gene mutations. *Cancer Biol Ther.*, 3: 1313-1321.

Sun, Z., Amsterdam, A., Pazour, G. J., Cole, D. G., Miller, M. S. and Hopkins, N. (2004) A genetic screen in zebrafish identifies cilia genes as a principal cause of cystic kidney. *Development.* 131: 4085-4093.

Supp, D. M., Brueckner, M., Kuehn, M. R., Witte, D. P., Lowe, L. A., McGrath, J., Corrales, J. and Potter, S. S. (1999) Targeted deletion of the ATP binding domain of left-right dynein confirms its role in specifying development of left-right asymmetries. *Development*, 126: 5495-5504.

Surpili, M. J., Delben, T. M. and Kobarg, J. (2003) Identification of proteins that interact with the central coiled-coil region of the human protein kinase NEK1. *Biochemistry.* 42: 15369-15376.

Takakura, A., Contrino, L., Beck, A. W. and Zhou, J. (2008) *Pkd1* inactivation induced in adulthood produces focal cystic disease. *J Am Soc Nephrol.*, 19: 2351-2363.

Tao, Y., Kim, J., Schrier, R. W. and Edelstein, C. L. (2005) Rapamycin markedly slows disease progression in a rat model of polycystic kidney disease. *J Am Soc Nephrol.*, 16: 46-51.

Tapon, N., Ito, N., Dickson, B. J., Treisman, J. E. and Hariharan, I. K. (2001) The Drosophila tuberous sclerosis complex gene homologs restrict cell growth and cell proliferation. *Cell*, 105: 345-355.

Tavazoie, S. F., Alvarez, V. A., Ridenour, D. A., Kwiatkowski, D. J. and Sabatini, B. L. (2005) Regulation of neuronal morphology and function by the tumor suppressors Tsc1 and Tsc2. *Nat Neurosci.*, 8: 1727-1734.

Tee, A.R., Fingar, D.C., Manning, B.D., Kwiatkowski, D.J., Cantley, L.C., and Blenis, J. (2002) Tuberous sclerosis complex-1 and -2 gene products function together to inhibit mammalian target of rapamycin (mTOR)-mediated downstream signalling. *Proc. Natl. Acad. Sci. USA*, 99: 13571–13576.

Tee, A. R., Manning, B. D., Roux, P. P., Cantley, L. C. and Blenis, J. (2003) Tuberous sclerosis complex gene products, Tuberin and Hamartin, control mTOR signalling by acting as a GTPase-activating protein complex toward Rheb. *Curr Biol.*, 13: 1259-1268.

Tee, A. R. and Blenis, J. (2005) mTOR, translational control and human disease. *Semin Cell Dev Biol.*, 16: 29-37.

The European Chromosome 16 Tuberous Sclerosis Consortium (1993) Identification and characterisation of the tuberous sclerosis gene on chromosome 16. *Cell*, 75: 1305-1315.

The European Polycystic Kidney Disease Consortium (1994) The polycystic kidney disease 1 gene encodes a 14kb transcript and lies within a duplicated region on chromosome 16. *Cell*, 77: 881-894.

The International Polycystic Kidney Disease Consortium. (1995) Polycystic kidney disease: the complete structure of the *PKD1* gene and its protein. *Cell*, 81: 289-298.

Thivierge, C., Kurbegovic, A., Couillard, M., Guillaume, R., Coté, O. and Trudel, M. (2006) Overexpression of *PKD1* causes polycystic kidney disease. *Mol Cell Biol.*, 26: 1538-1548.

Tobin, J. L. and Beales, P. L. (2007) Bardet-Biedl syndrome: beyond the cilium. *Pediatr Nephrol.*, 22: 926-936.

Torra, R., Badenas, C., San Millán, J. L., Pérez-Oller, L., Estivill, X. and Darnell, A. (1999) A loss-of-function model for cystogenesis in human autosomal dominant polycystic kidney disease type 2. *Am J Hum Genet.*, 65: 345-352.

Torres, V. E., Donovan, K. A., Scicli, G., Holley, K. E., Thibodeau, S. N., Carretero, O. A., Inagami, T., McAteer, J. A. and Johnson, C. M. (1992) Synthesis of renin by tubulocystic epithelium in autosomal-dominant polycystic kidney disease. *Kidney Int.*, 42: 364-373.

Torres, V. E., Bjornsson, J., King, B. F., Kumar, R., Zincke, H., Edell, E. S., Wilson, T. O., Hattery, R. R. and Gomez, M. R. (1995) Extrapulmonary lymphangioleiomyomatosis and lymphangiomatous cysts in tuberous sclerosis complex. *Mayo Clin Proc.*, 70: 641-648.

Torres, V. E. and Harris, P. C. (2007) Polycystic kidney disease: genes, proteins, animal models, disease mechanisms and therapeutic opportunities. *J Intern Med.*, 261: 17-31.

Torres, V. E. and Harris, P. C. (2006) Mechanisms of Disease: autosomal dominant and recessive polycystic kidney diseases. *Nat Clin Pract Nephrol.*, 2: 40-55.

Tsuchiya, H., Orimoto, K., Kobayashi, K. and Hino, O. (1996) Presence of potent transcriptional activation domains in the predisposing tuberous sclerosis (Tsc2) gene product of the Eker rat model. *Cancer Res.*, 56: 429-433.

Turco, A. E., Clementi, M., Rossetti, S., Tenconi, R. and Pignatti, P. F. (1996) An Italian family with autosomal dominant polycystic kidney disease unlinked to either the *PKD1* or *PKD2* gene. *Am J Kidney Dis.*, 28: 759-761.

Uhlmann, E. J., Apicelli, A. J., Baldwin, R. L., Burke, S. P., Bajenaru, M. L., Onda, H., Kwiatkowski, D. and Gutmann, D. H. (2002) Heterozygosity for the tuberous sclerosis complex (TSC) gene products results in increased astrocyte numbers and decreased p27-Kip1 expression in $TSC2^{+/-}$ cells. *Oncogene*, 21: 4050-4059.

Upadhya, P., Birkenmeier, E. H., Birkenmeier, C. S. and Barker, J. E. (2000) Mutations in a NIMA-related kinase gene, *Nek1*, cause pleiotropic effects including a progressive polycystic kidney disease in mice. *Proc Natl Acad Sci U S A*, 97: 217-221.

Van Adelsberg, J., Chamberlain, S. and D' Agati, V. (1997) Polycystin expression is temporally and spatially regulated during renal development. *Am J Physiol.*, 272: F602-F609.

Van Raay, T. J., Burn, T. C., Connors, T. D., Petry, L. R., Germino, G. G., Klinger, K. W. and Landes, G. M. (1996) A 2.5 kb polypyrimidine tract in the *PKD1* gene contains at least 23 H-DNA-forming sequences. *Microb Comp Genomics*, 1: 317-327.

van Slegtenhorst, M., de Hoogt, R., Hermans, C., Nellist, M., Janssen, B., Verhoef, S., Lindhout, D., van den Ouweland, A., Halley, D., Young, J. *et al.* (1997) Identification of the tuberous sclerosis gene *TSC1* on chromosome 9q34. *Science*, 277: 805-808.

van Slegtenhorst, M., Nellist, M., Nagelkerken, B., Cheadle, J., Snell, R., van den Ouweland, A., Reuser, A., Sampson, J., Halley, D., and van der Sluijs, P. (1998) Interaction between hamartin and tuberin, the *TSC1* and *TSC2* gene products. *Hum. Mol. Genet.*, 7: 1053-1057.

Verghese, H., Weidenfeld, R., Bertram, J. F., Ricardo, S. G. and Deane, J. A. (2008) Renal cilia display length alterations following tubular injury and are present early in epithelial repair. *Nephrol Dial Transplant.*, 23: 834-841.

Vézina, C., Kudelski, A. and Sehgal, S. N. (1975) Rapamycin (AY-22,989), a new antifungal antibiotic. I. Taxonomy of the producing streptomycete and isolation of the active principle. *J Antibiot (Tokyo)*, 28: 721-726.

Vogelstein, B. and Kinzler, K. W. (2004) Cancer genes and the pathways they control. *Nat Med.*, 10: 789-799.

Vogt, H. (1908) Zur Pathologie und pathologischen Anatomie der verschiedenen Idiotieform. *Monatsschr Psychiatr Neurol.*, 24: 106-150.

Wahl, P. R., Serra, A. L., Le Hir, M., Molle, K. D., Hall, M. N. and Wüthrich, R. P. (2006) Inhibition of mTOR with sirolimus slows disease progression in Han:SPRD rats with autosomal dominant polycystic kidney disease (ADPKD). *Nephrol Dial Transplant.*, 21: 598-604.

Wallingford, J. B. and Habas, R. (2005) The developmental biology of Dishevelled: an enigmatic protein governing cell fate and cell polarity. *Development*, 132: 4421-4436.

Waltereit, R., Welzl, H., Dichgans, J., Lipp, H. P., Schmidt, W. J. and Weller, M. (2006) Enhanced episodic-like memory and kindling epilepsy in a rat model of tuberous sclerosis. *J Neurochem.*, 96: 407-413.

Wang, J., Mark, S., Zhang, X., Qian, D., Yoo, S.J., Radde-Gallwitz, K., Zhang, Y., Lin, X., Collazo, A., Wynshaw-Boris, A., *et al.* (2005) Regulation of polarized extension and planar cell polarity in the cochlea by the vertebrate PCP pathway. *Nat. Genet.*, 37: 980-985.

Wang, Q., Pan, J. and Snell, W. J. (2006) Intraflagellar transport particles participate directly in cilium-generated signaling in *Chlamydomonas*. *Cell*, 125: 549-562.

Ward, C. J., Turley, H., Ong, A. C., Comley, M., Biddolph, S., Chetty, R., Ratcliffe, P. J., Gattner, K. and Harris, P. C. (1996) Polycystin, the polycystic kidney disease 1 protein, is expressed by epithelial cells in fetal, adult, and polycystic kidney. *Proc Natl Acad Sci U S A*, 93: 1524-1538.

Ward, C. J., Hogan, M. C., Rossetti, S., Walker, D., Sneddon, T., Wang, X., Kubly, V., Cunningham, J. M., Bacallao, R., Ishibashi, M., *et al.*, (2002) The gene mutated in autosomal recessive polycystic kidney disease encodes a large, receptor-like protein. *Nat Genet.*, 30: 259-269.

Ward, C. J., Yuan, D., Masyuk, T. V., Wang, X., Punyashthiti, R., Whelan, S., Bacallao, R., Torra, R., LaRusso, N. F., Torres, V. E. *et al.* (2003) Cellular and subcellular localization of the ARPKD protein; fibrocystin is expressed on primary cilia. *Hum. Mol. Genet.*, 12: 2703-2710.

Washecka, R. and Hanna, M. (1991) Malignant renal tumours in tuberous sclerosis. *Urology*, 37: 340-343.

Watnick, T. J., Torres, V. E., Gandolph, M. A., Qian, F., Onuchic, L. F., Klinger, K. W., Landes, G. and Germino, G. G. (1998) Somatic mutation in individual liver cysts supports a two-hit model of cystogenesis in autosomal dominant polycystic kidney disease. *Mol Cell*, 2: 247-251.

Watnick, T., He, N., Wang, K., Liang, Y., Parfrey, P., Hefferton, D., St George-Hyslop, P., Germino, G. and Pei, Y. (2000) Mutations of *PKD1* in ADPKD2 cysts suggest a pathogenic effect of trans-heterozygous mutations. *Nat Genet.*, 25: 143-144.

Webb, D. W., Fryer, A. E. and Osborne (1996) Morbidity associated with tuberous sclerosis: a population study. *Dev Med Child Neurol.*, 38: 146-155.

Weimbs, T. (2007) Polycystic kidney disease and renal injury repair: common pathways, fluid flow, and the function of polycystin-1. *Am J Physiol Renal Physiol.*, 293: F1423-F1432.

Weston, B. S., Bagnéris, C., Price, R. G. and Stirling, J. L. (2001) The polycystin-1 C-type lectin domain binds carbohydrate in a calcium-dependent manner, and interacts with extracellular matrix proteins in vitro. *Biochim Biophys Acta.*, 1536: 161-176.

Weston, B. S., Malhas, A. N. and Price, R. G. (2003) Structure-function relationships of the extracellular domain of the autosomal dominant polycystic kidney disease-associated protein, polycystin-1. *FEBS Lett.*, 538: 8-13.

Wheatley, D. N., Wang, A. M. and Strugnell, G. E. (1996) Expression of primary cilia in mammalian cells. *Cell Biol Int.*, 20: 73-81.

Wienecke, R., Konig, A. and DeClue, J. E. (1995) Identification of tuberin, the tuberous sclerosis-2 product. Tuberin possesses specific Rap1GAP activity. *J Biol Chem.*, 270: 16409-16414.

Wienecke, R., Maize, J. C. Jr, Shoarinejad, F., Vass, W. C., Reed, J., Bonifacino, J. S., Resau, J. H., de Gunzburg, J., Yeung, R. S. and DeClue, J. E. (1996) Co-localization of the *TSC2* product tuberin with its target Rap1 in the Golgi apparatus. *Oncogene*, 13: 913-923.

Wildonger, J., Jan, L. Y. and Jan, Y. N. (2008) The Tsc1-Tsc2 complex influences neuronal polarity by modulating TORC1 activity and SAD levels. *Genes Dev.*, 22: 2447-2453.

Wilson, C., Idziaszczyk, S., Parry, L., Guy, C., Griffiths, D. F. R., Lazda, E., Bayne, R. A. L., Smith, A. J. H., Sampson, J. R. and Cheadle, J. P. (2005) A mouse model of tuberous sclerosis 1 showing background specific early post-natal mortality and metastatic renal cell carcinoma. *Hum. Mol. Genet.*, 14: 1839-1850.

Wilson, C., Bonnet, C., Guy, C., Idziaszczyk, S., Colley, J., Humphreys, V., Maynard, J., Sampson, J. R. and Cheadle, J. P. (2006) *Tsc1* haploinsufficiency without mammalian target of rapamycin activation is sufficient for renal cyst formation in *Tsc1*$^{+/-}$ mice. *Cancer Res.*, 66: 7934-7938.

Wilson, P. D. (2001) Polycystin: new aspects of structure, function, and regulation. *J Am Soc Nephrol.*, 12: 834-845.

Wu, G., Tian, X., Nishimura, S., Markowitz, G. S., D'Agati, V., Park, J. H., Yao, L., Li, L., Geng, L., Zhao, H., Edelmann, W. and Somlo, S. (2002) Trans-heterozygous *Pkd1* and *Pkd2* mutations modify expression of polycystic kidney disease. *Hum Mol Genet.*, 11: 1845-1854.

Xu, X., Brodie, S. G., Yang, X., Im, Y. H., Parks, W. T., Chen, L., Zhou, Y. X., Weinstein, M., Kim, S. J. and Deng, C. X. (2000) Haploid loss of the tumor suppressor Smad4/Dpc4 initiates gastric polyposis and cancer in mice. *Oncogene*, 19: 1868-1874.

Yamamoto, Y., Jones, K. A., Mak, B. C., Muehlenbachs, A. and Yeung, R. S. (2002) Multicompartmental distribution of the tuberous sclerosis gene products, hamartin and tuberin. *Arch Biochem Biophys.*, 404: 210-217.

Yeung, R. S., Buetow, K. H., Testa, J. R. and Knudson, A. G. Jr. (1993) Susceptibility to renal carcinoma in the Eker rat involves a tumor suppressor gene on chromosome 10. *Proc Natl Acad Sci U S A*, 90: 8038-8042.

Yeung, R. S., Xiao, G. H., Jin, F., Lee, W. C., Testa, J. R. and Knudson, A. G. (1994) Predisposition to renal carcinoma in the Eker rat is determined by germ-line mutation of the tuberous sclerosis 2 (*TSC2*) gene. *Proc Natl Acad Sci U S A.*, 91: 11413-11416.

Yeung, R. S., Xiao, G. H., Everitt, J. I., Jin, F. and Walker, C. L. (1995) Allelic loss at the tuberous sclerosis 2 locus in spontaneous tumors in the Eker rat. *Mol Carcinog.*, 14: 28-36.

Yeung, R. S., Katsetos, C. D. and Klein-Szanto, A. (1997) Subependymal astrocytic hamartomas in the Eker rat model of tuberous sclerosis. *Am J Pathol.*, 151: 1477-1486.

Yoder, B. K., Richards, W. G., Sweeney, W. E., Wilkinson, J. E., Avener, E. D. and Woychik, R. P. (1995) Insertional mutagenesis and molecular analysis of a new gene associated with polycystic kidney disease. *Proc Assoc Am Physicians*, 107: 314-323.

Yoder, B. K., Hou, X. and Guay-Woodford, L. M. (2002) The polycystic kidney disease proteins, polycystin-1, polycystin-2, polaris, and cystin, are co-localized in renal cilia. *J Am Soc Nephrol.*, 13: 2508-2516.

Yoder, B. K., Mulroy, S., Eustace, H., Boucher, C. and Sandford, R. (2006) Molecular pathogenesis of autosomal dominant polycystic kidney disease. *Expert Rev Mol Med.*, 8: 1-22.

Yoder, B. K. (2007) Role of primary cilia in the pathogenesis of polycystic kidney disease. *J Am Soc Nephrol.*, 18: 1381-1388.

York, B., Lou, D. and Noonan, D. J. (2006) Tuberin nuclear localization can be regulated by phosphorylation of its carboxyl terminus. *Mol Cancer Res.*, 4: 885-897.

Yost, H. J. (2003) Left-right asymmetry: nodal cilia make and catch a wave. *Curr Biol.*, 13: R808-R809.

Yu, Y. and Bradley, A. (2001) Engineering chromosomal rearrangements in mice. *Nat Rev Genet.*, 2: 780-790.

Zaremba, J. (1968) Tuberous sclerosis: a clinical and genetical investigation. *J Ment Defic Res.*, 12: 63-80.

Zeng, L. H., Xu, L., Gutmann, D. H. and Wong, M. (2008) Rapamycin prevents epilepsy in a mouse model of tuberous sclerosis complex. *Ann Neurol.*, 63: 415-417.

Zerres, K., Mücher, G., Bachner, L., Deschennes, G., Eggermann, T., Kääriäinen, H., Knapp, M., Lennert, T., Misselwitz, J., von Mühlendahl, K. E. *et al.* (1994) Mapping of the gene for autosomal recessive polycystic kidney disease (ARPKD) to chromosome 6p21-cen. *Nat Genet.*, 7: 429-432.

Zhang, H., Cicchetti, G., Onda, H., Koon, H. B., Asrican, K., Bajraszewski, N., Vazquez, F., Carpenter, C. L. and Kwiatkowski, D. J. (2003) Loss of *Tsc1/Tsc2* activates mTOR and disrupts PI3K-Akt signaling through downregulation of PDGFR. *J Clin Invest.*, 112: 1223-1233.

Zhang, Q., Taulman, P. D. and Yoder, B. K. (2004) Cystic kidney diseases: all roads lead to the cilium. *Physiology (Bethesda)*, 19: 225-230.

Zhou, J. and Pei, Y. (2008) Autosomal dominant polycystic kidney disease. In: Molecular and Genetic Basis of Renal Disease. pp. 85-117, Mount, D. B. and Pollak, M. R. (eds.), Elsevier Saunders, Philadelphia, USA.